Mechanical properties of cells and modelling of structural instabilities in tissues

by

Somiealo Azote

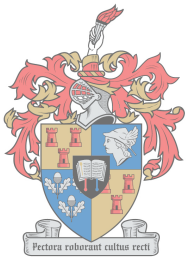

UNIVERSITEIT
iYUNIVESITHI
STELLENBOSCH
UNIVERSITY

Dissertation presented for the degree of Doctor of Philosophy
in the Faculty of Science at Stellenbosch University

Supervisor: Prof. Kristian Müller-Nedebock

December 2018

Declaration

By submitting this dissertation electronically, I declare that the entirety of the work contained therein is my own, original work, that I am the sole author thereof (save to the extent explicitly otherwise stated), that reproduction and publication thereof by Stellenbosch University will not infringe any third party rights and that I have not previously in its entirety or in part submitted it for obtaining any qualification.

Date: December 2018

Abstract

Mechanical properties of cells and modelling of structural instabilities in tissues

Somiealo

Department of Physics,
Stellenbosch University,
Private Bag X1, Matieland 7602, South Africa.

Dissertation: PhD

August 2018

Cells have inherent mechanical properties that can be modelled physically. Statistical physics approaches permit the understanding of deformation dependence by modelling the various elements of the cytoskeleton and combining these with the constraints and physical properties of the cell membrane. When cells combine to form more complex structures, including, for example, epithelial structures, the resulting structure also needs to be understood. We wish to understand the mechanical contribution to the elastic properties and stability of the cell within the tissue when branching actin cytoskeletal network emerge or grow and their structure, spatial organisation and orientational ordering geometrically constrained by the cell membrane.

Based on a grand canonical ensemble formalism by Frisch *et al.* [1] and Müller-Nedebock *et al.* [2], we model the structure of branching actin networks of living cell cytoskeletal filaments when these are rigidly contained with geometrical confining regions. The formalism allows a thermodynamic equilibrium calculation of density and orientational order density for filaments and branch points. We find distinct local orientation, order parameter and density profiles for network filament segments, as the degree of branching and the ratio of persistence lengths of the filaments to the confining region size are varied. These results suggest the role of the confinement in the structural properties and organization of branching actin networks inside the confining region. We next investigated the contribution of the elastic properties of the networks to the elastic properties and stability of the cells within tissues by computing

the free energies and forces of networks system. we find that tissue cells are stable against compression while cell under shear become unstable beyond a critical angle.

Uittreksel

Mechanical properties of cells and modelling of structural instabilities in tissues

Somiealo

Fisika Departement,
Stellenbosch Universiteit,
Privaatsak X1, Matieland 7602, Suid Afrika.

Proefskrif: PhD

Augustus 2018

Selle het inherente eienskappe wat met die fisika gemodelleer kan word. Statistiese fiska benaderingspunte laat toe om die vervormingsafhankliheid te verstaan deur die modellering van verskillende elemente van die sitoskelet en om dit met die randkondisies en fisiese eienskape van die selmembraan te kombineer. Wanneer selle gekombineer word om meer komplekse strukture te vorm, insluitende, byvoorbeeld, epitele strukture, dan moet die resulterende struktuur ook ondersoek word. Ons wil die meganiese bydrae tot die elastiese eienskappe en die stabiliteit van die sel as deel van die weefsel verstaan, wanneer vertakkende aktien netwerke ontstaan en groei, en hulle struktuur, organisasie in die ruimte deur die geometrie van die sel ingeperk word.

Gebaseer op n grootkanoniese formalisme van Frisch, et al., en van Müller-Nedebock et al. modelleer ons die struktuur van vertakkende aktien netwerke van dinamiese selle se sitoskeletfilamente wanneer hierdie tot starre geometriese gebiede beperk word. Die formalisme laat n berekening in die termodinamiese ewewig toe van die digtheid and orde in uitrigtings vir die filamente and vertakkingspunte. Ons bepaal duidelike lokale orientasie-, orderparameter- en digtheidsprofiele vir netwerk filamente, in afhanklkheid van hoe die graad van vertakking en die verhouding van die filamente se persistensielengte tot die grootte van die ingrensende gebied varieer. Hierdie resultate dui aan wat die rol van die ingrensing op die strukturele eienskappe en organisasie van die vertakkende aktien netwerke is binne die ingrensende gebied. Ons het ook ondersoek wat die bydrae van die elastiese eienskappe van die netwerke tot die elestiese eienskappe en stabiliteit van van die selle binnekant n weefsel is, deurdat die vrye energië en

kragte van die netwerkstelsel bepaal is. Ons vind dat weefsel stabiel teen samepersing is, terwyl dit onder skuifkragte bokant n kritieke hoek onstabiel raak.

Acknowledgements

I would like to express my special appreciation and thanks to my supervisor Professor Kristian K. Müller-Nedebock for all his advices, patience, motivation and support of my Ph.D research.

I would like to thank Dr. Kriel for some helpful discussions we had during my thesis.

I am so grateful to the Organisation for Women in Science for the Developing world (OWSD) and to the Swedish International Development Cooperation Agency (SIDA) who have funded this work, a big thank you. I thank also the National Research Foundation of South Africa (NRF) for their support.

I thank the African Instite for Matematical Sciences (AIMS) for opening me the doors of mathematical science researches.

To my AIMS's supervisor Professor Jean-Francois Joanny and to Doctor Rhoda Hawkins, I say thank you for having introduced me to the field of biophysics.

I would like to take this opportinuty to thank Professor Banna Magolmeena for his motivation and support. I thank also M. Kokou Gawonou N'Tsouaglo for the stimulating discussions about how to learn fast the programing languages, especially C/C++.

A special thank you to my office mates, Doctor Stanard Mebwe Patchong and Ishmael Takyi for the interesting discussions, and their support.

A big gratitude goes to my parents, family and family-in-law whom have always been by my side, for their love, prayers and support, a big thank you.

I am so grateful to my husband Hassikpezi Florent, thank you for your patience, motivating and loving heart.

I can not conclude without giving all the honor and glory to the Mighty God who has permitted this dream to become true!

Contents

List of Figures

List of Tables

Part I

Introductory chapter

Chapter 1

Introduction and background

1.1 Introduction and motivation

Living cells are constantly changing shape, interacting with their neighbouring cells, probing, pushing, pulling and crawling on their surrounding extracellular matrix. Most biological processes and functions, organ development, plants growth, wound healing and most cellular diseases are based on these mechanical activities that each cell of a tissue provide [3]. Known as the basic fundamental unit of life, an eukaryotic living cell (cell that make up animal and plants tissues) constitutes a whole system on its own. Initially thought of being a chemical liquid boundary by most of biologists [4, 5], cells possess a cluster of proteinic networks and organelles at their inner space which help to ensure most of their biological and mechanical functions. Cells can undergo mechanical instability or deformation when subjected to external geometrical constraints or force, in a similar manner as engineering materials [6], though they are way more complex. The mechanics of a typical living eukaryote cell is proven to generally originate from the structure, spatial organisation, alignment and elastic properties of its internal proteinic networks, called cytoskeleton [7–10].

Cryo-electron microscopy and fluorescent imaging techniques are often used to visualize the internal space of the cell in order to label the components that make up the cytoskeleton and determine their structural composition and properties [11, 12]. The cell cytoskeleton is constituted of actin filaments, microtubules and intermediate filaments. Also, diverse binding proteins exist inside the cell and serve as cross-linkers in the cytoskeletal networks formation. The function and mechanical properties of biopolymer filaments constituting the cell cytoskeletal networks are dictated by their structure, conformation, spatial organisation, orientational ordering and physical properties which, in turn, are considerably modified in geometrically confined or crowded spaces [13–16]. These biopolymer filaments under the effect of cell membrane confinement work in concert to contribute to the cell functions and to the elastic or mechanical stability of the cell. However, it is shown that the networks of actin filaments are most abundant proteins inside the cell and contribute most to the mechanical properties of the

cell. In fact, various drugs influence the mechanical integrity of different components of the cytoskeleton. This has been investigated using elasticity measurements with an atomic force microscope (AFM). Disaggregation of actin filaments causes the loss of the cell elasticity, while this does not happens for microtubules. This shows the importance of the actin network for the mechanical stability of living cells [17]. Actin filaments are directed and are semiflexible with persistence length similar to the cell dimension. They self-assemble into higher order structure inside the cell. In fact imaging of the interior of cell (crawling cell) shows a highly branched filamentous networks of actin at the cell periphery where branching via binding proteins such as the Arp2/3 protein complex, which initiate the branching of new actin filaments on existing ones at an angle of about 70°. It is shown that normal effect of cell membrane confinement on the structure, architecture, spatial organisation and orientational ordering of these branching actin networks under is fundamental for the cell mechanical stability [13, 18, 19].

Many cellular diseases, such as cancer and spreading of infected cell by viruses, as for example in cells infected by HIV, often originates from the abnormalities in the mechanics of the actin cytoskeleton which in turn is based on the structure, spatial organisation and orientational ordering of branching actin networks [20–23]. The structure, spatial organisation and orientational ordering of filaments of branching actin networks are in turned controlled by the geometrical confinements effects that the cell membrane introduce. Experimental researches showed that abnormal structural and spatial organization of actin and thus of the mechanics of cell can also lead for example to development and progression of atherosclerosis in adherent endothelial cells and non adherent leukocytes (white blood cells) [24–27]. Some authors found that genetic alteration in the structure of actin networks can lead to significant immunopathologic consequences and even to diseases such us alzheimer's diseases [27]. More, disruption of actin filaments and lack of their convenient spatial and orientational ordering affects multiple cell functions including motility, signal transduction and cell division, ultimately culminating in cell death [28] or in cancer cell formation and invasion [21–23]. Also the loss of contractility of heart muscle cells due to the lack of actin structural and spatial arrangement often cause heart failure [6, 29]. Actin networks are said to play a key role in establishing and spreading the HIV infection [20]. Therefore, failure in the cell actin networks structural and spatial organization under the effect of confinement can lead to the loss of the cells mechanical integrity, and this is unfavourable for the good functioning of cells within the tissue.
We are interested in investigating the contribution of confined branching actin cytoskeletal networks to the mechanical and structural properties and stability of tissue cells at thermodynamic equilibrium. The ability to model and understand how the cell membrane controls the structure, spatial organization and orientational ordering of the components that make up the cytoskeleton can allow to bring more light in the understanding of the elastic properties and stability of tissue cells.

Many researchers in biophysics model cells as a continuum material only (as visco-elastic fluid) using fundamentals laws of physics mainly of classical, continuum and fluid mechanics [30, 31]. There have been also many experimentals studies where experimental methods consist in general of a mechanical homogeneous perturbation of the cell in the form of an imposed deformation and then make observation of the static and dynamic responses of the cell. These include techniques such as atomic force microscopy (AFM), magnetic twisting cytometry (MTC), micropipette aspiration experiments, optical tweezers, shear-flow methods [32, 33]. But in reality cells are not homogeneous continuum materials but rather an heterogeneous composites. However both theoretical and experimental studies of the mechanics of cells and their cytoskeleton have known a lot of progress during the past 15 years with significant contributions for the development of novel theoretical models and experimental techniques in biotechnology and in medicine. The recent increasing number of cellular diseases, has motivated researchers in Biophysics and Biomathematics in trying to develop more theories and computational models of confined actin filaments to understand the relationship between the structural properties of actin biopolymers present everywhere in the internal space of the cell and the mechanical properties of living tissue cells. With the discovery that cell's mechanical properties depend on the mechanics of their underlying cytoskeletal networks, many new computational and theoretical approaches such as polymer-based-models have been developed to help understand the structural and thermodynamics behaviour of these. Alvarado *et al.* [34] and Silva *et al.* [13] in their study of the alignment of nematic and bundle semi-flexible filaments inside very small chambers, (size of order of μm), have reported that spatial confinement has a great impact on the conformational organization of actin filaments and also on their alignment. In fact, they used rectangular microchambers for their experiments whose length they compared to the filament persistence lengths and, depending on the density of the filaments, they found that the filaments align diagonaly (radially) or parallel to the cell's wall. This kind of ordering is also observed for the networks of microtubules under confinement [35]. There are also advanced experimental instruments that are developed to relate cells to their internal structures, such as MicroElectroMechanical systems (MEMS) devices with resolution size at cell scale, and even more advanced instruments capable of mechanically examining and confining single cytokeletal filament at forces and displacements smaller than a pN [6, 36, 37].

One of the principal objectives for doing and advancing all these researches is to come up with results that could assist in the diagnosis and treatment of the actin-based cell mechanical-related diseases such as cancer. But there are still many questions such as what is impact of the confinement effects on the structure, spatial organization and orientational ordering of branching actin networks and what is the consequence of these effects on the mechanical properties of tissue cells. It is evident that one has to answer these questions before being able to make efficient propositions toward a quantitative estimation of mechanical properties of cell and modelling of instabilities in tissues.

Actin filaments of the cytoskeletal networks are often described using coarse-grained model of semiflexible polymers with theoretical tools from statistical physics. In fact, many theorists in biophysics have developed polymer-based models to investigate the effects of confinement on the structure, behaviour, conformation, spatial and orientational organization of linear semiflexible biopolymers, either in their equilibrium or in their dynamical state [38–42]. Their studies allowed to know that semiflexible polymers are subject to strong confinement effects when they are confined in geometries with size smaller then their persistence lengths, which induce preferential in their alignment relatively to the confining region boundaries. These models allowed to understand the behaviour and some of the structural properties of linear actin filaments under cellular confinements. However, up to our knowledge, there exists no theory that has clearly investigated the effects of confinement on branching actin networks confined to finite regions at thermodynamics equilibrium.

In this thesis we model the branching cytoskeletal networks confined in various geometrical cells and we investigate on the effect of confinement on these branching actin networks. Our model is based on a grand canonical ensemble formalism at thermodynamics equilibrium developed for the study of linear semiflexible polymers in confining regions by other authors [1, 2, 43]. So we extend their model to branching actin networks. We show that a generalisation of the monomer ensemble technique [44] is particularly useful by the computational point of view, leading to density profiles of branching points, and orientations of filaments relatively to the cell boundaries. Our approach allows us to make predictions on the structure, spatial organization and ordering of branching actin networks under confinement. Using these quantitative results and exploring the free energy of the system, we investigate the relationship between structural properties of branching actin networks and the stability and elastic properties of cells within a tissue.

In what follows, we give a little background about the morphology of cells and the physics of its cytoskeleton. After that we give the outlines of this thesis.

1.2 Basic concepts about the physics of cell and their cytoskeleton

Living cells are the key characteristics of any living beings. We have two types of cells: eukaryotic cells which contain organelles such as nucleus with a huge compartiment and the prokaryotic cells which has no organelle, not even the nucleus. Most animal and plant tissues are made of eukaryotic cells. In contrast to prokaryotic cells which are single-celled organisms generally found in bacteria, eukaryotic cells can be single-celled or multicellular. We present here the

morphology of the eukaryotic tissue cells. Their sizes varies between 10 to 50μm in animal up to 100μm in plants. A single living cell is self-sufficient.

1.2.1 Morphology of eukaryotic animal and plant cells

Animal eukaryotic cells, Figure 1.1 , are composed of a plasma membrane (called cell membrane). It is a semi-permeable barrier made of the phospholipid bilayer that separate the cell and its external medium. In the inner of the cell is the cytoplasm which is the material between the nuclear envelope and the cell membrane. All the metabolic activity takes place in the cytoplasm. The nucleus is the greatest organelle (from the complex meshworks housed) in the cell. It is where the DNA giving the genetic informations is kept and RNA is transcribed. The endoplasmic reticulum ensures the transport for molecules needed for certain changes and functions of the cell. We have also the lysosome which constitutes the digestive system in the cell while the golgi bodies ensure the change or renewal of the protein molecules and are transformed into vesicles or stored in mitochondria. The latter one are the main energy source of the cell, it is where energy (ATP) is stored to aliment the activities of the cell. All these organelles are embedded in the cytosol which is an aqueous medium consisting of accessory proteins and fibrous macromolecules. The fibrous macromolecules is a three-dimensional complex meshworks called cytoskeleton. It maintains the shape of the cell as well as anchoring organelles and controls internal movement of structures. It contributes also to the intracellular transport. The rigidity of the cytoskeleton is reinforced by the membrane which maintains constant the cell volume, giving the cell unique mechanical properties and stability.

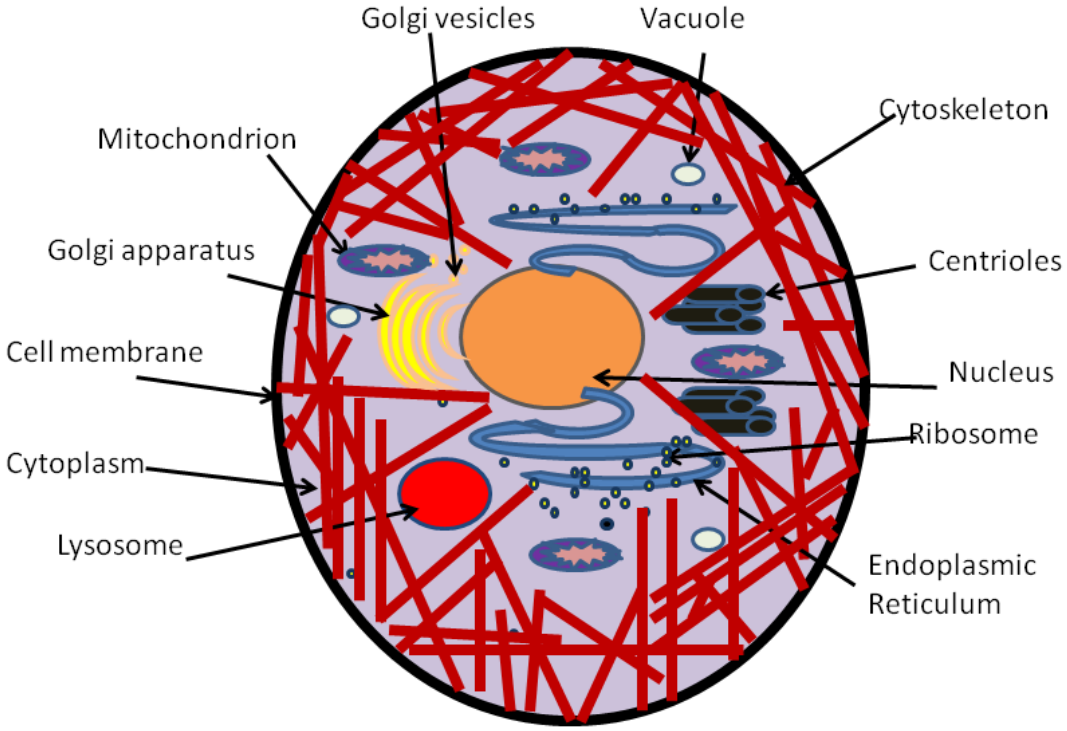

Figure 1.1: Depiction of an eukariotic cell of animals showing its differents components.

Like animal cells, **plant cells**, Figure 1.2, have a nucleus, cytoplasm, cell membrane, mitochondria and ribosomes. Beside these common features, plant cells possess rigid cell wall around their cell membrane which protects and gives the plant its structural texture. They have also chloroplasts and a permanent large vacuole. The latter occupy most of the interior space of the cell and only a very small thin area is occupied by the cytoskeleton. Thus, the cytoskeleton in plant cells generally presents thus a two-dimentional shape [8].

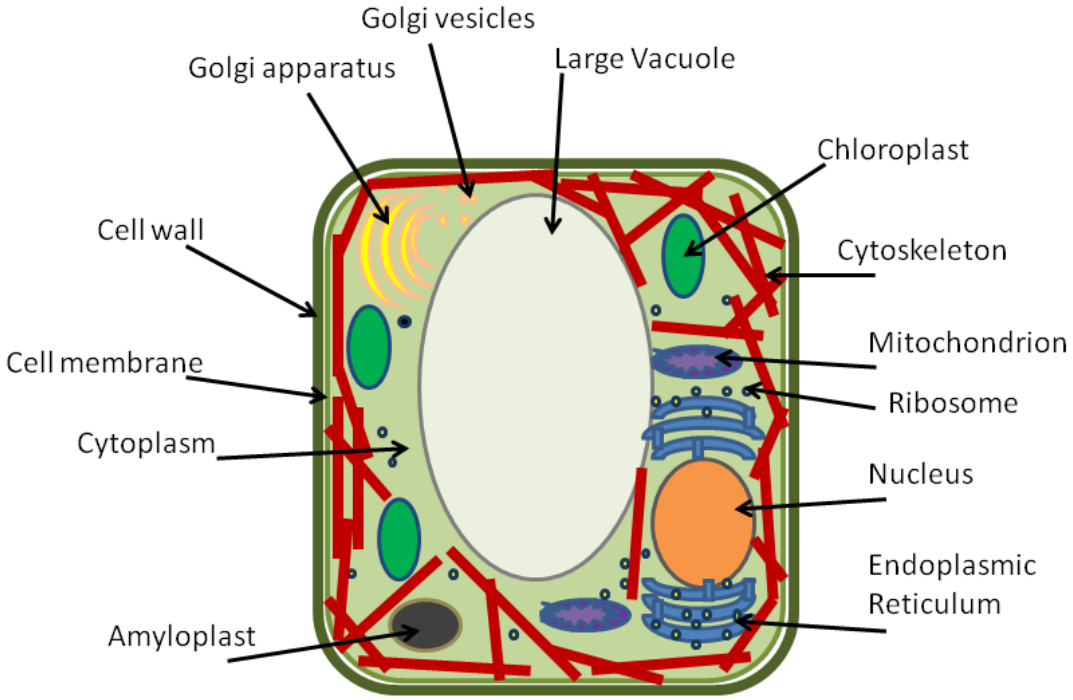

Figure 1.2: Depiction of an eukariotic cell of plants showing its differents components..

Each single cell is thought of as a self-sufficient material because of the numerous components it contains and that enables it to achieve most of its functions and its mechanical activities. We are interested in the study of the mechanical properties and stability of each tissue cell which are known to be ensured by the cell cytoskeleton. In what follows we define the components that make up the cell cytoskeleton.

1.2.2 Role and physical properties of the components of the cytoskeleton

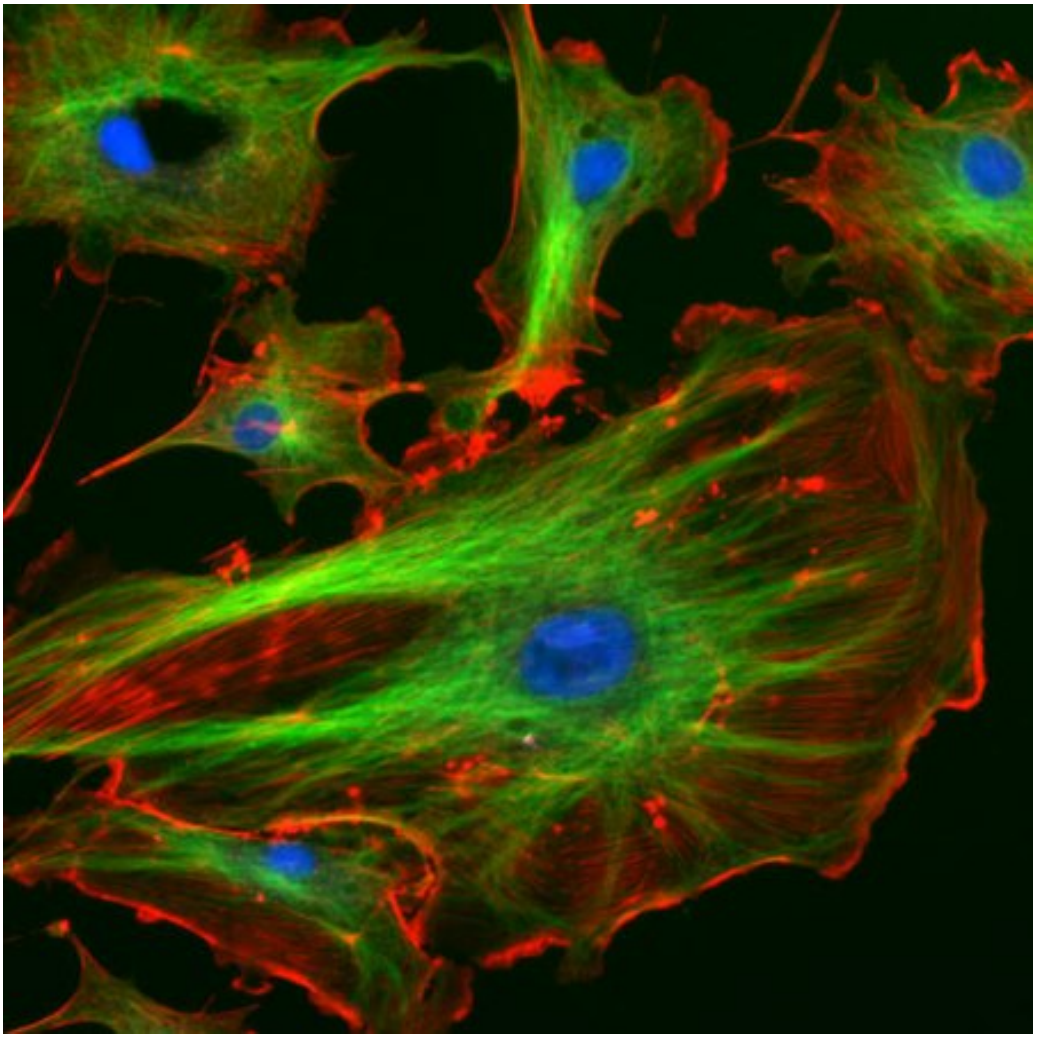

Figure 1.3: Image of eukaryotic cells cytoskeleton (Wikipedia). The networks in red represent the actin networls, in green we have the microtubule, the nucleus is reported in blue in the middle of the cytoskeleton.

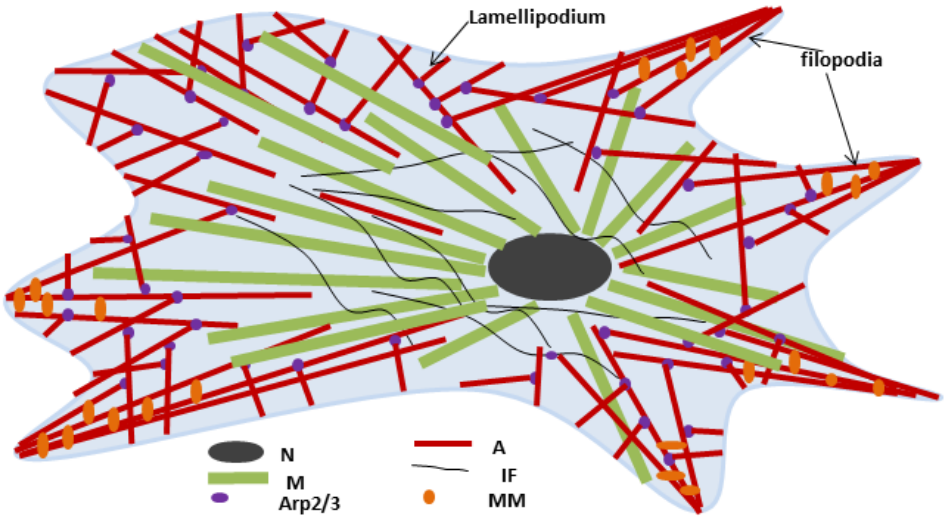

Figure 1.4: Cartoon of the cell cytoskeleton. The cartoon shows more clearly some of the differents components of the cell cytoskeleton. The filaments in red color are actin filaments (A), microtubules (M) are in green and the intermediate filaments are in black (IF) , the violet dots are the Arp2/3 protein complex, and motor proteins in orange color (MM). Actin network present a highly branched architecture at the leading edge of the cell called lamellipodium. The Arp2/3 protein complex are the nucleotors of the branching. We have the nucleus in the middle (which is not part of the cytoskeleton)

The cytoskeleton of eukaryotic cells is a complex dense network composed of three main types of biopolymer filaments namely the microtubules, the intermediate filaments and actin filaments. These filaments self-organise spatially into networks and work together to provide cell with mechanical support that enables cells to carry out essential physiological functions.

1.2.2.1 Role

Microtubules

Microtubules are made of fairly strong protein tubilins and are very rigid filaments and resistant to compression. They are in form of long hollow cylinders. They typically have a diameter of about 25nm of diameter (d) and a persistence length ℓ_p (it is a length that measures the stiffness of a polymer, see details in the subsection 1.2.3)of about 6mm [39, 45–47]. They are polar and thus have a plus and minus ends where the plus end is the end where the polymerization takes place while the depolymerization takes place at the minus end. The network of

microtubules function in the cell movement and in the cell division by mitosis especially in the formation of the miotic spindle apparatus. They are also involved in transport of vesicles, in mechanical support, organization of the cytoplasm, in motility and in maintaining the structural organization of the cell. They emerge from the centre of the cell towards the side of the cell. Microtubules are often modelled in continuum mechanics and statistical polymer physics as rigid (cylindrical) rods [45].

Intermediate filaments (IF)

Intermediate filaments are the flexible fibrous proteins. They help to enhance the mechanical integrity of cells against severe deformation. In fact they are the basic building blocks of intrinsically flexible, filamentous structures that are able to resist high mechanical stresses on the cell. They thus provide strength and support to the networks of microtubules and actin. Their diameter varies between 7nm and 10nm on average and possess a persistence length less that 1μm [39, 47, 48]. They are often modelled as flexible (freely jointed or as exhibiting random walks) using statistical mechanics tools.

Actin filaments

Actin filaments are thin semiflexible (visco elastic) polymers, two-stranded helical filament with diameter of about 8nm and of with a typical persistence length of about 17.7μm [39, 45–47, 49]. They possess a pointed end and a barbed end so they are directional. Actin filaments are polymerized from globular actin monomeric subunits called G-actin, which are the most abundant proteins inside the cell. The polymerization consists of a reversible process in which monomers add at the barbed end of the filament, which elongates to a certain length and then starts shrinking from both pointed ends. The shrinking mechanism is called depolymerisation. Actin constitutes the major component of the cell cytoskeleton. Actin networks are involved in many important biological processes and functions of the cells, including cell shape remodelling, cell division, differentiation, adhesion, motility or migration, transport and cell mechanosensing (which is the ability of a cell to sense mechanical cues of its microenvironment). Actin takes thus an exceptional position among the components of the cell cytoskeletal networks. Electron microscopy and fluorescence microscopy experiments showed that actin filaments are mainly polymerised beneath the plasma membrane and they constantly self-assemble into varieties of higher-order structural networks to provide mechanical support to the cell. In fact actin filaments can self-organize spatially and cross-link inside the cell either into bundle networks or into highly dense and branched tree-like networks. There are varieties of binding proteins which initiate or contribute to the formation of these actin networks. These proteins act depending

on the specific function or mechanical activity that the cell want to achieve. One of the binding proteins that we wish to know more about is the Arp2/3 protein complex. It has an essential role in the formation of lamellipodia and philopodia [50, 51]. In fact for the cell to move, it was shown that the Arp2/3 protein complex nucleates the polymerization of actin filaments and ensure the formation of the highly branched structures like tree-like networks at the leading edge of the cells. The Arp2/3 complex simultaneously controls nucleation of actin polymerization and initiates the branching and growth of new filaments to the side of existing filaments, at typical angle of 70°. In this process, the newly formed filaments activate other Arp2/3 complexes located at the periphery of the cell, facilitating the formation of more branched and dense networks of actin filaments which is proven to contribute most to the mechanical and thermodynamical stability of cells.

Filaments of actin networks are often studied using the coarse-grained model of semiflexible polymer with tools from statistical physics.

	Persistence length ℓ_p	diameter d
Actin	17.7μm	8nm
Microtubules	6mm	25nm
IF	$< 1\mu$m	10nm

Table 1.1: *Table summarizing the different length scales of cytoskeletal filaments.*

1.2.3 Example of polymer model for cytoskeletal filaments

Intermediate filaments

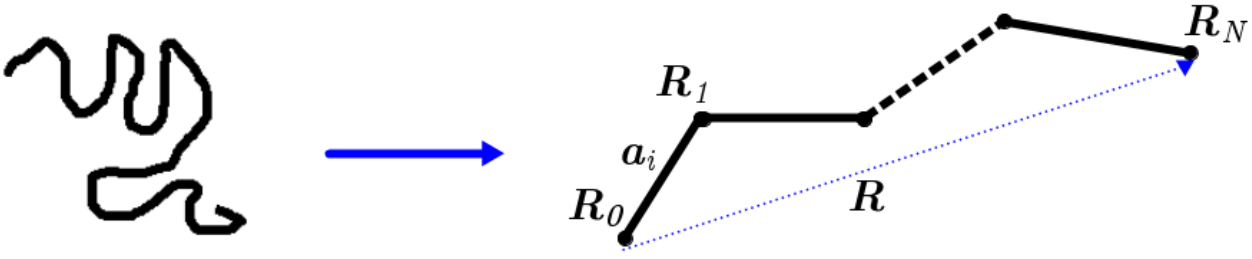

Figure 1.5: Intermediate filament modelled as freely jointed flexible polymer of N monomers. $\boldsymbol{a}_i = \boldsymbol{R}_i - \boldsymbol{R}_{i-1}$ are the chain bond vectors with size $|\boldsymbol{a}_i|$ where $\boldsymbol{R}$ is the end-to-end vector of the chain.

Intermediate filements are described as flexible polymer chains. Flexible chains in polymer physics, are modelled as freely jointed chain (no angular dependance between chain segments) of N oriented monomers subunits (Figure 1.5) of size a with $\boldsymbol{a}_i = \boldsymbol{R}_i - \boldsymbol{R}_{i-1}$. The average $\langle \boldsymbol{R} \rangle$ of the end-to-end vector of the chain is 0 i.e $\langle \boldsymbol{R} \rangle = \frac{1}{N} \sum_{i=1}^{i=N} \boldsymbol{a}_i = 0$. Therefore, this length is rather measured in term of its means square. The mean square is found to be: $\langle \boldsymbol{R}^2 \rangle = Na^2 = aL$ where

$L = Na$ is the contour length of the chain. A general end-to-end distance of a flexible polymer is thus obtained as $R \sim aN^{\nu}$ where ν is a scaling exponent equal to 1/2 for ideal chains where ideal chains are chains with no excluded volume effect. The segments of this type of chains are identical, while non-ideal chains consist of chains with excluded volume effects. Flexible chains exhibit thus a scaling behaviour and have a very small persistence length compared to its contour length $\ell_{\mathrm{p}} \ll L$. A broad study of flexible polymers can be found in reference [52].

Actin

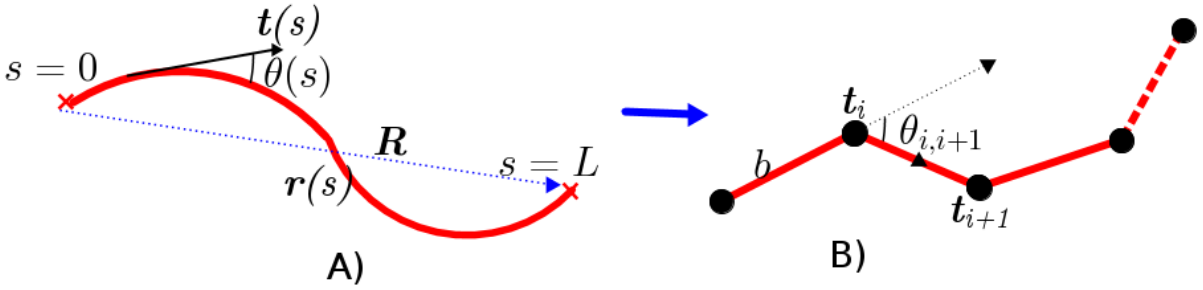

Figure 1.6: Actin modelled as semiflexible polymer. A) $\boldsymbol{r(s)}$ is the space curve of the chain where s is the arc length of the filament, $\boldsymbol{R}$ the end-to-end vector of the chain. $\boldsymbol{t}(s)$ is the tangent unit vector at arc length s of the chain and the angle $\theta(s)$ is the angle between pair of tangent vectors of the chain. B) Discrete version of semiflexible chains. The chain is described as made up of consecutive connection of monomers or segments where each segment is of length b and orientation $\boldsymbol{t}_i$, the tangent unit vector.

Actin filaments are modelled as sememiflexible polymers. Semiflexible polymers have been widely studied analytically by using the Kratky Porod chain model or worm-like chain model. it is a continuous description of the chain in which the chain is parametrized by space curve $\boldsymbol{r(s)}$ (Figure 1.6 A)) where s is the length along the curve. The Hamiltonian of the system is defined by

$$H[\boldsymbol{r}(s)] = \frac{k_b}{2}\int_0^L \mathrm{d}s \left(\frac{\mathrm{d}\boldsymbol{t}(s)}{\mathrm{d}s}\right)^2 \tag{1.1}$$

or

$$H[\boldsymbol{r}(s)] = \frac{k_b}{2}\int_0^L \mathrm{d}s \left(\frac{\mathrm{d}^2\boldsymbol{r}(s)}{\mathrm{d}s^2}\right)^2 \tag{1.2}$$

where $\boldsymbol{t}(s) = \frac{\mathrm{d}\boldsymbol{r}(s)}{\mathrm{d}s}$, is the tangent vector.

This Hamiltonian can be be used to express the partition function which can be calculated analytically by using the constraint of local inextensibility of semiflexible polymers $\delta(|\boldsymbol{t}(s)| - 1)$ for each s. However to model the semiflexible chain numerically, the discrete vesion is considered, (see Figure 1.6 B). The chain is made up of consecutive connection of monomers or segments where each segment i of the chain is of length b and orientation $\boldsymbol{t}_i$, the tangent unit vector. The contour length L of the chain is $L = Nb$, where N is the number of segments in the chain. The adjacent segments of the semiflexible chain are orientationally dependent. They

exhibit a bending stiffness between them. So a Boltzmann bending weight w is associated to this stiffness and is defined as:

$$w = e^{-\beta E_{i,i+1}} \tag{1.3}$$

where

$$E_{i,i+1} = \varepsilon \boldsymbol{t}_i.\boldsymbol{t}_{i+1}, \tag{1.4}$$

$\beta = 1/k_B T$ with k_B the Boltzmann constant and T the temperature; ε is the bending modulus.

The persistence length ℓ_p of a semiflexible chain is comparable to its contour length L. The tangent vectors of the chains are correlated and the correlation quantity $\langle \boldsymbol{t}_i \cdot \boldsymbol{t}_j \rangle$ of any pair of segments of the chain is:

$$\langle \boldsymbol{t}_i \cdot \boldsymbol{t}_j \rangle \sim e^{-\frac{|i-j|}{\ell_\mathrm{p}}} \tag{1.5}$$

The mean square of the end-to-end distance $\boldsymbol{R}$ is obtained in reference [53] as:

$$\langle \boldsymbol{R^2} \rangle = 2L\ell_\mathrm{p} \left(1 - \frac{\ell_\mathrm{p}}{L}(1 - e^{\ell_\mathrm{p}/L}) \right) \tag{1.6}$$

Using equation (1.6), one can see that for $\ell_\mathrm{p} \ll L$, we recover the case of the flexible chains.

Microtubules

Figure 1.7: Microtubule modelled as rigid polymer.

The model used to study of actin filaments is also valid for the study of microtubules except that in the present case we consider the persitence length of the polymer chain to be much greater than its contour length, i.e the chain is rigid. For a rigid chain, we have $\ell_\mathrm{p}/L \gg 1$ and in this limit, the mean square of the end-to-end distance defined in equation (1.6) becomes $\langle \boldsymbol{R^2} \rangle \simeq L^2$.
The persitence length is thus the most important measure that enables to classify cytoskeletal filaments in term of their stiffness.

All these thousands of proteins that make up the highly dense and complex cytoskeletal networks and the organelles described above are contained within the finite small size of the cell and they work together to ensure the cell physiological and mechanical functions. However, we are interested in the contribution of the branching actin networks to the mechanical stability

of the cells within the tissue.
Like the persistence length of microtubules, the persistence lengths of actin filaments constituting the actin networks are of order of magnitude similar to the size of the cell. Their spatial organization and orientational ordering inside the cell is constrained by the effect of the confinement that the cell membrane or wall introduces, since actin is the most abundant and form a dense branching networks in proximity of the cell membrane. Determining the effect of cell geometrical confinement on the formation and spatial arrangement of the branching cytoskeletal networks is crucial for the study and understanding of the structure and elastic properties of these networks, and their contribution to the emergent elastic or mechanical properties of cells and their tissues.

In the following chapter we presents some of the necessary physics and models that have been used or developed to investigate some of the physical properties of semiflexible linear chains and their networks under cellular confinement or compression. It enable us to get the background about the possible conformations, structure and mechanical properties that semi-flexible linear biopolymer possess. This allows to get the best understanding of our modelling of networks of branching actin filaments.

1.2.4 Confinement of semiflexible polymers

Theoretical models and simulations for the study of the semiflexible polymers in confining region exist (see amongst other, references [1, 2, 40, 41, 54–57, 57]). Most of them are based on the computation of the free energy F of the system. In reference [40, 41, 56, 57, 57], analytical modelling of a semiflexible polymer under confinement using polymer scaling laws [52, 58] enabled to find the scaling forms of the confinement free energy. In strong confinement regime (meaning the persistence length of the of the chain larger or equal to the confining region size) the free energy indicates that the chain exhibits a bending regime. This behaviour is not observed when the chain is confined in the geometry with size larger than the persistence length of the chain, i.e in the weak confinement regime. The free energy in that case has the scaling form similar to the one of flexible chains. So, similarly to the flexible chains, the semiflexible chain under weak confinement is not really influenced by the effect that the confinement introduces.

The study of confined semiflexible polymers in references [1, 2] is rather based on the grand canonical equilibrium calculations of the average density distribution profiles of the chain segments inside the confining regions. The results that they have obtained indicate that the chain segments density is high in the vicinity of the confining region boundary, while low near the center. This enabled them to predict the effect of confinements on the conformation and structural properties of semiflexible filaments in confining geometries.

Monte Carlo computer simulations results have also shown similar behaviour and properties of the confined semiflexible chains at equilibrium thermodynamic [54, 59–61]. It is observed that, at high chain segment concentration, the confined chain exhibits some structural ordering [54, 55, 61–63]

1.2.4.1 Order parameter field

In order to quantify the spatial and orientational arrangement of semiflexible polymers, the polymer bond orientational order parameters are often defined and computed [41, 54, 57]. For example Liu *et al.* [54] defined a specific order parameters Q for the confined chain system in terms of the change in the orientation of the tangent vector $\boldsymbol{t}$ of the semiflexible polymer chain. They define it as:

$$Q = \left\langle \int \mathrm{d}s\, \boldsymbol{t}(s) \times \frac{\partial \boldsymbol{t}(s)}{\partial s} \right\rangle \tag{1.7}$$

Using these order parameters they find that when the semiflexible chain is subjected to strong confinement, the free energy of the system is dominated by the bending energy, and thus the chain bends and wraps around the confining region in order to minimize the free energy cost. For chains with no preferred bending orientation the order parameter Q is 0.

The models of the confined system we presented in the above are done in the canonical ensemble which represents the theoretical framework for a closed system energy with the heat bath. However, biological systems are open ones. They can thus exchange both energy and matter with their surroundings. So in our study we model the confined branching actin networks in the grand canonical ensemble. In the section that follows we introduce the grand canonical ensemble formalism and talk also discuss the advantages of modelling the confinement of semiflexible polymers (actin) or their networks in that ensemble.

1.2.5 Grand canonical ensemble and ensemble averages

Grand canonical ensemble has the properties of being at thermodynamic equilibrium. In fact, beside being at statistical equilibrium, thermal equilibrium and mechanical equilibrium which also are the properties of the canonical ensemble, the grand canonical ensemble also have the properties of chemical equilibrium. So any system of the grand canonical exchange energy and particles with the reservoir. This ensemble is thus convenient for the study of the cellular system which are said to be at equilibrium thermodynamics at macroscopic scale [64]. So modelling the polymer system in this ensemble enable to combine the macroscopic level or aspect of the system (thermodynamics) with its microscopic partner theory of equilibrium statistical mechanics. We wish to use it here because equilibrium calculations would be a first step, which

is also technically feasible. We know that living cells are definitely not in equilibrium not in equilibrium but our calculations provide a kind of prediction for long times or *in vitro* grown cytoskeleton, or dead cells. This can be a kind of basis for comparison from which one can explores nonequilibrium behaviour in the future.
The principal quantity in grand canonical ensemble is the grand canonical partition function $\mathfrak{Z}(\mu, V, T)$ defined as:

$$\mathfrak{Z}(\mu, V, T) = \sum_{N=0}^{\infty} (e^{\beta\mu})^N \mathcal{Z}_N. \tag{1.8}$$

where $\mathcal{Z}_N = \int e^{-\beta H(p,q)}$ is the canonical partition function of a system of polymer chains of N monomers, μ the chemical potential and (p, q) are the positional and orientational degrees of freedom of monomers in the system. We can redefine the grand canonical partition function as

$$\mathfrak{Z}(\mu, V, T) = \sum_{N=0}^{\infty} (z)^N \mathcal{Z}_N. \tag{1.9}$$

where $z = z_0 e^{\beta\mu}$ is the activity or fugacity of the monomer. The advantage of using the grand canonical formalism is that, one can define the monomer activity or fugacity z as an external field acting on the chain segments and inducing a geometrical confinement of the chain. This also induce inhomogeneities in the confined system and is compatible with the physical situation existing in the living cell, where there are actin filaments of various lengths and conformation. More details are in the next Chapter .
The termodynamics of the system is connected to the mechanical properties of the system through the equation of state given by

$$PV = k_B T \ln \mathfrak{Z}(\mu, V, T) \tag{1.10}$$

and through the the grand potential Γ defined as:

$$\Gamma = -k_B T \ln \mathfrak{Z}(\mu, V, T) \tag{1.11}$$

The average density of monomers in the confining region can also be calculated using the following definition

$$\langle \varrho \rangle = \frac{\partial \ln \mathfrak{Z}(\mu, V, T)}{\partial z} \tag{1.12}$$

In the presence of excluded volume effects between chain segment, it is difficult to compute the defined grand canonical partition. Self-consistent field theory is often used to make the problem more tractable.

1.2.6 Self-consistent field theory for polymer system (SCFT)

Generally used for many body system, the SCFT is applied to polymer system in order to coarse-grain it as a system consisting of one segment embedded inside an external or an auxiliary field, also called mean field, which can be seen as an average potential created by the rest of the

segments of the system. This is basically achieved by using either the Hubbard-Stratonovich transformation, or the delta-functional transformation, to convert the grand canonical partition function defined over the many degree of freedoms of the chain system into a functional integral representation over an auxiliary field function [65–68]. Next, using the mean field approximation [66, 67, 69], one can compute the grand partition function of the system. This theory is thus very useful for the study of confined inhomogeneous polymer systems at thermodynamic equilibrium.

1.3 Conclusion

In this chapter, we have broadly introduced and motivated the aim of our study of the mechanical properties of living tissues cells. We have defined some polymer physics concepts for the cells cytoskeleton, which is the machinery that is responsible in the cell mechanical properties. Stiffness is one of the key characteristic in the study of polymers filaments and their networks, whether synthetics or biological polymers. Polymers are classified to be flexible, semi-flexible or rigid according to their stiffness. The cytoskeletal filaments can fall within these three categories of chains. Intermediate filament are flexible i.e $\ell_{\mathrm{p}} \ll L$, actin filament are semiflexible meaning $\ell_{\mathrm{p}} \simeq L$ and microtubules are rigid, i.e $\ell_{lp}/L \gg 1$.
We are particularly interested in the properties of the confined semiflexible filaments because our aim is to investigate the spatial organization and orientational ordering and structural properties of actin networks under cellular confinement, and then see how these are coupled to the mechanical properties and stability of the cell.
We therefore looked at the existing models for confined semiflexible networks.

We found that, to introduce the confinement effect, one needs to define a third length length scale which is the size (diameter D in case of sphere) of the confining geometrical region, besides the contour length and the persistence length. Either the persistence length or the diameter can be varied in order to determine the change in the structure and conformational properties of the chains in comparison to their properties in the bulk or in their unconfined state.

For many models of confined polymers, the free energy of the chain system is calculated to predict the confinement effects on the filaments. Semiflexible linear polymers are subject to strong confinement effect when confined in region with size equal or smaller than their persistence length and they can adopt conformations different to the ones in bulk and they bend in order to minimize the free energy of the system.
The models we have discussed above are mainly about linear polymer chains. What about polymers chains that are not linear? We are also interested in the study of confined networks of semi-flexible filaments that present a tree-like structures.
It is proven that the stiffness of semiflexible polymers increase as the functionality of the filament increases [70]. Therefore, stiffness also depends on the structure and architecture of the polymer filament and we guess that the effect of confinement may also depend on the chains

architecture and structure. In eukaryotic living cell, actin filaments that compose the actin networks possess various structures and architectures. Filaments can be linear or branched. Experimental works have shown that the angular branching of actin have a strong impact on the elastic properties of actin networks [71]. So, does branched semiflexible polymer filaments and their networks behave differently under confinement, and does branching contributes to the stability of cell? To respond to these question, we aim to investigate the confinement effects on the spatial arrangement and ordering of filaments of branching actin networks at thermomodynamics equilibrium.

Outlines of the thesis

The outlines of the thesis are as follows:

Chapter 2

Here, we introduce in this chapter, the monomers grand ensemble formalism for confined semiflexible linear chain(s). We define a grand canonical partition function for confined chains and then derive their density and order parameter field distributions. We apply the formalism to linear actin filament under cellular confinement where the mutual interactions between chain segments are neglected. This is a variation or developement of an existing theoretical model [1, 2].

Chapter 3

Here we extend the monomers ensemble formalism to include the branching. We model branching tree-like actin networks confined in geometrical finite regions in the absence of mutual interactions between segments of the networks. We derive the expressions of the densities and order parameter field distributions for the confined branched networks. Non linear integral equations are used to express the density distributions. We present a numerical method which we use to compute these quantities. This chapter is completely new work for branching building upon the ideas of Chapter 2.

Chapter 4

In this chapter we present the results for various types of confined branching actin networks and we make a quantitative prediction of the effect of confinement on the structure, spatial organization and orientational ordering of branching cytoskeletal actin networks under cellular confinement. Both Chapter 4 and Chapter 5 are results for structure in confinement. These have not been obtained by similar methods, and not at all for branching.

Chapter 5

Here we confine the branching actin networks with excluded volume effects between networks segments. We use the self-consistent mean field approach to calculate the grand canonical partition function and then derive new expressions for the density distributions and order parameter. The density profiles are reported in non-linear integral equation which we compute numerically.

Chapter 6

In this chapter, we investigate the contribution of branching actin cytoskeletal networks under cellular confinement to the mechanical properties and stability of cells within living tissues. We also address questions on how the mechanical behaviour of cells is related to the structural and architectural properties of the confined branching actin networks. We have used our tools to examine mechanical properties. The properties are our own predictions, using comparison of free energies typically applied to polymer networks. This chapter is a small variation of the work by Cates and Edwards. It might need considerable further development by others.

Chapter 7

This chapter presents an alternative mean field approach to investigate the elastic properties of branching actin networks. We model the living cell and their branching cytoskeletal networks as an elastic composite material. The model is based on the linear theory of disordered fibre-reinforced composites developed by Cates and Edwards [72]. The effective Green function formalism is used to study some of the elastic properties of an elastic media star-like branched filaments are embedded.

Chapter 8

This chapter consist of the general summary of this thesis and then provides an outlooks for future works.

Appendix

The Appendix presents the details of the calculations we performed in this thesis.

Part II

Density field theory for confined branching cytoskeletal networks

Chapter 2

Introduction of monomer ensemble formalism for semiflexible linear polymer chains and confinement

2.1 Introduction

Semiflexible polymers are ubiquitous in nature and are often found in confined environments. Their conformations and structures in confined state can differ substentially from those of the bulk [14, 54, 55, 73, 74]. Examples of semiflexible polymers under confinement are biological macromolecules such as the actin filaments of the living eukaryotic cell cystoskeleton. The structual properties, spatial organization and ordering of actin networks inside the cell are greatly influenced by the cell membrane confinement effect [13]. So to investigate these properties, several models and approaches, experimental, computational and analytical tools have been developed to study their functions, conformation, structures, their dynamical and equilibrium properties in bulk and in confined state (amongst other, see[43, 53, 61, 75–77]).

Researchers in Biophysics use tools from statistical physics and develop methods for the study of their structural and physical properties. In the recent years, field theoretical techniques have been often and successfully used for theoretical modelling of semiflexible filaments and their networks [1, 53, 67, 69, 78, 79].

We are interested in the equilibrium properties of individual linear semiflexible filament and of their networks under confinement constraints. One of the theoretical approaches or techniques is the monomer ensemble formalism developed earlier by Frisch *et al.* [1] for non-interacting linear flexible chains. It is a field-like density functional theory used to study the behaviour of non-interacting semi-flexible linear polymer chains in equilibrium thermodynamics [2]. The statistical ensemble associated to the monomeric units of the chains is the grand canonical ensemble. Ordered monomers of the ensemble link together to form stiff polymer chains with

bonds oriented and localised in space.
When these polymer chains are confined inside a specific finite geometrical domain, the method allows to investigate the density distribution profiles of the linear chain segments and to calculate the degree of polymerisation or the number of these segments. As a consequence, this helps to make predictions on the conformation, the spatial organisation and on the structural and physical properties of semiflexible linear polymers filaments under the effect of confinement.
Most semiflexible filaments, such as actin filaments are polar or oriented. The rigid membrane or wall of the confining region may induce the orientational ordering of semiflexible chains and their networks. However previous calculations [1, 2] have not looked at the effect of confinement on the filament orientational ordering inside the confining region.
We introduce the monomer ensemble formalism in this chapter. We propose new analytical and numerical schemes for the calculation of the densities and number of chain segments in a confining region. We also propose an order parameter field in order to quantify the alignment of polymer chain(s) (segments) inside the confining region.
In the first section of this chapter, we define the grand canonical partition function for a single chain and for a composite of chains in the ensemble. We use the grand partition function to derive the expressions for the average density distribution functions in the second section. In the third section we introduce the idea of confinement of semiflexible polymers relevant for the study of composites of linear actin filaments under cellular confinement of the filaments. In the final section we define an order parameter field for the system.

2.2 Description of the model: Grand canonical partition function

We use a field theoretical monomer ensemble model to describe the formation and behaviour of linear semiflexible polymer chain(s) in thermodynamics equilibrium. The key is to define a grand canonical partition function for semiflexible chain(s) system.

We use a discrete description to present the mechanism of the semiflexible polymer chain(s) formation.
We consider a system of large number of monomers in equilibrium in the grand canonical representation. The ensemble is controlled by the activity of the monomers, also called the fugacity z. Monomers of the ensemble link one after the other linearly in an ordered manner through the fugacity z and form linear chain(s), see Figure 2.1. We treat the monomers of the polymer chain as physically having a length or size different to zero by characterizing them as the chain segments. So we mean the same thing when we say (number of) monomers of a polymer chain or (number of) bonds or segments of a polymer chain.

Each monomer or bond of a chain has two ends and each end has a local geometrical position $\boldsymbol{r}_i$ and orientation $\hat{\boldsymbol{n}}_i$ (it indicates the direction in which a monomer connect to its neighbour and form a bond) and they correspond to the degree of freedoms of the bond. The fugacity z of a bond or monomer is a function of all the degrees of freedom of the monomers which are $\boldsymbol{r}_i$ and $\hat{\boldsymbol{n}}_i$ the position and orientation of the starting end of a segment, and $\boldsymbol{r}'_i$ and $\hat{\boldsymbol{n}}'_i$ the position and orientation of the second end of a segment inside the chain, and is defined by:

$$z(\boldsymbol{r}_i, \hat{\boldsymbol{n}}_i, \boldsymbol{r}'_i, \hat{\boldsymbol{n}}'_i) = z_0 e^{(-\beta\varphi(\boldsymbol{r}_i, \hat{\boldsymbol{n}}_i, \boldsymbol{r}'_i, \hat{\boldsymbol{n}}'_i))}, \tag{2.1}$$

where z_0 is a constant and represent the degree of filament elongation, φ is a chemical potential field associated to each monomers in the system, $\beta = 1/k_{\mathrm{B}}T$ is the Boltzmann constant and i is any bond of the chain.
The filament growth factor or fugacity z acts as a local force field on each segment of the chain. It is enhanced by a propagator or a Green function $\mathcal{G}$.

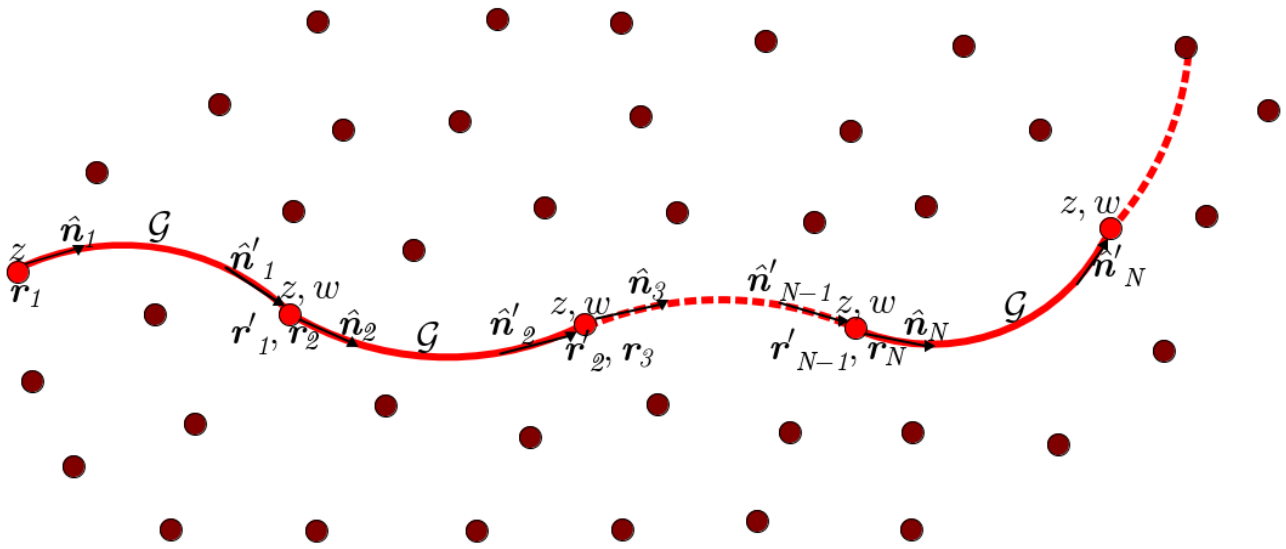

Figure 2.1: *Depiction of a grown semiflexible polymer chain of ordered monomers or bonds in the ensemble. The monomers or bonds that belongs to the chain are in red colour. Each monomer has two ends with the starting end starting at a position* $\boldsymbol{r}$ *and the other end at position* $\boldsymbol{r}'$ *and each end has an orientation* $\hat{\boldsymbol{n}}$*. $\mathcal{G}$ is the propagator or the Green function that characterises the segments of the chain as straight line of size ℓ and ensure that both ends of a segment have the same orientation. z is the monomer activity called fugacity and w is the Boltzmann weight factor associated to the pairwise bending stiffness between monomers of the chain. The red dots are the starting points of each monomer or bond of the chain and the dots in brown colour are the starting points of neighbours monomers.*

$\mathcal{G}$ is also a function of positions $\boldsymbol{r}$ and orientations $\hat{\boldsymbol{n}}$ of the ends of the segments of the chain and is given by:

$$\mathcal{G}(\boldsymbol{r}_i, \hat{\boldsymbol{n}}_i, \boldsymbol{r}'_i, \hat{\boldsymbol{n}}'_i) = \delta(\boldsymbol{r}'_i - (\boldsymbol{r}_i + \ell\hat{\boldsymbol{n}}_i))\delta(\hat{\boldsymbol{n}}_i - \hat{\boldsymbol{n}}'_i). \tag{2.2}$$

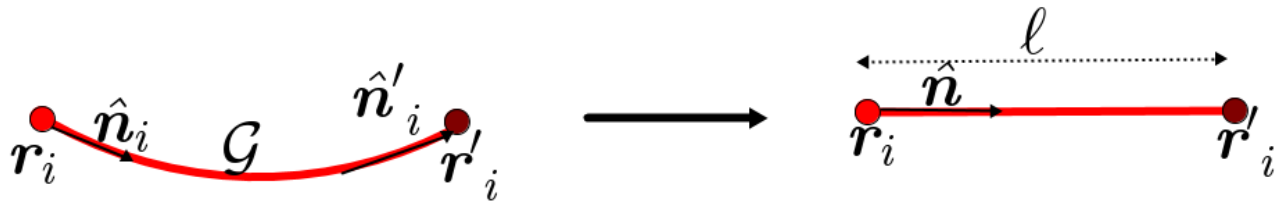

Figure 2.2: Visual depiction of the action of the propagator $\mathcal{G}$. $\mathcal{G}$ applies to each segment of the semiflexible chain and transform it into a straight segment of length ℓ ($\boldsymbol{r}'_i = \boldsymbol{r}_i + \ell\hat{\boldsymbol{n}}_i$) and orientation $\hat{\boldsymbol{n}} = \hat{\boldsymbol{n}}_i = \hat{\boldsymbol{n}}'_i$.

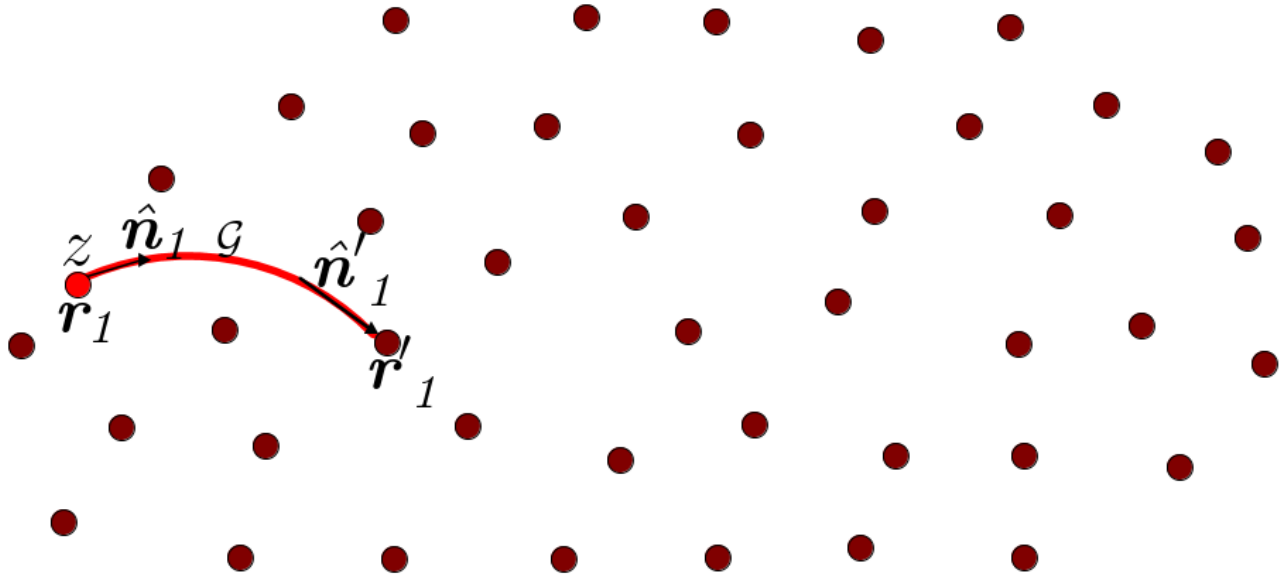

Figure 2.3: Depiction of a semiflexible chain of one bond. The monomer of the chain is in red colour. It has two ends with the starting end starting at a position $\boldsymbol{r}$ and the other end at position $\boldsymbol{r}'$ and each end has an orientation $\hat{\boldsymbol{n}}$. $\mathcal{G}$ is the propagator or the Green function that characterises the segments of the chain as straight line of size ℓ and ensure that both ends of a segment have the same orientation. z is the monomer activity called fugacity and w is the Boltzmann weight factor associated to the pairwise bending stiffness between monomers of the chain. The red dots are the starting points of each monomer or bond of the chain and the dots in brown colour are the starting points of neighbours monomers.

This propagator or Green function $\mathcal{G}$ allows to treat each segment of the chain as straight line of size ℓ and to ensure that both ends of a segment have the same orientation. We characterize the role of $\mathcal{G}$ in Figure 2.2.

The polymer chain segments exhibit a pairwise bond bending stiffness via a bending potential energy of Boltzmann weight factor w. It enable the chain to keep its semiflexibility. w is a function of the positions of the junction between any two adjacent bonds i and j of the chain and also a function of the orientations of the bonds. It is given by:

$$w(\boldsymbol{r}'_i, \hat{\boldsymbol{n}}'_i, \boldsymbol{r}_j, \hat{\boldsymbol{n}}_j) = w(\hat{\boldsymbol{n}}'_i, \hat{\boldsymbol{n}}_j)\delta(\boldsymbol{r}'_i - \boldsymbol{r}_j) \tag{2.3}$$

where

$$w(\hat{\boldsymbol{n}}'_i, \hat{\boldsymbol{n}}_j) = w_0 e^{-\beta \hat{\boldsymbol{n}}'_i \cdot \hat{\boldsymbol{n}}_j}. \tag{2.4}$$

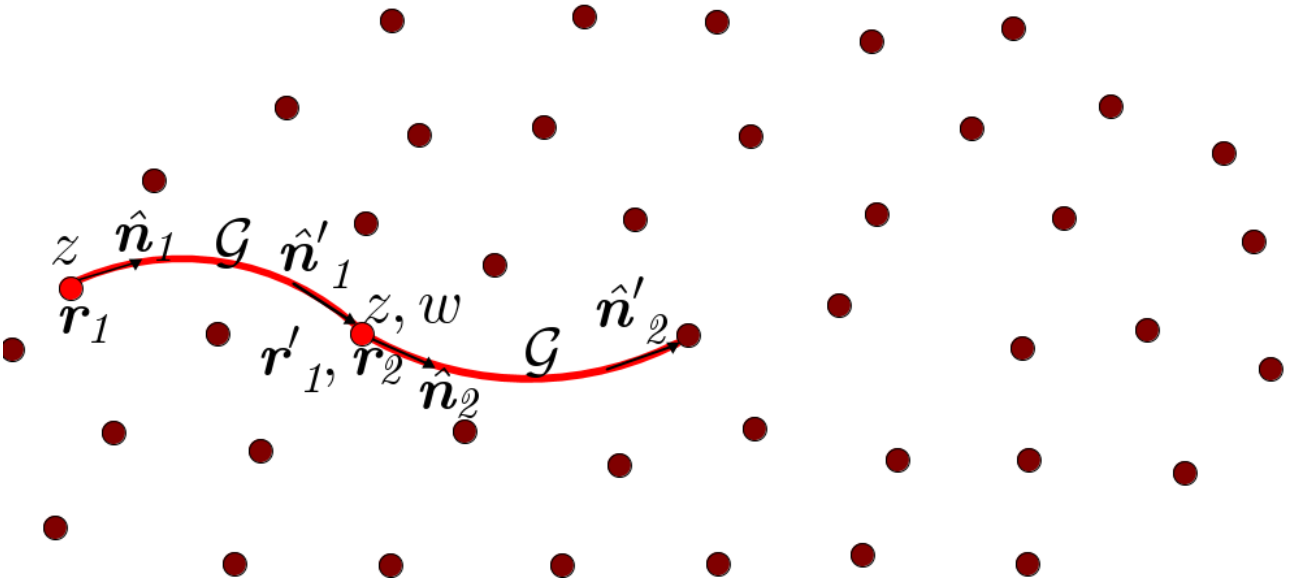

Figure 2.4: Depiction of a semiflexible chain of two bonds.

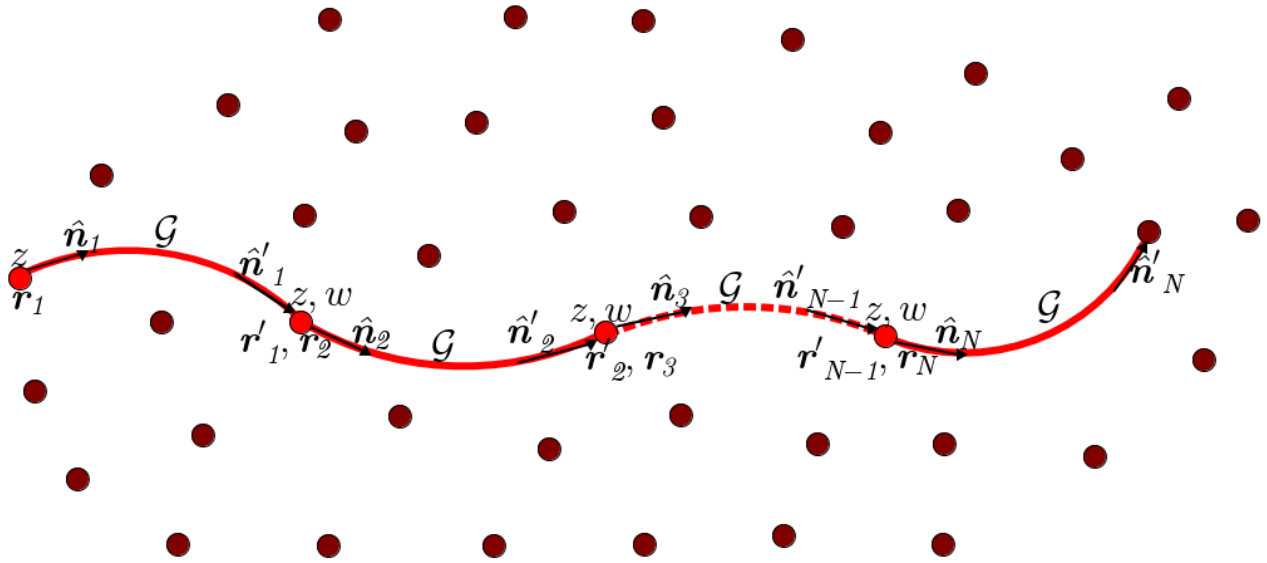

Figure 2.5: *Depiction of a semiflexible chain consisting of N bonds. The monomers or bonds that belongs to the chain are in red colour. Each monomer has two ends with the starting end starting at a position $\boldsymbol{r}$ and the other end at position $\boldsymbol{r}'$ and each end has an orientation $\hat{\boldsymbol{n}}$. $\mathcal{G}$ is the propagator or the Green function that characterises the segments of the chain as straight line of size ℓ and ensure that both ends of a segment have the same orientation. z is the monomer activity called fugacity and w is the Boltzmann weight factor associated to the pairwise bending stiffness between monomers of the chain. The red dots are the starting points of each monomer or bond of the chain and the dots in brown colour are the starting points of neighbours monomers.*

The factor $\delta(\boldsymbol{r}'_i - \boldsymbol{r}_j)$ ensures that the stiffness applies at the junction which is the point where the end of the adjacent segments of the chain meet.

The above presentation constitute the full discrete model that describe the growth of a semiflexible chain of infinite length of monomers (Figure 2.1) in thermal equilibrium. In this model,

the semiflexible polymer chain can grow, prune and then grow again under the activity z of the monomers. So, a grand canonical partition function for the single semiflexible polymer chain can be defined. We can also generalize this definition for a composite of large number of non-interacting semiflexible chains.

2.2.1 Single semiflexible linear chain

Our modelling is a simplified model of semiflexible polymer chain and the description is similar to an ideal freely jointed polymer chain because we neglect the excluded volume effect between monomers meaning that the monomers do not see each other or there is no mutual monomer interactions.

The segments or monomers of the chains can have variable orientations and positions. So the chains have variable configurations corresponding to the various possible lengths, positions and orientations that the polymer chain(s) can have.

The grand canonical partition function can be defined for the single semiflexible polymer chain of monomers at thermodynamic equilibrium. The grand partition function $\mathfrak{Z}$ of a single linear chain is thus a generating functional which is the sum of all possible conformation or configurations of the chain growing under the activity of the fugacity z.

For each configuration, all possible states of the chain are counted. It corresponds to the summation or to the integration over all possible positions and orientations (of the bonds) of the chain. For a good understanding of how we define the grand partition function for a single linear polymer chain, let us first present the mathematical representation of few configurations of the polymer chain and the corresponding partition functions. Figures 2.3, 2.4 and 2.5 show respectively, the chains of length one segment, 2 segments, and N segments.

First, we define the partition functions $\mathfrak{Z}_1$ for the chain of 1 segment, $\mathfrak{Z}_2$ for the chain of segments and $\mathfrak{Z}_N$ for the chain of N segments. The partition function of a chain of N monomers is the sum over all possible conformations i.e all possible positions and orientations of the chain and the partition function is the sum of all possible configurations of chains for N monomers. The partition function $\mathfrak{Z}_1$ is mathematically defined by:

$$\mathfrak{Z}_1 = \int\int \mathrm{d}^3\boldsymbol{r}_1\mathrm{d}^2\hat{\boldsymbol{n}}_1\mathrm{d}^3\boldsymbol{r}'_1\mathrm{d}^2\hat{\boldsymbol{n}}'_1 z(\boldsymbol{r}_1,\hat{\boldsymbol{n}}_1,\boldsymbol{r}'_1,\hat{\boldsymbol{n}}'_1)\mathcal{G}(\boldsymbol{r}_1,\hat{\boldsymbol{n}}_1,\boldsymbol{r}'_1,\hat{\boldsymbol{n}}'_1) \tag{2.5}$$

where each integral symbol is a short hand notation of multiple integrals over all degrees of freedom $(\hat{\boldsymbol{n}}, \boldsymbol{r})$ of the chain segments.

The partition function $\mathfrak{Z}_2$ of a chain of size two bonds is

$$\begin{aligned}\mathfrak{Z}_2 = \int\int\int\int \mathrm{d}^3\boldsymbol{r}_1\mathrm{d}^2\hat{\boldsymbol{n}}_1\mathrm{d}^3\boldsymbol{r}'_1\mathrm{d}^2\hat{\boldsymbol{n}}'_1\mathrm{d}^3\boldsymbol{r}_2\mathrm{d}^2\hat{\boldsymbol{n}}_2\mathrm{d}^3\boldsymbol{r}'_2\mathrm{d}^2\hat{\boldsymbol{n}}'_2 z(\boldsymbol{r}_1,\hat{\boldsymbol{n}}_1,\boldsymbol{r}'_1,\hat{\boldsymbol{n}}'_1)\mathcal{G}(\boldsymbol{r}_1,\hat{\boldsymbol{n}}_1,\boldsymbol{r}'_1,\hat{\boldsymbol{n}}'_1)\\ w(\boldsymbol{r}'_1,\hat{\boldsymbol{n}}'_1,\boldsymbol{r}_2,\hat{\boldsymbol{n}}_2)z(\boldsymbol{r}_2,\hat{\boldsymbol{n}}_2,\boldsymbol{r}'_2,\hat{\boldsymbol{n}}'_2)\mathcal{G}(\boldsymbol{r}_2,\hat{\boldsymbol{n}}_2,\boldsymbol{r}'_2,\hat{\boldsymbol{n}}'_2).\end{aligned} \tag{2.6}$$

The partition function $\mathfrak{Z}_N$ of a chain of size two bonds is

$$\begin{aligned}\mathfrak{Z}_N = \int\ldots\int \mathrm{d}^3\boldsymbol{r}_1\mathrm{d}^2\hat{\boldsymbol{n}}_1\boldsymbol{r}'_1\mathrm{d}^2\hat{\boldsymbol{n}}'_1\mathrm{d}^3\boldsymbol{r}_2\mathrm{d}^2\hat{\boldsymbol{n}}_2\mathrm{d}^3\boldsymbol{r}'_2\mathrm{d}^2\hat{\boldsymbol{n}}'_2\ldots\mathrm{d}^3\boldsymbol{r}_N\mathrm{d}^2\hat{\boldsymbol{n}}_N\boldsymbol{r}'_N\mathrm{d}^2\hat{\boldsymbol{n}}'_N\\ z(\boldsymbol{r}_1,\hat{\boldsymbol{n}}_1,\boldsymbol{r}'_1,\hat{\boldsymbol{n}}'_1)\mathcal{G}(\boldsymbol{r}_1,\hat{\boldsymbol{n}}_1,\boldsymbol{r}'_1,\hat{\boldsymbol{n}}'_1)w(\boldsymbol{r}'_1,\hat{\boldsymbol{n}}'_1,\boldsymbol{r}_2,\hat{\boldsymbol{n}}_2)z(\boldsymbol{r}_2,\hat{\boldsymbol{n}}_2,\boldsymbol{r}'_2,\hat{\boldsymbol{n}}'_2)\mathcal{G}(\boldsymbol{r}_2,\hat{\boldsymbol{n}}_2,\boldsymbol{r}'_2,\hat{\boldsymbol{n}}'_2)\\ \ldots z(\boldsymbol{r}_{N-1},\hat{\boldsymbol{n}}_{N-1},\boldsymbol{r}'_{N-1},\hat{\boldsymbol{n}}'_{N-1})\mathcal{G}(\boldsymbol{r}_{N-1},\hat{\boldsymbol{n}}_{N-1},\boldsymbol{r}'_{N-1},\hat{\boldsymbol{n}}'_{N-1})w(\boldsymbol{r}'_{N-1},\hat{\boldsymbol{n}}'_{N-1},\boldsymbol{r}_N,\hat{\boldsymbol{n}}_N)\\ z(\boldsymbol{r}_N,\hat{\boldsymbol{n}}_N,\boldsymbol{r}'_N,\hat{\boldsymbol{n}}'_N)\mathcal{G}(\boldsymbol{r}_N,\hat{\boldsymbol{n}}_N,\boldsymbol{r}'_N,\hat{\boldsymbol{n}}'_N)\end{aligned} \tag{2.7}$$

Replacing the equations (2.1), (2.2), (2.3) in (2.7) and integrating, we get:

$$\begin{aligned}\mathfrak{Z}_N = \int\ldots\int \mathrm{d}^3\boldsymbol{r}_1\mathrm{d}^2\hat{\boldsymbol{n}}_1\mathrm{d}^3\boldsymbol{r}_2\mathrm{d}^2\hat{\boldsymbol{n}}_2\ldots\mathrm{d}^3\boldsymbol{r}_N\mathrm{d}^2\hat{\boldsymbol{n}}_N z(\boldsymbol{r}_1,\hat{\boldsymbol{n}}_1)w_1(\hat{\boldsymbol{n}}_1,\hat{\boldsymbol{n}}_2)z(\boldsymbol{r}_2,\hat{\boldsymbol{n}}_2)\\ \ldots w(\hat{\boldsymbol{n}}_{N-1},\hat{\boldsymbol{n}}_N)z(\boldsymbol{r}_N,\hat{\boldsymbol{n}}_N)\end{aligned} \tag{2.8}$$

where

$$z(\boldsymbol{r}_i,\hat{\boldsymbol{n}}_i) = z_0 e^{(-\beta\varphi(\boldsymbol{r}_i,\hat{\boldsymbol{n}}_i,\boldsymbol{r}_i+\ell\hat{\boldsymbol{n}}_i,\hat{\boldsymbol{n}}_i))} \tag{2.9}$$

The grand canonical partition function $\mathfrak{Z}$ of a single semiflexible polymer filament is then the sum of the partition funtions of all possible chains or confugarations of chain that can be formed in the limit of N going to infinity. In other words:

$$\mathfrak{Z} = 1 + \sum_{N=1}^{\infty}\mathfrak{Z}_N \tag{2.10}$$

Where $1 = \mathfrak{Z}_0$.

We rewrite $\mathfrak{Z}$ in full as

$$\begin{aligned}\mathfrak{Z} = 1 + \sum_{N=1}^{\infty}\int\ldots\int \mathrm{d}^3\boldsymbol{r}_1\mathrm{d}^2\hat{\boldsymbol{n}}_1\mathrm{d}^3\boldsymbol{r}_2\mathrm{d}^2\hat{\boldsymbol{n}}_2\ldots\mathrm{d}^3\boldsymbol{r}_N\mathrm{d}^2\hat{\boldsymbol{n}}_N\, z(\boldsymbol{r}_1)z(\boldsymbol{r}_1,\hat{\boldsymbol{n}}_1)w(\hat{\boldsymbol{n}}_1,\hat{\boldsymbol{n}}_2)\\ z(\boldsymbol{r}_2,\hat{\boldsymbol{n}}_2)\ldots w(\hat{\boldsymbol{n}}_{N-1},\hat{\boldsymbol{n}}_N)z(\boldsymbol{r}_N,\hat{\boldsymbol{n}}_N).\end{aligned} \tag{2.11}$$

We rewrite the expansion of w and z as vectors over the positions eigenstates as:

$$z(\boldsymbol{r},\hat{\boldsymbol{n}}) = \langle\boldsymbol{r},\hat{\boldsymbol{n}}|z|\boldsymbol{r},\hat{\boldsymbol{n}}\rangle \tag{2.12}$$

where $\boldsymbol{r}$ and $\hat{\boldsymbol{n}}$ are the positions and orientations of polymer chain segments or monomers.

We also write

$$w(\hat{\boldsymbol{n}}, \hat{\boldsymbol{n}}') = \langle \boldsymbol{r}, \hat{\boldsymbol{n}} | w\delta(\boldsymbol{r}, \boldsymbol{r}') | \boldsymbol{r}', \hat{\boldsymbol{n}}' \rangle \tag{2.13}$$

Following Frisch and Percus formulation [1], we rewrite the grand canonical partition function $\mathfrak{Z}$ as:

$$\begin{aligned} \mathfrak{Z} = 1 + \sum_{N=1}^{\infty} \int \dots \int \mathrm{d}^3\boldsymbol{r}_1 \mathrm{d}^2\hat{\boldsymbol{n}}_1 \mathrm{d}^3\boldsymbol{r}_2 \mathrm{d}^2\hat{\boldsymbol{n}}_2 \dots \mathrm{d}^3\boldsymbol{r}_N \mathrm{d}^2\hat{\boldsymbol{n}}_N \langle \boldsymbol{r}_1, \hat{\boldsymbol{n}}_1 | z | \boldsymbol{r}_1, \hat{\boldsymbol{n}}_1 \rangle \\ \langle \boldsymbol{r}_1, \hat{\boldsymbol{n}}_1 | w\delta(\boldsymbol{r}_1, \boldsymbol{r}_2) | \boldsymbol{r}_2, \hat{\boldsymbol{n}}_2 \rangle \langle \boldsymbol{r}_2, \hat{\boldsymbol{n}}_2 | z | \boldsymbol{r}_2, \hat{\boldsymbol{n}}_2 \rangle \dots \langle \boldsymbol{r}_{N-1}, \hat{\boldsymbol{n}}_{N-1} | z | \boldsymbol{r}_{N-1}, \hat{\boldsymbol{n}}_{N-1} \rangle \\ \langle \boldsymbol{r}_{N-1}, \hat{\boldsymbol{n}}_{N-1} | w\delta(\boldsymbol{r}_{N-1}, \boldsymbol{r}_N) | \boldsymbol{r}_N, \hat{\boldsymbol{n}}_N \rangle \langle \boldsymbol{r}_N, \hat{\boldsymbol{n}}_N | z | \boldsymbol{r}_N, \hat{\boldsymbol{n}}_N \rangle. \end{aligned} \tag{2.14}$$

The integration over all spatial locations and orientations is $|\boldsymbol{I}\rangle$ i.e:

$$\int \mathrm{d}^3\boldsymbol{r} \mathrm{d}^2\hat{\boldsymbol{n}} \, |\boldsymbol{r}, \hat{\boldsymbol{n}}\rangle \langle \boldsymbol{r}, \hat{\boldsymbol{n}}| = |\boldsymbol{I}\rangle \tag{2.15}$$

and

$$\sum_{\boldsymbol{r}, \hat{\boldsymbol{n}}} |\boldsymbol{r}, \hat{\boldsymbol{n}}\rangle = |\mathbf{1}\rangle \tag{2.16}$$

Thus after integration, we obtain:

$$\mathfrak{Z} = 1 + \sum_{N=1}^{\infty} \langle \mathbf{1} | z(wz)^{N-1} | \mathbf{1} \rangle. \tag{2.17}$$

We have a geometric sum and we average it over the total number of the monomers composing the linear chain and get:

$$\mathfrak{Z} = 1 + \langle \mathbf{1} | z(\boldsymbol{I} - wz)^{-1} | \mathbf{1} \rangle. \tag{2.18}$$

Where $\boldsymbol{I}$ is the identity matrix.

We are now going to define the grand canonical partition function for a system of non-interacting semi-flexible chains composite in an infinitely large system .

2.2.2 System of many noninteracting linear semiflexible polymer chains

To determine the grand canonical partition function of a composite system of semiflexible filaments, we consider that each single polymer filament is part of an ensemble of noninteracting linear polymers chains (in an infinitely large enclosure) whose density per unit length of the

system is controlled by an artificial polymer activity ς [1]. The grand canonical partition function $\mathfrak{Z}_T$ of the composite of linear semiflexible polymer filaments is given by:

$$\mathfrak{Z}_T = e^{\varsigma \mathfrak{Z}}, \tag{2.19}$$

where ς is the fugacity of each polymer of the composite and $\mathfrak{Z}$ the grand canonical partition function for a single chain. The grand partition function is obtained in terms of an exponential series due to the fact that the chains do not interact. They do not see each other meaning they are identical and one can switch them around.
The grand canonical partition functions for the composite of semiflexible linear polymer chains serves as a generating function for thermal averages. In the next section we define and derive the expression for the mean number of confined polymer chains, the average density distributions of the chain segments and the number-average degree of polymerization.

2.3 Average numbers and average density distribution functions

Here we introduce the definitions and derive the expressions for different quantities for average numbers and densities of chains and their bonds which we compute at later stage of this thesis.

2.3.1 Average number of chains

The average number of semiflexible polymer chains N_{chains} confined in a finite geometrical region is given by:

$$N_{\text{chains}} = \frac{\varsigma}{\mathfrak{Z}_T}\frac{\partial \mathfrak{Z}_T}{\partial \varsigma} = \varsigma \mathfrak{Z} \tag{2.20}$$

In the following we calculate the average density distribution of filament segments inside the confining region.

2.3.2 Average density of chain segments of the composite

The average density distribution of chain segments of a composite of semiflexible chains is given by the following general definition of mean density in the grand canonical ensemble:

$$\varrho(\boldsymbol{r}, \hat{\boldsymbol{n}}) = \frac{z(\boldsymbol{r}, \hat{\boldsymbol{n}})}{\mathfrak{Z}_T}\frac{\delta \mathfrak{Z}_T}{\delta z(\boldsymbol{r}, \hat{\boldsymbol{n}})}, \tag{2.21}$$

a functional of the activity of the chain bonds or fugacity $z(\boldsymbol{r}, \hat{\boldsymbol{n}})$ and its expression is obtained by calculating the functional derivative of the grand canonical partition function $\mathfrak{Z}_T$.

Since there is no interactions between the polymer chains, the average density of segments of the composite (equation 2.17) is the same as multiplying the fugacity ς of each chain to the average density of segments of a single chain $\varrho_s(\boldsymbol{r}, \hat{\boldsymbol{n}})$:

$$\varrho(\boldsymbol{r},\hat{\boldsymbol{n}}) = \varsigma\varrho_s(\boldsymbol{r},\hat{\boldsymbol{n}}) \tag{2.22}$$

where $\varrho_s(\boldsymbol{r},\hat{\boldsymbol{n}})$ is given by

$$\varrho_s(\boldsymbol{r},\hat{\boldsymbol{n}}) = \frac{z(\boldsymbol{r},\hat{\boldsymbol{n}})}{\mathfrak{Z}}\frac{\delta\mathfrak{Z}}{\delta z(\boldsymbol{r},\hat{\boldsymbol{n}})}. \tag{2.23}$$

To obtain the expressions for the densities we need to do the functional derivation of $\mathfrak{Z}$. We calculate the functional derivative of $\mathfrak{Z}$ (equation 2.11) by using the definitions of functional derivation given in Appendix Section A.1. We obtain the expression of $\varrho_s(\boldsymbol{r},\hat{\boldsymbol{n}})$ to be

$$\varrho(\boldsymbol{r},\hat{\boldsymbol{n}}) = \frac{z(\boldsymbol{r},\hat{\boldsymbol{n}})}{\mathfrak{Z}}\Phi(\boldsymbol{r},\hat{\boldsymbol{n}})\Psi(\boldsymbol{r},\hat{\boldsymbol{n}}). \tag{2.24}$$

Where

$$\begin{cases} \Psi(\boldsymbol{r},\hat{\boldsymbol{n}}) = \langle \boldsymbol{r},\hat{\boldsymbol{n}}|(\boldsymbol{I}-wz)^{-1}|\mathbf{1}\rangle \\ \Phi(\boldsymbol{r},\hat{\boldsymbol{n}}) = \langle \mathbf{1}|(\boldsymbol{I}-zw)^{-1}|\boldsymbol{r},\hat{\boldsymbol{n}}\rangle \end{cases}. \tag{2.25}$$

$\Phi(\boldsymbol{r},\hat{\boldsymbol{n}})\Psi(\boldsymbol{r},\hat{\boldsymbol{n}})$ represents the probability of having on average a chain bond or segment ate position $\boldsymbol{r}$ and orientation $\hat{\boldsymbol{n}}$. We distinguish the difference between Ψ and Φ due to the fact that the filaments are oriented and that filament can grow starting from the root (a root in graph theory means the starting point or node of a tree) or starting from the leave (the leave is the end node of a tree). In fact zw is not equal to wz due to the orientation of the filaments.

Ψ and Φ represent quantities associated to the average density distributions and are used for the construction of all possible configurations of the filaments of the networks. The integration of the quantity $z(\boldsymbol{r},\hat{\boldsymbol{n}})\Psi(\boldsymbol{r},\hat{\boldsymbol{n}})$ or $z(\boldsymbol{r},\hat{\boldsymbol{n}})\Phi(\boldsymbol{r},\hat{\boldsymbol{n}})$ over all possible monomer or bonds locations $\boldsymbol{r}$ and orientations $\hat{\boldsymbol{n}}$, gives us the same expression of the grand canonical partition function as the one we have obtained in equation (2.13). So we can expressed the grand partition function as linear function of $\Psi(\boldsymbol{r},\hat{\boldsymbol{n}})$ or $\Phi(\boldsymbol{r},\hat{\boldsymbol{n}})$ as:

$$\mathfrak{Z} = 1 + \int_{\boldsymbol{r},\hat{\boldsymbol{n}}} \mathrm{d}^3\boldsymbol{r}\mathrm{d}^2\hat{\boldsymbol{n}}\, z(\boldsymbol{r},\hat{\boldsymbol{n}})\Psi(\boldsymbol{r},\hat{\boldsymbol{n}}). \tag{2.26}$$

or

$$\mathfrak{Z} = 1 + \int_{\boldsymbol{r},\hat{\boldsymbol{n}}} \mathrm{d}^3\boldsymbol{r}\mathrm{d}^2\hat{\boldsymbol{n}}\, z(\boldsymbol{r},\hat{\boldsymbol{n}})\Phi(\boldsymbol{r},\hat{\boldsymbol{n}}) \tag{2.27}$$

The compution of the grand canonical partition functions and the densities are thus dependent on Ψ and Φ values. So we need to find an appropriate way to interpret and calculate the quantities Ψ and Φ given by equations (2.21).

2.3.3 (Resulting) Integral equation form of Ψ and Φ

An easy way to understand how to compute the functional Ψ and Φ is to convert Ψ and Φ into functional integral equations. We obtain the integral form for Ψ and Φ using the following algebraic definition:

$$\boldsymbol{A}\boldsymbol{A}^{-1} = \boldsymbol{I}. \tag{2.28}$$

Where A is an invertible matrix. $(\boldsymbol{I} - wz)$ is a positive definite matrix, so:

$$\begin{aligned} \sum_{\boldsymbol{r}',\hat{\boldsymbol{n}}'} \langle \boldsymbol{r}, \hat{\boldsymbol{n}} | (\boldsymbol{I} - wz) | \boldsymbol{r}', \hat{\boldsymbol{n}}' \rangle \langle \boldsymbol{r}', \hat{\boldsymbol{n}}' | (\boldsymbol{I} - wz)^{-1} | \boldsymbol{r}'', \hat{\boldsymbol{n}}'' \rangle &= \langle \boldsymbol{r}, \hat{\boldsymbol{n}} | \boldsymbol{r}'', \hat{\boldsymbol{n}}'' \rangle \\ &= \delta(\boldsymbol{r} - \boldsymbol{r}'') \delta(\hat{\boldsymbol{n}} - \hat{\boldsymbol{n}}'') \\ &= \boldsymbol{I}. \end{aligned} \tag{2.29}$$

Similarly using Ψ in equation 2.25, we write:

$$\begin{aligned} \sum_{\boldsymbol{r},\hat{\boldsymbol{n}}} \langle \boldsymbol{r}', \hat{\boldsymbol{n}}' | (\boldsymbol{I} - wz) | \boldsymbol{r}, \hat{\boldsymbol{n}} \rangle \Psi(\boldsymbol{r}, \hat{\boldsymbol{n}}) &= \sum_{\boldsymbol{r},\hat{\boldsymbol{n}}} \langle \boldsymbol{r}', \hat{\boldsymbol{n}}' | (\boldsymbol{I} - wz) | \boldsymbol{r}, \hat{\boldsymbol{n}} \rangle \langle \boldsymbol{r}, \hat{\boldsymbol{n}} | (\boldsymbol{I} - wz) | \mathbf{1} \rangle \\ &= \langle \boldsymbol{r}', \hat{\boldsymbol{n}}' | \mathbf{1} \rangle \\ &= \mathbf{1}. \end{aligned}$$

equivalent to the integral form

$$\int_{\boldsymbol{r},\hat{\boldsymbol{n}}} \mathrm{d}^3\boldsymbol{r}\mathrm{d}^2\hat{\boldsymbol{n}} \langle \boldsymbol{r}', \hat{\boldsymbol{n}}' | (\boldsymbol{I} - wz) | \boldsymbol{r}, \hat{\boldsymbol{n}} \rangle \Psi(\boldsymbol{r}, \hat{\boldsymbol{n}}) = \langle \boldsymbol{r}', \hat{\boldsymbol{n}}' | \mathbf{1} \rangle = 1 \tag{2.30}$$

We then have Ψ in term of linear integral equation as:

$$\Psi(\boldsymbol{r}, \hat{\boldsymbol{n}}) = 1 + \int_{\boldsymbol{r}',\hat{\boldsymbol{n}}'} \mathrm{d}^3\boldsymbol{r}'\mathrm{d}^2\hat{\boldsymbol{n}}' w(\hat{\boldsymbol{n}}, \hat{\boldsymbol{n}}') z(\boldsymbol{r}, \hat{\boldsymbol{n}}') \Psi(\boldsymbol{r}, \hat{\boldsymbol{n}}') \tag{2.31}$$

Similarly we obtain the integral equation deriving from Φ as:

$$\Phi(\boldsymbol{r}, \hat{\boldsymbol{n}}) = 1 + \int_{\boldsymbol{r}',\hat{\boldsymbol{n}}'} \mathrm{d}^3\boldsymbol{r}'\mathrm{d}^2\hat{\boldsymbol{n}}' \tilde{z}(\boldsymbol{r}, \hat{\boldsymbol{n}}') w(\hat{\boldsymbol{n}}, \hat{\boldsymbol{n}}') \Phi(\boldsymbol{r}, \hat{\boldsymbol{n}}') \tag{2.32}$$

For a segment to form, the activity z in the expression of Ψ acts in the orientation n while $\tilde{z}$ in the expression of Φ acts in the opposite orientation $\hat{\boldsymbol{n}}' = -\hat{\boldsymbol{n}}$. That is why we put the difference between the two activities by naming the activity in the expression of Ψ, z and the activity in Φ, $\tilde{z}$. We can rewrite Ψ and Φ in shorthand notation as:

$$\Psi = 1 + wz\Psi \tag{2.33}$$

and

$$\Phi = 1 + \tilde{z}w\Phi \tag{2.34}$$

We can represent the equations for Ψ and Φ diagrammatically as:

Figure 2.6: *Diagram for linear Ψ function. The cross circles on this diagram are the roots of the chains and we do not integrate over the position and oriention of the root. It indicates that a filament can grow starting from the root. We distinguish the root from the leave due to the fact that filaments are oriented.*

and

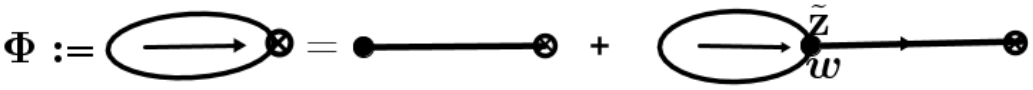

Figure 2.7: *Diagram for linear Φ function. The cross circles on this diagram are the leaves of the chains and we do not integrate over the position and oriention of the leaves. It indicates that a filament can grow starting from the the leave.*

Expansion of equations (2.33) or (2.34) leads to a linear series in Ψ or Φ. We recursively replace the expression for Ψ in its expressions and get a series expansion as

$$\Psi = 1 + wz + wzwz + wzwzwz + \ldots + wzwzwzwz \ldots wz\Psi \tag{2.35}$$

In the same way we write Φ as a linear series

$$\Phi = 1 + zw + zwzw + zwzwzw + \ldots + zwzwzw \ldots zw\Phi \tag{2.36}$$

Or diagrammatically as:

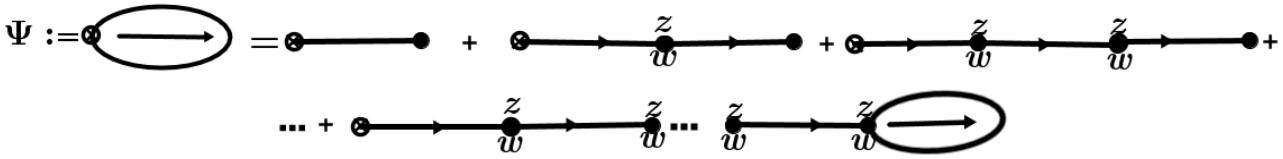

We can easily solve numerically for Ψ and Φ for a given fugacity z acting on each segment of the chains and for a given Boltzmann weight w that links the segments into linear chains.

We are interested to investigate the behaviour and properties of semiflexible cytoskeletal filaments under the effect of confinement from the cell membrane. For that, we define the fugacity z as an external potential that is induced by the confinement of the polymer chains. We also define a specific Boltzmann factor w such that its embed the bending stiffness between the chain segments.

2.4 Confinement

The fugacity z and the weight factor w are the most important parameters of the system that we need to define in order to compute for Ψ and Φ. Specifically, a finite chemical potential field (action of the field restricted to a field) is require in order to ensure the confinement of the polymer chains in a finite geometry and then compute the grand canonical partition functions, the average densities and numbers and also of chain segments inside the confining region. The persistence length of the polymer chains is also required and is the length which enable to scale the system under study. We express it in term of the bending energetics and compare it with the size of the confining region.

2.4.1 Confining field and bending stiffness

The action of the external potential field or fugacity z is caused by the confinement of filaments and the field acts only on segments of chains that form inside the confined domain. We define it as:

$$\varphi(\boldsymbol{r},\hat{\boldsymbol{n}},\boldsymbol{r}+\ell\hat{\boldsymbol{n}},\hat{\boldsymbol{n}}) = \begin{cases} 0, & \text{if } \boldsymbol{r}\in\mathbb{L} \quad \text{and } \boldsymbol{r}+\ell\hat{\boldsymbol{n}}\in\mathbb{L} \\ \infty, & \text{otherwise} \end{cases} \tag{2.37}$$

So we have

$$z(\boldsymbol{r},\hat{\boldsymbol{n}}) = z_0\theta(\boldsymbol{r},\hat{\boldsymbol{n}}) \tag{2.38}$$

for the calculation of Ψ and

$$\tilde{z}(\boldsymbol{r},\hat{\boldsymbol{n}}) = z_0\theta(\boldsymbol{r},-\hat{\boldsymbol{n}}) \tag{2.39}$$

for the calculation of Φ, where we define

$$\theta(\boldsymbol{r},\hat{\boldsymbol{n}}) = \begin{cases} 1, & \text{if } \boldsymbol{r}\in\mathbb{L} \text{ and } \boldsymbol{r}+\ell\hat{\boldsymbol{n}}\in\mathbb{L} \\ 0, & \text{otherwise} \end{cases} \tag{2.40}$$

$\mathbb{L}$ represents the confining region and ℓ the chain segment or bond length.
This external field (fugacity) serves as the boundary condition required for the chain segment to be inside the confining region. So, the external field φ or the fugacity z controls or defines the geometry of the confining regions the field.

In chapter 5 of this thesis, we show result for the semiflexible chains confined in various geometries of cell including spherical, square (2d) or cubic (3d), rectangular and triangular shape. Modelling the confinement of chains in various geometry allows us to see, how the structure and physical properties of the chains are related to the confining cell geometry.

We appropriately redefine the weight w associated to the bending energy or stiffness between adjacent bonds (recall that we treat the monomer of the confined chain as bonds or segments) by normalizing it. We have:

$$w(\hat{\boldsymbol{n}}, \hat{\boldsymbol{n}}') = \frac{w_0}{\mathcal{N}_w} e^{\beta\epsilon\hat{\boldsymbol{n}}\cdot\hat{\boldsymbol{n}}'}. \tag{2.41}$$

where

$$\mathcal{N}_w = \sum_{\hat{\boldsymbol{n}}'} w(\hat{\boldsymbol{n}}, \hat{\boldsymbol{n}}') \tag{2.42}$$

$\mathcal{N}_w$ is used to normalize the weight factor w_0. In fact we use this normalization factor for numerical purpose. It helps to keep the volume of the defined confining region finite.
ϵ is the bending constant or the bending modulus and is related to the persistence lengths of the confined chains.

2.4.2 Persistence length

The persistence length is defined as the length at which a vector drawn tangent to the polymer chain is no longer correlated in space with any tangent vector of the polymer [80]. It is the characteristic measure used to quantify the stiffness of a semiflexible polymer chain. In the thermodynamic, limit the persistence lengths describe how well the position of one section of a polymer is correlated to another section in the thermodynamic limit [81]. Beyond this length the semiflexible polymer chain loses its thermal properties.
In our model, the persistence length couples the polymer chains stiffness to the system length scales such as the size of the the confining domain.

So we aim here to express the persistence length of an unconfined chains in terms of the bending energy or bending stiffness between the bonds of the polymer chain and then compare it with the size of the semiflexible chain confining region.

We consider a discrete semiflexible polymer chain Fig 2.8 living on triangular lattice where the monomers or bonds of the chains occupy the bonds of the lattice. We wish to calculate the persistence length of the very long chain at thermodynamic equilibrium.

The persistence length is related to the correlation between the first bond or tangent vector and the last bond vector of the chain. We first consider the portion of the chain that is in the domain $[a, a+N]$ and we calculate the correlation function $\langle \boldsymbol{t}_a \cdot \boldsymbol{t}_{N+a} \rangle$ between the chain end segments. We use the weight factor given by equation (2.36) associated to the bending stiffness between the chain bonds to define the partition function for the single chain system. However

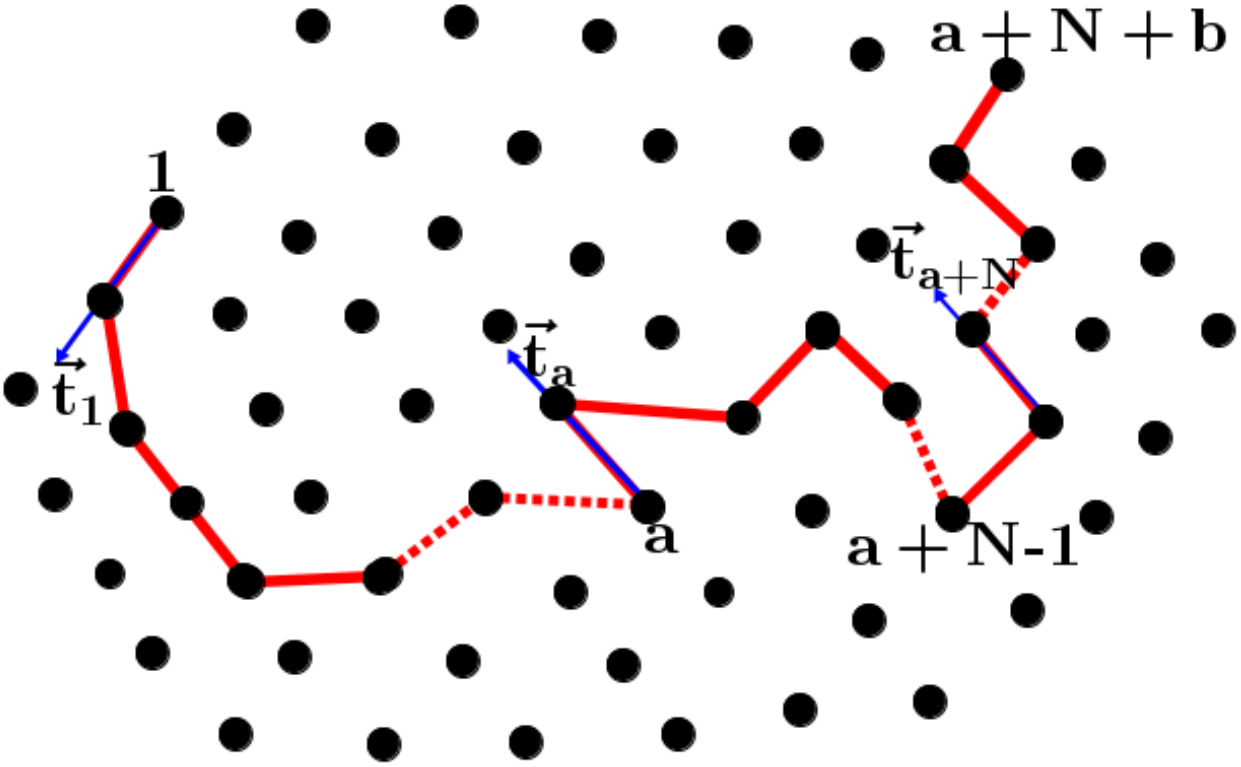

Figure 2.8: A very long semiflexible polymer chain discretized like a freely jointed chain on a 2D triangular lattice. The black dots represent the monomers (bonds) positions and the red segments along vectors $\boldsymbol{t}$ represente the monomers orientations

we express it here in term of the tangent vectors which have the same meaning as the unit vector $\hat{\boldsymbol{n}}$ that we have used so far.

The Boltzmann weight is given by:

$$w(i, i+1) = e^{c\boldsymbol{t}_i \cdot \boldsymbol{t}_{i+1}}. \tag{2.43}$$

we define the partition function $\mathcal{Z}$ of the full polymer chain of $M = a + b + N$ monomers. The partition function is given by:

$$\mathcal{Z} = \sum_{\boldsymbol{t}_i} \prod_{i=1}^{M-1} w(i, i+1). \tag{2.44}$$

and the correlation quantity between the tangent vector $\boldsymbol{t}_a$ and $\boldsymbol{t}_{N+a}$ is

$$\langle \boldsymbol{t}_a \cdot \boldsymbol{t}_{N+a} \rangle = \frac{1}{\mathcal{Z}} \sum_{\boldsymbol{t}_i} \boldsymbol{t}_a \cdot \boldsymbol{t}_{N+a} \prod_{i=1}^{M-1} w(i, i+1). \tag{2.45}$$

We use the transfer matrix formalism [82] to express the partition so that we can compute the correlation between the tangent vectors.

As the transfer matrix defined in the case of one dimensional Potts model is associated to the

different states of the spin in one dimension, we define the transfer matrix of the polymer chain of N monomers following the orientations of the bonds of the chain on a lattice. Then we calculate the persistence length of the polymer chain in the thermodynamic limit ($N \longrightarrow \infty$). We do the calculations for a polymer chain that is living on a two dimensional (2d) triangular lattice (six possible directions) and on a three dimensional (3d) lattice (twelve possible directions).

So depending on the defined lattice, there exist a transfer matrix $\mathbb{T}$ such that:

$$w(i, i+1) = \langle \boldsymbol{t}_i | \mathbb{T} | \boldsymbol{t}_{i+1} \rangle. \tag{2.46}$$

and

$$\prod_{i=1}^{N-1} w(i, i+1) = \langle \boldsymbol{t}_1 | \mathbb{T} | \boldsymbol{t}_2 \rangle \langle \boldsymbol{t}_2 | \mathbb{T} | \boldsymbol{t}_3 \rangle \cdots \langle \boldsymbol{t}_{N-1} | \mathbb{T} | \boldsymbol{t}_N \rangle. \tag{2.47}$$

So

$$\mathcal{Z} = \sum_{t_1, t_M} \langle \boldsymbol{t}_1 | \mathbb{T}^{M-1} | \boldsymbol{t}_M \rangle. \tag{2.48}$$

To calculate the sum defined above, we define the following set of vectors

$$\begin{aligned} m = \{&(1,0,0,0,0,0), (0,1,0,0,0,0), (0,0,1,0,0,0), \\ &(0,0,0,1,0,0), (0,0,0,0,1,0), (0,0,0,0,0,1)\}. \end{aligned} \tag{2.49}$$

corresponding to the possible directions for each bonds or tangent vectors on the lattice (here the 2D triangular lattice) $\boldsymbol{t}_i = \{\hat{x}, -\hat{x}, \hat{y}, -\hat{y}, \hat{v}, -\hat{v}\}$.
Thus

$$\mathcal{Z} = \sum_{m, m'=1}^{4} \langle m | \mathbb{T}^{M-1} | m' \rangle. \tag{2.50}$$

In 2d triangular lattice, the transfer matrix is given by:

$$\mathbb{T} = \begin{pmatrix} e^{\epsilon} & e^{-\epsilon} & e^{0.5\epsilon} & e^{-0.5\epsilon} & e^{-0.5\epsilon} & e^{0.5\epsilon} \\ e^{-\epsilon} & e^{\epsilon} & e^{-0.5\epsilon} & e^{0.5\epsilon} & e^{0.5\epsilon} & e^{-0.5\epsilon} \\ e^{0.5\epsilon} & e^{-0.5\epsilon} & e^{\epsilon} & e^{-\epsilon} & e^{0.5\epsilon} & e^{-0.5\epsilon} \\ e^{-0.5\epsilon} & e^{0.5\epsilon} & e^{-\epsilon} & e^{\epsilon} & e^{-0.5\epsilon} & e^{0.5\epsilon} \\ e^{-0.5\epsilon} & e^{0.5\epsilon} & e^{0.5\epsilon} & e^{-0.5\epsilon} & e^{\epsilon} & e^{-\epsilon} \\ e^{0.5\epsilon} & e^{-0.5\epsilon} & e^{-0.5\epsilon} & e^{0.5\epsilon} & e^{-\epsilon} & e^{\epsilon}. \end{pmatrix} \tag{2.51}$$

$\mathbb{T}$ is diagonalizable so, there exist a matrix $\mathbb{A}$ such that $\mathbb{A}.\mathbb{A}^{-1} = \mathbb{I}$ =identity matrix and $\mathbb{A}^{-1}\mathbb{T}\mathbb{A} = \mathbb{D}$ where $\mathbb{D}$ is the diagonal matrix.

So we recall: $\mathbb{L} = \mathbb{A}^{-1}$ and $\mathbb{R} = \mathbb{A}$

We have $\mathbb{R}\mathbb{L} = \mathbb{I}$,so let rewrite

$$\begin{aligned} \mathcal{Z} &= \sum_{m,m'=1}^{4} \langle m|\mathbb{R}\mathbb{L}\mathbb{T}\mathbb{R}\mathbb{L}\mathbb{T}\mathbb{R}\mathbb{L}\cdots\mathbb{T}\mathbb{R}\mathbb{L}|m'\rangle \qquad (2.52)\\ &= \sum_{m,m'=1}^{4} \langle m|\mathbb{R}\underbrace{(\mathbb{L}\mathbb{T}\mathbb{R})(\mathbb{L}\mathbb{T}\mathbb{R})\mathbb{L}\cdots\mathbb{T}\mathbb{R}}_{M-1 \quad times}\mathbb{L}|m'\rangle \qquad (2.53)\\ &= \sum_{m,m'=1}^{4} \langle m|\mathbb{R}\mathbb{D}^{M-1}\mathbb{L})|m'\rangle. \qquad (2.54) \end{aligned}$$

One finds that

$$\mathfrak{P} = \mathrm{Tr}(\mathbb{D}^{M-1}) \qquad (2.55)$$

with the same reasoning the correlation quantity becomes

$$\begin{aligned} \langle \boldsymbol{t}_a \cdot \boldsymbol{t}_{N+a}\rangle = \frac{1}{\mathcal{Z}} \sum_{\boldsymbol{t}_1,\boldsymbol{t}_a,\boldsymbol{t}_{a+N},\boldsymbol{t}_b} \boldsymbol{t}_a \cdot \boldsymbol{t}_{N+a}\langle \boldsymbol{t}_1|\mathbb{R}\mathbb{D}^a\mathbb{L}|\boldsymbol{t}_a\rangle\langle \boldsymbol{t}_a|\mathbb{R}\mathbb{D}^{N-1}\mathbb{L}|\\ \boldsymbol{t}_{a+N}\rangle\langle \boldsymbol{t}_{a+N}|\mathbb{R}\mathbb{D}^b\mathbb{L}|\boldsymbol{t}_b\rangle. \end{aligned} \qquad (2.56)$$

or, more explicitly,

$$\begin{aligned} \langle \boldsymbol{t}_a \cdot \boldsymbol{t}_{N+a}\rangle = \frac{1}{\sum_i \lambda_i^{a+b+N-1}} \sum_{m,m'} \mathbb{R}\mathbb{D}^a\mathbb{L}|m\rangle\langle m|\mathcal{R}\mathbb{D}^{N-1}\mathbb{L}|m'\rangle\\ \langle m'|\mathbb{R}\mathbb{D}^b\mathbb{L}|1\rangle \times \cos\theta_{mm'}. \end{aligned} \qquad (2.57)$$

where θ is the angle between the consecutive bonds vectors.

We can now find the expression for the persistence length ℓ_{p}.

$$\langle \boldsymbol{t}_a \cdot \boldsymbol{t}_{N+a}\rangle \sim e^{-\frac{N}{\ell_{\mathrm{p}}}} \qquad (2.58)$$

Thus

$$\ell_{\mathbf{p}} \sim -\frac{N}{\ln\left(\langle \boldsymbol{t}_a \cdot \boldsymbol{t}_{N+a}\rangle\right)} \qquad (2.59)$$

We find that for very large number of monomers,

$$\ell_{\mathbf{p}} \sim \frac{1}{\ln \frac{\lambda_{\mathbf{Max}}}{\lambda_{\mathbf{Max\text{-}second}}}} \tag{2.60}$$

Where $\lambda_{\mathbf{Max}}$ is the largest eigen value of the transfer matrix and $\lambda_{\mathbf{Max\text{-}second}}$ the second largest.

We compute the persistence length of the unconfined chain and plot it as a function of the bending modulus on Figure 2.9.

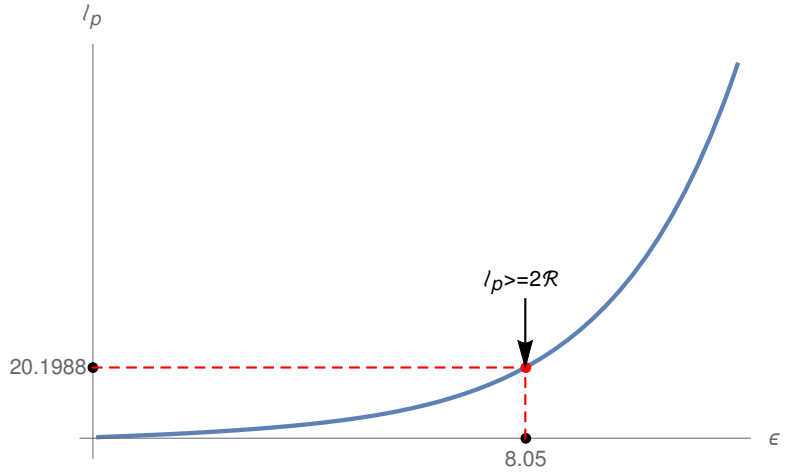

Figure 2.9: *Plot of the persistence length of a polymer chain living on the 3D cubic plus digonals lattice as function of* ϵ

The equation (2.60) for the persistence length is important because it enables us to investigate the properties and conformational behaviour or changes of the polymer chains as it grows under the action of the monomers activity or fugacity z inside the confining finite cell region. We compare the persistence length of the chains to the diameter of the confining region by fixing the ratio at approximately 1. This choice makes the filament semiflexible as well as keeps the size of the confing region finite while with the average number or degree of polymerisation of the polymer filament is increasing.

Let D be size of the confining region (for example the diameter of a spherical confining region) and N the average number of polymerisation of the polymer filament which can be assumed to be equal to contour length of the filament in case of semi-flexible filament.
So for

- $\ell_{\mathrm{p}} \simeq N > D$ we have semi-flexible polymer chain that is subjected to strong effect of the confinement.
- $\ell_{\mathrm{p}} \simeq N \sim D$ we are at the transition between strong and weak confinement.

- $\ell_p \simeq N < D$ we have weak confinement effect.

These comparisons thus allow to investigate the confined chains behaviour and their physical properties.

We are also interested in the ordering of the semiflexible polymer chains inside the confining region. We define an order parameter that enable us to quantifies the effect of confinement on the orientation of the polymer chains in our model.

2.5 Definition of the radial order parameter field

We aim to quantify in our model the alignement of semiflexible filaments in confining regions. In fact this investigation is relevant for the understanding of how actin cytoskeletal networks self-organize and align inside the cell under the effect of cell membrane confinement. It has been shown using electron and fluorescent microscopy techniques that interesting ordering phenomena occur at the cell confining membrane or wall [83]. The conformation, behaviour and alignment of semiflexible cytoskeletal filaments change when subjected to strong confinement and their physical properties become totally different to the one observed in the bulk [73].
In our model, the segments of the polymer chains can have preferred orientation inside the confining domain or they can be isotropically oriented. For preferred orientation, the chain segments can either align perpendicular to the confining region wall or they can align parallel to it. Whereas for isotropic distribution of filaments, all orientations are equally possible. We use cosine of the angle between the chain segments orientation and the radial unit vector $\hat{\boldsymbol{u}}$ function of the position bonds $\hat{\boldsymbol{u}} = \boldsymbol{r}/|\boldsymbol{r}|$ to describe the ordering of the chains relatively to the cell membranes and we choose to measure $\boldsymbol{r}$ from the centre of some symetrical confining . In our model the degree orientational ordering or alignement is entirely (controlled) measured by the radial parameter field distribution defined by:

$$Q(\boldsymbol{r}) = \sum_{\hat{\boldsymbol{n}}} \frac{1}{2}(1 - 3(\hat{\boldsymbol{u}} \cdot \hat{\boldsymbol{n}})^2)\varrho(\boldsymbol{r}, \hat{\boldsymbol{n}}). \tag{2.61}$$

for chains confined in three dimensions (3d) and

$$Q(\boldsymbol{r}) = \sum_{\hat{\boldsymbol{n}}} (1 - 2(\hat{\boldsymbol{u}} \cdot \hat{\boldsymbol{n}})^2)\varrho(\boldsymbol{r}, \hat{\boldsymbol{n}}). \tag{2.62}$$

for chains confined in two dimensions (2d).
For a small angle between $\hat{\boldsymbol{u}}$ and $\hat{\boldsymbol{n}}$ i.e for $\boldsymbol{u} \parallel \hat{\boldsymbol{n}}$ (the segments of the chains align parallel to the radial vector $\hat{\boldsymbol{u}}$ and thus perpendicular to the cell wall) and this correspond to negative sign of the radial order parameter field distribution.
For an angle between $\hat{\boldsymbol{u}}$ and $\hat{\boldsymbol{n}}$ avoid to 90° i.e for $\hat{\boldsymbol{u}} \perp \hat{\boldsymbol{n}}$, the filaments are perpendicular to the radial vector $\hat{\boldsymbol{u}}$ and thus parallel to the cell wall, and we have a positive radial order field distribution in that case.

For the order parameter field distribution equal to 0, we have an isotropic distribution of filament inside the confining region.

2.6 Conclusion

In summary, we have introduced the grand canonical monomer ensemble formalism for semiflexible chains in this chapter. We have defined a grand canonical partition function for a system of semiflexible linear polymer chains. We used it to derive the expressions for the average density distributions, the degree of polymerisation or mean number of chains segments and the average number of chains. We have also introduce the idea of semiflexible chains confinement in finite regions and we defined the parameters that are the confining external field, the chains bond bending stiffness and the persistence length of the polymer chains, useful for numerical computation of the quantities defined above. We next have defined an order parameter field that allows to quantify the degree of orientational alignment of the polymer chains relatively to the cell membrane under the effect of confinement. This model is very convenient for the study of linear actin cytoskeletal filaments under cellular confinement.

However, actin filaments inside living eukaryotic cell can be linear or can branch and form tree-like structures such as what is observed at the leading edge of a moving cell. So in the next chapter, we extend the monomer ensemble formalism to model branching cytoskeletal networks in confining regions.

Chapter 3

Branching cytoskeletal networks in confining region

3.1 Introduction

Actin filaments making up the cytoskeletal actin networks have various architectures and structures. They can be linear or have branched architecture and they are treated as semiflexible and oriented filaments.

Actin filaments form a highly dense and branched network at the cell periphery, especially in motile cells. Inside the living cell, their growth, elongation, branching, spatial rearrangement and their orientational ordering are often restricted by the cell membrane because of the similarity between their persistence length and the cell size [13, 34, 84–86]. Actin filaments and their networks are involved in many cellular functions mainly mechanical activities of the cell. However the constraint due to cell size confinement strongly influence their structural organization, behaviour, conformations and their physical properties. Branching networks are the most subjected to the confinement effects since they mainly form at the vicinity of the cell membrane. Many diseases such as cancer result sometime from the failure in the actin networks structure, ordering and spatial organization which are said to be controlled by cell geometry and confinement [87, 88]. It is thus important to investigate the effect of cell membrane confinement on actin networks. Experimental and theoretical models for the study of the effect of confinement on linear semiflexible (actin) polymer chains exist [13, 14, 34, 54, 55, 74, 85, 86], but none of them has effectively investigated in a quantitative way the correlation between the confinement effects from the cell membrane and the spatial and orientational organisation of branching networks of semiflexible filaments. These effects might have different degrees of influence depending on the architecture and structure of filaments composing the networks, since branched filaments or networks are stiffer than composites of linear chains [70, 71]. We wish to model branching cytoskeletal networks inside confining regions and quantitatively determine the confinement effect on the spatial organisation, orientational ordering and on the structural

properties of these networks.

We are interested in the study of the physical properties that are relevant to branching cytoskeletal actin networks that grow via the cellular binding Arp2/3 protein complex in eukaryotic cells [89]. The Arp2/3 protein complex ensure the nucleation of the actin filaments polymerisation and growth and then initiates the branching of new filaments on existing ones approximately at 70° angle [51, 90, 91]. We aim to determine the density distributions and order parameter field profiles of these networks confined inside cells with size comparable to the persistence length of the filaments in order to predict the effect of the cell membrane confinement on the spatial organisation and orientation of branching actin networks at thermodynamic equilibrium.
The monomer ensemble formalism for single semiflexible filament we have introduced in Chapter 2 is extended the formalism to branching networks in the grand canonical ensemble. We structured the chapter as follow:

In the first section we present the model and then we conveniently redefine the grand canonical partition function for a network of branching filaments without any kind of interactions between filament segments. In the section that follows we define and derive the expressions for the average densities of segments of the networks from which will result new integrals equations. We also make choice of the appropriate parameters in order to compute the grand partition function, the densities and the order profiles. In the third (last) section we describe the numerical method which we have developed in order to implement the integral equations for the computation of all the relevant quantities.

3.2 Description of the model

We model the branching actin cytoskeletal networks in confining regions. We consider an infinite number of G-actin monomers and of Arp2/3 protein complex inside a cell with finite size. We consider the cell system as a bath or reservoir from which monomers and proteins are taken to form the filaments and the networks. The mechanism of semiflexible polymer chains formation stays the same as in the case of single filament except that here, the polymer chain can branch as it grows to form a tree-like network. We neglect the mutual monomer interaction and also their interaction with the confining membrane or wall. We characterize the activity of each G-actin monomer by a chemical potential field or fugacity z. It enables monomers to connect with their nearest neighbours successively, elongate and form linear filaments. New filaments branching off from existing (linear or branched) chains can occur via a fugacity ζ that mimic the activity of the Arp2/3 protein complex and form a branched networks of filaments without any loop (tree-like structure) as shown by Figure 3.1. Each monomer or bond of the formed network is localised and labelled by its position $\boldsymbol{r}$ and by its orientation $\hat{\boldsymbol{n}}$. The activity of monomers or fugacities z and ζ are function of positions of the monomers and their orientations inside the confining medium.

In Figure 3.1, we model the filaments growing into linear and branched chains. While first or old filaments are elongating linearly in a particular orientation $\hat{\boldsymbol{n}}$, new filaments bind on old filament at 70° angle and elongate in a direction $\hat{\boldsymbol{n}}'$ where the Arp2/3 protein complex serve as junction between the mother and the daughter filaments. The branching network is thus composed of both linear and branched filaments.

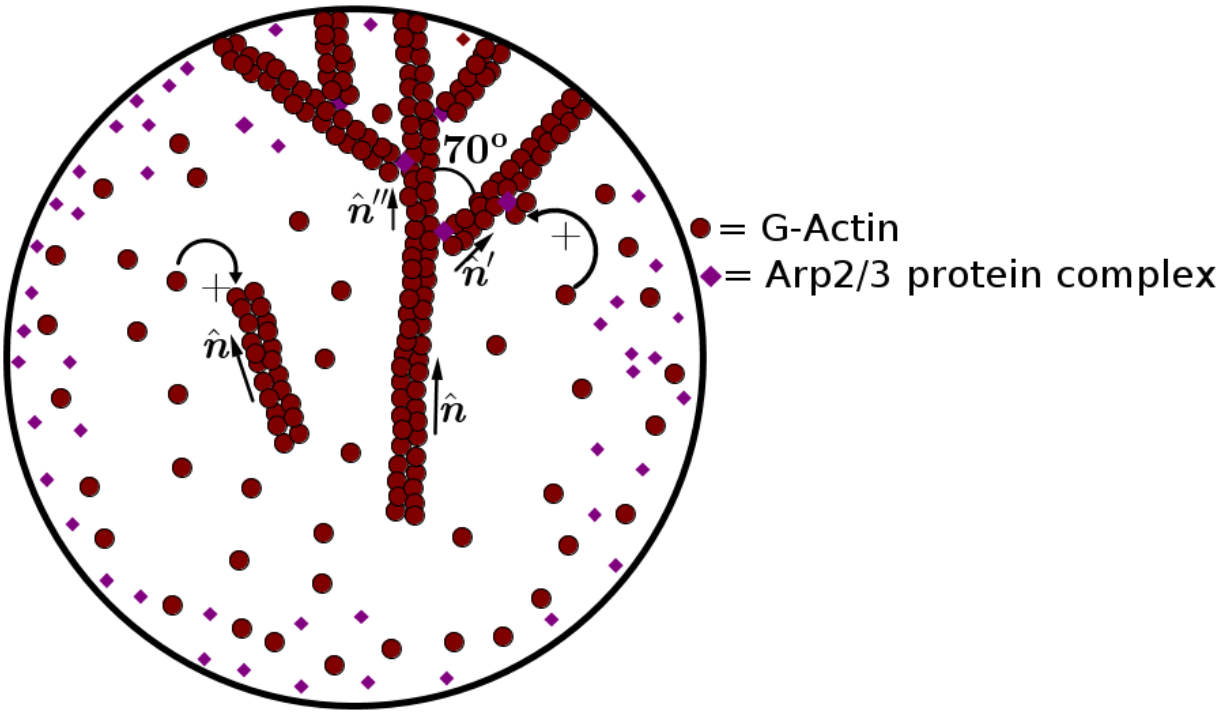

Figure 3.1: Depiction of the growth and branching of the actin filements via the Arp2/3 protein complex inside a spherical cell with rigid membrane. We have inside the sphere which we represent here on the figure by a circular shape in black, G-actin monomers in red that link linearly and form a linear filament with orientation $\hat{\boldsymbol{n}}$. The model and formalism we have introduced in Chapter 3 of this thesis applies to the linear actin chain formation. Inside the sphere, we have also branching actin filaments. As the filament grows in the direction $\hat{\boldsymbol{n}}$, the Arp2/3 in violet protein complex attach to the filament and nucleate the binding of the G-actin monomer in orientation $\hat{\boldsymbol{n}}'$ leading to the growth of new filament on existing one at 70° angle. The arrow with the plus indicate the adding of G-actin monomer at the actin filament growing end to ensure its linear elongation or at the top of the Arp2/3 protein at the side of the old filament to ensure the growth of the branching filament. A branching or tree-like network thus grows and possibly fills the confining spherical cell.

We descibe more explicitly the mathematical representation of the branching actin networks on 3.2.

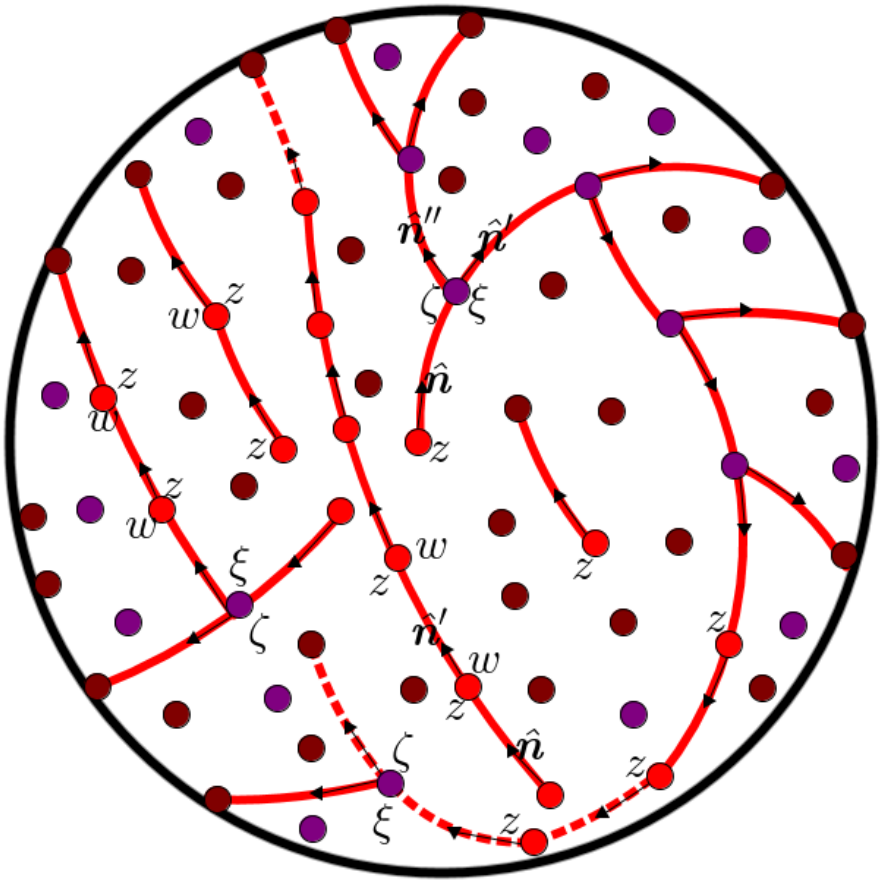

Figure 3.2: *Mathematical representation of a grown branching actin network. It contains various configurations of branched filaments and linear filaments. The monomers or bonds that belongs to the chain of the networks are in red color. Each monomer has two ends with the starting end starting at a position* $\boldsymbol{r}$ *and the other end at position* $\boldsymbol{r}'$ *and each end has an orientation* $\hat{\boldsymbol{n}}$*.* $\mathcal{G}$ *is the propagator or the Green function that characterises the segments of the chain as straight line of size* ℓ *and ensure that both ends of a segment have the same orientation.* z *is the monomer activity called fugacity and* w *is the Boltzmann weight factor associated to the pairwise bending stiffness between monomers of the chain. The red dots are the starting points of each monomer or bond of the chain and the dots in brown colour are the starting points of neighbours monomers. The proteins in violet represent the binding proteins (Arp2/3 protein complex) that ensure the branching of the filaments*

Since actin filament is semiflexible, there is a stiffness between bounds of the filament that enable it to keep its semiflexiblity. We have previously defined the bending weight w that couples the angular orientations between bonds of the linear chains.

We now want to present the mathematical formalism that allows us to obtain the grand canonical partitions functions for the system of branching actin networks.

3.2.1 Networking and the grand canonical partition function of confined branching networks

The actin filaments of the network that we grow, have variable lengths and conformations because they can be pruned, and then grow again by branching or by elongating into linear filaments. So we can define a grand canonical partition function for this branching networks at thermodynamic equilibrium.

In order to define the grand canonical partition function, we need to define a bending weight ξ (function of the positions and orientations of the segments of the network) which associate to the stiffness between bonds that are involved in junctions or in branching points, the fugacity ζ associated to the branching points and the propagator $\mathcal{G}$ (function of the positions and orientations of a segment ends) that makes the segments of the filament straight in order ensure that both end of a segment have the same orientation. $\mathcal{G}$ is the same as the one we have defined in Figure 2.2 or in equation (2.2).

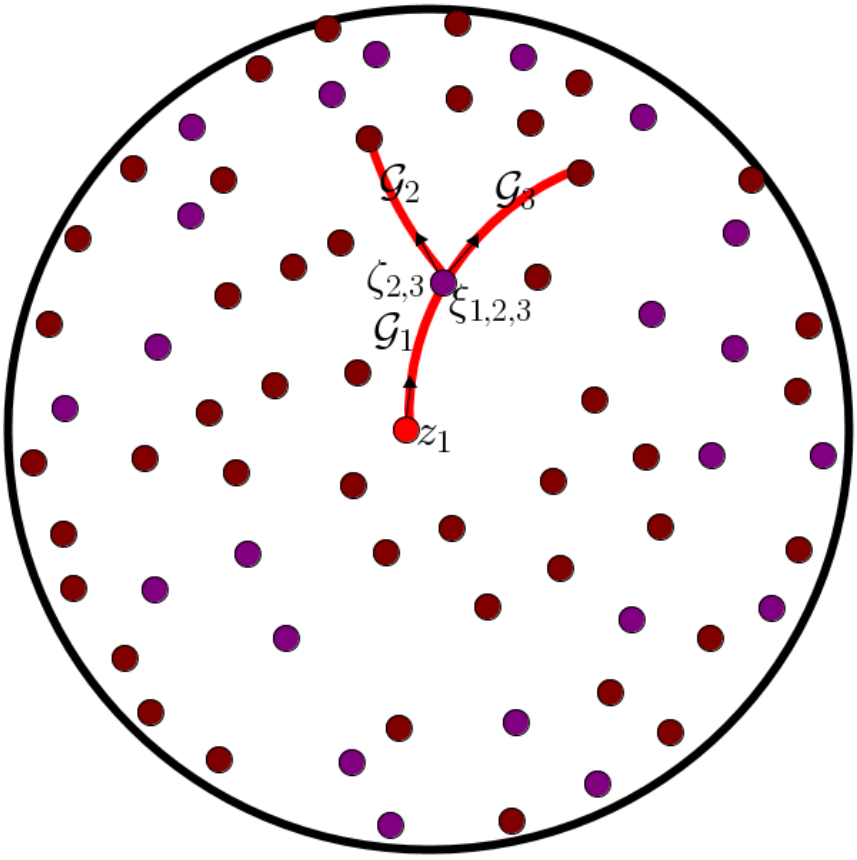

Figure 3.3: *Depiction of a branched filament consisting of 3 bonds. The monomers or bonds that belongs to the chain of the networks are in red color. Each monomer has two ends with the starting end starting at a position* $\boldsymbol{r}$ *and the other end at position* $\boldsymbol{r}'$ *and each end has an orientation* $\hat{\boldsymbol{n}}$*.* $\mathcal{G}$ *is the propagator or the Green function that characterises the segments of the chain as straight line of size* ℓ *and ensure that both ends of a segment have the same orientation.* z *is the monomer activity called fugacity and* w *is the Boltzmann weight factor associated to the pairwise bending stiffness between monomers of the chain. The red dots are the starting points of each monomer or bond of the chain and the dots in brown colour are the starting points of neighbours monomers. The proteins in violet represent the binding proteins (Arp2/3 protein complex) that ensure the branching of the filaments*

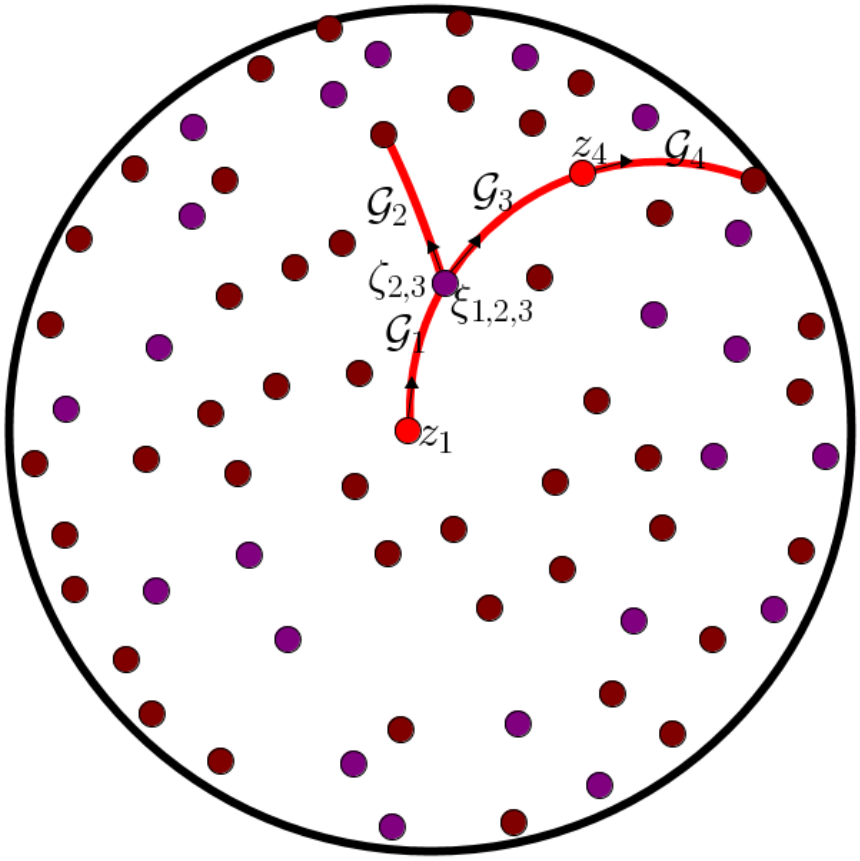

Figure 3.4: *Depiction of a branched filament consisting of 4 bonds. The monomers or bonds that belongs to the chain of the networks are in red colour. Each monomer has two ends with the starting end starting at a position* $\boldsymbol{r}$ *and the other end at position* $\boldsymbol{r}'$ *and each end has an orientation* $\hat{\boldsymbol{n}}$*.* $\mathcal{G}$ *is the propagator or the Green function that characterises the segments of the chain as straight line of size* ℓ *and ensure that both ends of a segment have the same orientation.* z *is the monomer activity called fugacity and* w *is the Boltzmann weight factor associated to the pairwise bending stiffness between monomers of the chain. The red dots are the starting points of each monomer or bond of the chain and the dots in brown colour are the starting points of neighbours monomers. The proteins in violet represent the binding proteins (Arp2/3 protein complex) that ensure the branching of the filaments*

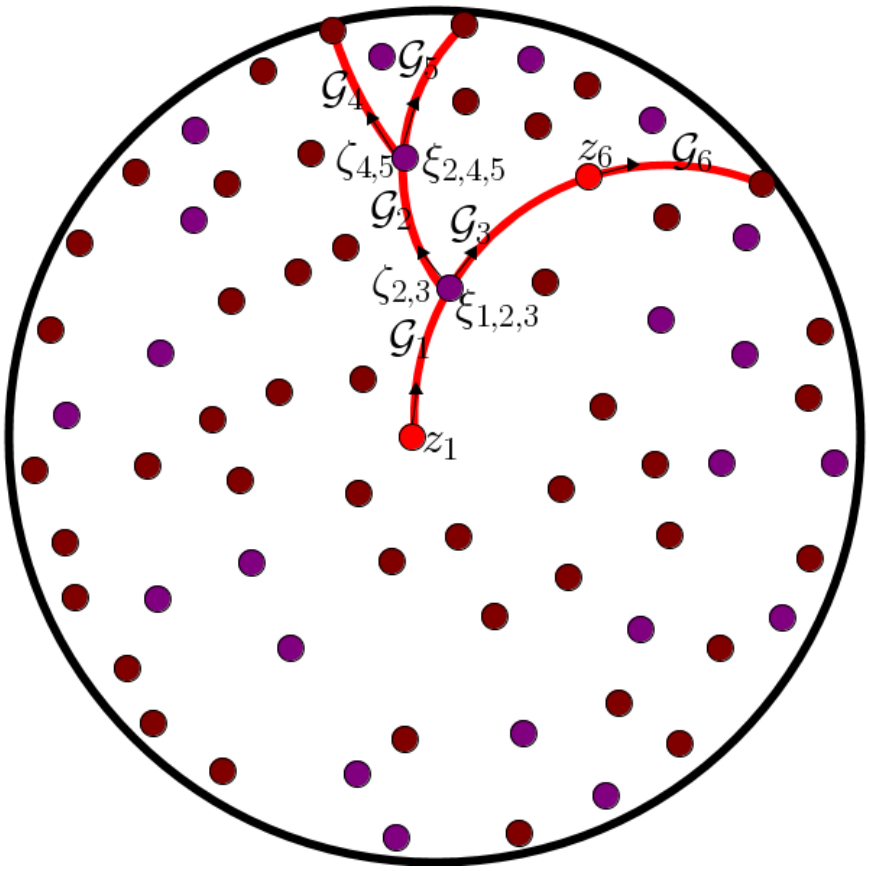

Figure 3.5: *Depiction of a branched filament consisting of 6 bonds. The monomers or bonds that belongs to the chain of the networks are in red color. Each monomer has two ends with the starting end starting at a position* $\boldsymbol{r}$ *and the other end at position* $\boldsymbol{r}'$ *and each end has an orientation* $\hat{\boldsymbol{n}}$*.* $\mathcal{G}$ *is the propagator or the Green function that characterises the segments of the chain as straight line of size* ℓ *and ensure that both ends of a segment have the same orientation.* z *is the monomer activity called fugacity and* w *is the Boltzmann weight factor associated to the pairwise bending stiffness between monomers of the chain. The red dots are the starting points of each monomer or bond of the chain and the dots in brown colour are the starting points of neighbours monomers. The proteins in violet represent the binding proteins (Arp2/3 protein complex) that ensure the branching of the filaments*

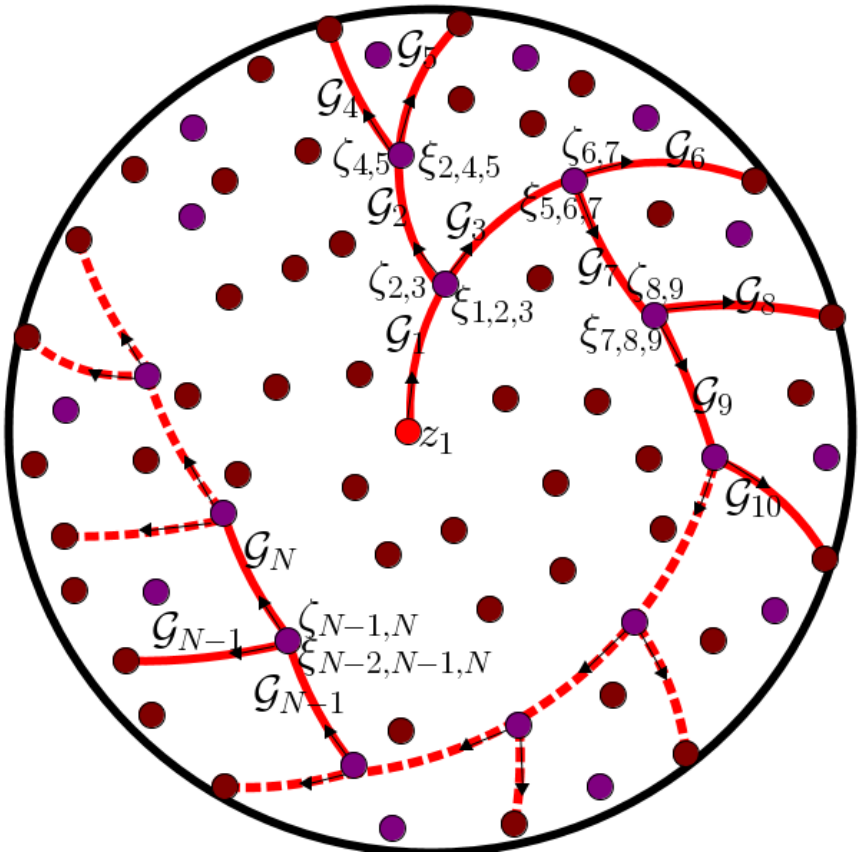

Figure 3.6: *Depiction of a branched filament consisting of N bonds. The monomers or bonds that belongs to the chain of the networks are in red color. Each monomer has two ends with the starting end starting at a position $\boldsymbol{r}$ and the other end at position $\boldsymbol{r}'$ and each end has an orientation $\hat{\boldsymbol{n}}$. $\mathcal{G}$ is the propagator or the Green function that characterises the segments of the chain as straight line of size ℓ and ensure that both ends of a segment have the same orientation. z is the monomer activity called fugacity and w is the Boltzmann weight factor associated to the pairwise bending stiffness between monomers of the chain. The red dots are the starting points of each monomer or bond of the chain and the dots in brown colour are the starting points of neighbours monomers. The proteins in violet represent the binding proteins (Arp2/3 protein complex) that ensure the branching of the filaments.*

define the Boltzman weight ξ as

$$\xi_{i,j,k} = \xi(\boldsymbol{r}'_i, \hat{\boldsymbol{n}}'_i, \boldsymbol{r}_j, \hat{\boldsymbol{n}}_j, \boldsymbol{r}_k, \hat{\boldsymbol{n}}_k) = \delta(\boldsymbol{r}'_i - \boldsymbol{r}_k)\delta(\boldsymbol{r}'_i - \boldsymbol{r}_k)\xi(\hat{\boldsymbol{n}}'_i, \hat{\boldsymbol{n}}_j, \hat{\boldsymbol{n}}_k) \tag{3.1}$$

Where the functions delta $\delta(\boldsymbol{r}'_i - \boldsymbol{r}_k)\delta(\boldsymbol{r}'_i - \boldsymbol{r}_k)$ ensure that the segments j, and k branch at the same end point of the existing segment i. The chemical field or fugacity ζ associated to the branching points is function of the degrees of freedom $(\boldsymbol{r}, \hat{\boldsymbol{n}})$ of the segments that emerge from the branching junction or point. It is defined as:

$$\zeta_{j,k} = (\boldsymbol{r}_j, \hat{\boldsymbol{n}}_j, \boldsymbol{r}'_j, \hat{\boldsymbol{n}}'_j, \boldsymbol{r}_k, \hat{\boldsymbol{n}}_k, \boldsymbol{r}'_k, \hat{\boldsymbol{n}}'_k) = \delta(\boldsymbol{r}_j - \boldsymbol{r}_k)e^{-\beta\phi(\boldsymbol{r}_j, \hat{\boldsymbol{n}}_j, \boldsymbol{r}'_j, \hat{\boldsymbol{n}}'_j, \boldsymbol{r}_k, \hat{\boldsymbol{n}}_k, \boldsymbol{r}'_k, \hat{\boldsymbol{n}}'_k)} \tag{3.2}$$

where $\delta(\boldsymbol{r}_j - \boldsymbol{r}_k)$ is there to ensure that at each branching point, two segments branch off at the same points and $\phi(\boldsymbol{r}_j, \hat{\boldsymbol{n}}_j, \boldsymbol{r}'_j, \hat{\boldsymbol{n}}'_j, \boldsymbol{r}_k, \hat{\boldsymbol{n}}_k, \boldsymbol{r}'_k, \hat{\boldsymbol{n}}'_k)$ is the chemical potential field.
As a reminder,

$$\mathcal{G}_i(\boldsymbol{r}_i, \hat{\boldsymbol{n}}_i, \boldsymbol{r}'_i, \hat{\boldsymbol{n}}'_i) = \delta(\boldsymbol{r}'_i - (\boldsymbol{r}_i + \ell\hat{\boldsymbol{n}}_i))\delta(\hat{\boldsymbol{n}}_i - \hat{\boldsymbol{n}}'_i) \tag{3.3}$$

where ℓ is the bond length. and

$$z_i = z(\boldsymbol{r}_i, \hat{\boldsymbol{n}}_i, \boldsymbol{r}'_i, \hat{\boldsymbol{n}}'_i) = z_0 e^{(-\beta\varphi(\boldsymbol{r}_i, \hat{\boldsymbol{n}}_i, \boldsymbol{r}'_i, \hat{\boldsymbol{n}}'_i))} \tag{3.4}$$

In order to make clear how we define the grand canonical partition function for the confined branching networks, we start by defining the partitions for few configurations which consist of branching and branched filaments of respectively of 3, 4, 6 and N bonds (see Figure 3.3, Figure 3.4, Figure 3.5 and Figure 3.6). We call branched filament a filament that are of functionality 3, meaning that we have 3 segments that are conneted at each junction of the filament (example of filaments on Figure 3.3 and 3.6) while branching filament are of functionality 2 and 3 (example of3.4).

We define the partition function of the branched filament consisting of 3 bonds of Figure 3.3 in shorthand notation as:

$$\mathfrak{Z}_3 = \int_{\boldsymbol{r}_1, \hat{\boldsymbol{n}}_1, \boldsymbol{r}'_1, \hat{\boldsymbol{n}}'_1} \int_{\boldsymbol{r}_2, \hat{\boldsymbol{n}}_2, \boldsymbol{r}'_2, \hat{\boldsymbol{n}}'_2} \int_{\boldsymbol{r}_3, \hat{\boldsymbol{n}}_3, \boldsymbol{r}'_3, \hat{\boldsymbol{n}}'_3} z_1 \mathcal{G}_1 \xi_{1,2,3} \mathcal{G}_2 \zeta_{2,3} \mathcal{G}_3 \tag{3.5}$$

or in full

$$\begin{aligned} \mathfrak{Z}_3 = \int\int\int & \mathrm{d}^3\boldsymbol{r}_1 \mathrm{d}^2\hat{\boldsymbol{n}}_1 \mathrm{d}^3\boldsymbol{r}'_1 \mathrm{d}^2\hat{\boldsymbol{n}}'_1 \mathrm{d}^3\boldsymbol{r}_2 \mathrm{d}^2\hat{\boldsymbol{n}}_2 \mathrm{d}^3\boldsymbol{r}'_2 \mathrm{d}^2\hat{\boldsymbol{n}}'_2 \mathrm{d}^3\boldsymbol{r}_3 \mathrm{d}^2\hat{\boldsymbol{n}}_3 \mathrm{d}^3\boldsymbol{r}'_3 \mathrm{d}^2\hat{\boldsymbol{n}}'_3 \\ & z(\boldsymbol{r}_1, \hat{\boldsymbol{n}}_1, \boldsymbol{r}'_1, \hat{\boldsymbol{n}}'_1) \mathcal{G}(\boldsymbol{r}_1, \hat{\boldsymbol{n}}_1, \boldsymbol{r}'_1, \hat{\boldsymbol{n}}'_1) \xi(\boldsymbol{r}'_1, \hat{\boldsymbol{n}}'_1, \boldsymbol{r}_2, \hat{\boldsymbol{n}}_2, \boldsymbol{r}_3, \hat{\boldsymbol{n}}_3) \\ & \mathcal{G}(\boldsymbol{r}_2, \hat{\boldsymbol{n}}_2, \boldsymbol{r}'_2, \hat{\boldsymbol{n}}'_2) \zeta(\boldsymbol{r}_2, \hat{\boldsymbol{n}}_2, \boldsymbol{r}'_2, \hat{\boldsymbol{n}}'_2, \boldsymbol{r}_3, \hat{\boldsymbol{n}}_3, \boldsymbol{r}'_3, \hat{\boldsymbol{n}}'_3) \mathcal{G}(\boldsymbol{r}_3, \hat{\boldsymbol{n}}_3, \boldsymbol{r}'_3, \hat{\boldsymbol{n}}'_3) \end{aligned} \tag{3.6}$$

Replacing equations (3.8),(3.3), (3.4) and (3.1) in equation (3.6) and integrating we get:

$$\mathfrak{Z}_3 = \int\int\int \mathrm{d}^3\boldsymbol{r}_1 \mathrm{d}^2\hat{\boldsymbol{n}}_1 \mathrm{d}^3\boldsymbol{r}_2 \mathrm{d}^2\hat{\boldsymbol{n}}_2 \mathrm{d}^3\boldsymbol{r}_3 \mathrm{d}^2\hat{\boldsymbol{n}}_3 \, z(\boldsymbol{r}_1, \hat{\boldsymbol{n}}_1) \xi(\hat{\boldsymbol{n}}_1, \hat{\boldsymbol{n}}_2, \hat{\boldsymbol{n}}_3) \zeta(\boldsymbol{r}_2, \hat{\boldsymbol{n}}_2, \boldsymbol{r}_3, \hat{\boldsymbol{n}}_3). \tag{3.7}$$

where

$$\zeta(\boldsymbol{r}_j, \hat{\boldsymbol{n}}_j, \boldsymbol{r}_k, \hat{\boldsymbol{n}}_k) = \delta(\boldsymbol{r}_j - \boldsymbol{r}_k) e^{-\beta\phi(\boldsymbol{r}_j, \hat{\boldsymbol{n}}_j, \boldsymbol{r}_j + \ell\hat{\boldsymbol{n}}_j, \hat{\boldsymbol{n}}'_j, \boldsymbol{r}_k, \hat{\boldsymbol{n}}_k, \boldsymbol{r}_k + \ell\hat{\boldsymbol{n}}_k, \hat{\boldsymbol{n}}_k)} \tag{3.8}$$

The shorthand notation of equation (3.7) is

$$\mathfrak{Z}_3 = \int_{\boldsymbol{r}_1, \hat{\boldsymbol{n}}_1} \int_{\boldsymbol{r}_2, \hat{\boldsymbol{n}}_2} \int_{\boldsymbol{r}_3, \hat{\boldsymbol{n}}_3} z \mathcal{G} \xi \mathcal{G} \zeta \mathcal{G} \tag{3.9}$$

The partition function for a branching filament consisting of 4 bonds (Figure 3.4) is

$$\begin{aligned} \mathfrak{Z}_4 = \int\int\int\int\int & \mathrm{d}^3\boldsymbol{r}_1 \mathrm{d}^2\hat{\boldsymbol{n}}_1 \mathrm{d}^3\boldsymbol{r}_2 \mathrm{d}^2\hat{\boldsymbol{n}}_2 \mathrm{d}^3\boldsymbol{r}_3 \mathrm{d}^2\hat{\boldsymbol{n}}_3 \mathrm{d}^3\boldsymbol{r}_4 \mathrm{d}^2\hat{\boldsymbol{n}}_4 \mathrm{d}^3\boldsymbol{r}_5 \mathrm{d}^2\hat{\boldsymbol{n}}_5 \, z(\boldsymbol{r}_1, \hat{\boldsymbol{n}}_1) \xi(\hat{\boldsymbol{n}}_1, \hat{\boldsymbol{n}}_2, \hat{\boldsymbol{n}}_3) \\ & \times \zeta(\boldsymbol{r}_2, \hat{\boldsymbol{n}}_2, \boldsymbol{r}_3, \hat{\boldsymbol{n}}_3) w(\hat{\boldsymbol{n}}_2, \hat{\boldsymbol{n}}_4) z(\boldsymbol{r}_4, \hat{\boldsymbol{n}}_4)) w(\hat{\boldsymbol{n}}_3, \hat{\boldsymbol{n}}_5) z(\boldsymbol{r}_5, \hat{\boldsymbol{n}}_5) \end{aligned} \tag{3.10}$$

Similarly we define the partition function for other configuration of the branching actin networks. Recall that the branching actin networks consist of linear, branching and branched networks. So The grand canonical partition function $\mathfrak{Z}$ is equal to the sum of all possible

configurations of the linear actin filaments, of the branching filaments and all possible configurations of the branched filaments in the thermodynamics limit (N going to infinity). So we write the grand canonical partition function $\mathfrak{Z}$ as:

$$
\begin{aligned}
\mathfrak{Z} = 1 &+ \int \mathrm{d}^3\boldsymbol{r}_1\mathrm{d}^2\hat{\boldsymbol{n}}_1\, z(\boldsymbol{r}_1,\hat{\boldsymbol{n}}_1)+ \\
&\int\int \mathrm{d}^3\boldsymbol{r}_1\mathrm{d}^2\hat{\boldsymbol{n}}_1\mathrm{d}^3\boldsymbol{r}_2\mathrm{d}^2\hat{\boldsymbol{n}}_2\, z(\mathbf{r}_1,\hat{\boldsymbol{n}}_1)w(\hat{\boldsymbol{n}}_1,\hat{\boldsymbol{n}}_2)z(\boldsymbol{r}_2,\hat{\boldsymbol{n}}_2)+ \\
&\int\int\int \mathrm{d}^3\boldsymbol{r}_1\mathrm{d}^2\hat{\boldsymbol{n}}_1\mathrm{d}^3\boldsymbol{r}_2,\mathrm{d}^2\hat{\boldsymbol{n}}_2\mathrm{d}^3\boldsymbol{r}_3\mathrm{d}^2\hat{\boldsymbol{n}}_3\, z(\boldsymbol{r}_1,\hat{\boldsymbol{n}}_1)w(\hat{\boldsymbol{n}}_1,\hat{\boldsymbol{n}}_2)z(\boldsymbol{r}_2,\hat{\boldsymbol{n}}_2) \\
&\times w(\hat{\boldsymbol{n}}_2,\hat{\boldsymbol{n}}_3)z(\boldsymbol{r}_3,\hat{\boldsymbol{n}}_3) \\
&+ \int\int\int\int \mathrm{d}^3\boldsymbol{r}_1\mathrm{d}^2\hat{\boldsymbol{n}}_1\mathrm{d}^3\boldsymbol{r}_2\mathrm{d}^2\hat{\boldsymbol{n}}_2\mathrm{d}^3\boldsymbol{r}_3\mathrm{d}^2\hat{\boldsymbol{n}}_3\mathrm{d}^3\boldsymbol{r}_4\mathrm{d}^2\hat{\boldsymbol{n}}_4\, z(\boldsymbol{r}_1,\hat{\boldsymbol{n}}_1)w(\hat{\boldsymbol{n}}_1,\hat{\boldsymbol{n}}_2)z(\boldsymbol{r}_2,\hat{\boldsymbol{n}}_2) \\
&\times w(\hat{\boldsymbol{n}}_2,\hat{\boldsymbol{n}}_3)z(\boldsymbol{r}_3,\hat{\boldsymbol{n}}_3)w_1(\hat{\boldsymbol{n}}_3,\hat{\boldsymbol{n}}_4)z(\boldsymbol{r}_4,\hat{\boldsymbol{n}}_4) \\
&+ \ldots + \int\ldots\int \mathrm{d}^3\boldsymbol{r}_1\mathrm{d}^2\hat{\boldsymbol{n}}_1\mathrm{d}^3\boldsymbol{r}_2\mathrm{d}^2\hat{\boldsymbol{n}}_2\ldots\mathrm{d}^3\boldsymbol{r}_N\mathrm{d}^2\hat{\boldsymbol{n}}_N\, z(\boldsymbol{r}_1,\hat{\boldsymbol{n}}_1)w_1(\hat{\boldsymbol{n}}_1,\hat{\boldsymbol{n}}_2)z(\boldsymbol{r}_2,\hat{\boldsymbol{n}}_2) \\
&\times \ldots w(\hat{\boldsymbol{n}}_{N-1},\hat{\boldsymbol{n}}_N)z(\boldsymbol{r}_N,\hat{\boldsymbol{n}}_N) \\
&+ \int\int\int \mathrm{d}^3\boldsymbol{r}_1\mathrm{d}^2\hat{\boldsymbol{n}}_1\mathrm{d}^3\boldsymbol{r}_2\mathrm{d}^2\hat{\boldsymbol{n}}_2\mathrm{d}^3\boldsymbol{r}_3\mathrm{d}^2\hat{\boldsymbol{n}}_3\, z(\boldsymbol{r}_1,\hat{\boldsymbol{n}}_1)\xi(\hat{\boldsymbol{n}}_1,\hat{\boldsymbol{n}}_2,\hat{\boldsymbol{n}}_3)\zeta(\boldsymbol{r}_2,\hat{\boldsymbol{n}}_2,\boldsymbol{r}_3,\hat{\boldsymbol{n}}_3) \\
&+ \int\int\int\int \mathrm{d}^3\boldsymbol{r}_1\mathrm{d}^2\hat{\boldsymbol{n}}_1\mathrm{d}^3\boldsymbol{r}_2\mathrm{d}^2\hat{\boldsymbol{n}}_2\mathrm{d}^3\boldsymbol{r}_3\mathrm{d}^2\hat{\boldsymbol{n}}_3\mathrm{d}^3\boldsymbol{r}_4\mathrm{d}^2\hat{\boldsymbol{n}}_4\, z(\boldsymbol{r}_1,\hat{\boldsymbol{n}}_1)\xi(\hat{\boldsymbol{n}}_1,\hat{\boldsymbol{n}}_2,\hat{\boldsymbol{n}}_3)\zeta(\boldsymbol{r}_2,\hat{\boldsymbol{n}}_2,\boldsymbol{r}_3,\hat{\boldsymbol{n}}_3) \\
&w(\hat{\boldsymbol{n}}_2,\hat{\boldsymbol{n}}_4)z(\boldsymbol{r}_4,\hat{\boldsymbol{n}}_4) \\
&+ \int\int\int\int\int \mathrm{d}^3\boldsymbol{r}_1\mathrm{d}^2\hat{\boldsymbol{n}}_1\mathrm{d}^3\boldsymbol{r}_2\mathrm{d}^2\hat{\boldsymbol{n}}_2\mathrm{d}^3\boldsymbol{r}_3\mathrm{d}^2\hat{\boldsymbol{n}}_3\mathrm{d}^3\boldsymbol{r}_4\mathrm{d}^2\hat{\boldsymbol{n}}_4\mathrm{d}^3\boldsymbol{r}_5\mathrm{d}^2\hat{\boldsymbol{n}}_5\, z(\boldsymbol{r}_1,\hat{\boldsymbol{n}}_1)\xi(\hat{\boldsymbol{n}}_1,\hat{\boldsymbol{n}}_2,\hat{\boldsymbol{n}}_3) \\
&\times \zeta(\boldsymbol{r}_2,\hat{\boldsymbol{n}}_2,\boldsymbol{r}_3,\hat{\boldsymbol{n}}_3)w(\hat{\boldsymbol{n}}_2,\hat{\boldsymbol{n}}_4)z(\boldsymbol{r}_4,\hat{\boldsymbol{n}}_4))w(\hat{\boldsymbol{n}}_3,\hat{\boldsymbol{n}}_5)z(\boldsymbol{r}_5,\hat{\boldsymbol{n}}_5) \\
&+ \int\int\int\int\int \mathrm{d}^3\boldsymbol{r}_1\mathrm{d}^2\hat{\boldsymbol{n}}_1\mathrm{d}^3\boldsymbol{r}_2\mathrm{d}^2\hat{\boldsymbol{n}}_2\mathrm{d}^3\boldsymbol{r}_3\mathrm{d}^2\hat{\boldsymbol{n}}_3\mathrm{d}^3\boldsymbol{r}_4\mathrm{d}^2\hat{\boldsymbol{n}}_4\mathrm{d}^3\boldsymbol{r}_5\mathrm{d}^2\hat{\boldsymbol{n}}_5\, z(\boldsymbol{r}_1,\hat{\boldsymbol{n}}_1)\xi(\hat{\boldsymbol{n}}_1,\hat{\boldsymbol{n}}_2,\hat{\boldsymbol{n}}_3) \\
&\times \zeta(\boldsymbol{r}_2,\hat{\boldsymbol{n}}_2,\boldsymbol{r}_3,\hat{\boldsymbol{n}}_3)\xi(\hat{\boldsymbol{n}}_2,\hat{\boldsymbol{n}}_4,\hat{\boldsymbol{n}}_5)\zeta(\boldsymbol{r}_4,\hat{\boldsymbol{n}}_4,\boldsymbol{r}_5,\hat{\boldsymbol{n}}_5) + \ldots
\end{aligned}
\tag{3.11}
$$

The equation (3.11) can be rewritten in terms of sum as:

$$
\begin{aligned}
\mathfrak{Z} = 1 &+ \sum_{N=1}^{\infty} \int \dots \int \mathrm{d}^3\boldsymbol{r}_1 \mathrm{d}^2\hat{\boldsymbol{n}}_1 \mathrm{d}^3\boldsymbol{r}_2 \mathrm{d}^2\hat{\boldsymbol{n}}_2 \dots \mathrm{d}^3\boldsymbol{r}_{N-1} \mathrm{d}^2\hat{\boldsymbol{n}}_{N-1} \mathrm{d}^3\boldsymbol{r}_N \mathrm{d}^2\hat{\boldsymbol{n}}_N \, z(\boldsymbol{r}_1, \hat{\boldsymbol{n}}_1) w(\hat{\boldsymbol{n}}_1, \hat{\boldsymbol{n}}_2) \\
&\times z(\boldsymbol{r}_2, \hat{\boldsymbol{n}}_2) \dots w(\hat{\boldsymbol{n}}_{N-1}, \hat{\boldsymbol{n}}_N) z(\boldsymbol{r}_N, \hat{\boldsymbol{n}}_N) \\
&+ \sum_{N=1}^{\infty} \int \dots \int \mathrm{d}^3\boldsymbol{r}_1 \mathrm{d}^2\hat{\boldsymbol{n}}_1 \mathrm{d}^3\boldsymbol{r}_2 \mathrm{d}^2\hat{\boldsymbol{n}}_2 \mathrm{d}^3\boldsymbol{r}_3 \mathrm{d}^2\hat{\boldsymbol{n}}_3 \mathrm{d}^3\boldsymbol{r}_4 \mathrm{d}^2\hat{\boldsymbol{n}}_4 \, z(\boldsymbol{r}_1, \hat{\boldsymbol{n}}_1) \xi(\hat{\boldsymbol{n}}_1, \hat{\boldsymbol{n}}_2, \hat{\boldsymbol{n}}_3) \zeta(\boldsymbol{r}_2, \hat{\boldsymbol{n}}_2, \boldsymbol{r}_3, \hat{\boldsymbol{n}}_3) \\
&\times w(\hat{\boldsymbol{n}}_2, \hat{\boldsymbol{n}}_4) z(\boldsymbol{r}_4, \hat{\boldsymbol{n}}_4) \dots z(\boldsymbol{r}_{N-1}, \hat{\boldsymbol{n}}_{N-1}) w(\hat{\boldsymbol{n}}_{N-1}, \hat{\boldsymbol{n}}_N) z(\boldsymbol{r}_N, \hat{\boldsymbol{n}}_N) \\
&+ \sum_{N=1}^{\infty} \int \dots \int \mathrm{d}^3\boldsymbol{r}_1 \mathrm{d}^2\hat{\boldsymbol{n}}_1 \mathrm{d}^3\boldsymbol{r}_2 \mathrm{d}^2\hat{\boldsymbol{n}}_2 \mathrm{d}^3\boldsymbol{r}_3 \mathrm{d}^2\hat{\boldsymbol{n}}_3 \mathrm{d}^3\boldsymbol{r}_4 \mathrm{d}^2\hat{\boldsymbol{n}}_4 \mathrm{d}^3\boldsymbol{r}_5 \mathrm{d}^2\hat{\boldsymbol{n}}_5 \mathrm{d}^3\boldsymbol{r}_6 \mathrm{d}^2\hat{\boldsymbol{n}}_6 \\
&z(\boldsymbol{r}_1, \hat{\boldsymbol{n}}_1) \xi(\hat{\boldsymbol{n}}_1, \hat{\boldsymbol{n}}_2, \hat{\boldsymbol{n}}_3) \zeta(\boldsymbol{r}_2, \hat{\boldsymbol{n}}_2, \boldsymbol{r}_3, \hat{\boldsymbol{n}}_3) \xi(\hat{\boldsymbol{n}}_2, \hat{\boldsymbol{n}}_4, \hat{\boldsymbol{n}}_5) \zeta(\boldsymbol{r}_4, \hat{\boldsymbol{n}}_4, \boldsymbol{r}_5, \hat{\boldsymbol{n}}_5) w(\hat{\boldsymbol{n}}_4, \hat{\boldsymbol{n}}_6) \\
&\times z(\boldsymbol{r}_6, \hat{\boldsymbol{n}}_6) \dots z(\boldsymbol{r}_{N-1}, \hat{\boldsymbol{n}}_{N-1}) w(\hat{\boldsymbol{n}}_{N-1}, \hat{\boldsymbol{n}}_N) z(\boldsymbol{r}_N, \hat{\boldsymbol{n}}_N) + \dots \\
&+ \sum_{N=1}^{\infty} \int \dots \int \mathrm{d}^3\boldsymbol{r}_1 \mathrm{d}^2\hat{\boldsymbol{n}}_1 \mathrm{d}^3\boldsymbol{r}_2 \mathrm{d}^2\hat{\boldsymbol{n}}_2 \mathrm{d}^3\boldsymbol{r}_3 \mathrm{d}^2\hat{\boldsymbol{n}}_3 \mathrm{d}^3\boldsymbol{r}_4 \mathrm{d}^2\hat{\boldsymbol{n}}_4 \mathrm{d}^3\boldsymbol{r}_5 \mathrm{d}^2\hat{\boldsymbol{n}}_5 \, z(\boldsymbol{r}_1, \hat{\boldsymbol{n}}_1) \xi(\hat{\boldsymbol{n}}_1, \hat{\boldsymbol{n}}_2, \hat{\boldsymbol{n}}_3) \\
&\times \zeta(\boldsymbol{r}_2, \hat{\boldsymbol{n}}_2, \boldsymbol{r}_3, \hat{\boldsymbol{n}}_3) \xi(\hat{\boldsymbol{n}}_2, \hat{\boldsymbol{n}}_4, \hat{\boldsymbol{n}}_5) \zeta(\boldsymbol{r}_4, \hat{\boldsymbol{n}}_4, \boldsymbol{r}_5, \hat{\boldsymbol{n}}_5) \dots \xi(\hat{\boldsymbol{n}}_{N-3}, \boldsymbol{n}_{N-1}, \hat{\boldsymbol{n}}_N) \\
&\times \zeta(\boldsymbol{r}_{N-1}, \hat{\boldsymbol{n}}_{N-1}, \boldsymbol{r}_N, \hat{\boldsymbol{n}}_N).
\end{aligned}
\tag{3.12}
$$

We rewrite (3.12) in shorthand notation as:

$$
\begin{aligned}
\mathfrak{Z} = &\sum_{N=0}^{\infty} \int_{\boldsymbol{r}_1, \hat{\boldsymbol{n}}_1} \dots \int_{\boldsymbol{r}_N, \hat{\boldsymbol{n}}_N} zwz \dots zwz \\
&+ \sum_{N=0}^{\infty} \int_{\boldsymbol{r}_1, \hat{\boldsymbol{n}}_1} \dots \int_{\boldsymbol{r}_N, \hat{\boldsymbol{n}}_N} z\xi\zeta wz \dots zwz \\
&+ \sum_{N=0}^{\infty} \int_{\boldsymbol{r}_1, \hat{\boldsymbol{n}}_1} \dots \int_{\boldsymbol{r}_N, \hat{\boldsymbol{n}}_N} z\xi\zeta\xi\zeta wz \dots zwz \\
&\dots \\
&+ \sum_{N=0}^{\infty} \int_{\boldsymbol{r}_1, \hat{\boldsymbol{n}}_1} \dots \int_{\boldsymbol{r}_N, \hat{\boldsymbol{n}}_N} z\xi\zeta\xi\zeta \dots \zeta\xi\zeta
\end{aligned}
\tag{3.13}
$$

Where the first term in right hand of the equation (3.13) is the sum of all possible configurations of linear filaments of the network, the second term is the sum of all possible configuration of filaments having only one branching points, the third term is count all possible configurations of filaments with two branching. We continue till we reach the last term of the equation which is the sum of all possible configurations of the branched filaments.

One can illustrate the grand canonical partition function using diagram as follow: We see that we can conveniently define quantities Ψ and Φ for branching networks such that we express the grand canonical partition analytically as.

$$
\mathfrak{Z} = 1 + \int_{\boldsymbol{r}, \hat{\boldsymbol{n}}} \mathrm{d}^3\boldsymbol{r} \mathrm{d}^2\hat{\boldsymbol{n}} z(\boldsymbol{r}, \hat{\boldsymbol{n}}) \Psi(\boldsymbol{r}, \hat{\boldsymbol{n}}) \tag{3.14}
$$

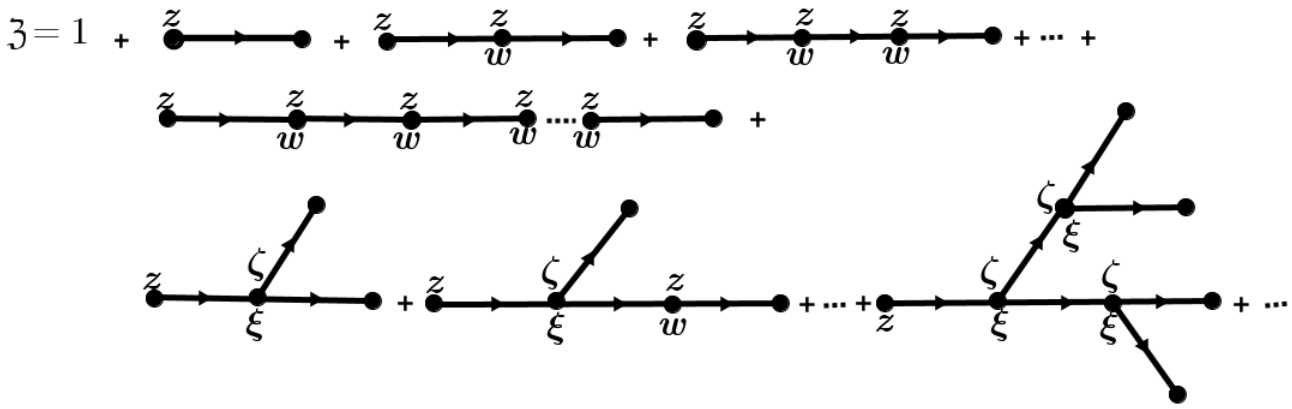

Figure 3.7: *Diagrammatic represention of the grand canonical partition function* $\mathfrak{Z}$ *for branching cytoskeletal networks.*

or

$$\mathfrak{Z} = 1 + \int_{\boldsymbol{r},\hat{\boldsymbol{n}}} \mathrm{d}^3\boldsymbol{r}\mathrm{d}^2\hat{\boldsymbol{n}}\tilde{z}(\boldsymbol{r},\hat{\boldsymbol{n}})\Psi(\boldsymbol{r},\hat{\boldsymbol{n}}) \tag{3.15}$$

So we define the functions of Ψ and and Φ by the following non-linear integral equations:

$$\Psi(\boldsymbol{r},\hat{\boldsymbol{n}}) = 1 + \int_{\boldsymbol{r},\hat{\boldsymbol{n}}} \mathrm{d}^3\boldsymbol{r}'\mathrm{d}^2\hat{\boldsymbol{n}}' w(\hat{\boldsymbol{n}},\hat{\boldsymbol{n}}')z(\boldsymbol{r},\hat{\boldsymbol{n}}')\Psi(\boldsymbol{r},\hat{\boldsymbol{n}}')+ \int_{\boldsymbol{r}',\hat{\boldsymbol{n}}',\boldsymbol{r}'',\hat{\boldsymbol{n}}''} \mathrm{d}^3\boldsymbol{r}'\mathrm{d}^2\hat{\boldsymbol{n}}'\mathrm{d}^3\boldsymbol{r}''\mathrm{d}^2\hat{\boldsymbol{n}}''\xi(\boldsymbol{r},\hat{\boldsymbol{n}},\hat{\boldsymbol{n}}',\hat{\boldsymbol{n}}'')\zeta(\boldsymbol{r},\hat{\boldsymbol{n}}',\hat{\boldsymbol{n}}'')\Psi(\mathbf{r}',\hat{\boldsymbol{n}}')\Psi(\boldsymbol{r}'',\hat{\boldsymbol{n}}'') \tag{3.16}$$

and

$$\Phi(\boldsymbol{r},\hat{\boldsymbol{n}}) = 1 + \int_{\boldsymbol{r},\hat{\boldsymbol{n}}} \mathrm{d}^3\boldsymbol{r}'\mathrm{d}^2\hat{\boldsymbol{n}}'\tilde{z}(\boldsymbol{r},\hat{\boldsymbol{n}}')w(\hat{\boldsymbol{n}},\hat{\boldsymbol{n}}')\Psi(\mathbf{r},\hat{\boldsymbol{n}}')+ \int_{\boldsymbol{r}',\hat{\boldsymbol{n}}',\boldsymbol{r}'',\hat{\boldsymbol{n}}''} \mathrm{d}^3\boldsymbol{r}'\mathrm{d}^2\hat{\boldsymbol{n}}'\mathrm{d}^3\boldsymbol{r}''\mathrm{d}^2\hat{\boldsymbol{n}}''\xi(\boldsymbol{r},\hat{\boldsymbol{n}},\boldsymbol{n}',\boldsymbol{n}'')\tilde{\zeta}(\boldsymbol{r},\boldsymbol{n}',\hat{\boldsymbol{n}}'')\Psi(\boldsymbol{r}',\boldsymbol{n}')\Phi(\boldsymbol{r}'',\hat{\boldsymbol{n}}''). \tag{3.17}$$

If we set ζ to 0 we see that we recover the equation (2.11) of the grand canonical partition function and thus the integral equations (2.28 and (2.30) for single semiflexible linear chain system. We can represent equation (3.16) and equation (3.17) digramatically as:

One can for example check that by replacing recursively the equation (3.16) for $\Psi(\boldsymbol{r},\hat{\boldsymbol{n}})$ in the

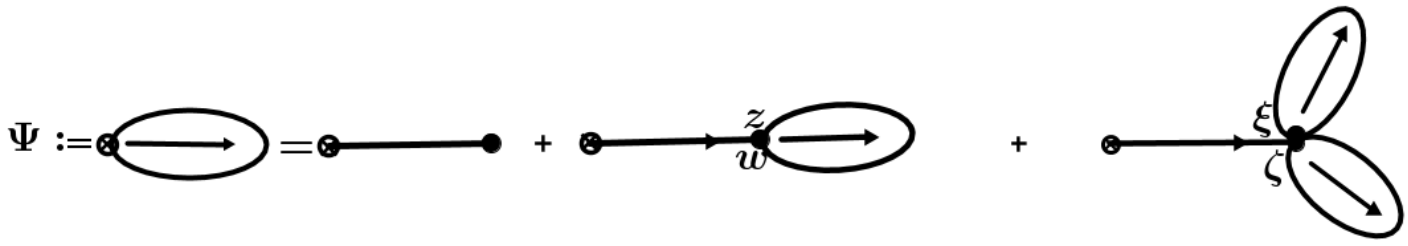

Figure 3.8: *Diagram for* Ψ *functional*

equation (3.14) we recover the expression for the grand canonical partition function of equation

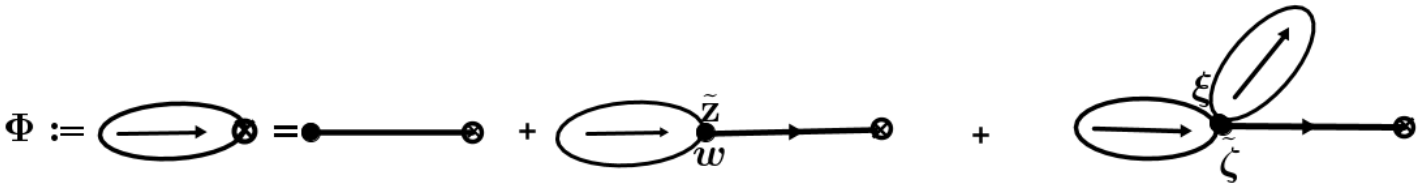

Figure 3.9: *Diagram for* Φ *functional*

(3.12)

Where of z and $\tilde{z}$ are the fugacity associated to the activity of monomers involved in respectively the quantity Ψ and Φ and ζ and $\tilde{\zeta}$ are fugacities associated to the activity of the binding proteins (Arp2/3) at junction in respectively Ψ and Φ. w is the Boltzmann weight associated to the stiffness between bonds of linear chains and ξ is the Boltzmann weight associated to the bending stiffness between bonds that are involved in branching points.

Ψ and Φ equations are non-linear coupled integral equation and thus difficult to solve analytically. So we aim to solve these equations by developing a self-consistent numerical method. We need to appropriately make a choice of the chemical potential field or the fugacity ζ associated to the branching points (which also controls the geometry of the confining region) and the Boltzmann weigth ξ. We have already defined w and z in Chapter 2 and they are given by equations (3.12). With

$$\phi(\boldsymbol{r},\hat{\boldsymbol{n}},\boldsymbol{r}',\hat{\boldsymbol{n}}') = \begin{cases} 0, & \text{if} \boldsymbol{r} \in \mathbb{L} \text{ and } \boldsymbol{r}+\ell\hat{\boldsymbol{n}} \in \mathbb{L} \\ \text{ and } & \boldsymbol{r}+\ell\hat{\boldsymbol{n}}' \in \mathbb{L} \\ \infty, & \text{otherwise} \end{cases} \tag{3.18}$$

We define

$$\zeta(\boldsymbol{r},\hat{\boldsymbol{n}},\boldsymbol{r}',\hat{\boldsymbol{n}}') = \delta(\boldsymbol{r}-\boldsymbol{r}')\zeta(\boldsymbol{r},\hat{\boldsymbol{n}},\hat{\boldsymbol{n}}') \tag{3.19}$$

where

$$\zeta(\boldsymbol{r},\hat{\boldsymbol{n}},\hat{\boldsymbol{n}}') = \zeta_0 \times \begin{cases} 1, & \text{if} \boldsymbol{r} \in \mathbb{L} \text{ and } \boldsymbol{r}+\ell\hat{\boldsymbol{n}} \in \mathbb{L} \\ \text{ and } & \boldsymbol{r}+\ell\hat{\boldsymbol{n}}' \in \mathbb{L} \\ 0, & \text{otherwise} \end{cases} \tag{3.20}$$

and

$$\tilde{\zeta}(\boldsymbol{r},\hat{\boldsymbol{n}},\boldsymbol{r}',\hat{\boldsymbol{n}}') = \delta(\boldsymbol{r}-\boldsymbol{r}')\tilde{\zeta}(\boldsymbol{r},\hat{\boldsymbol{n}},\hat{\boldsymbol{n}}') \tag{3.21}$$

where

$$\tilde{\zeta}(\boldsymbol{r},\hat{\boldsymbol{n}},\hat{\boldsymbol{n}}') = \zeta_0 \times \begin{cases} 1, & \text{if } \boldsymbol{r}\in\mathbb{L} \text{ and } \boldsymbol{r}-\ell\hat{\boldsymbol{n}}\in\mathbb{L} \\ \text{and} & \boldsymbol{r}-\ell\hat{\boldsymbol{n}}'\in\mathbb{L} \\ 0, & \text{otherwise} \end{cases} \tag{3.22}$$

ξ embeds also the stiffness of the bonds and the correlations between the branched bonds orientations at branching points which we consider to be Gaussian. We choose ξ to be:

$$\xi(\boldsymbol{r},\hat{\boldsymbol{n}},\hat{\boldsymbol{n}}',\hat{\boldsymbol{n}}'') = \frac{\mathcal{N}_w}{\mathcal{N}_\xi} w(\hat{\boldsymbol{n}},\hat{\boldsymbol{n}}') \times e^{\left(-\xi_0\left(\hat{\boldsymbol{n}}\cdot\hat{\boldsymbol{n}}''-\cos\alpha\right)^2-\xi_1\left(\hat{\boldsymbol{n}}'\cdot\hat{\boldsymbol{n}}''-\cos\alpha\right)^2\right)}. \tag{3.23}$$

where α is the chosen branching angle depending on the chosen lattice, ξ_0 ,ξ_1 the junctions stiffness parameters. Our choice of the Boltzmann weight for the junctions is based on the bending rigidity between the filaments segment. However any other choices of Boltzmann weight can be made for the junctions.

With the knowledge of the grand canonical partition function we can now compute the average density distributions of filament segments composing the actin branching networks.

3.3 Average density distributions

Here we compute separately the average density distribution of chain segments that are involved only in linear chains $\varrho_z(\boldsymbol{r},\hat{\boldsymbol{n}})$ and the average density of chains segments of the network that are involved in junctions (branching points) $\varrho_j(\boldsymbol{r},\hat{\boldsymbol{n}})$. To calculate the average density of segments of the networks that are involved in junctions $\varrho_j(\boldsymbol{r},\hat{\boldsymbol{n}})$, we calculate first the average density of junction $\varrho_\zeta(\boldsymbol{r},\hat{\boldsymbol{n}})$. As previously defined in chapter 3, the average density distribution of:

- bonds that are not involved in the junction $\varrho_z(\boldsymbol{r},\hat{\boldsymbol{n}})$ is given by:

$$\varrho_z(\boldsymbol{r},\hat{\boldsymbol{n}}) = \frac{z(\boldsymbol{r},\hat{\boldsymbol{n}})}{\mathfrak{Z}}\frac{\delta\mathfrak{Z}}{\delta z(\boldsymbol{r},\hat{\boldsymbol{n}})} \tag{3.24}$$

  After taking the funtional derivative we have:

$$\varrho_z(\boldsymbol{r},\hat{\boldsymbol{n}}) = \frac{z(\boldsymbol{r},\hat{\boldsymbol{n}})}{\mathfrak{Z}}\Phi(\boldsymbol{r},\hat{\boldsymbol{n}})\Psi(\boldsymbol{r},\hat{\boldsymbol{n}}). \tag{3.25}$$

- junctions or branching points $\varrho_\zeta(\boldsymbol{r},\hat{\boldsymbol{n}})$ is:

$$\varrho_\zeta(\boldsymbol{r},\hat{\boldsymbol{n}}) = \frac{\zeta(\boldsymbol{r},\hat{\boldsymbol{n}}',\hat{\boldsymbol{n}}'')}{\mathfrak{Z}}\frac{\delta\mathfrak{Z}}{\delta\zeta(\boldsymbol{r},\hat{\boldsymbol{n}}',\hat{\boldsymbol{n}}'')} \tag{3.26}$$

  After taking the functional derivation of equation (3.14) (see Appendix Section A.1) for the derivation we have:

$$\varrho_\zeta(\boldsymbol{r},\hat{\boldsymbol{n}}) = \frac{\zeta(\boldsymbol{r},\hat{\boldsymbol{n}}',\hat{\boldsymbol{n}}'')}{\mathfrak{Z}}\Phi(\boldsymbol{r},\hat{\boldsymbol{n}})\Psi(\boldsymbol{r},\hat{\boldsymbol{n}}')\Psi(\boldsymbol{r},\hat{\boldsymbol{n}}'') \tag{3.27}$$

- bonds that are involved in the branching points $\varrho_j(\boldsymbol{r},\hat{\boldsymbol{n}})$ is given by:

$$\varrho_j(\boldsymbol{r},\hat{\boldsymbol{n}}) = 2\varrho_\zeta(\boldsymbol{r},\hat{\boldsymbol{n}}) \tag{3.28}$$

where two stand for the fact that we have two segments that emerge at each junction of the network. The total average density distribution of filament segments of the networks inside the confining cell is thus given by:

$$\varrho(\boldsymbol{r},\hat{\boldsymbol{n}}) = \varrho_z(\boldsymbol{r},\hat{\boldsymbol{n}}) + \varrho_j(\boldsymbol{r},\hat{\boldsymbol{n}}). \tag{3.29}$$

Using the obtained total density of filament segments of the network inside the confining domain, we calculate the order parameter field using equation 2.61 and 2.62 for respectively 3d and 2d networks enabling us to make quantitative prediction on the alignment of branching actin networks under geometrical confinement.
We can express the total density in terms of the monomers or bonds positions only as:

$$\varrho(\boldsymbol{r}) = \sum_{\hat{\boldsymbol{n}}} \varrho(\boldsymbol{r},\hat{\boldsymbol{n}}). \tag{3.30}$$

The average degree of polymerization $\langle N\rangle$ (the the total number of filaments segments inside the confined region) of the chains of the confined network is equal to the sum of number of bonds that are involved in junctions and the number of bonds that make up the linear chains. It is given by

$$\langle N\rangle = \sum_{\boldsymbol{r}} \varrho(\boldsymbol{r}) \tag{3.31}$$

In order to compute the grand canonical partition functions, the density distributions, the average number or degree of polymerisation of filaments and the order parameter fields for linear single semiflexible linear chain, for a composite of linear semiflexible chains and for branching actin networks, we have developed a numerical method that enabled us to implement and compute the resulting integral equations obtained above.

3.4 Numerical method

3.4.1 Description

We describe the numerical methods for modelling branching cytoskeletal networks (actin networks) of semiflexible polymer chains under confinement. The computation consist of solving recursively the non-linear integral equation (3.16) for the quantity $\Psi(\boldsymbol{r},\hat{\boldsymbol{n}})$ and the equation (3.17) for $\Phi(\boldsymbol{r},\hat{\boldsymbol{n}})$.
We model networks in two dimension and networks in three dimension since we are interested to the properties that are relevant to eukaryotic cells which include plant and animal cells. In fact generally plant cells have a very large vacuole which occupy most of the interior space of the cell and only a very small thin area is occupied by the cytoskeleton leading to the two dimensional

shape of the cytoskeleton [92], while the animal cells cytoskeleton present a 3d shape [93]. it is interesting to observe whether there are obvious differences between the properties of 2d and 3d networks.

We need a discrete monomer system in order to solve the non-linear integral equations given by equations (3.16) and equation (3.17). So we consider that the confined polymer chains that are formed live on the lattice where the chain segments occupy the lattice bonds.

The position and orientation of the chains segments are discretized in the lattice frame and thus the integral equations are solved self-consistently on the lattice.

Lattice model techniques are coarse-grained methods widely used in many polymer physics researches and simulations such as proteins folding simulations on lattices [94, 95], union/find algorithm, depth-first search or Monte Carlo simulation that are used in graph theory to construct binary trees, in percolation theory or for simulation of the random work of polymeric material [96]. In our case, there is no randomness, all possible configurations of networks that can be formed by the interaction between nearest neighbours on the lattice are counted.

To obtain two (2d) and three dimensional (3d) shapes of the cytoskeletal networks and to ensure that filament branching angle is in the range of experimental observation (between 58° and 78°) [90, 97], we choose to do the numerical implementations on 2d triangular lattice to obtain the 2d networks and on 3d triangular lattice for 3d cytoskeletal networks. We did the numerical implementation also on cubic-plus-diagonal lattice for 3d networks and obtained similar results.

3.4.2 Choice of the 2d and 3d lattices

3.4.2.1 2d triangular lattice

We consider a 2d triangular lattice model of $N \times N$ sites. 2d triangular lattice has the coordination number equal to 6 and is thus more favourable to maximize a 2d shape for the confining region. Each bond of the lattice has 6 possibles orientations to their nearest-neighbour. The monomers or bonds of the chains occupy the lattice bonds and are confined inside a finite geometrical region. The discrete linkage between bonds to form confined polymer chains is controlled by the activity or fugacity z_0 which controls also the confining geometry of the chains. The excluded volume effect on monomers is neglected. So, each monomer or bond of the chains does not see each other and they have six possible orientations or directions on the two triangular lattices.

A 2d triangular lattice allows also branching of filaments at 60° angle which is in the range of the angles of branching via Arp2/3 protein complex inside the real living cells with optimal branching at 70°.

In order to localise the nearest neighbour positions we need to know the lattice basis units vectors and the integer coordinates of the lattice sites or points. In 2d triangular lattice with unit length between nearest neighbour monomers, the integers coordinates of the nearest neighbours of a lattice point $P = (X, Y)$ are:$(X + 1, Y)$, $(X - 1, Y)$,$(X, Y + 1)$,$(X, Y - 1)$,$(X - 1, Y + 1)$

$,(X+1,Y-1)$.
This means that the nearest neighbours of the site at the position $(X,Y)=(0,0)$ are $(1,0)$, $(-1,0)$, $(0,1)$, $(0,-1)$, $(1,0)$,$(-1,1)$, $(1,-1)$.
The geometrical basis unit vectors are:

$$\begin{cases} \hat{x} = \pm(1,0) \\ \hat{y} = \pm(\frac{1}{2}, \frac{\sqrt{3}}{2}) \\ \hat{w} = \pm(\hat{y}-\hat{x}) = \pm(-\frac{1}{2}, \frac{\sqrt{3}}{2}) \end{cases}, \tag{3.32}$$

leading to the geometrical position P of any monomer or bonds $(\overrightarrow{OP})$ on the 2D triangular lattice is given by:

$$\overrightarrow{OP} = (X_g, Y_g) = X\hat{x} + Y\hat{y}. \tag{3.33}$$

where X, $Y \in \mathbb{Z}$. One can consider using rather the hexagonal packing geometrical coordinates given by:

$$(X_g, Y_g) = (X, \frac{\sqrt{3}}{2}Y) \quad \texttt{for} \quad Y \quad \text{even.} \tag{3.34}$$

$$(X_g, Y_g) = (X + \frac{1}{2}, \frac{\sqrt{3}}{2}Y) \quad \text{for} \quad Y \quad \text{odd.} \tag{3.35}$$

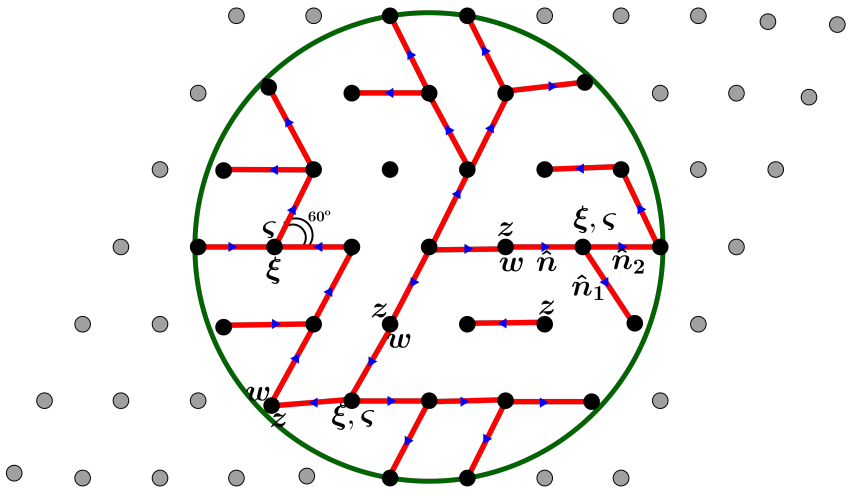

Figure 3.10: *example of configuration of branching network on 2d triangular lattice. We have the lattice sites that are in the confining domain in black and those out of the confining domain in grey. The polymer chain bonds are in red and their orientation in blue.*

3.4.2.2 3d triangular lattice

We consider the 3d triangular lattice with a size $N \times N \times N$ sites on which we form the three dimensional networks. Each lattice point have 12 nearest-neighbours. This high coordination

number enable to maximize the approximation of a 3d space. The monomers or bonds of the chains occupy the lattice bonds. So each monomer of the chain has 12 possible directions. The 3d triangular lattice is formed of layers of square lattices in parallel planes and is formed by a closest cubic packing of spheres [94]. The 3d triangular lattice is obtained by considering the two primary unit vectors $\hat{x}$ and $\hat{y}$ specifying the x and y axes of each square lattice and adding to them a primary axis along a unit vector $\hat{z}$ which is at an angle of $2\pi/3$ from both x and y. The distance between two adjacent planes is $\sqrt{2}/2$. These planes support two consecutive layers of square lattices. The three dimensional triangular lattice ensure the same distance between nearest-neighbours and beside the fact that this 3d lattice give good approximation of the 3d shape, it also allows to mimic the branching of actin filaments at 60° angle.
We have 6 basis unit vectors $\hat{x}, \hat{y}, \hat{z}, \hat{u}, \hat{v}, \hat{w}$ on the 3d triangular lattice which are defined as

$$\begin{cases} \hat{x} = \pm(1,0,0) \\ \hat{y} = \pm(0,1,0) \\ \hat{z} = \pm(-\frac{1}{2}, -\frac{1}{2}, \frac{\sqrt{2}}{2}) \\ \hat{u} = \pm(\hat{x}+\hat{z}) = \pm(\frac{1}{2}, -\frac{1}{2}, \frac{\sqrt{2}}{2}) \\ \hat{v} = \pm(\hat{y}+\hat{z}) = \pm(-\frac{1}{2}, \frac{1}{2}, \frac{\sqrt{2}}{2}) \\ \hat{w} = \pm(\hat{x}+\hat{y}+\hat{z}) = \pm(\frac{1}{2}, \frac{1}{2}, \frac{\sqrt{2}}{2}) \end{cases} . \tag{3.36}$$

Each lattice point position P on the lattice is represented by its integer coordinates (X, Y, Z) where $X, Y, Z \in \mathbb{Z}$ and the integer coordinates of the nearest neighbours of P are:

$$\{(X \pm 1, Y, Z), \quad (X, Y \pm 1, Z), \quad (X, Y, Z \pm 1), \\ (X \pm 1, Y, Z \pm 1), \quad (X, Y \pm 1, Z \pm 1), \quad (X \pm 1, Y \pm 1, Z \pm 1)\} \tag{3.37}$$

The nearest neighbours of the origin $(X, Y, Z) = (0, 0, 0)$ for example are:

$$\begin{cases} \pm(1,0,0), \quad \pm(0,1,0), \quad \pm(0,0,1), \\ \pm(1,0,1), \quad \pm(0,1,1), \quad \pm(1,1,1) \end{cases} \tag{3.38}$$

The corresponding cartesion position vector of P from the origin of the lattice O is given by:

$$\overrightarrow{OP} = (X_c, Y_c, Z_c) = X\hat{x} + Y\hat{y} + Z\hat{z}. \tag{3.39}$$

meaning that:

$$\begin{cases} X_c = X - \frac{1}{2} \\ Y_c = Y - \frac{1}{2} \\ Z_c = \frac{Z}{\sqrt{2}} \end{cases} \tag{3.40}$$

3.4.2.3 Algorithm

The two chemical potential fields z and ζ (z associated to actin monomers and responsible for filaments elongation and ζ associated to Arp2/3 protein and responsible for branching) ensure respectively the elongation and the branching of the polymer filaments. Each monomer of the chains occupy the lattice bonds with size the unit length of the lattice. Bonds are oriented in any of the possible directions of the lattice (6 possible directions on 2d triangular lattice, 12 on 3d triangular lattice and 14 possible direction on the cubic-plus-diagonal lattice) and this allow monomers to connect successively with their nearest neighbour in particular orientation and form directed filaments. Monomers that are in the confining region can branch on existing linear filaments at 60° angle and form tree-like structure without loop. We show an example of network configuration in Figure 3.10.

The knowledge of the position of each monomer or bonds on the lattice and of the basis minimal vectors helps to convert the integer lattice into Cartesian coordinates. We define a confining region $\mathbb{L}$ that have a size D, on the lattice which we compare with the persistence length ℓ_{p} of actin filament. All the essential parameters such the fugacity, the Boltzmann weight associated to the bond bending and the one associated to junctions are computed. Only monomers that are inside the confining region are activated. The possible bond orientations or basis vectors allow us to check whether the new bonds that connect to a polymer chains is inside the confining region or not.

The fugacities $z(\boldsymbol{r},\hat{\boldsymbol{n}})$ and $\zeta(\boldsymbol{r},\hat{\boldsymbol{n}}_1,\hat{\boldsymbol{n}}_2)$ associated, respectively, to filaments elongation and branching controls the spherical region boundary limit. This limit is obtained by setting the fugacities to 0 for filament length $L \geq D$ and this is translated into the following boundary conditions:

$$z(\boldsymbol{r},\hat{\boldsymbol{n}}) = z_0 \times \begin{cases} 1, & \text{if } \boldsymbol{r} \in \mathbb{L} \text{ and } \boldsymbol{r} + \ell\hat{\boldsymbol{n}} \in \mathbb{L} \\ 0, & \text{otherwise} \end{cases} \tag{3.41}$$

and

$$\tilde{z}(\boldsymbol{r},\hat{\boldsymbol{n}}) = z_0 \times \begin{cases} 1, & \text{if } \boldsymbol{r} \in \mathbb{L} \text{ and } \boldsymbol{r} - \ell\hat{\boldsymbol{n}} \in \mathbb{L} \\ 0, & \text{otherwise} \end{cases} \tag{3.42}$$

$$\zeta(\boldsymbol{r},\hat{\boldsymbol{n}}_1,\hat{\boldsymbol{n}}_2) = \zeta_0 \times \begin{cases} 1, & \text{if } \boldsymbol{r} \in \mathbb{L} \text{ and } \boldsymbol{r} + \ell\hat{\boldsymbol{n}}_1 \in \mathbb{L} \\ \text{and} & \boldsymbol{r} + \ell\hat{\boldsymbol{n}}_2 \in \mathbb{L} \\ 0, & \text{otherwise} \end{cases} \tag{3.43}$$

and

$$\tilde{\zeta}(\boldsymbol{r},\hat{\boldsymbol{n}}_1,\hat{\boldsymbol{n}}_2) = \zeta_0 \times \begin{cases} 1, & \text{if } \boldsymbol{r} \in \mathbb{L} \text{ and } \boldsymbol{r} - \ell\hat{\boldsymbol{n}}_1 \in \mathbb{L} \\ \text{and} & \boldsymbol{r} - \ell\hat{\boldsymbol{n}}_2 \in \mathbb{L} \\ 0, & \text{otherwise} \end{cases} \tag{3.44}$$

We check if $\boldsymbol{r} - \boldsymbol{r}_c$ and $\boldsymbol{r} + \ell\hat{\boldsymbol{n}} - \boldsymbol{r}_c$ are positions inside the confining region then the fugacities are different of 0. $\boldsymbol{r}_c$ is the position of the center of the sphere.

We proceed by solving recursively the non-linear integral equation (3.16) and equation (3.17). To start the recursion, we assign initial guesses to Ψ and Φ which we call respectively Ψ_0 and Φ_0 living on the lattice. Ψ_0 and Φ_0 are function of position $\boldsymbol{r}$ and direction $\hat{\boldsymbol{n}}$. $\hat{\boldsymbol{n}}$ can be any the 6 directions if it on 2d triangular lattice or one of the 12 directions if 3d triangular lattice and $\boldsymbol{r}$ is any geometrical monomer point position on the defined lattice.
Either we have no bond, i.e no filament formation, and then $\Psi(\boldsymbol{r},\hat{\boldsymbol{n}})$ and $\Phi(\boldsymbol{r},\hat{\boldsymbol{n}})$ are set to 1 or bonds are formed and then $\Psi(\boldsymbol{r},\hat{\boldsymbol{n}})$ and $\Phi(\boldsymbol{r},\hat{\boldsymbol{n}})$ are locally calculated as follow.

- Calculation of new Ψ on the lattice:

Ψ is calculated at each position $\boldsymbol{r}$ and orientation $\hat{\boldsymbol{n}}$. The filaments can grow from any monomer point of the lattice as long as this monomer is inside the confining region. So a Monomer at position $\boldsymbol{r}$ connect with a monomers at position $\boldsymbol{r}_1 = \boldsymbol{r} + \ell\hat{\boldsymbol{n}}$ where ℓ is the lattice unit length and we choose to set it to 1. $\hat{\boldsymbol{n}}$ is one of the 6 (2d triangular lattice), 12 (3d triangular lattice) or possible directions. The monomer or bond at positions $\boldsymbol{r}_1$ and orientation $\hat{\boldsymbol{n}}_1$ branches with with the bond at position $\boldsymbol{r}_1$ and orientation $\hat{\boldsymbol{n}}_2$ on the lattice and form a tree-like filament or a junction. Each of the monomers then reaches respectively the monomers or bonds at positions $\boldsymbol{r}_2$ and $\boldsymbol{r}_3$. We write this description as follow:

$$\rightarrow \boldsymbol{r}_1 \begin{cases} \nearrow \boldsymbol{r}_2 = \boldsymbol{r}_1 + \ell\hat{\boldsymbol{n}}_1 \\ \searrow \boldsymbol{r}_3 = \boldsymbol{r}_1 + \ell\hat{\boldsymbol{n}}_2. \end{cases} \tag{3.45}$$

A new Ψ on the lattice as function of position $\boldsymbol{r}$ and direction $\hat{\boldsymbol{n}}$ is then computed itteratively. For the first iteration (iteration=1) we have:

$$\begin{aligned} \Psi(\boldsymbol{r},\hat{\boldsymbol{n}}) = 1 &+ \sum_{\hat{\boldsymbol{n}}_1} w_0(\hat{\boldsymbol{n}},\hat{\boldsymbol{n}}_1) z(\boldsymbol{r},\hat{\boldsymbol{n}}_1) \Psi_0(\boldsymbol{r}_1,\hat{\boldsymbol{n}}_1) \\ &+ \sum_{\hat{\boldsymbol{n}}_1}\sum_{\hat{\boldsymbol{n}}_2} \xi(\hat{\boldsymbol{n}},\hat{\boldsymbol{n}}_1,\hat{\boldsymbol{n}}_2)\zeta(\boldsymbol{r},\hat{\boldsymbol{n}}_1,\hat{\boldsymbol{n}}_2)\Psi_0(\boldsymbol{r}_2,\hat{\boldsymbol{n}}_1)\Phi_0(\boldsymbol{r}_3,\hat{\boldsymbol{n}}_2). \end{aligned} \tag{3.46}$$

Then, the solution for quantity Ψ for all networks configuration on the lattice is obtained. and we check if the obtained solution converge. The convergence criterion is that $\frac{|\Psi-\Psi_0|}{\Psi}$ must approach some small number (typically we choose 10^{-6}). If the convergence criteria is not satisfied, the newly calculated Ψ become the old Ψ and then the iteration continues until we get a convergent solution for Ψ.

- The computation of $\Phi(\boldsymbol{r},\hat{\boldsymbol{n}})$ is similar to the computation of $\Psi(\boldsymbol{r},\hat{\boldsymbol{n}})$ with a minor difference:

In the current case the monomers binding and branching works as follow:

$$\boldsymbol{r} \rightarrow \boldsymbol{r}_1 \quad = \quad \boldsymbol{r} - \ell\hat{\boldsymbol{n}} \tag{3.47}$$

$$\rightarrow \boldsymbol{r}_1 \begin{cases} \nearrow \boldsymbol{r}_2 = \boldsymbol{r}_1 + \ell\hat{\boldsymbol{n}}_1 \\ \searrow \boldsymbol{r}_3 = \boldsymbol{r}_1 - \ell\hat{\boldsymbol{n}}_2. \end{cases} \tag{3.48}$$

And then calculate $\Phi(\boldsymbol{r}, \hat{\boldsymbol{n}})$ for the first itteration as:

$$\Phi(\boldsymbol{r}, \hat{\boldsymbol{n}}) = 1 + \sum_{\hat{\boldsymbol{n}}_1} w_0(\hat{\boldsymbol{n}}, \hat{\boldsymbol{n}}_1)\tilde{z}(\boldsymbol{r}, \hat{\boldsymbol{n}}_1)\tilde{\Psi}_0(\boldsymbol{r}_1, \hat{\boldsymbol{n}}_1) + \sum_{\hat{\boldsymbol{n}}_1}\sum_{\hat{\boldsymbol{n}}_2} \xi(\hat{\boldsymbol{n}}, \hat{\boldsymbol{n}}_1, \hat{\boldsymbol{n}}_2)\tilde{\zeta}(\boldsymbol{r}, \hat{\boldsymbol{n}}_1, \hat{\boldsymbol{n}}_2)\Psi_0(\boldsymbol{r}_2, \hat{\boldsymbol{n}}_1)\Phi_0(\boldsymbol{r}_3, \hat{\boldsymbol{n}}_2). \tag{3.49}$$

Here also, the equation is iterated until we get the convergent solution for Φ.
After obtaining the convergent solution for Ψ and Φ, we compute the grand partition function, the spatial density distributions and the nematic order field for different type of networks, typed according to their stiffness and their structures.

3.5 Conclusion

Actin filaments are the most abundant of the cell cytoskeleton. They self-organise into a varieties of high order structures in order to insure the cell mechanical stability. One of these high order structure is the branching actin networks obtained via the Arp2/3 proteins complex which span the internal space of the cell with specific orientational alignment and allows the cell to deform its shape in order to probe its environment or to move. However the structure, spatial organization and ordering is strongly correlated to the effect of confinement that the cell membrane introduce. This correlation is not very well explored and understood especially for branching actin networks. It has been the aim of this chapter to develop a model and a numerical tool in order to investigate and quantify the effect of confinement on the actin networks structure and properties.
We have extended the grand canonical monomer ensemble formalism to branching semiflexible cytoskeletal networks in confining regions. Using this formalism we have been able to define a grand canonical partition function for the networks with parameters that mimic the the formation of linear filaments and the branching mechanism. We have conveniently defined non-linear integral equations relating the quantities Ψ and Φ to the grand canonical partition that we have defined. We used the grand canonical canonical partitions function to derive the expressions for the density, number and order distributions of filament segments and junctions. We found that the densities are also dependent of the quantities Ψ and Φ. We have next introduce a computational technique that enabled us to solve self-consistently the non-linear integral equations. We used the numerical solutions for Ψ and Φ to compute the grand canonical partition function, densities, the average number of polymerisation and the order parameter fields.

In the chapter that follows, we discuss the results and make quantitative predictions of the effect of confinement on the behaviour, structure, orientational ordering, conformation and spatial organization of branching actin cytoskeletal networks (under cellular confinements).

Chapter 4

Densities profiles and ordering of filaments of branching actin networks in confining cells

4.1 Introduction

In this chapter we present the results of our models for branching actin cytoskeletal networks confined in finite geometrical regions in the absence of excluded volume effect between filament segments. We neglect also the interactions between the chains and the confining region. The results consist of the profiles of the density distributions of networks filaments segments, their polarisations, the radial order parameter fields of these filaments and their degree of polymerisation inside the confining regions, which results we obtained from numerical computation.

The density is one of the physical measures that allows the quantification of the concentration of physical structures inside a geometrical region. It is often used in equilibrium polymer physics to measure the local average distribution and the number or degree of polymerization of confined polymers filaments relatively to the confining membrane surface allowing to investigate the change in their structure, conformation and their physical properties under the effect of the confining region boundary [1, 2, 98, 99]. The conformation and structure of growing actin branching filamentous networks are often controlled or constrained by the cell geometrical boundary because living cells sizes and the persistence length of actin filaments are of the same order of magnitude [45, 46, 49, 92, 100]. Many theoretical studies and coarse-grained computer simulations have been conducted to investigate the effects of confinement on the behaviour, conformations and properties of individual or networks of linear semiflexible polymers [13, 40, 54, 57, 101–104] and these studies have been very useful for understanding some of the physical properties and behaviour of linear actin filaments and other semiflexible biopolymers (such as DNA and microtubules) under cellular confinement. Experimental studies on animal

living cells using super-resolution microscopy enabled to investigate the density distribution of actin filaments relative to the cell membrane [93, 98, 99]. Joanny *et al.* [99] calculated the density profiles and showed that filaments of actin networks are asymmetrically distributed inside the cell with a high density close to the cell membrane making up the actin cortex [99]. Other autors reported also that long semiflexible filaments and thus actin networks made up of long linear actin filaments are under a strong confinement effect due to the finite size of the cell[13, 34, 73]. However cell cytoskeletal actin filaments are found in higher order structures inside the cell. Imaging of the interior of living eukaryotic cells using electron and fluorescence microscopy has shown a highly branched and dense actin structures in the vicinity of the cell membrane [34, 85, 86, 105–107]. But for our knowledge there is no model that has been developed to explore quantitatively the effects of cell membrane confinement on the structure, the spatial organization and ordering of branching actin networks (with branching occuring via the Arp2/3 protein complex) in thermodynamics equilibrium.

When polar or oriented semiflexible chains or their networks are confined inside a sphere of size much smaller than their persistence length, they locally arrange themselves into orientationally ordered structures [13, 41, 108]. The knowledge of the average density and order parameter field profiles of the segments of branching actin networks confined in a finite region with size comparable to the persistence length of actin filaments can allow us to quantify the effect of confinement on these actin networks with regard to their topologies or architecture.

In our model we are able to construct different types of networks of semiflexible (actin) filaments by varying the parameters z and ζ corresponding to networks dominated by short actin filaments, networks dominated by long linear actin filaments and branched networks by varying the parameters z and ζ. We implement the model numerically with the numerical method presented in section 4 of Chapter 3. The numerical implementation permit to compute the density distributions and the order parameter fields of the segments of filaments that make them up the branching actin networks confined in cells with various geometries. We also calculate also the average degree of polymerisation of filaments and the polarization profiles of the networks. To facilitate the numerical implementation, we choose to confine the branching actin networks inside cell that have symmetric geometries such as cell with spherical shape, cubic shape, square or equilateral triangle shape (for 2d networks) and then measure the profiles of the networks in these various geometries. However we focus on the results for networks confined in spherical cells that have rigid walls.

In the second section of the present chapter, we define the domain of validity of our model. It corresponds to domain in which our numerical results are still convergent even in the absence of the confinement effects on the networks. We next present in the third section the results of the radial order parameter fields, average density profiles and the degree of polymerization of

actin chain segments of the different confined structural networks that we have modelled. To investigate how the confined branching actin networks respond to any kind of perturbation, we introduce an external field in the system analogous to the magnetized system. The result of this is presented in the fourth section. Finally we conclude

4.2 Domain of validity of the model

We make sure that our model and numerical results are still valid in the absence of confinement by defining a domain of validity that corresponds to the limit beyond which the numerical results or solutions for unconfined semiflexible or actin filaments networks of the model diverge. For a network free of any confinement constraint, the centre of mass of the network is translationally and rotationally invariant. Ψ and Φ are in this case not dependant of the position and orientation vectors, $\boldsymbol{r}$ and $\hat{\boldsymbol{n}}$ which means Ψ and Φ are constant. Using the normalized discrete equations (3.46) and (3.49), we see that the constant values of Ψ_0 and Φ_0 must satisfy

$$\Psi_0 = 1 + z_0\Psi_0 + \zeta_0\Psi^2 \tag{4.1}$$

$$\Phi_0 = 1 + \tilde{z}_0\Phi_0 + \tilde{\zeta}_0\Psi_0\Phi_0 \tag{4.2}$$

The existence of the solutions is obtained only for values of ζ_0 and z_0 for which the discriminant of equation (4.1) is positive

$$(1 - z_0)^2 \geq 4\zeta_0 \tag{4.3}$$

This condition applies also for the equation (4.2).
The single physical solution of that quadratic equation is

$$\Psi_0 = \frac{1}{2\zeta_0}\left(1 - z_0 - \sqrt{(1-z_0)^2 - 4\zeta_0}\right) \text{ and} \tag{4.4}$$

$$\Phi_0 = \frac{1}{1 - z_0 - \zeta_0\Psi_0}. \tag{4.5}$$

The densities of filaments and branches in unconfined conditions where the chain segments are growing and branching on a lattice of sites N is then defined as:

$$\varrho_{0,\mathrm{f}} = \frac{n_\mathrm{d} z_0 \Psi_0 (1 + \Psi_0)}{1 + n_\mathrm{d} z_0 N \Psi_0} \tag{4.6}$$

which leads to the number of filaments and branches as

$$N_{0,\mathrm{f}} = 1 + \Psi_0 \tag{4.7}$$

$$N_{0,\mathrm{b}} = \frac{\zeta_0}{z_0} n_\mathrm{d}^2 \Psi_0^2 \tag{4.8}$$

Obtaining the domain of the validity allows us to make the best choice of ζ_0 and z_0 values for the numerical computation. We thus use ζ_0 and z_0 values that fall in the domain defined by equation (4.3). So the results we obtain are within the defined domain.
In the following section we show the results and make predictions on the physical properties and structural behaviour of networks that can be formed in the validity domain that we defined.

4.3 Result and discusions

We model two (2d) and three dimensional (3d) branching actin networks confined in a spherical cell. Let us recall the modelling method and the important parameters that we use to build our model.

The network chains and branching point occupy a 2d triangular lattice for 2d networks and a 3d triangular lattice for 3d networks. The network segments are the same size and equal to one lattice bond length which we choose to be 1. The spherical confining cell with diameters D comparable to the persistence length of actin filaments is thus defined in the lattice frame. Figure 4.1 shows the profile of the spherical confining region in the absence of any chain. The typical persistence length of an unconfined actin filament is ($\ell_{\rm p} \sim 17.7\mu$m) [45]. We choose the confining region diameter such that $\ell_{\rm p}/D \sim 17.7/D \sim 1.2$. We define the confining region such that the ratio $\ell_{\rm p}/D \sim 1.2$ (stiff networks). In our model the persistence length of a filament is expressed in term of the bending energy between adjacent bonds of the filaments. So we confine the 2d networks in spherical cell with the ratio $\ell_{\rm p}/D = 60/50 \sim 1.2$ and the corresponding bending modulus used in Boltwmann weight factor associated to the bending stiffness between chain segments (2.41) is $\varepsilon = 8.15/k_{\rm B}T$. For 3d networks we choose the ratio $\ell_{\rm p}/D = 30/25 \sim 1.2$ and the corresponding value of ε is $8.124/k_{\rm B}T$. We set the parameter ξ_0 and ξ_1 used in the equation (3.23) defining the Boltzmann weight associated to branching points equal to 1. The chemical potential field parameter z_0 associated to actin monomer activities, acts as an external field on chain segments and ensure the linear chain elongation as it increases in one hand and on the order hand it creates the confining effect on the networks and thus control the geometry of the confining region. In the meanwhile under the action of the fugacity ζ_0 associated to the binding proteins (Arp2/3 protein complex), new filaments can grow branching off from existing one, at 60° angle and as we increases the value of ζ_0, the confined linear chains become more and more branched thus forming a branched network. Therefore we can vary ζ_0 and z_0 in order to grow networks with various structures and architectures. From here the average density distribution of segments and branching points, the degree of polymerization and the radial order parameter field of confined branching semiflexible chain can be determined to describe the branching actin network behaviour, the conformation of chains making up the networks, their spatial organisation, orientational ordering and thus the networks equilibrium properties.

4.3.1 Density profiles

To investigate the effect that the confining cell membrane or wall has on the structural properties of confined branching networks, we compute the total density as function of the polymer segments (monomers) local positions $\boldsymbol{r}$ ($\boldsymbol{r} = (x, y)$ for 2d networks and $\boldsymbol{r} = (x, y, z)$ for 3d) inside the confining domain following the self-consistent numerical scheme that we describe in section 3.4.1 of Chapter 3 of this thesis. Recall that we recursively solve the non-linear inte-

gral equation for $\Psi(\boldsymbol{r},\hat{\boldsymbol{n}})$ and $\Phi(\boldsymbol{r},\hat{\boldsymbol{n}})$ (equations (3.46) and (3.49)) in a self-consistent manner and we use their convergent solution to compute relevant quantities including the total density $\varrho(\boldsymbol{r}) = \sum_{\hat{\boldsymbol{n}}} \varrho(\boldsymbol{r},\hat{\boldsymbol{n}})$ where $\varrho(\boldsymbol{r},\hat{\boldsymbol{n}})$ is the probability or a density of finding a chain segment at a position $\boldsymbol{r}$ and orientation $\hat{\boldsymbol{n}}$ inside the confining region and is given by equation (3.29). The average density of filament segments of the networks inside the confining domain is normalised and summed to obtain the average number or degree of polymerisation of filament segments $\langle N\rangle$ given by $\langle N\rangle = \sum_{\boldsymbol{r}} \varrho(\boldsymbol{r})$.

The variation of z_0 and ζ_0 allow to obtain different type of confined networks of filaments, different in term of their structures. As we vary the two parameters value, we can grow a network dominated by short linear filaments of length $L = \langle N\rangle < D$ with few branching, a network dominated by long linear filaments of length $L > D$ with few branching, a networks with comparable length scales which constituted of linear filaments of length $L \sim D \sim \ell_{\mathrm{p}}$ with significant number of branching points or a branched networks which is obtained for a large enough values of z_0 and ζ_0 such that $(1 - z_0)^2 \sim 4\zeta_0$.

We thus do the computation and present the profiles for four types of networks that we describe above. Each of these networks is modelled in 2d and 3d triangular lattices and confined in spherical cell with rigid membrane or wall. The numerical results show distinct differences between the density distribution profiles of filament segments of these different networks. However the results for networks modelled in 2d and 3d are similar.

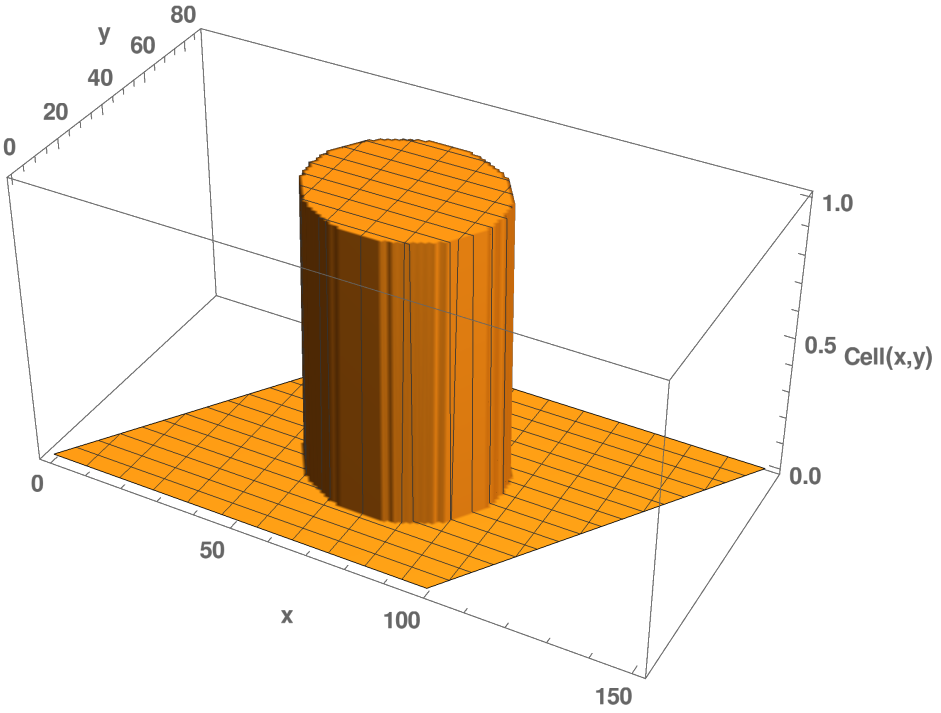

Figure 4.1: Profile of the circular confining region in the absence of any actin polymer chain.

4.3.1.1 2d networks

Networks dominated by short linear filaments ($L < D$)

We present here the profiles of the average density of filament segments of the network dominated by short linear chains modelled on two dimensional lattice. It is obtained for ζ_0 close to zero and small z_0 ($(1 - z_0)^2 > 4\zeta_0 \sim 0$). Figure 4.2 and Figure 4.3 are the three dimensional plots of the density profiles. We plot the three dimensional shape to show the shape of the spherical cell while confining a specific type of network.

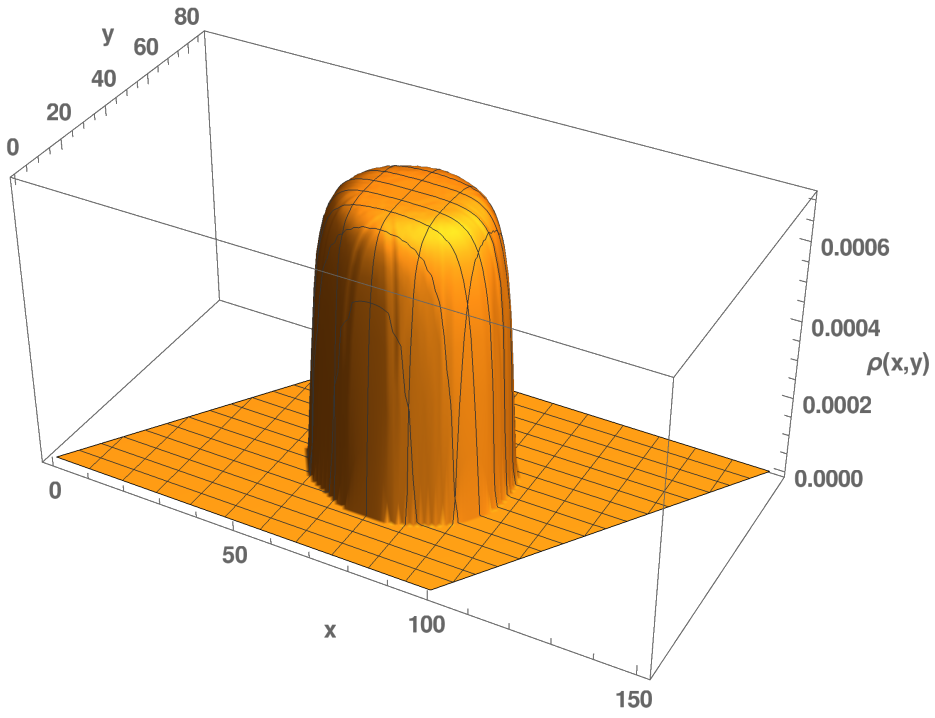

Figure 4.2: The graph is the three dimensional plot of the density profile of the actin networks dominated by short filaments ($L < D$) with little branching confined in sphere. This type of network is modelled in 2d and obtained for growth or chain elongation parameter $z_0 = 0.5$ values, and for the branch formation parameter $\zeta_0 = 0.001$. We observe a convex-shaped density distribution of the chain segments with a plateau towards the middle of the sphere.

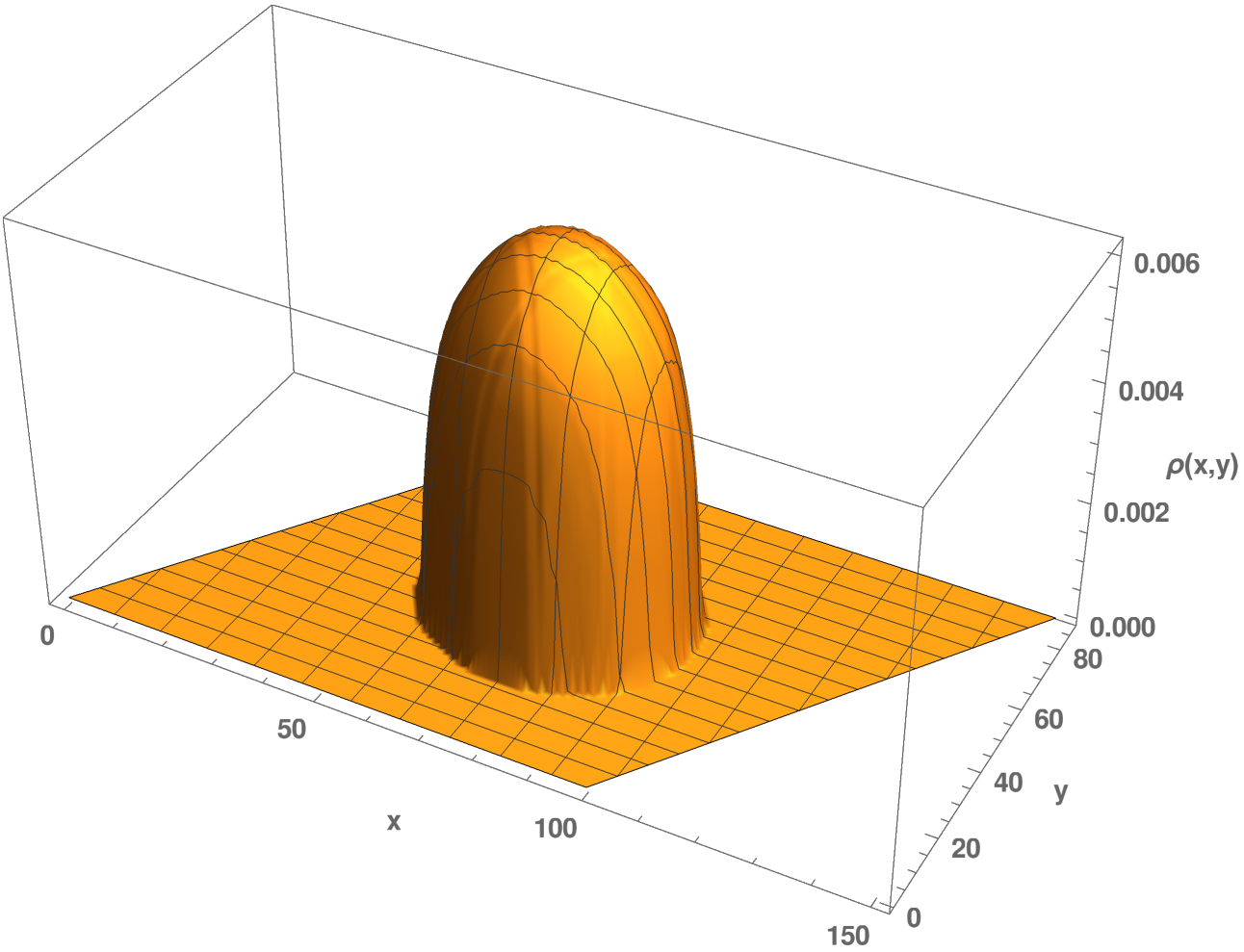

Figure 4.3: Three dimensional plots of the density profiles of network segments for $\zeta_0 = 0.001$ and values, $z_0 = 0.6$. Here we still have the networks dominated by short filaments ($L < D$). However the filaments are longer and a high concentration of chain segments is observed in the middle of the sphere (higher than the one we have obtained in Figure 4.2). We observe a distribution of filament segments with higher density in the centre of spherical confining cell.

We can see more clearly the distribution of the chain segments of the networks by plotting its density profile through the centre of the sphere. Figure 4.4 and Figure 4.5 are the profiles of the networks through the centre of the sphere. Because we have a symmetric confining region, the plots in x, y or z direction of the density profiles for networks modelled on 2d or 3d triangular lattices are the same.

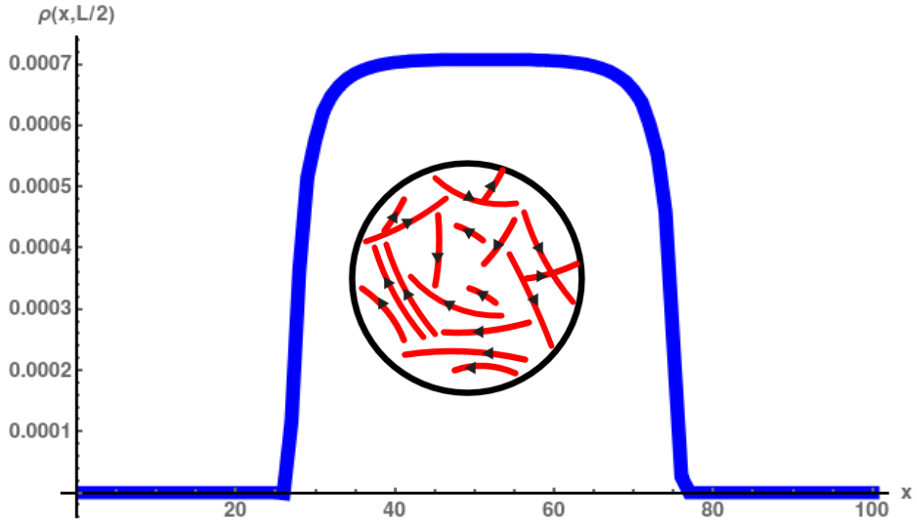

Figure 4.4: Plot of the densty profile of segments through the centre of the sphere in x direction of the network dominated by short linear filaments ($L < D$) modelled on 2d triangular lattice. The filaments elongation and branching parameter values are $z_0 = 0.5$ and $\zeta_0 = 0.001$. The inset is a cartoon representing the spherical geometry confining the network of actin filaments in red on the graph and it is there to illustrate the type of the networks for which the this density profile is obtained.

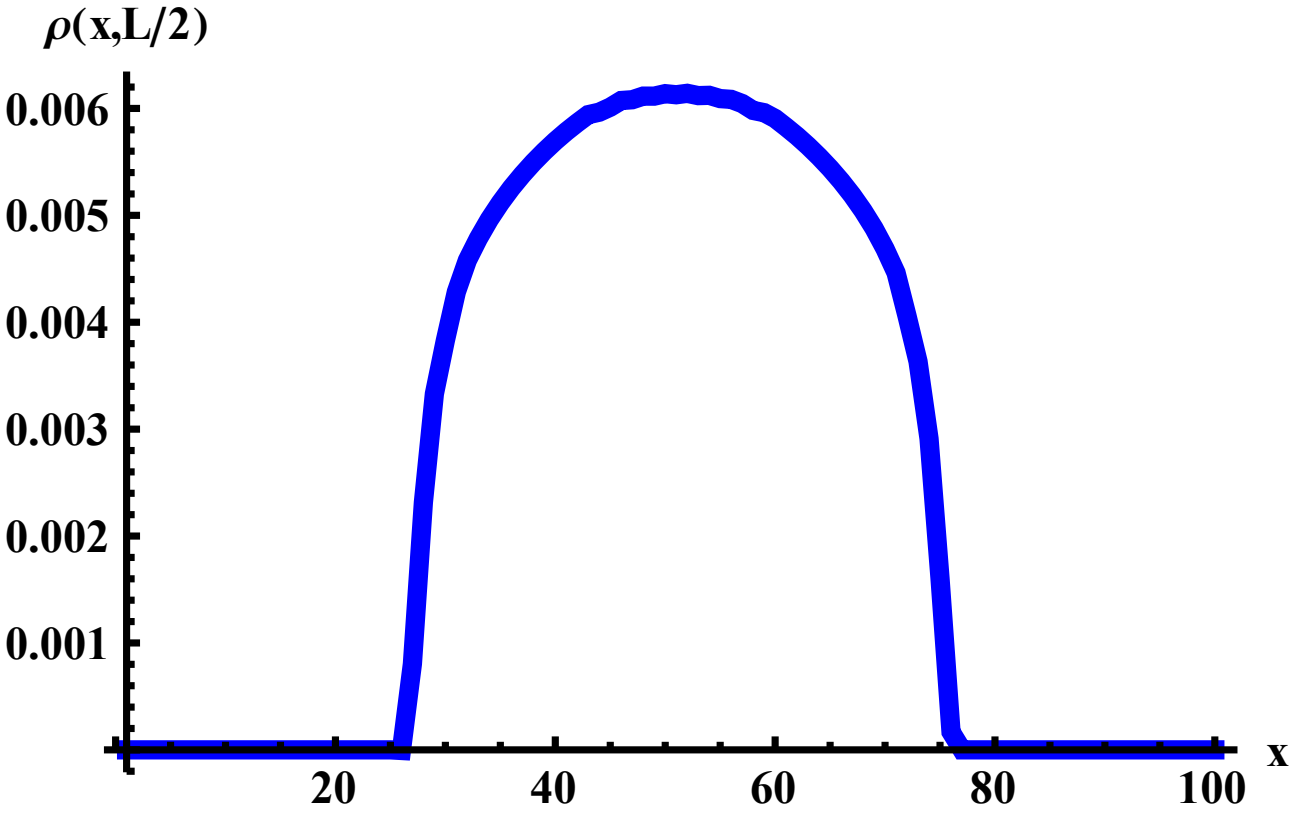

Figure 4.5: Plot of the densty profile of segments throught the centre of the sphere in x direction of the network dominated by short linear filaments ($L < D$) modelled on 2d triangular lattice. The profile of the network we show is obtained for filaments elongation and branching parameter values $z_0 = 0.6$ and $\zeta_0 = 0.001$.

The density profiles of confined networks dominated by short filaments show that the filaments are much denser towards the centre of the sphere. This is explained by the fact that for semiflexible polymers or for actin filament shorter than the confining sphere diameter ($L < D$), most chain or chain segments move toward the centre of the sphere to seek more available volume to orient and translate comfortably and thus maximize their number of accessible conformations [41, 54, 55, 61]. Consequently, the structure and spatial organisation of network of short actin filaments are weakly influenced by the confining effect that the cell membrane introduce [43, 55, 75, 103] .

The networks with comparable length scales ($L \sim D \sim \ell_{\mathbf{p}}$)

The networks with comparable length scales are formed at points (ζ_0 , z_0) values for which most of the linear filaments are either of length comparable to the size of the confining region $L \sim D \sim \ell_{\mathrm{p}}$ or the branching become significant. At these points, we start observing a small indent in the middle of the profile suggesting a decrease of the number of segments in the middle of the sphere leading to inhomogeneities in the density distribution of network segments, see Figure 4.6 for three dimensional plots of the density profile and 4.7 for the profile of the segments of the networks with comparable length scales through the middle of the sphere. For our model, the inhomogeneous distribution stands for the high distribution of filament or filament segments of the actin networks at the vicinity of the confining cell membrane or wall while low near the center of the confining cell.

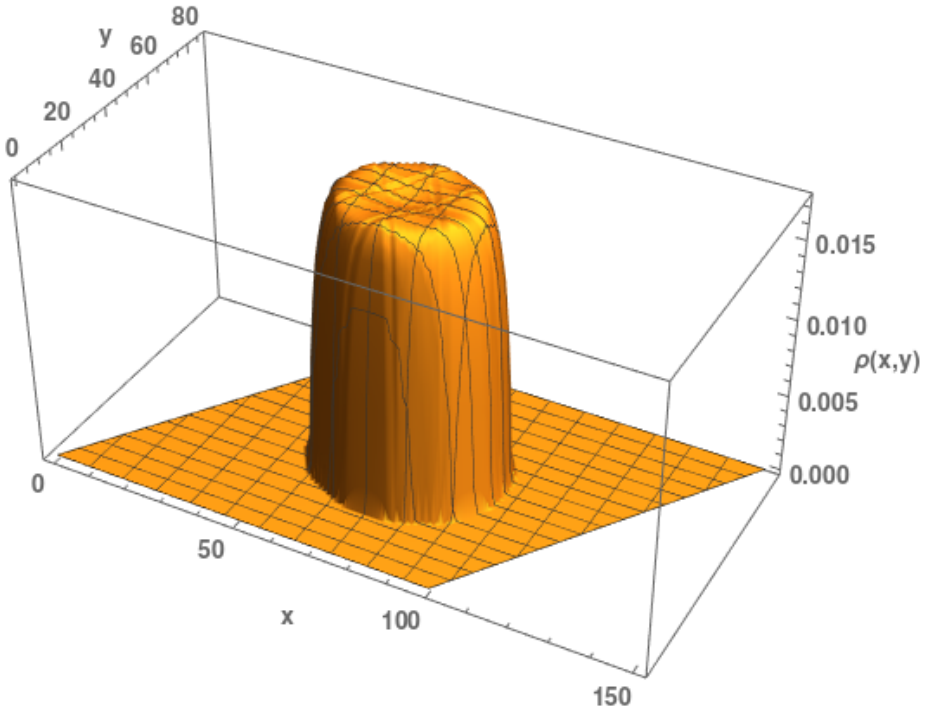

Figure 4.6: Three dimensional plot of the density profile of the segments of the networks in which the length of the filaments are comparable to the seize of the confining region ($L \sim D$). We plot this density profile for $\zeta_0 = 0.001$ and $z_0 = 0.69$. The small dip in the middle of the density profile suggessts a decrease of segment distribution in the centre of the sphere.

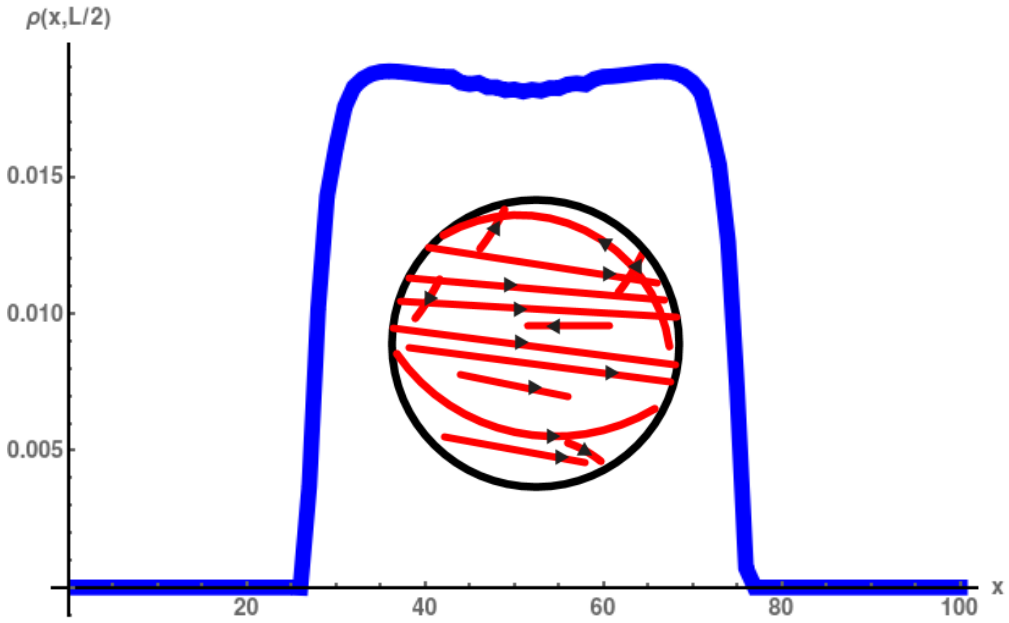

Figure 4.7: Density profile through the centre of the sphere in x direction of the segments of the networks in which the length of the filaments are equal to the seize of the confining region ($L \sim D$). We plot this density profile for $\zeta_0 = 0.001$ and $z_0 = 0.69$. The small dip in the middle of the density profile suggessts a decrease of segment distribution in the centre of the sphere. The inset is a cartoon representing the spherical geometry confining the network of actin filaments in red on the graph and it is there to illustrate the type of the networks for which the this density profile is obtained.

This inhomogeneity may be due to the fact that the filaments no longer have freedom to orient and self-organize freely inside the confining cell because the filament lengths reach the size of the confining cell. So the filaments of the networks formed at these at this points (ζ_0 ,z_0) start feeling the effect of confinement that the cell membrane introduce. The available accessible conformation and orientation for these filaments start reducing, so they start bending in order to minimize the free energy of the system [43, 60, 109, 110].

Networks dominated by long linear filaments ($L > D$)

The actin networks dominated by long linear filaments are obtained for $(1 - z_0)^2 > 4\zeta_0$ with large value of z_0 while the degree of branching parameter ζ_0 is kept at very small values (ζ_0 close to 0) meaning that we have very few branching of filaments. We present here the density profile of this type of networks and we show this profile on three dimensional graph in Figure 4.8. We plot also the profile of the network through the centre of the sphere in x direction on Figure 4.9. The density profile shows that under the effect of confinements the confined branching networks dominated by long linear filaments are inhomogeneously distributed. We observe a high average density distribution of chains or chain segments at the periphery of the confining cell while the density becomes low in the centre of the confining region. Many studies suggest

that when long linear semiflexible polymer filaments are confined in a finite geometry with size smaller than their persistence lengths or smaller than their unconfined sizes, they are strongly affected by the presence of the confining membrane. This reduces their available configurations and they bend and occupy the periphery of the confining cell membrane thus minimizing the free energy of the system [41, 62, 75, 111].

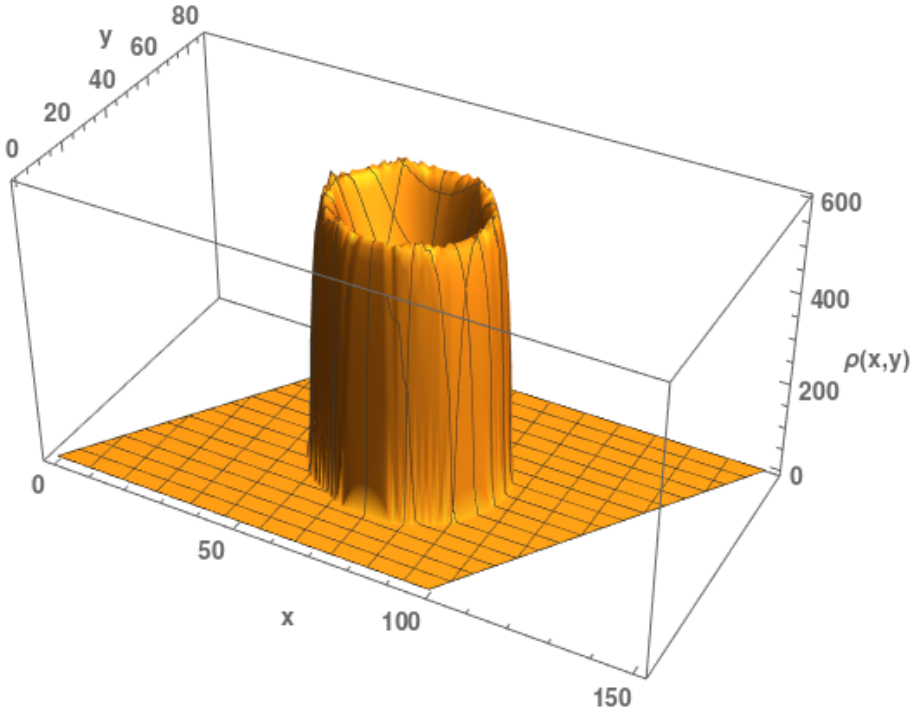

Figure 4.8: Three dimensional plot of the density profile of the segments of the networks dominated by long linear filaments with little branching. The length of the filaments in this networks are greater than the seize of the confining region ($L > D$). We plot this density profile for $\zeta_0 = 0.001$ and $z_0 = 0.75$. We observe a huge decrease of the average density of segments in the middle of the spheres while the profile shows a high density distrisbution at the periphery of the confining spherical cell.

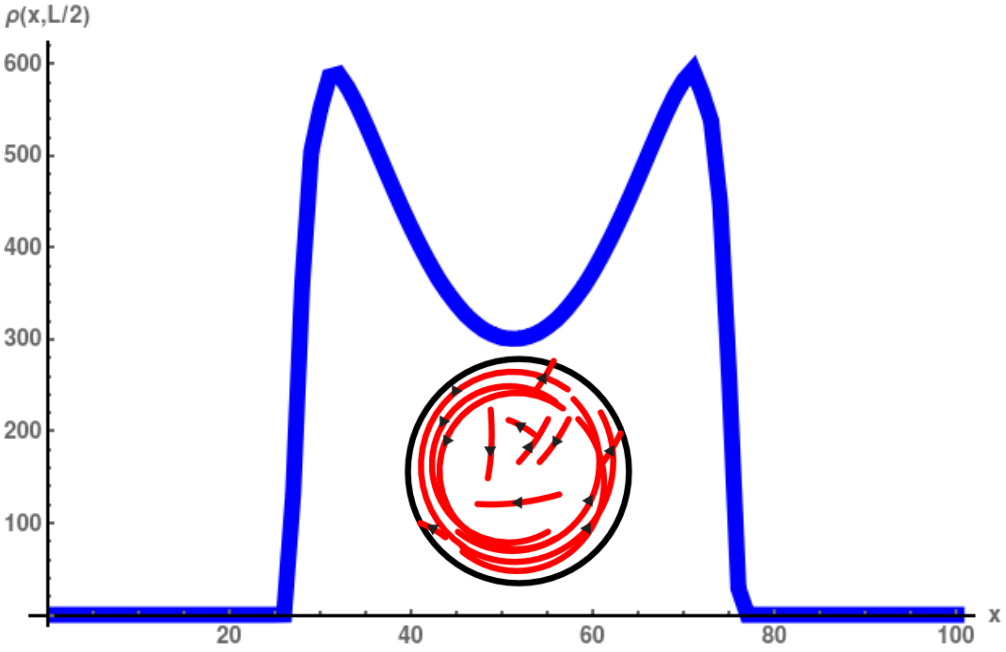

Figure 4.9: Graph of the density profile of the segments of the networks dominated by long linear filaments with few branching through the centre of the sphere in x direction. The length of the linear filaments are greater than the seize of the confining region ($L > D$). We plot this density profile for $\zeta_0 = 0.001$ and $z_0 = 0.75$. We observe a huge decrease of the average density of segments in the middle of the spheres while the profile shows a high density distribution at the periphery of the confining spherical cell. The inset is a cartoon representing the spherical geometry confining the network of actin filaments in red on the graph and it is there to illustrate the type of the networks for which the this density profile is obtained. It shows the filaments of the networks wrapped around the cell. This drawing becomes more understandable when we look at the radial order parameter field profile of this type of networks in the Figure 4.23.

Branched networks

To obtain a branched network we choose z_0 and ζ_0 for which $(1-z_0)^2 \sim 4\zeta_0$. The density profile, Figure A.3 or Figure 4.11, of the system of branched networks shows an inhomogeneous density distribution profile of filaments of the network with a high density of segments close to the cell membrane or cell wall. Increasing of the branching parameter ζ_0 increases the number of branching points especially at the vicinity of the cell membrane leading to the inhomogeneous distribution of filaments that we observe.

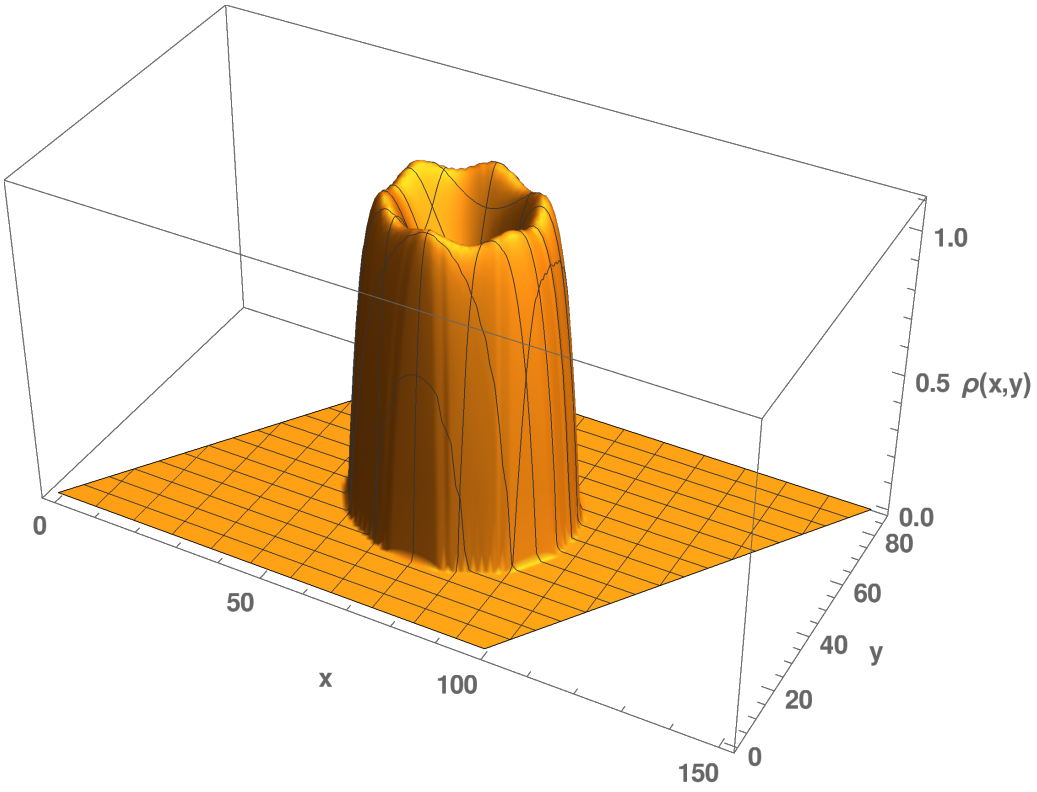

Figure 4.10: Three dimensional plot of the density profile of the segments of the branched networks. It is obtained for $(1-z_0)^2 \sim 4\zeta_0$. We plot this density profile for $\zeta_0 = 0.06$ and $z_0 = 0.516$. We observe a huge decrease of the average density of segments in the middle of the spheres while the profile shows a high density distribution at the periphery of the confining spherical cell.

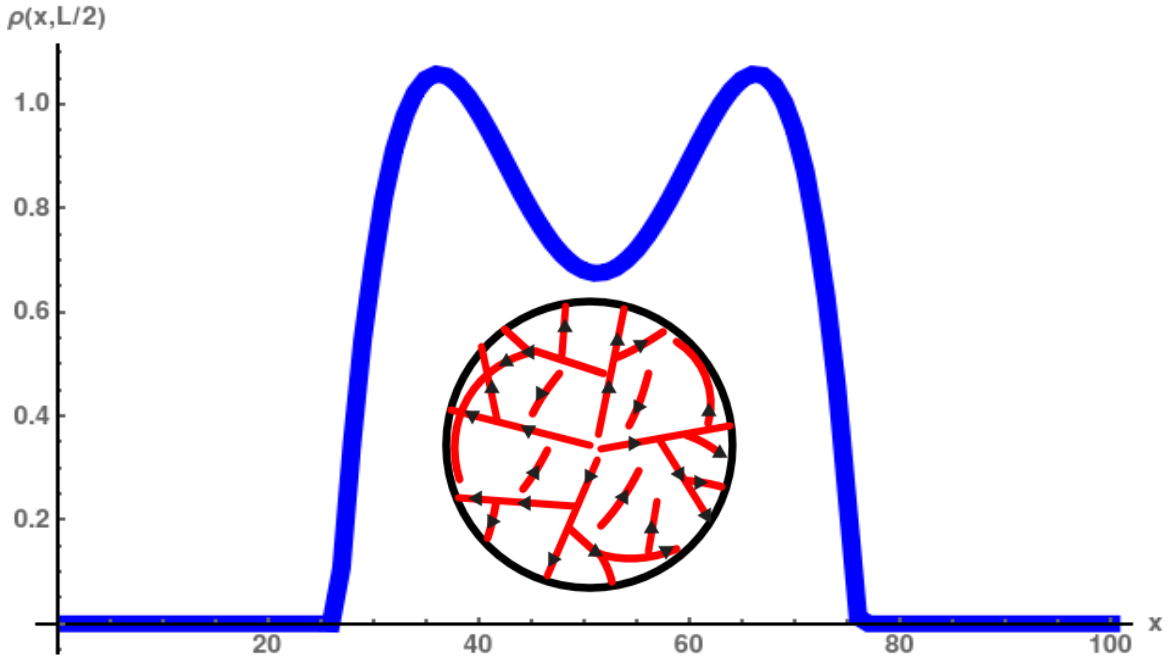

Figure 4.11: Graph of the density profile of the segments of a branched network through the centre of the sphere in x direction. It is obtained for $(1-z_0)^2 \sim 4\zeta_0$. We plot this density profile for $\zeta_0 = 0.06$ and $z_0 = 0.516$. The profile shows a high increase of the average density of segments as we go from the centre to the periphery of the confining spherical cell suggesting an inhomogeneous distribution of chain segments of the branched confined networks. The inset is a cartoon representing the spherical geometry confining the network of actin filaments in red on the graph and it is there to illustrate the type of the networks for which the this density profile is obtained. It shows the filaments of the networks that are highly branched at the vicinity of the cell and pointing straight to the cell membrane and with very few bent filaments at the edge. This drawing becomes more understandable when we look at the radial order parameter field profile of this type of networks in the Figure 4.25.

4.3.1.2 3d networks

In this section we plot the profiles of the 3d networks modelled on the 3d triangular lattice. Their density profiles are similar to the density profiles of the networks that are modelled on 2d triangular lattice (3d networks). So the observation and arguments we made in the case of the 2d networks are also valid for these 3d networks. So in the following we plot the graphs for the different type of networks that we modelled on the 3d triangular lattice.

Networks dominated by short linear filaments ($L < D$)

Figure 4.12 and Figure 4.13 represent the three dimensional plots and the profiles through the centre of the density of branching actin networks dominated by short linear filaments modelled on the 3d triangular lattice.

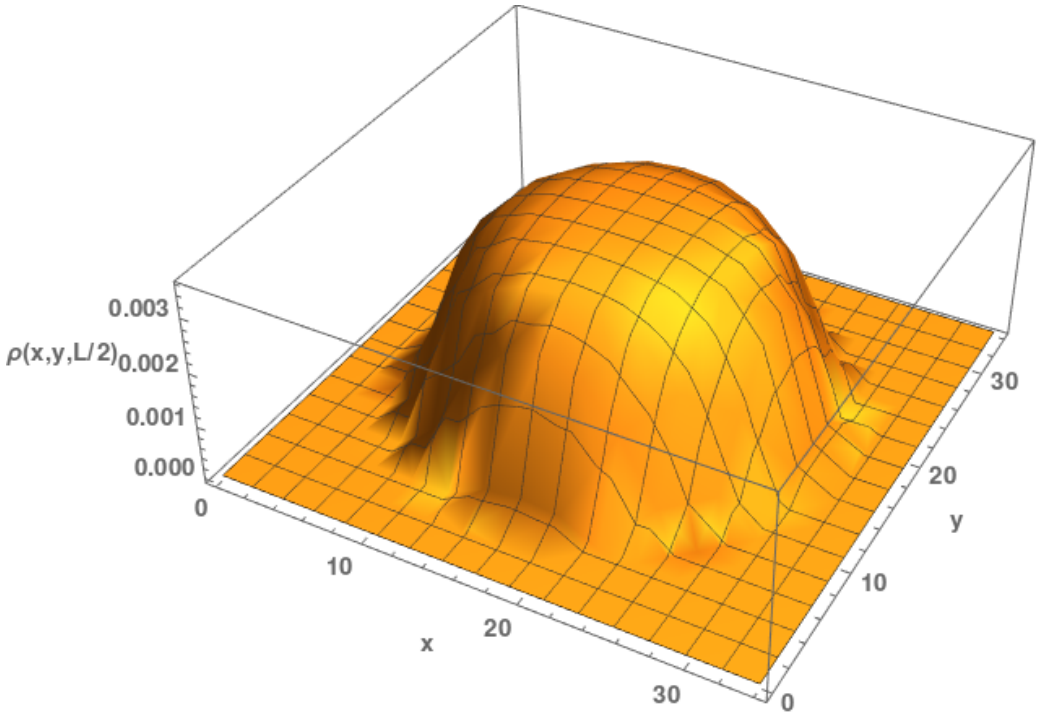

Figure 4.12: The graph is the three dimensional plot of the density profile of 3d actin networks dominated by short filaments ($L < D$) with few branching confined in sphere. It is obtained for growth or chain elongation parameter $z_0 = 0.31$ values, and for the branch formation parameter $\zeta_0 = 0.001$. We observe a convex-shaped density distribution of the chain segments with a plateau in the middle of the sphere.

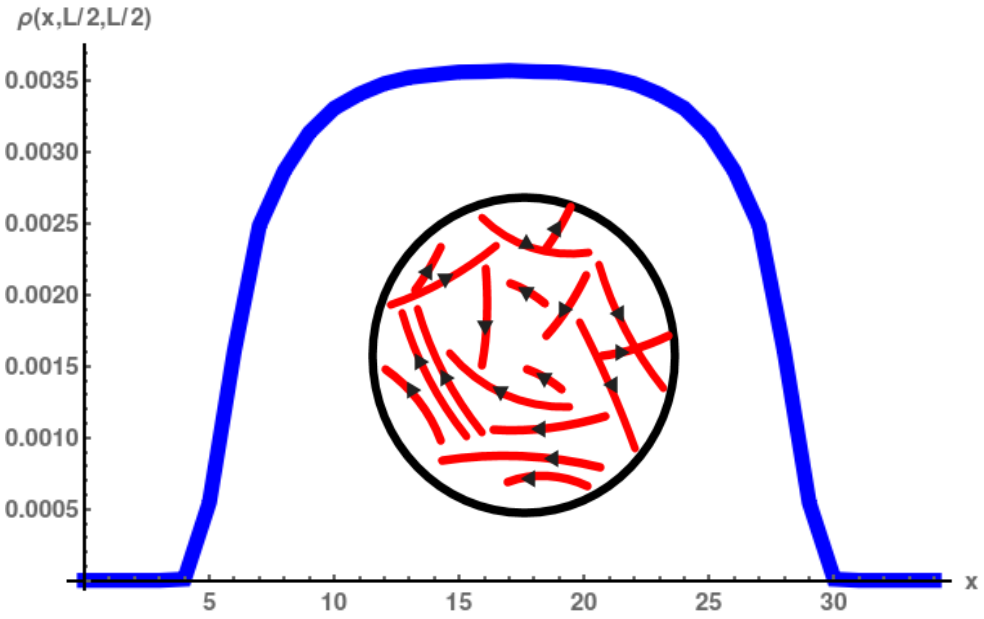

Figure 4.13: Plot of the density profile of segments through the centre of the sphere in x direction of the 3d network dominated by short linear filaments ($L < D$) modelled on 3d triangular lattice. The filaments elongation and branching parameter values are $z_0 = 0.31$ and $\zeta_0 = 0.001$. The inset is a cartoon representing the spherical geometry confining the network of actin filaments in red on the graph and it is there to illustrate the type of the networks for which the this density profile is obtained.

Networks dominated by long linear filaments

Figure 4.14 are Figure 4.15 represent the three dimensional plots and the profiles through the centre of the density of actin chain segments of the networks dominated by long linear filaments.

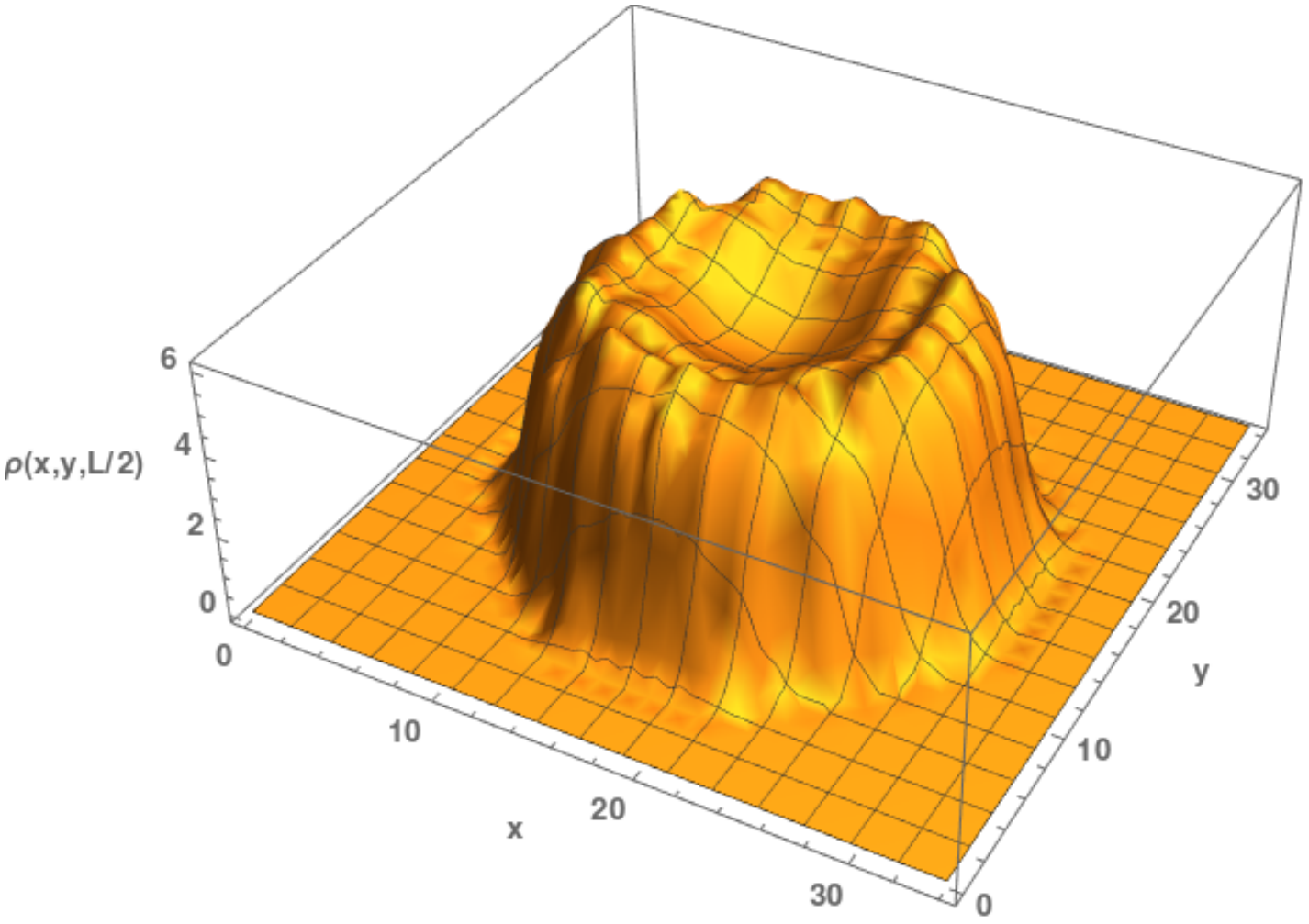

Figure 4.14: Three dimensional plot of the density profile of the segments of the networks dominated by long linear filaments with few branching. The length of the filaments in this networks are greater than the seize of the confining region ($L > D$). We plot this density profile for $\zeta_0 = 0.00001$ and $z_0 = 0.71$. We observe a huge decrease of the average density of segments in the middle of the spheres while the profile shows a high density distrisbution at the periphery of the confining spherical cell.

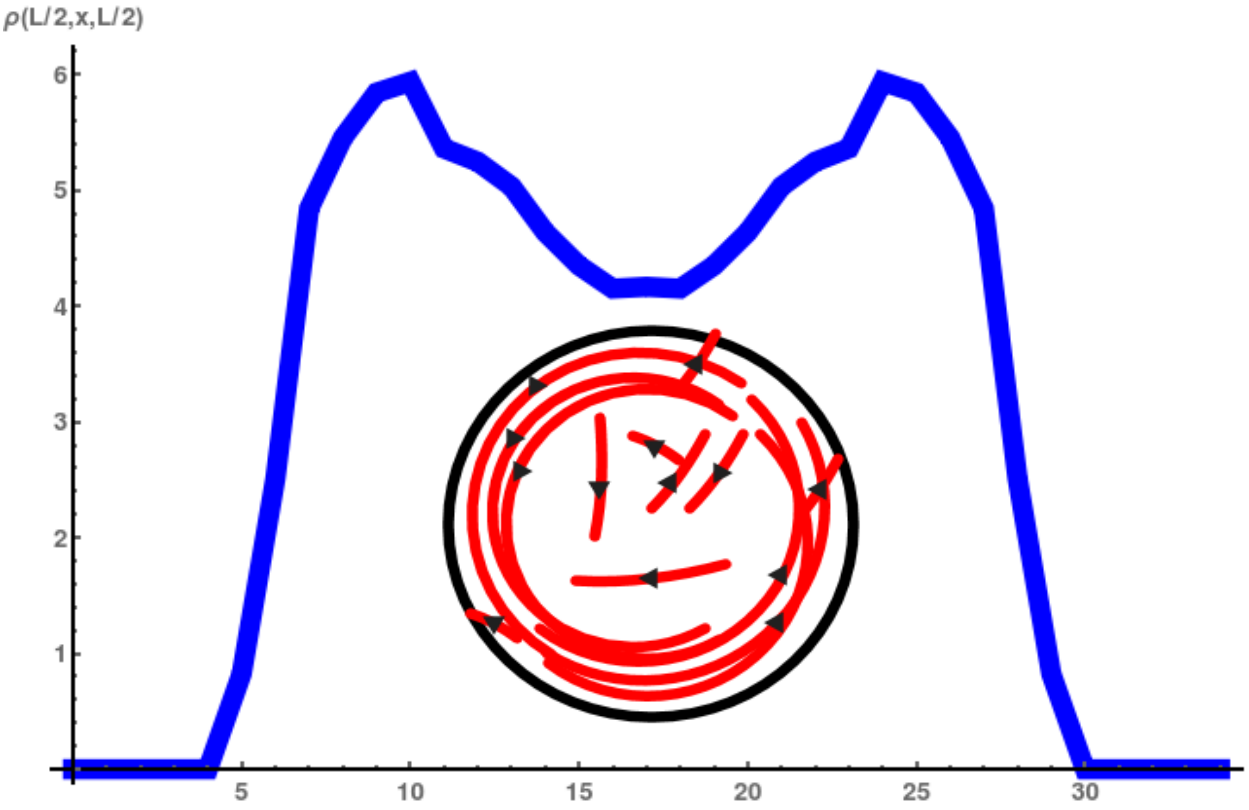

Figure 4.15: Graph of the density profile of the segments of the networks dominated by long linear filaments with few branching through the centre of the sphere in x direction. The length of the linear filaments are greater than the size of the confining region ($L > D$). We plot this density profile for $\zeta_0 = 0.00001$ and $z_0 = 0.71$. We observe a huge decrease of the average density of segments in the middle of the spheres while the profile shows a high density distribution at the periphery of the confining spherical cell. The inset is a cartoon representing the spherical geometry confining the network of actin filaments in red on the graph and it is there to illustrate the type of the networks for which the this density profile is obtained. It shows the filaments of the networks wrapped around the cell. This drawing becomes more understandable when we look at the radial order parameter field profile of this type of networks in the Figure 4.29.

Branched networks

We remark that in 3d, a very small increase of ζ_0 from $\zeta_0 \sim 0$ to $\zeta_0 > 0$ while $z_0 > 0$ leads to a highly branched networks. Figure 4.16 and Figure 4.17 represent the three dimensional plots and the profiles through the centre of the density of actin chain segments of the branched networks.

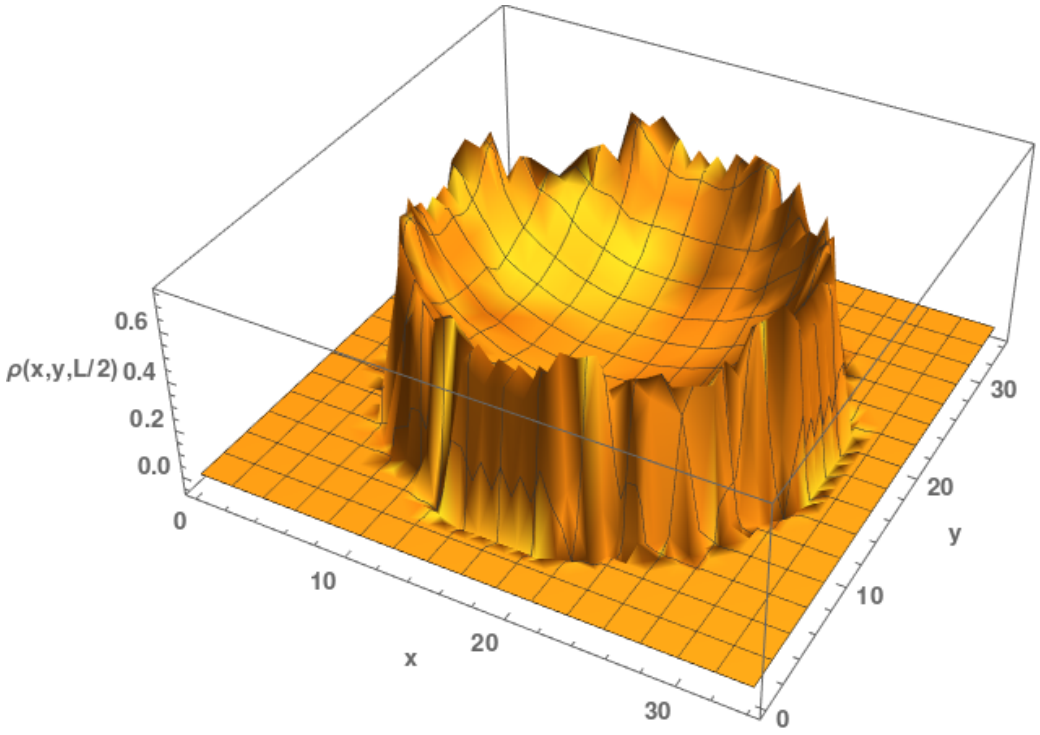

Figure 4.16: Three dimensional plot of the density profile of the segments of the branched networks. It is obtained for $(1-z_0)^2 \geq 4\zeta_0$. We plot this density profile for $\zeta_0 = 0.0049$ and $z_0 = 0.5$. We observe a huge decrease of the average density of segments in the middle of the spheres while the profile shows a high density distribution at the periphery of the confining spherical cell.

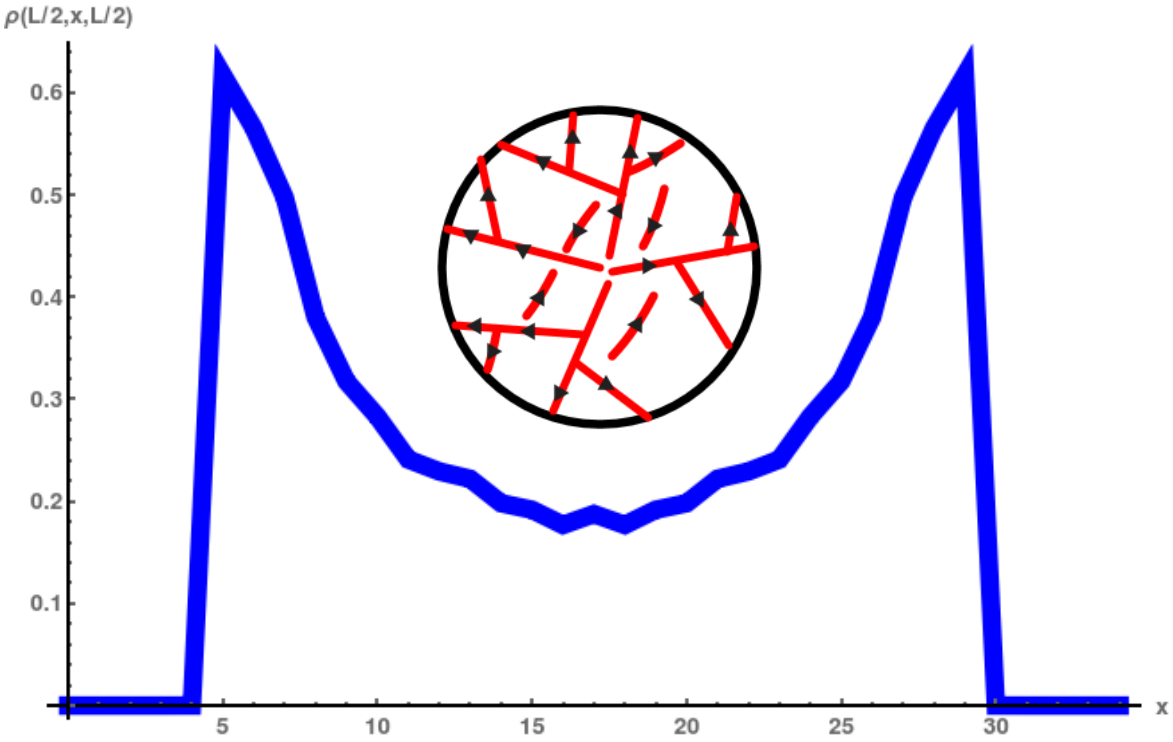

Figure 4.17: Graph of the density profile of the segments of a branched network through the centre of the sphere in x direction. It is obtained for $(1-z_0)^2 > 4\zeta_0$. We plot this density profile for $\zeta_0 = 0.0049$ and $z_0 = 0.5$. The profile shows a high increase of the average density of segments as we go from the centre to the periphery of the confining spherical cell suggesting an inhomogeneous distribution of chain segments of the branched confined networks. The inset is a cartoon representing the spherical geometry confining the network of actin filaments in red on the graph and it is there to illustrate the type of the networks for which the this density profile is obtained. It shows the filaments of the networks that are highly branched at the vicinity of the cell and pointing straight to the cell membrane. This drawing becomes more understandable when we look at the radial order parameter field profile of this type of networks in the Figure 4.31.

The knowledge of the average density distribution permit to calculate the total mean number of filaments segments $\langle N \rangle$ that make up the different type of actin networks that we study.

4.3.1.3 Tables of the average number density for some ζ_0 and z_0 values for 2d and 3d networks

The total average degree of polymerization or number of the segments $\langle N \rangle$ of the different type of networks that we modelled are summarized in the following tables.

z_0 \ ζ_0	0.15	0.13	0.1	0.05	0.01	0.005	0.001	0.0005	0.0
0.143	**50.522133**	48.831915	4.624645	1.97	1.311589	1.292229	1.286047	1.285854	1.285790
	0.927797	0.845215	0.714108	0.342226	0.019454	0.004929	0.000198	0.000050	0.0
0.2074	107.56	**49.903545**	5.137452	2.145977	1.504501	1.485928	1.480002	1.479817	1.479756
	0.950333	**0.909478**	0.693967	0.302480	0.016024	0.004047	0.000162	0.000041	0.0
0.30451	113.2225	95.000	**50.311434**	2.807552	1.944647	1.921190	1.913722	1.913488	1.913411
	0.941123	0.90133	**0.868432**	0.298036	0.015020	0.003786	0.000152	0.000038	0.0
0.485825	–	–	–	**50.496638**	3.860215	3.779904	1.913722	1.913488	1.913411
	–	–	–	**0.736603**	0.022776	0.005728	0.000152	0.000038	0.0
0.6681	–	–	–	155.1111	**50.128394**	21.601760	15.321	10.896127	10.889906
	–	–	–	0.40100	**0.193685**	0.028055	0.00234	0.000266	0.0
0.6894	–	–	–	445.2333	200.3455	**50.510584**	40.005	16.167672	16.140957
	–	–	–	0.22200	0.10012	**0.058259**	0.001	0.000455	0.0
0.697	–	–	–	500.3533	432.0021	153.12	**50.487543**	**50.312257**	**50.255180**
	–	–	–	0.13222	0.112344	0.00588	**0.002428**	**0.000602**	**0.0**

Table 4.1: *For each couple of points (ζ_0, z_0), we calculate the total average number of bonds $\langle N \rangle$ and the ratio r of the number of bonds that are involved in branching points over the total number of the bonds of the networks modelled in 2d. The first values in each cell stand for $\langle N \rangle$ and the second values are r . The bold values are the values at which we start observing the inhomogeneity in the networks either because the the degree of branching has increased and thus the branching start increasing at the cell periphery or the filaments are at transition points values (ζ_0, z_0) which correspond to the points for which $L = \langle N \rangle = D$.*

z_0 \ ζ_0	0.08	0.07	0.06	0.05	0.01	0.005	0.001	0.0005	0.0
0.143	**25.522133**	12.831915	8.624645	5.97	4.311589	2.292229	1.286047	1.285854	1.285790
	0.927797	0.845215	0.714108	0.342226	0.019454	0.004929	0.000198	0.000050	0.0
0.2074	70.3445	**24.903545**	5.137452	2.145977	1.504501	1.485928	1.480002	1.479817	1.479756
	0.94332	**0.909478**	0.693967	0.30241	0.01601	0.00403	0.000162	0.000041	0.0
0.30451	40.1223	35.9932	**25.3111**	12.8075	11.94469	1.92150	1.91371	3	1.913411
	0.93222	0.81010	**0.868432**	0.298036	0.015020	0.003786	0.000152	0.000038	0.0
0.485825	100.1234	83.932	46.3343	**24.496638**	3.860215	3.779904	1.913722	1.913488	1.913411
	0.89012	0.74222	0.72002	**0.736603**	0.022776	0.005728	0.0152	0.0038	0.0
0.6681	–	–	–	–	**25.128394**	11.601760	11.0012	10.896127	10.889906
	–	–	–	–	**0.193685**	0.0680515	0.05	0.00266	0.0
0.6894	–	–	–	–	52.4567	**24.510584**	17.4563	16.167672	16.140957
	–	–	–	–	0.06113	**0.05825**	0.00222	0.000455	0.0
0.697	–	–	–	–	85.2232	46.2178	**24.487543**	**24.712257**	**25.255180**
	–	–	–	–	0.0442	0.02333	**0.00242**	**0.00062**	**0.0**

Table 4.2: *For each couple of points (ζ_0, z_0), we calculate the total average number of bonds $\langle N \rangle$ and the ratio r of the number of bonds that are involved in branching points over the total number of the bonds of the networks modelled in 3d. The first values in each cell stand for $\langle N \rangle$ and the second values are r . The bold values are the values at which we start observing the inhomogeneity in the networks either because the the degree of branching has increased and thus the branching start increasing at the cell periphery or the filaments are at transition points values (ζ_0, z_0) which correspond to the points for which $L = \langle N \rangle = D$.*

As mentioned previously, networks of cytoskeletal actin filaments can spatially arranges themselves into varieties of orientationally ordered structures under the effect of cell membrane confinement [13]. Using our model, we quantify not only the effect of confinement on the structure and conformations of branching actin networks by computing their density profiles in the confining geometrical regions, but we also compute the radial order parameter field profiles of the different networks that we modelled. In what follows we recall the definition of the radial order parameter field and present the order profiles that we get for the different types of networks that we have modelled.

4.3.2 Radial order parameter field profiles

We quantitatively investigate the effect of confinement on ordering or alignment of the filaments of branching actin networks with various topology by computing the radial order parameter field (given by equation ((4.9)) for 3d networks and by equation ((4.10)) for 2d networks) for the different actin networks for which the density profiles have been shown in the sections above. The radial order parameter field $Q(\boldsymbol{r})$ is defined for networks modelled in 3d as:

$$Q(\boldsymbol{r}) = \sum_{\hat{\boldsymbol{n}}} \frac{1}{2}(1 - 3(\hat{\boldsymbol{u}} \cdot \hat{\boldsymbol{n}})^2)\varrho(\boldsymbol{r}, \hat{\boldsymbol{n}}) \tag{4.9}$$

and for networks modelled in 2d as:

$$Q(\boldsymbol{r}) = \sum_{\hat{\boldsymbol{n}}} \frac{1}{2}(1 - 2(\hat{\boldsymbol{u}} \cdot \hat{\boldsymbol{n}})^2)\varrho(\boldsymbol{r}, \hat{\boldsymbol{n}}) \tag{4.10}$$

where $\hat{\boldsymbol{u}}$ is the radial unit vector defined by the positions of the bonds of the filaments in the confining region by $\hat{\boldsymbol{u}} = \boldsymbol{r}/|\boldsymbol{r}|$ with its origin in the centre of the confining sphere, $\boldsymbol{r}$ the local position of the chain segments inside the confining region and $\hat{\boldsymbol{n}}$ their orientations. According to our definition of the order parameter field, if the segments of the actin networks align along the radial vector ($\hat{\boldsymbol{u}} \parallel \boldsymbol{n}$), we get a negative order parameter field ($Q(\boldsymbol{r}) < 0$), if the segments align perpendicular to it ($\hat{\boldsymbol{u}} \perp \boldsymbol{n}$), we get a positive order field ($Q(\boldsymbol{r}) > 0$) and if the segments of the networks are isotropically oriented, the order parameter field have value 0 ($Q(\boldsymbol{r}) = 0$). Therefore, the radial order parameter field distribution equal to 0 corresponds to a perfectly isotropic networks inside the confining region and positive radial order parameter field profiles points out the parallel alignment of the filaments to the confining cell membrane whereas negative radial order parameter field means the filaments are perpendicular or are pointing straight to the cell membrane.
Similar order parameter field have been previously used to investigate the ordering of linear semiflexible chains confined in a slit [57]. The profile of the order parameter we define serve thus as a quantitative measure of the alignment of the filaments of the networks with respect to the cell membrane or to the confining region boundary, at thermodynamics equilibrium.

In the following, we present the radial order parameter field profiles for the networks modelled in 2d and those modelled in 3d which show a similar results. Depending on the type and structure of the networks, We observe three main confinement regimes: we have weak, strong and strong-resistant confinement. We predict from our model that at thermodynamic equilibrium, the networks of long linear actin filaments are affected by the strong confinement, while the the networks of short filaments are weakly influenced by the effect of confinement [13, 43, 54, 56, 57, 103, 109]. The branched networks though subjected to a strong confinement, exhibit a high resistance to the effect of confinement. We have also the order profiles for the transition or crossover networks which is made up of actin filaments of length similar to the

size of the spherical confining region.

4.3.2.1 2d networks

Networks dominated by short linear filaments ($L < D$)

Figure 4.18 and Figure 4.19 represent the three dimensional plots of the radial order parameter field profiles and the profiles through the centre of the sphere of the 2d actin networks dominated by short filaments. The order profile shows that the network chain segments that are near the centre of the sphere are isotropically distributed while the segments close to the cell boundary have preference of aligning parallel to the cell wall. This confirm the argument that networks of semiflexible or actin filaments with lengths shorter than the confining region size are under weak confinement effect [43, 103] and are free to orient and translate and thus align relatively to the confining membrane as they prefer.

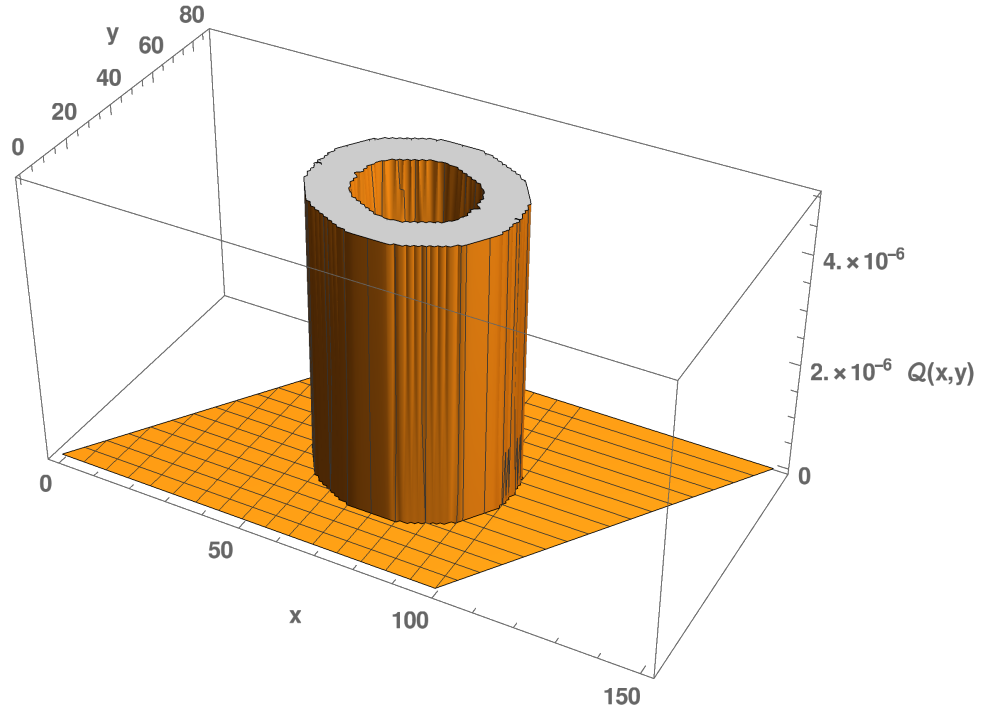

Figure 4.18: Three dimensional plot of the radial order parameter field profile of the 2d actin networks dominated by short filaments ($L \leq D$) with few branching under sperical confinement. It is obtained for growth or chain elongation parameter $z_0 = 0.5$ values, and for the branch formation parameter $\zeta_0 = 0.001$. The graph shows a positive order parameter profile at the vicinity of the spherical cell indicating a parallel alignment of segments that are close to the wall while the order profile toward the centre of the cell is 0. This indicates that the filaments are isotropically distributed in the middle of the sphere.

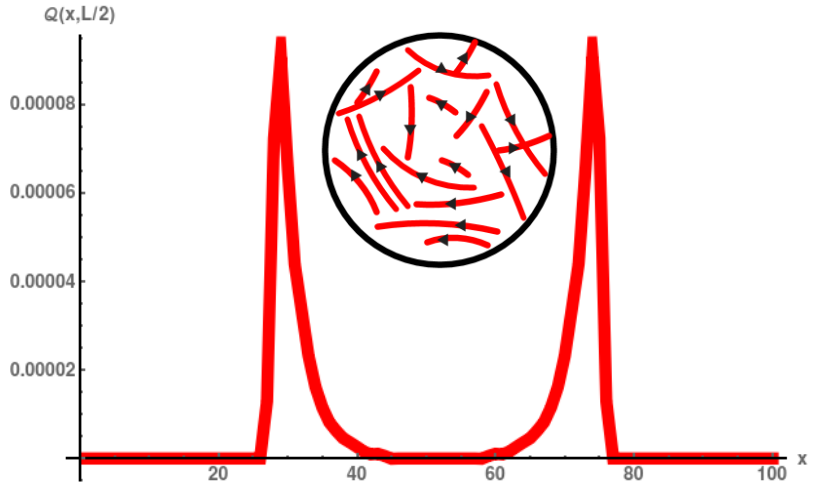

Figure 4.19: Plot of radial order parameter field profile of segments throught the centre of the sphere in x direction of 2d networks dominated by short linear filaments ($L \leq D$) modelled on 2d triangular lattice. The filaments elongation and branching parameter values are $z_0 = 0.5$ and $\zeta_0 = 0.001$. The inset is a cartoon representing the spherical geometry confining the network of actin filaments in red on the graph and it is there to illustrate the type of the networks for which the radial order parameter field profile is obtained.

We are now going to present the order profile of the networks composed of filaments of length similar to the confining region.

The networks with comparable length scales ($L \sim D \sim \ell_{\mathbf{p}}$)

In Figure 4.20 we have the three dimensional plot of the order profile and Figure 4.21 the order profile through the centre of the sphere of the networks with comparable length scales. At the edge of the confining sphere, we observe a parallel alignment of chain segments with the spherical confining cell membrane or wall. As we move toward the middle of the sphere, we see that the filament segments align radially or perpendicular to the confining wall, while in the the middle of the sphere, we have an isotropic distribution of actin filaments segments. At this state, the networks start feeling the influence of strong cell membrane confinement.

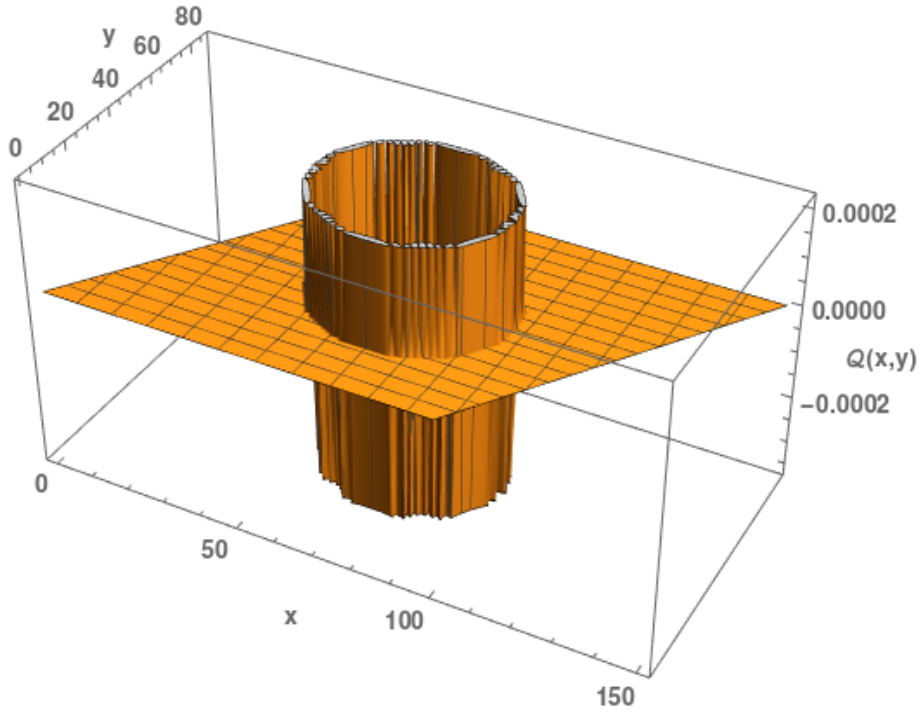

Figure 4.20: Three dimensional plot of the radial order parameter field profile of the networks with comparable length scales ($L \sim D \sim \ell_p$). The profile we present here obtained for $z_0 = 0.69$ and $\zeta_0 = 0.001$. The order field is positive at the very edge of the cell, negative as we move towards the centre and 0 in the middle.

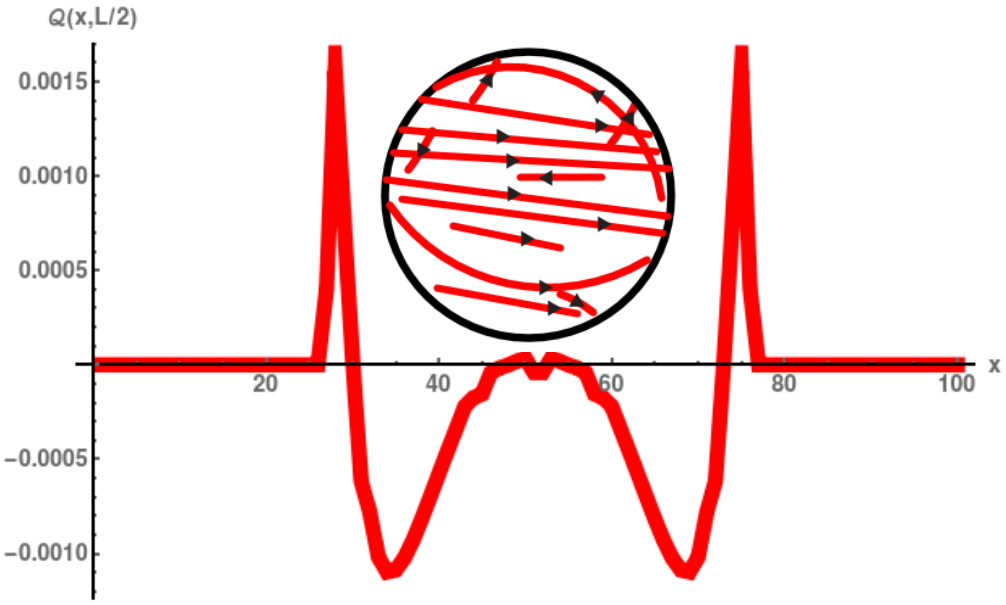

Figure 4.21: Plot of radial order parameter field profile of segments throught the centre of the sphere in x direction of the networks with comparable length scales ($L \sim D \sim \ell_p$). The profile we present is obtained for $z_0 = 0.69$ and $\zeta_0 = 0.001$. The inset is a cartoon representing the spherical geometry confining the network of actin filaments in red on the graph and it is there to illustrate the type of the networks for which the radial order parameter field profile is obtained.

Next we present the order parameter profiles for networks dominated by long linear filaments $L > D$.

Networks dominated by long linear filaments $L > D$

Here we show the results of the model for branching actin networks dominated by long linear filament confined in a spherical region. The results show positive radial order parameter field profiles of the networks dominated by long linear filaments at the periphery of the cell, see Figures 4.22 for the graph plotted in three dimension and Figure 4.23 for the profile of the networks through the centre of the sphere.

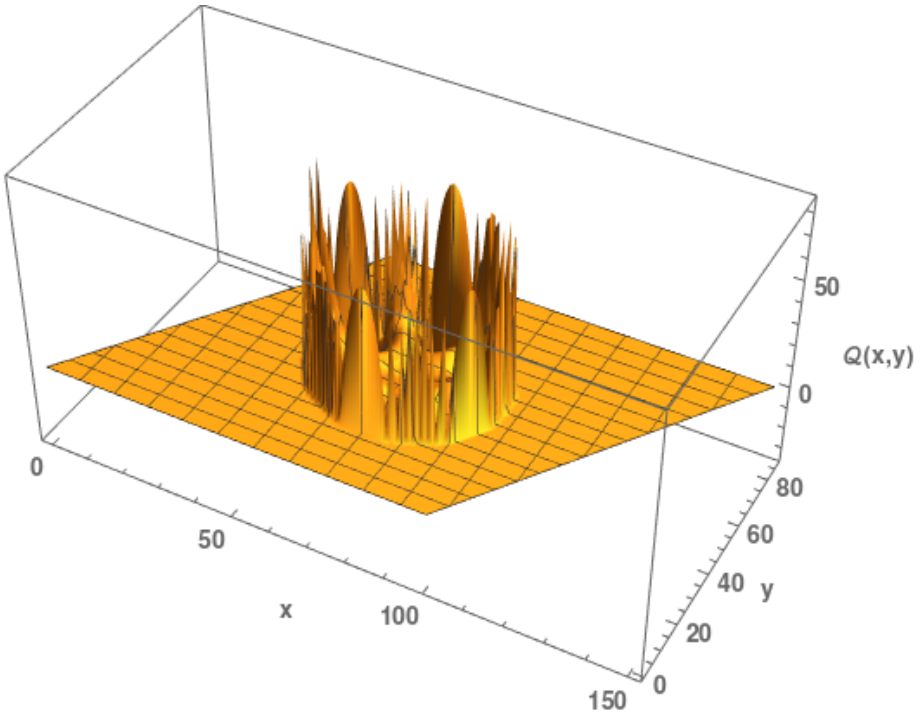

Figure 4.22: The graph of the three dimensional plot of the order parameter field profile of 2d networks dominated by long linear filaments $L > D$. The graph is obtained for $z_0 = 0.75$ and $\zeta_0 = 0.001$. The order parameter field is positive at the periphery of confining region while 0 in the centre of the sphere. This indicates that long linear filaments bend and wrap around the cell while the few shorter filaments that are in the middle of the cell are isotropically distributed.

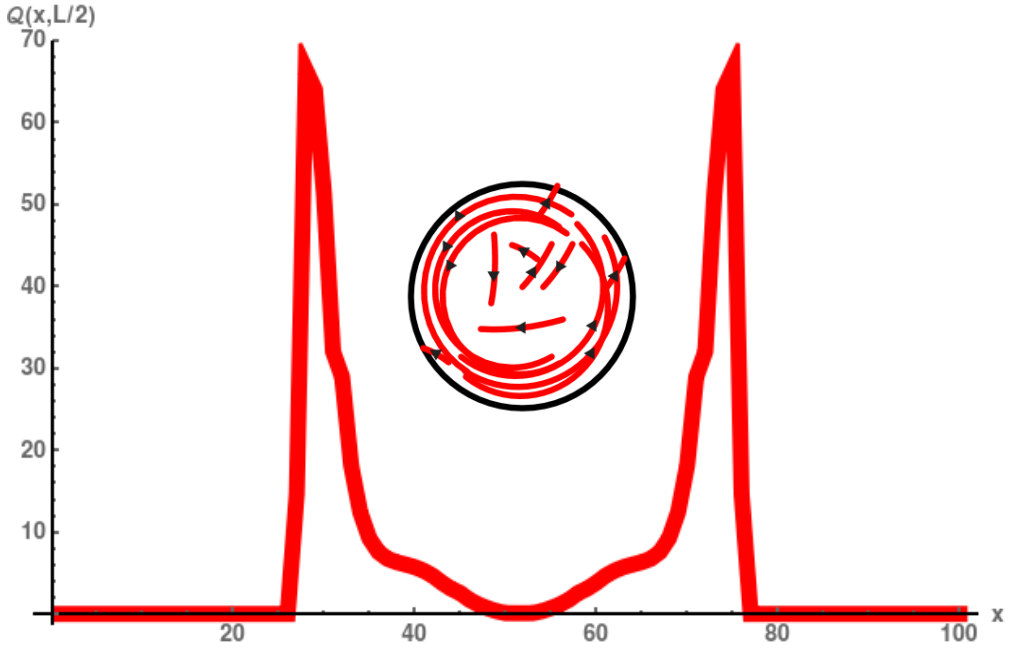

Figure 4.23: Plot of radial order parameter field profile of segments through the centre of the sphere in x direction. This graph of the of 2d networks dominated by long linear actin filaments is obtained for $z_0 = 0.75$ and $\zeta_0 = 0.001$. The inset is a cartoon representing the spherical geometry confining the network of actin filaments in red on the graph and it is there to illustrate the type of the networks for which the radial order parameter field profile is obtained.

The density profiles of this type of networks shows a high concentration of chains segments at the periphery of the cell and low towards the centre of the confining sperical region (Figure 4.8 and 4.9 or 4.14 and 4.15). So most filaments of the networks are located at the cell periphery and aligned parallel to the cell wall. In fact semiflexible polymers lose their accessible conformations, when confined to finite regions (here sphere) of the same size or of size greater than their persistence lengths [41, 54, 75]. So to minimize the free energy of the network system, under the effect of confinement, bend and wrap around the confining cell membrane or wall [41, 43, 62, 75]. The results from our model therefore are in agreement with previous studies. Branching actin networks dominated by long linear filaments are subjected to strong confinement regime when confined in geometries with sizes smaller than their persistence lengths.
We have also obtained the order parameter profiles for branched actin networks and we present it the section that follows.

Branched networks

The order parameter field profiles for 2d branched networks are plotted in three dimension on Figure A.4 and the profile through the centre of the sphere in Figure 4.25). We have a negative profile of the networks with very small positive values at the periphery of cell while 0 in the middle of the sphere. We predict that the filaments align perpendicularly (pointing radially

straight) to the cell wall. We have previously seen that the density distribution of segments of branched actin networks is very high at the cell periphery and low toward the centre (Figure A.3 and 4.16 or 4.11 and 4.17). We argue that this density may be due to the increasing of branching of filaments at the cell periphery under the effect of confinement giving to the networks a highly branched architecture. Tree-like networks of semiflexible filaments are highly stiff [84, 85, 112] and difficult to bend. The strong confinement effect from the rigid cell membrane on branched actin networks is thus cancelled by the stiffness induced by the branching via Arp2/3 protein complex. So branched networks of actin or semiflexible filaments we modelled, resist the strong confinement effects. However for two dimensional branched networks we observe few filaments that bent at the cell periphery.

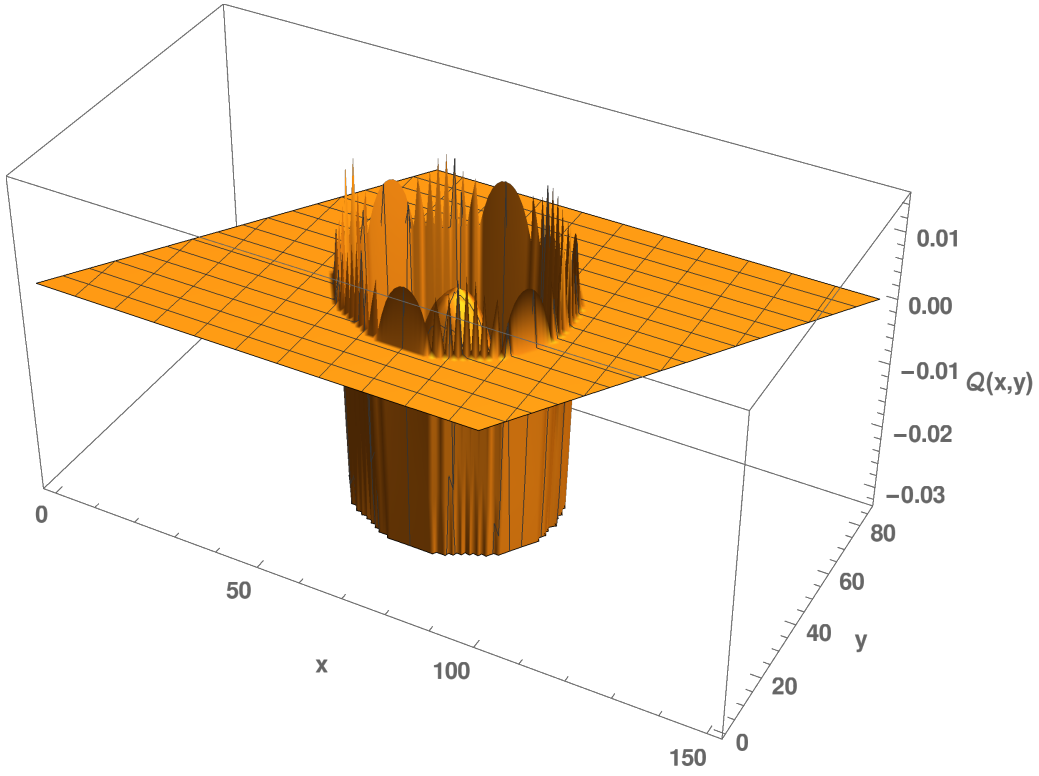

Figure 4.24: Radial order parameter field profile of 2d branched networks plotted in three dimension. The profile we show is obtained for $z_0 = 0.516$ and $\zeta_0 = 0.06$. We have negative order parameter field with very small positive values at the vicinity of the cell. This indicate that filaments of segments of the branched networks align perpendicular or point straight to the confining. Only very few filament bent. The chain segments are isotropically distributed in the middle of the sphere.

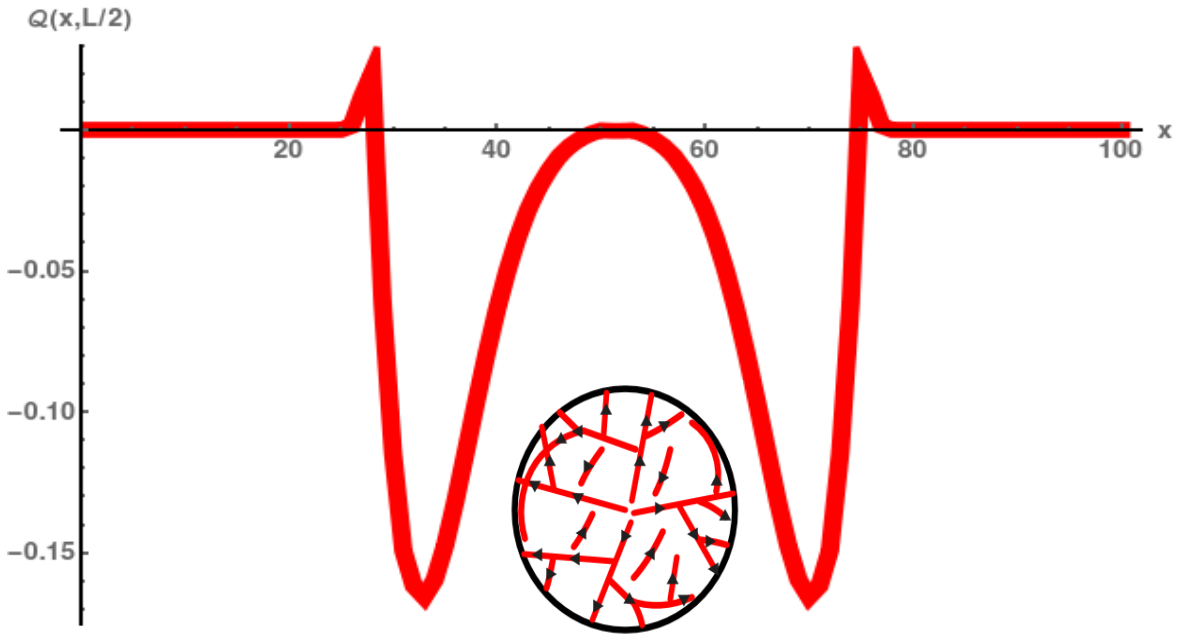

Figure 4.25: Plot of radial order parameter field profile of 2d branched networks segments through the centre of the sphere in x direction. The graph is obtained for $z_0 = 0.516$ and $\zeta_0 = 0.06$. The inset is a cartoon representing the spherical geometry confining the network of actin filaments in red on the graph and it is there to illustrate the type of the networks for which the radial order parameter field profile is obtained.

We obtained similar results of the order parameter field profiles for the different types of branching actin networks modelled in 3d.

4.3.2.2 3d networks

The discussion we made for the results in the case of 2d networks are also valid for the case of the 3d networks except a slight difference we observe between the order profiles of confined branched networks modelled in 3d and the confined 2d branched networks. The order parameter for 3d branched networks is totally negative (meaning all filaments of the 3d networks are aligned perpendicular i.e point straight to the cell wall, Figure 4.31) while for 2d networks there are few filaments that bent at the vicinity of the spherical confining cell, see Figure 4.25.

Networks dominated by short linear filaments ($L < D$)

Figure 4.26 and Figure 4.27 represent the three dimensional plots and the profiles through the centre of the radial order parameter field of actin networks dominated by short filaments modelled on the 3d triangular lattice.

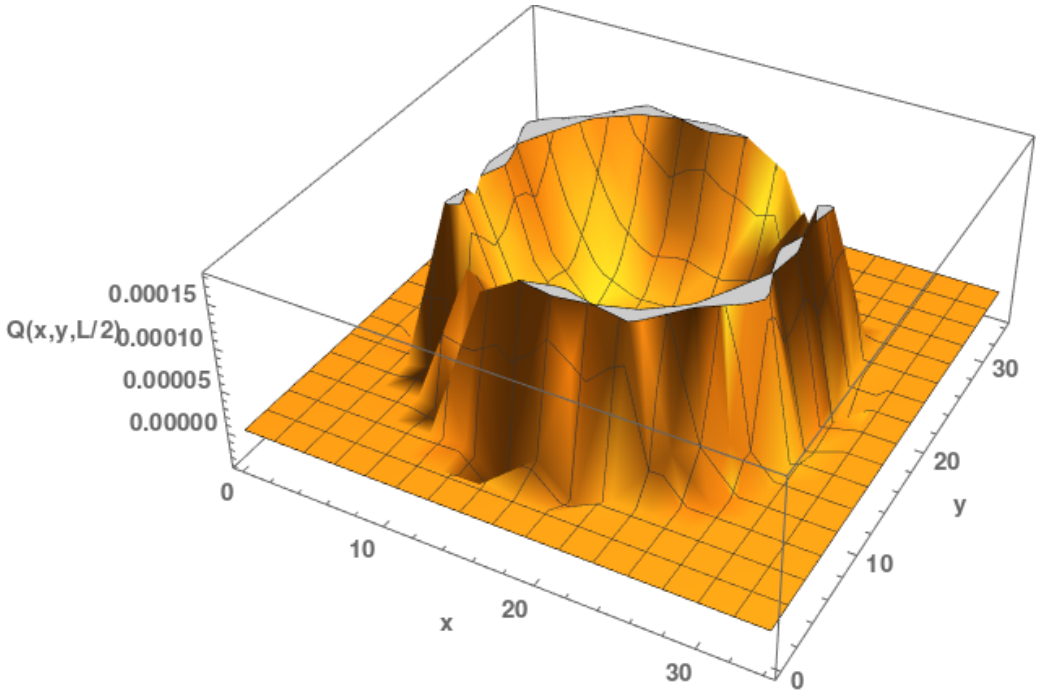

Figure 4.26: Three dimensional plot of the radial order parameter field profile of the 3d actin networks dominated by short filaments ($L \leq D$) with few branching under sperical confinement. It is obtained for growth or chain elongation parameter $z_0 = 0.31$ values, and for the branch formation parameter $\zeta_0 = 0.001$. The graph shows a positive order parameter profile at the vicinity of the spherical cell indicating a parallel alignment of segments that are close to the wall while the order profile toward the centre of the cell is 0. It indicates that the filaments are isotropically distributed in the middle of the sphere.

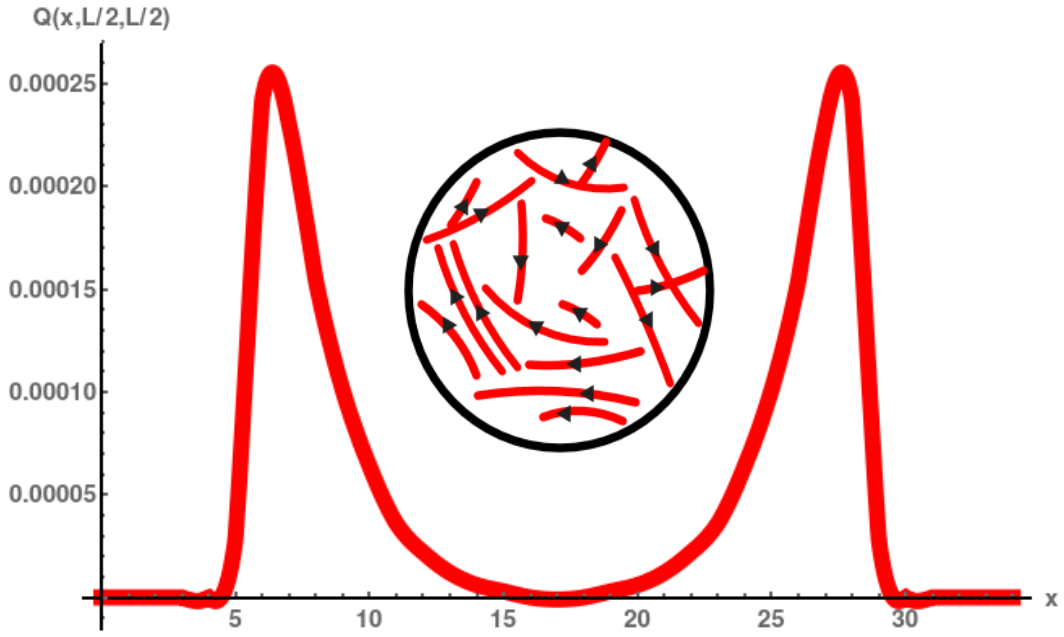

Figure 4.27: Plot of radial order parameter field profile of segments through the centre of the sphere in x direction of 3d networks dominated by short linear filaments ($L \leq D$). The filaments elongation and branching parameter values are $z_0 = 0.31$ and $\zeta_0 = 0.001$. The inset is a cartoon representing the spherical geometry confining the network of actin filaments in red on the graph and it is there to illustrate the type of the networks for which the radial order parameter field profile is obtained.

Networks dominated by long linear filaments $L > D$

In Figure 4.28 and Figure 4.29, we have the three dimensional plots and the profiles through the centre of the radial order parameter field of 3d actin networks dominated by long linear filaments.

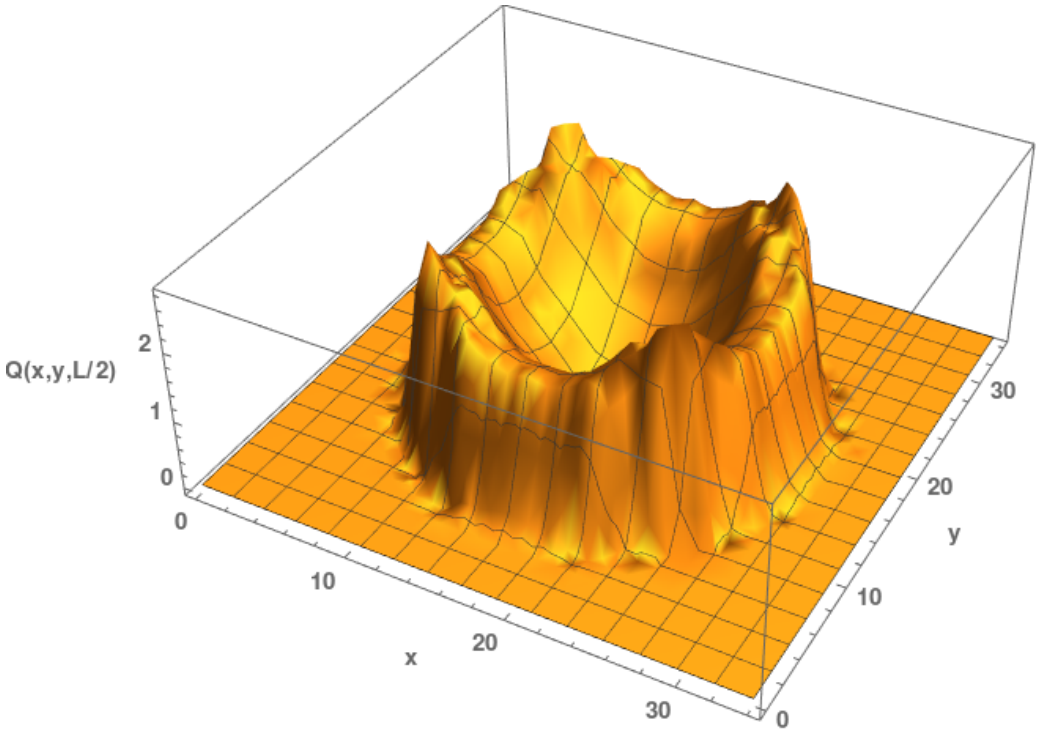

Figure 4.28: The graph of the three dimensional plot of the order parameter field profile of 3d networks dominated by long linear filaments $L > D$. The graph is obtained for $z_0 = 0.71$ and $\zeta_0 = 0.00001$. The order parameter field is positive at the periphery of confining region while 0 in the centre of the sphere. This indicates that long linear filaments bend and wrap around the cell while the few shorter filaments that are in the middle of the cell are isotropically distributed.

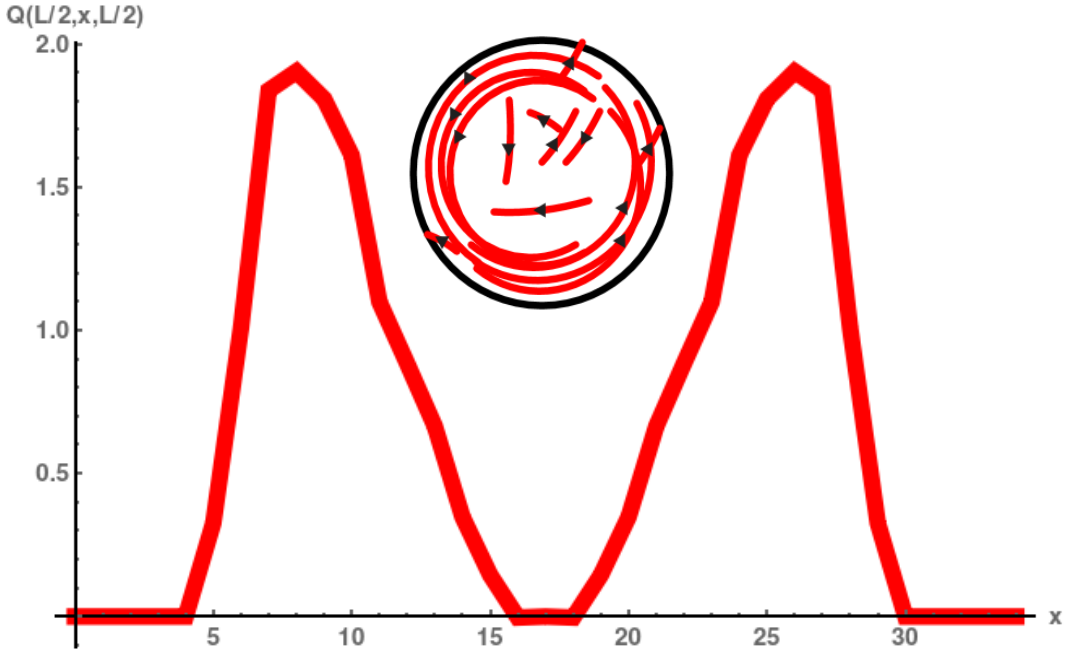

Figure 4.29: Plot of radial order parameter field profile of segments through the centre of the sphere in x direction. This graph of the of 3d networks dominated by long linear actin filaments is obtained for $z_0 = 0.71$ and $\zeta_0 = 0.00001$. The inset is a cartoon representing the spherical geometry confining the network of actin filaments in red on the graph and it is there to illustrate the type of the networks for which the radial order parameter field profile is obtained.

Branched networks

Figure 4.30 are Figure 4.31 represent the three dimensional plots and the profiles through the centre of the radial order parameter field of of the branched actin networks modelled on the 3d triangular lattice.

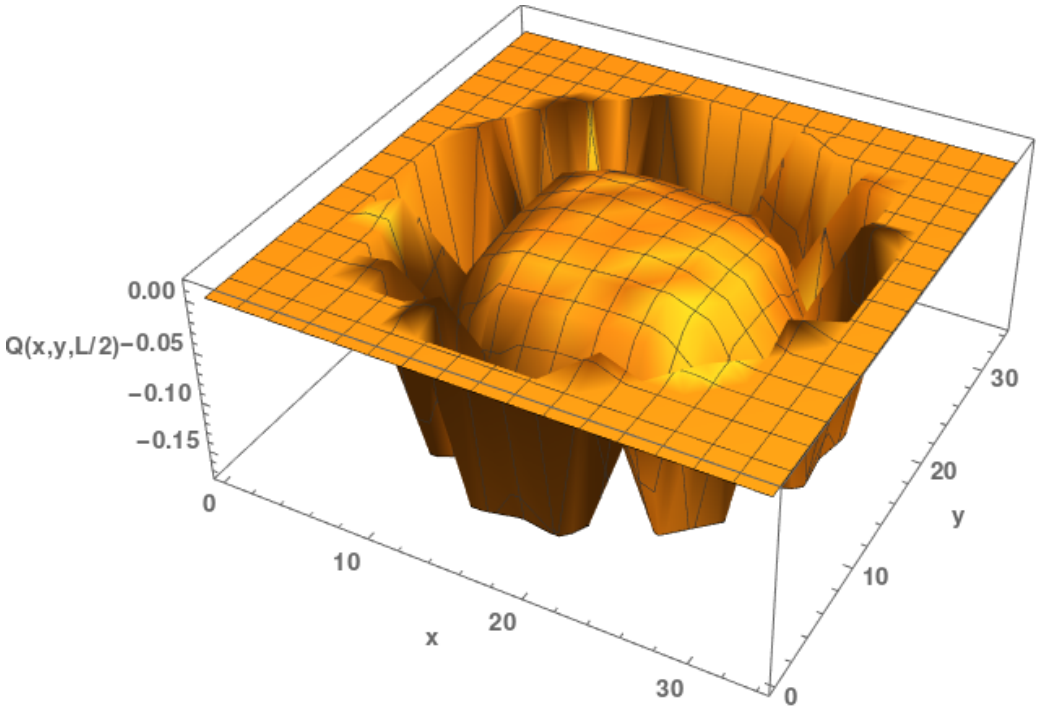

Figure 4.30: Radial order parameter field profile of 3d branched networks plotted in three dimensions. The profile we show is obtained for $z_0 = 0.5$ and $\zeta_0 = 0.0049$. We have negative order parameter field at the vicinity of the cell and 0 order close and in the middle of the confining sphere. This indicate that all filaments of 3d branched networks align perpendicular or point straigh to the confining sphere. The chain segments are isotropically distributed in the middle of the sphere.

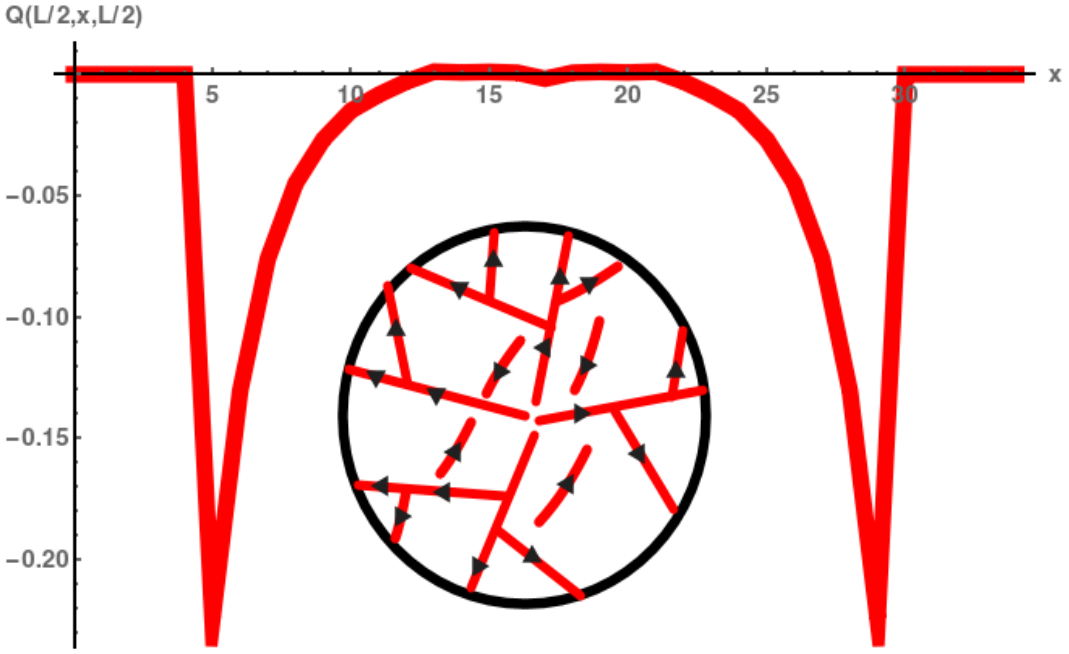

Figure 4.31: Plot of radial order parameter field profile of 3d branched networks segments through the centre of the sphere in x direction. The graph is obtained for $z_0 = 0.5$ and $\zeta_0 = 0.0049$. The inset is a cartoon representing the spherical geometry confining the network of actin filaments in red on the graph and it is there to illustrate the type of the networks for which the radial order parameter field profile is obtained.

In the section that follows we present a phase diagram that shows the domains of the different networks that we have studied above, according to their properties.

4.3.3 Phase Diagrams (ζ_0, z_0)

We have sumarized all the results above on a phase diagrams (ζ_0, z_0) for 2d networks and for 3d networks. On this phase diagrams we present three different domains for (ζ_0, z_0) corresponding to the domains of the networks dominated by short filaments with few branching, network dominated by long linear filaments and branched networks. The points of (ζ_0, z_0) for which we obtain the networks with comparable length scales ($L \sim D \sim \ell_p$) are used to draw the lines separating the domains of the three types of networks.

To obtain the graph of the phase diagrams Figure 4.32 for 2d networks and Figure 4.33 for 3d networks, we have computed the average densities and the order parameters fields for many points (ζ_0, z_0) that are in the domain of validity of our model given by the equation (4.3). The density and order field profiles we obtained at these points allowed us to partition the validity domain into three distinct zones which corresponds to the three different types of networks that we have studied above.

The phase diagram is presented as follows: the networks formed in the yellow dots zone are obtained for small value of $z_0 > 0$ while $\zeta_0 \sim 0$ and the properties of the branching networks that are formed correspond to those dominated by short linear filaments which are homogeneously distributed inside the confining cell with parallel alignment preference.
The density profiles of networks segments we have obtained for points in the black triangle zone shows a high density distribution of chain segments the confining cell periphery while low in the centre of the spherical region with a positive order field profile at the cell periphery. These properties correspond to the networks dominated by long linear chains with little branching, inhomogeneously distributed inside the confining region and isotropic distribution of segment in the centre.

Curvature of the density near centre	average order parameter	
> 0	> 0	black triangles
> 0	< 0	red square
< 0	> 0	yellow dots (circles)

Table 4.3: *Summary of the description of the phase diagrams*

The points (ζ_0, z_0) in the red squares zone on the phase diagram satisfy $(1 - z_0)^2 \simeq 4\zeta_0$. This zone corresponds to confined branched networks which segment density profiles show an inhomogeneous distribution of filament segments with negative order parameter fields.

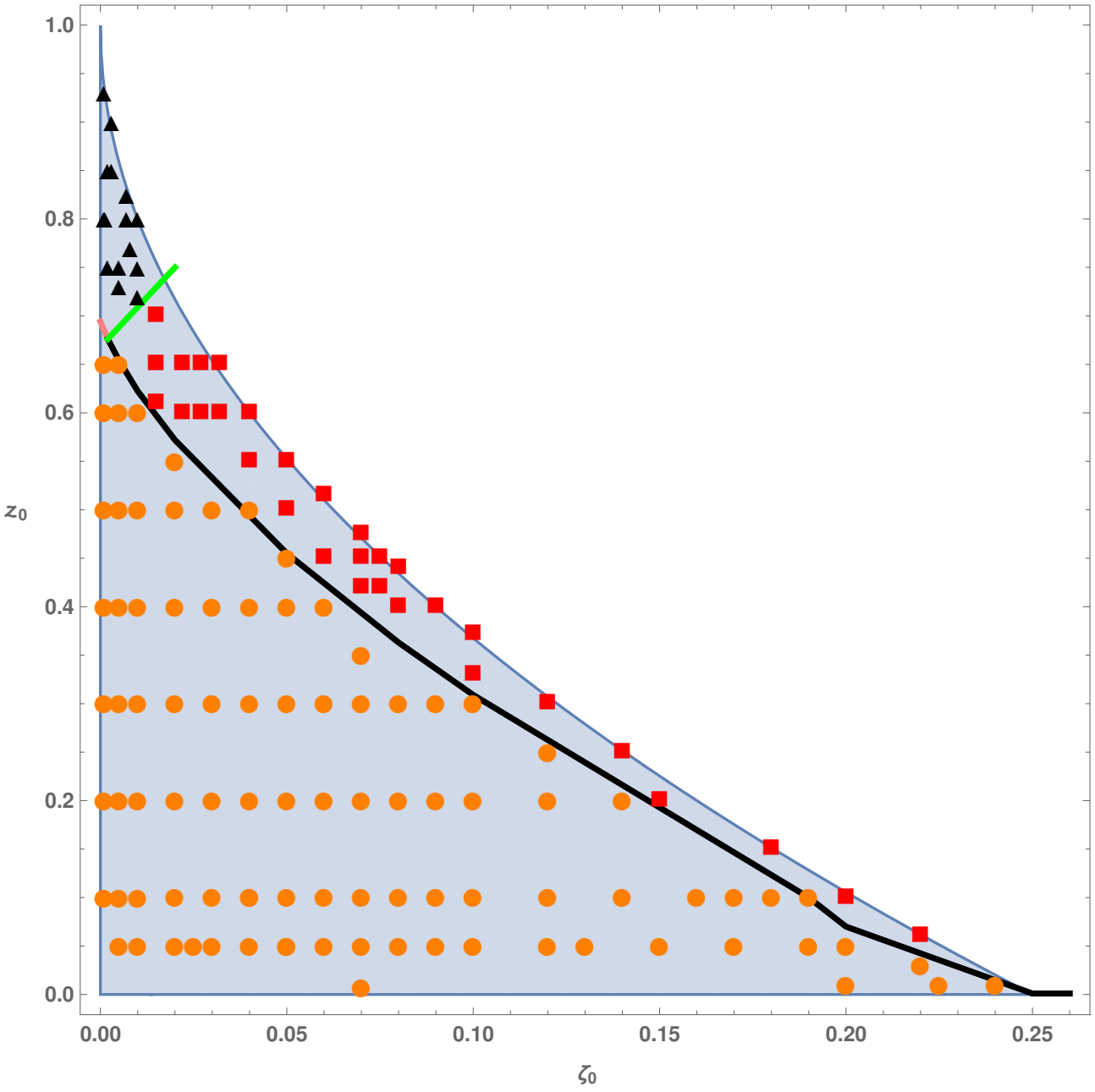

Figure 4.32: Phase diagrams (ζ_0, z_0) for 2d networks. It shows the domains of the three studied type of networks. The number densities of filaments segments are plotted as we vary the filament elongation parameter z_0 and the branching parameter ζ_0. On this phase diagram, the yellow dots zone corresponds to the domain of the branching networks that are dominated by short actin filaments with few branching. The black triangle domain is mainly composed of long linear actin chains formation with few branching. In the red squares domain, we have very branched networks. The points of the line separating the different domain correspond to (ζ_0, z_0) values for which we obtain the transition networks. The blue zone indicate the domain in which our numerical result is valid (domain of validity) given by the equation (4.3).

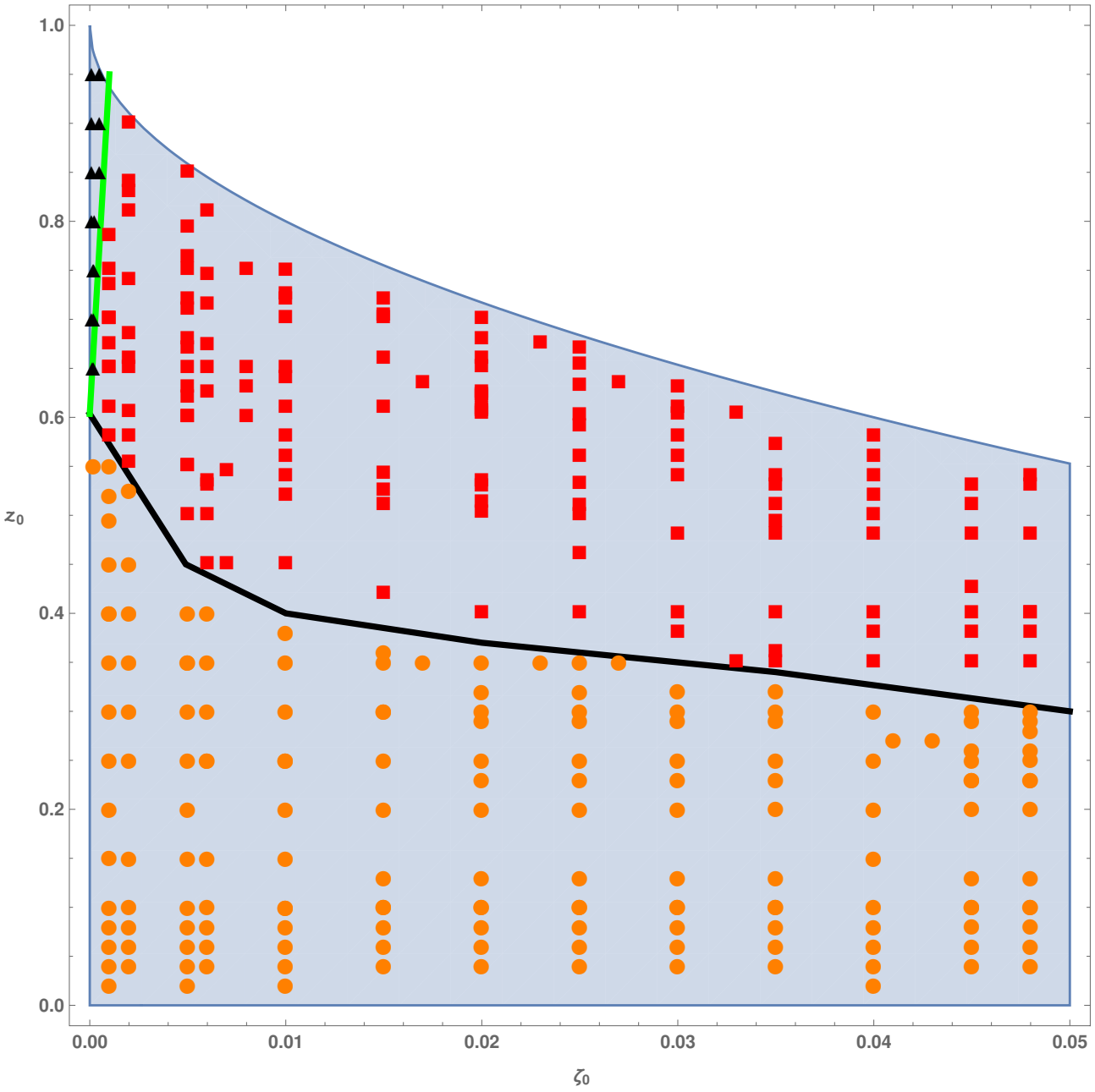

Figure 4.33: Phase diagrams (ζ_0, z_0) for 3d networks. It shows the domains of the three studied types of networks. The number densities of filaments segments are plotted as we vary the filament elongation parameter z_0 and the branching parameter ζ_0. On this phase diagram, the yellow dots zone corresponds to the domain of the branching networks that are dominated by short actin filaments with few branching. The black triangle domain is mainly composed of long linear actin chains formation with few branching. In the red squares domain, we have very branched networks. The points of the line separating the different domain correspond to (ζ_0, z_0) values for which we obtain the transition networks. The blue zone indicate the domain in which our numerical result is valid (domain of validity) given by the equation (4.3).

In summary, the knowledge of the densities and the radial order parameter fields profiles of the networks we have modelled enabled us to classify these networks into different types (typed according to their behaviour, structure, topology, spatial and orientational organization and thus according to their properties) and then locate them on the phase diagram.

The actin filaments of the confined branching networks that we have modelled are polarized i.e oriented. So in the presence of an external field in oriented or polar confined neworks system, one can expect to see a change in the networks behaviour and orientation either spontaneously or linearly. In the next section we wish to investigate how the confined branching actin networks that we modelled respond to perturbation.

We notice that the free energies show no noticeable discontinuties when crossing between regions on the diagram. Crossing the solid black line is defined by a definite change of sign of the density curvature in the centre. Since the cells are not homogeneous with order parameter varying along the radius, and the cell is finite, this is not a classical phase transition, but more like a cross-over between regimes of fundamentally different occupation of filaments inside the cell.

4.3.4 Response of confined branching actin Networks to perturbation

Analogously to the approach used for calculation of the magnetization $\mathbf{m}$ in the case of the Ising model, we introduce a new field in our system that imposes a preferential direction to the segments or filaments of the confined branched network and we measure the response of the network that we call vorticity V. In this case we redefine the fugacity $z(\boldsymbol{r}, \boldsymbol{n})$ to be

$$z'(\boldsymbol{r}, \boldsymbol{n}) = z(\boldsymbol{r}, \hat{\boldsymbol{n}}) e^{\eta \hat{B} \cdot (\hat{\boldsymbol{n}} \times \hat{\boldsymbol{u}})} \tag{4.11}$$

where η is analogous to the field h in the Ising model and V analogous to m. V is given by

$$V = \frac{1}{\mathcal{Z}} \frac{\delta \mathcal{Z}}{\delta \eta} \mid_{\eta=0} = \langle [\hat{B} \cdot (\hat{\boldsymbol{n}} \times \hat{\boldsymbol{u}})] \rangle \tag{4.12}$$

where $\hat{\boldsymbol{u}}$ is the radial unit vector taken from the of the sphere and $\hat{\boldsymbol{B}}$ the unit vector indicating the orientation of the field η.
We plot the vorticity as function of η and we found out that for different values of the stiffness ζ_0 of the networks, the networks respond linearly without breaking of the symmetry, see Figure 4.36. We plot also the different curve of $V(\eta)$ corresponding to different values of the growth factor z_0, see Figure 4.37 . We have obtained in that case also a linear response of the system.

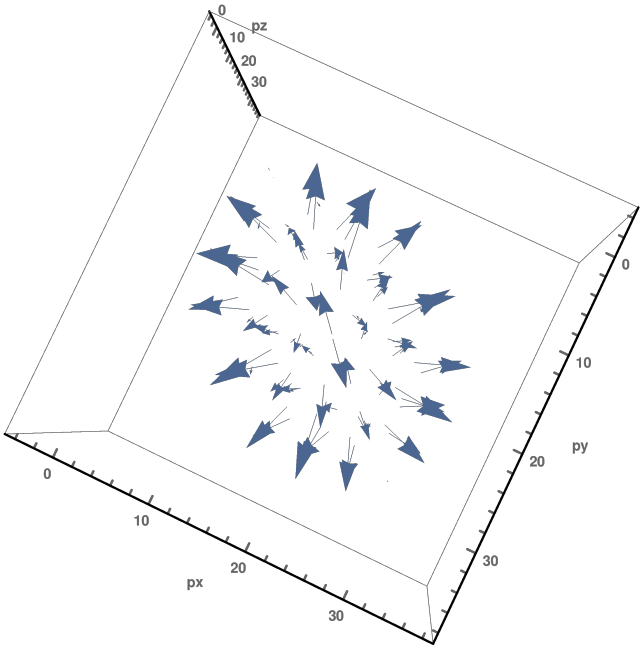

Figure 4.34: *Plot of the polarization for the field $\eta = 0$. It shows the direction in which the networks grow in the absence of external field. The networks grow from the centre towards the boundary of the confining cell.*

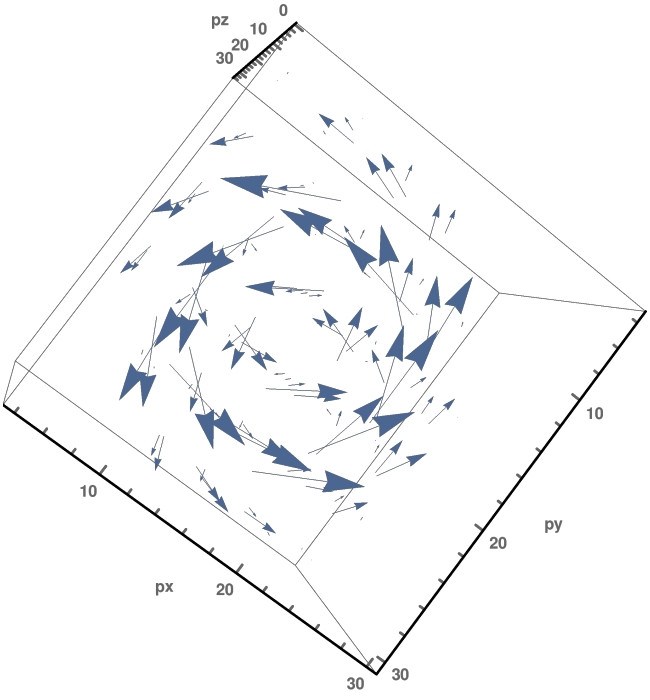

Figure 4.35: *The polarization of the branching networks in the presence of the external field, with $\eta = 0.4$. We observe that the networks grow in the orientation of the external field.*

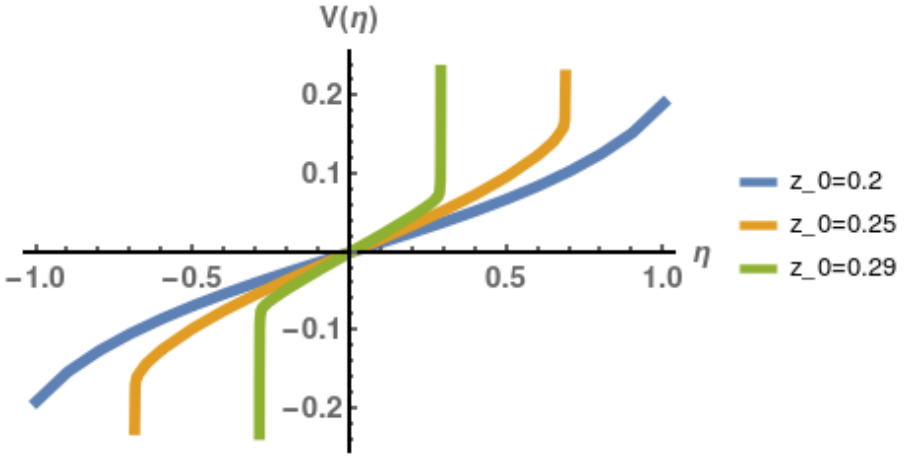

Figure 4.36: *Plot of the response of the networks as function of η and for three different growth parameter z_0 values, ζ_0 being fixed at 0.1. The sharp changes in the curves is correspond to the value η for which our numerical calculation diverges.*

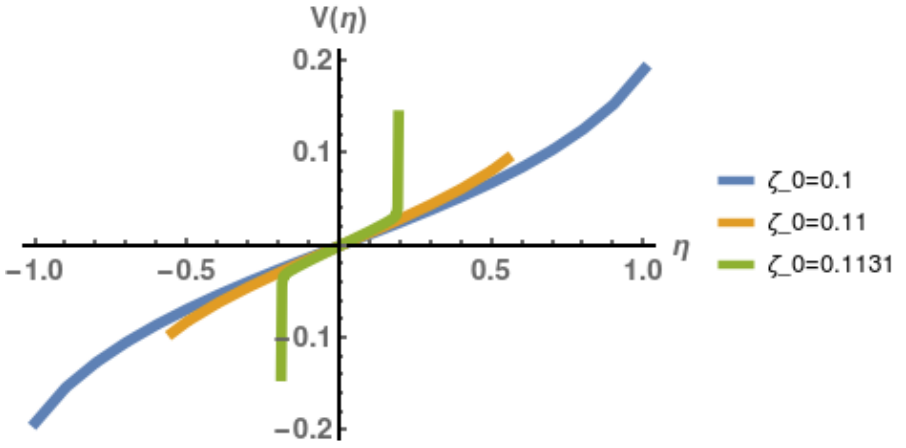

Figure 4.37: *Plot of the response of the networks as function of η and for three different stiffness ζ_0 values, z_0 being fixed at 0.2. The sharp changes in the curves is correspond to the value η for which our numerical calculation diverges.*

We observe a linear response of the branching actin network in the presence of an external field, see Figure 4.36 and 4.37, a result which is not very interesting as we expected. However the profile of the polarisation vector of the networks shows that the chain segments of the branching networks grow radially in the absence of external field, while in the presence of an external field with orientation along the magnetic field vector B (which we have chosen to be along the y axis for 3d networks), filament segments align in the direction of the field, see Figure 4.34 and 4.35.

4.4 Conclusion

Using the four main parameters, namely the persistence length of actin filament ℓ_p, the confining region diameter D, the filament elongation parameter z_0 and the filament branching parameter ζ_0, we have been able to construct various types of confined 2d and 3d branching actin networks (where the branching mimic the dendritic branching of actin filaments inside living eukaryotic cell via Arp2/3 protein complex) with various topologies and structure and predict some of their physical properties and structures when subjected to confinement. We got similar results for 2d and 3d networks.

The computation of the average density distribution of filament segments of the networks allowed us to make quantitative predictions of the effect of cell membrane confinement on the structure, conformation and behaviour of the actin networks. We showed that the networks of actin filaments made up mainly of long linear filaments and the branched networks are inhomogeneously distributed inside the cell whith a high density at the cell periphery [13, 98, 99]. This is due to the loss of available accessible conformations of the filaments of the networks as they grow and become longer than the confining cell size [41]. We computed also the order parameter field that allowed us to predict the influence of the confinement on the spatial organization and alignment of the different actin networks that we have grown. The order parameter field profile showed that networks dominated by long linear filaments experience strong confinement effect. They bent and wrap around the cell to minimize the free energy of the system [41, 43, 61, 109, 110]. Whereas the branched networks, though they experience a strong confinement effect do not bent. They rather point straight or perpendicular to the cell membrane or wall. This may be due to the high stiffness rate that branching via Arp2/3 protein complex introduce in the network system [71].

We calculated also the degree of polymerisation of the networks inside the spherical confining region as the values of change. We have next summarized our finding on a phase diagram for networks modelled in two dimension and for networks in 3d.

To see how the branching networks that we grow react to an external field similar to introducing magnetization in the case of Ising model, we remark that the network response which we name networks vorticity is linear. However the polarization of the networks shows that the introduction of the external field align the filaments of the networks in the direction of the field. Our model can be tested experimentally use all the parameters we defined above and also the using the average number of segments that we have obtained. We argue that our results mimic very well the properties and behaviour of actin networks via which they ensure cell function and mechanical stability. Fluorescent imaging of cells is able to inform one about filament density and it is also possible to gain orientational data (Tsugawa *et al.* [35] showed this for microtubules). We note that colleagues in Stellenbosch can confine cells using fibronetin substrates [113]. In principle, these tools can be combined to produce data relevant to our results.

We have also looked at the branching actin networks confined in cells with other geometries, namely cubic cell for 3d networks, square ,rectangular and triangular cells for networks modelled in 2d. The results we got are similar to the results we have obtained for networks confined in spherical geometry, see Appendix A2. The quantitative results from our models shows that regardless to the geometry of the confining region, the cell membrane or wall induces strong confinement constraints on branching cytoskeletal actin networks to control their conformations, their spatial organisation, orientational ordering, behaviour, conformation and this with respect of networks structures and architectures.

We study in the next chapter the properties of confined branching actin networks in which pair interactions between network chain segments are non negligible.

Chapter 5

Self-consistent and mean field theory for confined branching cytoskeletal networks

5.1 Introduction

In living cells, the function of biomacromolecules constituting the cell cytoskeleton is dictated by their structure, conformation, spatial organisation, orientational ordering and physical properties which, in turn, are considerably modified in geometrically confined or crowded spaces [13–16]. The knowledge of the structural and thermodynamic properties of confined semiflexible cytoskeletal filaments and their networks are of interest in medicine, in biotechnology and even in industrial applications.
For that, in Chapter 2 and Chapter 3 of this thesis we model the linear actin filaments and branching actin networks in confining region by considering that they are in the grand canonical monomer ensemble representation. In these models, we consider that the polymer chains are only subject to a backbone interaction which consist of the confining external fields z and ζ. Recall that actin filament inside the cell constitute an inhomogeneous networks [93, 98, 99] and the fields z and ζ, in our model induce the inhomogeneity (filaments elongation, branching and pruning) in the network system and they control also the geometry of the confining region. However natural or biological semiflexible polymers exhibit intra-chain interactions [98] and we should include these interactions. Two semiflexible polymers chains may appear to be similar on the macroscale, but a small difference in interactions between the segments of these chains may give rise to a great difference in their behaviour when confined in finite region. it is of great importance to understand how the presence of the interactions between the segments constituting the actin chains give rise to changes in the thermodynamic properties, behaviour and conformations of linear actin polymer chains and their branching networks inside confining regions.

In the present chapter, we aim to include in our model an interaction potential that takes

care of or that mimics these intra- semiflexible chain interactions. So beside the external fields z and ζ, we consider that there is an attractive interactions between any pair of monomers or segments of the actin polymer filaments. It is not obvious to directly derive and compute the relevant quantities such as the grand canonical partition function and thus of the densities, number of chain segments and the order field of the interacting monomer-based model that we build due to the fact that the interaction between segments introduce a correlation between each segment with the rest of the segments of the chain. It is a complex system and is similar to many-body problem. There exist methods that are commonly used is such situation such as the mean field theory to make the problem tractable or simpler. The mean field theory is a method in which the interaction of all the other individual particles (segments or monomers) with any given individual particle is approximated by a single averaged effect allowing to simplify the many-body problem into a one-body problem.
We implement the mean field technique by introducing a Hubbard-Stratonovich (H-S) transformation to convert the many interacting chain segments system into a statistical mean field-theorical model [69, 81] for which there exist approximation techniques that facilitate the computation of the relevant physical quantities. The theoretical handling of these field-theoretic polymeric model has been made possible by the development of the self-consistent field theory (SCFT) using statistical physics tools (Edward 1965, de Gennes, 1969 [69]). This theory has been widely and successfully used to understand and predict the properties of (confined) inhomogeneous polymer systems and also their microscopic conformations and behaviour [14, 44, 67, 114–116]. So, using the mean field approximation or SCFT also known as saddle point approximation, we envisage to compute the density of confined actin network filament segments, their order parameter field and their degree of polymerisation in the presence of the mutual monomers interactions.

In the first section of this chapter, we redefine the grand canonical partition functions for a system of confined linear actin filaments and for a system of confined branching cytoskeletal networks in the presence of monomer mutual interactions. Using the H-S transformations we express these grand partition functions as functional integrals of only chemical potential and auxiliary fields. In the second sections we compute the average density distributions of the chain segments of the confined branching networks using the SCFT approach. This also enable the computation of the average number of chain segments and their radial order parameter fields. In the final section, we present the results and make predictions.

5.1.1 The grand canonical partition of confined actin polymers in the presence of mutual monomer interactions

We wish to investigate the effect of the mutual monomer interactions on the structure, spatial organisation, ordering, conformation and the properties of confined actin networks in thermo-

dynamic equilibrium.

So, taking into account the mutual interaction or the excluded volume effects on the segments of the confined actin chains, we define the grand canonical partition function first for the confined linear actin polymer chains under confinement and after we extend this definition to confined branching networks which is made up of both linear and branched filaments.

5.1.2 Confined linear actin polymer chain

Recall that the linear actin chain is formed and embedded inside the confining domain by a chemical potential field that ensures the monomer activity, called fugacity z which acts as an external field and allows the linear elongation of the filament and also controls the confining geometry. This field is function of the positions and orientations of bonds of the chains. Since the actin filament is semiflexible, there exist a Boltzmann weight w associated to the bending stiffness between the chain bonds and is function of the positions and the angular orientations of the bonds. As a reminder, we rewrite here the definition of z and w. They are given by:

$$z(\boldsymbol{r}, \hat{\boldsymbol{n}}) = z_0 \theta(\boldsymbol{r}, \hat{\boldsymbol{n}}) \tag{5.1}$$

for the calculation of Ψ where

$$\theta(\boldsymbol{r}, \hat{\boldsymbol{n}}) = z_0 \times \begin{cases} 1, & \text{if } \boldsymbol{r} \in \mathbb{L} \text{ and } \boldsymbol{r} + \ell\hat{\boldsymbol{n}} \in \mathbb{L} \\ 0, & \text{otherwise} \end{cases} \tag{5.2}$$

and

$$w(\hat{\boldsymbol{n}}, \hat{\boldsymbol{n}}') = \frac{w_0}{\mathcal{N}_w} e^{\beta\epsilon \hat{\boldsymbol{n}}\cdot\hat{\boldsymbol{n}}'}. \tag{5.3}$$

where

$$\mathcal{N}_w = \sum_{\hat{\boldsymbol{n}}'} w(\hat{\boldsymbol{n}}, \hat{\boldsymbol{n}}') \tag{5.4}$$

We now define an interacting potential $V(\boldsymbol{r}, \boldsymbol{r}')$ between any pair monomers or segments at any positions $\boldsymbol{r}$ and $\boldsymbol{r}'$ of the chain. So, in the presence of interactions, the grand canonical partition

function of the single semiflexible linear (actin) chain becomes:

$$\begin{aligned}
\mathfrak{Z} = 1 + &\int \mathrm{d}^3\boldsymbol{r}_1\mathrm{d}^2\hat{\boldsymbol{n}}_1\, z(\boldsymbol{r}_1,\hat{\boldsymbol{n}}_1)+\\
&\int\int \mathrm{d}^3\boldsymbol{r}_1\mathrm{d}^2\hat{\boldsymbol{n}}_1\mathrm{d}^3\boldsymbol{r}_2\mathrm{d}^2\hat{\boldsymbol{n}}_2\, z(\mathbf{r}_1,\hat{\boldsymbol{n}}_1)w(\hat{\boldsymbol{n}}_1,\hat{\boldsymbol{n}}_2)z(\boldsymbol{r}_2,\hat{\boldsymbol{n}}_2)e^{-\beta V(\boldsymbol{r}_1-\boldsymbol{r}_2)}+\\
&\int\int\int \mathrm{d}^3\boldsymbol{r}_1\mathrm{d}^2\hat{\boldsymbol{n}}_1\mathrm{d}^3\boldsymbol{r}_2,\mathrm{d}^2\hat{\boldsymbol{n}}_2\mathrm{d}^3\boldsymbol{r}_3\mathrm{d}^2\hat{\boldsymbol{n}}_3\, z(\boldsymbol{r}_1,\hat{\boldsymbol{n}}_1)w(\hat{\boldsymbol{n}}_1,\hat{\boldsymbol{n}}_2)z(\boldsymbol{r}_2,\hat{\boldsymbol{n}}_2)\\
&\times w(\hat{\boldsymbol{n}}_2,\hat{\boldsymbol{n}}_3)z(\boldsymbol{r}_3,\hat{\boldsymbol{n}}_3)e^{-\beta(V(\boldsymbol{r}_1-\boldsymbol{r}_2)+V(\boldsymbol{r}_2-\boldsymbol{r}_3)+V(\boldsymbol{r}_1-\boldsymbol{r}_3))}+\\
&\int\int\int\int \mathrm{d}^3\boldsymbol{r}_1\mathrm{d}^2\hat{\boldsymbol{n}}_1\mathrm{d}^3\boldsymbol{r}_2\mathrm{d}^2\hat{\boldsymbol{n}}_2\mathrm{d}^3\boldsymbol{r}_3\mathrm{d}^2\hat{\boldsymbol{n}}_3\mathrm{d}^3\boldsymbol{r}_4\mathrm{d}^2\hat{\boldsymbol{n}}_4\, z(\boldsymbol{r}_1,\hat{\boldsymbol{n}}_1)w(\hat{\boldsymbol{n}}_1,\hat{\boldsymbol{n}}_2)z(\boldsymbol{r}_2,\hat{\boldsymbol{n}}_2)\\
&\times w(\hat{\boldsymbol{n}}_2,\hat{\boldsymbol{n}}_3)z(\boldsymbol{r}_3,\hat{\boldsymbol{n}}_3)w_1(\hat{\boldsymbol{n}}_3,\hat{\boldsymbol{n}}_4)z(\boldsymbol{r}_4,\hat{\boldsymbol{n}}_4)\\
&\times e^{-\beta(V(\boldsymbol{r}_1-\boldsymbol{r}_2)+V(\boldsymbol{r}_2-\boldsymbol{r}_3)+V(\boldsymbol{r}_3-\boldsymbol{r}_4)+V(\boldsymbol{r}_1-\boldsymbol{r}_3)+V(\boldsymbol{r}_1-\boldsymbol{r}_4)+V(\boldsymbol{r}_2-\boldsymbol{r}_4))}+\\
&\ldots+\int\ldots\int \mathrm{d}^3\boldsymbol{r}_1\mathrm{d}^2\hat{\boldsymbol{n}}_1\mathrm{d}^3\boldsymbol{r}_2\mathrm{d}^2\hat{\boldsymbol{n}}_2\ldots\mathrm{d}^3\boldsymbol{r}_N\mathrm{d}^2\hat{\boldsymbol{n}}_N\, z(\boldsymbol{r}_1,\hat{\boldsymbol{n}}_1)w_1(\hat{\boldsymbol{n}}_1,\hat{\boldsymbol{n}}_2)z(\boldsymbol{r}_2,\hat{\boldsymbol{n}}_2)\\
&\times\ldots w(\hat{\boldsymbol{n}}_{N-1},\hat{\boldsymbol{n}}_N)z(\boldsymbol{r}_N,\hat{\boldsymbol{n}}_N)e^{-\beta(V(\boldsymbol{r}_1-\boldsymbol{r}_2)+\ldots+V(\boldsymbol{r}_{N-1}-\boldsymbol{r}_N))}+\ldots.
\end{aligned} \tag{5.5}$$

Where we have illustrated the Boltzmann weight factor associated to the interaction between any pair of segments (i,j) of the chain by $e^{-\beta V(\boldsymbol{r}_i-\boldsymbol{r}_j)}$.
We can rewrite it as

$$\begin{aligned}
\mathfrak{Z} = 1+\sum_{N=1}^{\infty}\int\ldots\int \mathrm{d}^3\boldsymbol{r}_1\mathrm{d}^2\hat{\boldsymbol{n}}_1\mathrm{d}^3\boldsymbol{r}_2\mathrm{d}^2\hat{\boldsymbol{n}}_2\ldots\mathrm{d}^3\boldsymbol{r}_{N-1}\mathrm{d}^2\hat{\boldsymbol{n}}_{N-1}\mathrm{d}^3\boldsymbol{r}_N\mathrm{d}^2\hat{\boldsymbol{n}}_N\, z(\boldsymbol{r}_1,\hat{\boldsymbol{n}}_1)w(\hat{\boldsymbol{n}}_1,\hat{\boldsymbol{n}}_2)\\
\times z(\boldsymbol{r}_2,\hat{\boldsymbol{n}}_2)\ldots w(\hat{\boldsymbol{n}}_{N-1},\hat{\boldsymbol{n}}_N)z(\boldsymbol{r}_N,\hat{\boldsymbol{n}}_N)e^{-\frac{1}{2}\beta\sum_i^N\sum_j^N V(\boldsymbol{r}_i-\boldsymbol{r}_j)}.
\end{aligned} \tag{5.6}$$

Where the factor (1/2) in the expression of the segment-segment interaction weight $e^{-\frac{1}{2}\beta\sum_i^N\sum_j^N V(\boldsymbol{r}_i-\boldsymbol{r}_j)}$ is there to correct the double counting of each pair of segments of the chain in the double sum. Next, we define the grand canonical partition functions to the branching networks.

5.1.3 Confined branching actin networks

As we described previoiously in Chapter 3, to form the branching networks, we include in the confined linear chain system, the parameter ξ and ζ associated to the stiffness between segments that connect to the branching points and to the activity of the branching points. $\zeta(\boldsymbol{r},\hat{\boldsymbol{n}})$ is the chemical potential field or fugacity that mimic the activity of the branching or binding proteins (Arp2/3 protein complex) and is given by:

$$\zeta(\boldsymbol{r},\hat{\boldsymbol{n}},\boldsymbol{r}',\hat{\boldsymbol{n}}') = \delta(\boldsymbol{r}-\boldsymbol{r}')\zeta(\boldsymbol{r},\hat{\boldsymbol{n}},\hat{\boldsymbol{n}}') \tag{5.7}$$

where

$$\zeta(\boldsymbol{r},\hat{\boldsymbol{n}},\hat{\boldsymbol{n}}') = \zeta_0\times\begin{cases}1, & \text{if}\boldsymbol{r}\in\mathbb{L}\text{ and }\boldsymbol{r}+\ell\hat{\boldsymbol{n}}\in\mathbb{L}\\ \text{ and} & \boldsymbol{r}+\ell\hat{\boldsymbol{n}}'\in\mathbb{L}\\ 0, & \text{otherwise}\end{cases} \tag{5.8}$$

The Boltzman weight $\xi(\hat{\boldsymbol{n}}, \hat{\boldsymbol{n}}', \hat{\boldsymbol{n}}'')$ ($\hat{\boldsymbol{n}}, \hat{\boldsymbol{n}}'$and $\hat{\boldsymbol{n}}''$) are the orientations of the segments that meet at branching points) associated to the bending stiffness between segments that meet at the branching points is:

$$\xi(\hat{\boldsymbol{n}}, \hat{\boldsymbol{n}}', \hat{\boldsymbol{n}}'') = \frac{\mathcal{N}_w}{\mathcal{N}_\xi} w(\hat{\boldsymbol{n}}, \hat{\boldsymbol{n}}') \times e^{\left(-\xi_0\left(\hat{\boldsymbol{n}}\cdot\hat{\boldsymbol{n}}''-\cos\alpha\right)^2-\xi_1\left(\hat{\boldsymbol{n}}'\cdot\hat{\boldsymbol{n}}''-\cos\alpha\right)^2\right)}. \tag{5.9}$$

The grand canonical partition function for the branching networks in the presence of the mutual monomer or segments of the network interaction is given by:

$$\begin{aligned}
\mathfrak{Z} = 1 &+ \int \mathrm{d}^3\boldsymbol{r}_1 \mathrm{d}^2\hat{\boldsymbol{n}}_1\, z(\boldsymbol{r}_1, \hat{\boldsymbol{n}}_1) + \\
&\int\int \mathrm{d}^3\boldsymbol{r}_1 \mathrm{d}^2\hat{\boldsymbol{n}}_1 \mathrm{d}^3\boldsymbol{r}_2 \mathrm{d}^2\hat{\boldsymbol{n}}_2\, z(\mathbf{r}_1, \hat{\boldsymbol{n}}_1) w(\hat{\boldsymbol{n}}_1, \hat{\boldsymbol{n}}_2) z(\boldsymbol{r}_2, \hat{\boldsymbol{n}}_2) e^{-\beta V(\boldsymbol{r}_1-\boldsymbol{r}_2)} + \\
&\int\int\int \mathrm{d}^3\boldsymbol{r}_1 \mathrm{d}^2\hat{\boldsymbol{n}}_1 \mathrm{d}^3\boldsymbol{r}_2, \mathrm{d}^2\hat{\boldsymbol{n}}_2 \mathrm{d}^3\boldsymbol{r}_3 \mathrm{d}^2\hat{\boldsymbol{n}}_3\, z(\boldsymbol{r}_1, \hat{\boldsymbol{n}}_1) w(\hat{\boldsymbol{n}}_1, \hat{\boldsymbol{n}}_2) z(\boldsymbol{r}_2, \hat{\boldsymbol{n}}_2) \\
&\times w(\hat{\boldsymbol{n}}_2, \hat{\boldsymbol{n}}_3) z(\boldsymbol{r}_3, \hat{\boldsymbol{n}}_3) e^{-\beta(V(\boldsymbol{r}_1-\boldsymbol{r}_2)+V(\boldsymbol{r}_2-\boldsymbol{r}_3)+V(\boldsymbol{r}_1-\boldsymbol{r}_3))} + \\
&\int\int\int\int \mathrm{d}^3\boldsymbol{r}_1 \mathrm{d}^2\hat{\boldsymbol{n}}_1 \mathrm{d}^3\boldsymbol{r}_2 \mathrm{d}^2\hat{\boldsymbol{n}}_2 \mathrm{d}^3\boldsymbol{r}_3 \mathrm{d}^2\hat{\boldsymbol{n}}_3 \mathrm{d}^3\boldsymbol{r}_4 \mathrm{d}^2\hat{\boldsymbol{n}}_4\, z(\boldsymbol{r}_1, \hat{\boldsymbol{n}}_1) w(\hat{\boldsymbol{n}}_1, \hat{\boldsymbol{n}}_2) z(\boldsymbol{r}_2, \hat{\boldsymbol{n}}_2) \\
&\times w(\hat{\boldsymbol{n}}_2, \hat{\boldsymbol{n}}_3) z(\boldsymbol{r}_3, \hat{\boldsymbol{n}}_3) w_1(\hat{\boldsymbol{n}}_3, \hat{\boldsymbol{n}}_4) z(\boldsymbol{r}_4, \hat{\boldsymbol{n}}_4) \\
&\times e^{-\beta(V(\boldsymbol{r}_1-\boldsymbol{r}_2)+V(\boldsymbol{r}_2-\boldsymbol{r}_3)+V(\boldsymbol{r}_3-\boldsymbol{r}_4)+V(\boldsymbol{r}_1-\boldsymbol{r}_3)+V(\boldsymbol{r}_1-\boldsymbol{r}_4)+V(\boldsymbol{r}_2-\boldsymbol{r}_4))} + \\
&\ldots + \int \ldots \int \mathrm{d}^3\boldsymbol{r}_1 \mathrm{d}^2\hat{\boldsymbol{n}}_1 \mathrm{d}^3\boldsymbol{r}_2 \mathrm{d}^2\hat{\boldsymbol{n}}_2 \ldots \mathrm{d}^3\boldsymbol{r}_N \mathrm{d}^2\hat{\boldsymbol{n}}_N\, z(\boldsymbol{r}_1, \hat{\boldsymbol{n}}_1) w_1(\hat{\boldsymbol{n}}_1, \hat{\boldsymbol{n}}_2) z(\boldsymbol{r}_2, \hat{\boldsymbol{n}}_2) \\
&\times \ldots w(\hat{\boldsymbol{n}}_{N-1}, \hat{\boldsymbol{n}}_N) z(\boldsymbol{r}_N, \hat{\boldsymbol{n}}_N) e^{-\beta(V(\boldsymbol{r}_1-\boldsymbol{r}_2)+\ldots+V(\boldsymbol{r}_{N-1}-\boldsymbol{r}_N))} + \\
&\int\int\int \mathrm{d}^3\boldsymbol{r}_1 \mathrm{d}^2\hat{\boldsymbol{n}}_1 \mathrm{d}^3\boldsymbol{r}_2 \mathrm{d}^2\hat{\boldsymbol{n}}_2 \mathrm{d}^3\boldsymbol{r}_3 \mathrm{d}^2\hat{\boldsymbol{n}}_3\, z(\boldsymbol{r}_1, \hat{\boldsymbol{n}}_1) \xi(\hat{\boldsymbol{n}}_1, \hat{\boldsymbol{n}}_2, \hat{\boldsymbol{n}}_3) \zeta(\boldsymbol{r}_2, \hat{\boldsymbol{n}}_2, \boldsymbol{r}_3, \hat{\boldsymbol{n}}_3) \\
&\times e^{-\beta(V(\boldsymbol{r}_1-\boldsymbol{r}_2)+V(\boldsymbol{r}_2-\boldsymbol{r}_3)+V(\boldsymbol{r}_1-\boldsymbol{r}_3))} + \\
&\int\int\int\int \mathrm{d}^3\boldsymbol{r}_1 \mathrm{d}^2\hat{\boldsymbol{n}}_1 \mathrm{d}^3\boldsymbol{r}_2 \mathrm{d}^2\hat{\boldsymbol{n}}_2 \mathrm{d}^3\boldsymbol{r}_3 \mathrm{d}^2\hat{\boldsymbol{n}}_3 \mathrm{d}^3\boldsymbol{r}_4 \mathrm{d}^2\hat{\boldsymbol{n}}_4\, z(\boldsymbol{r}_1, \hat{\boldsymbol{n}}_1) \xi(\hat{\boldsymbol{n}}_1, \hat{\boldsymbol{n}}_2, \hat{\boldsymbol{n}}_3) \zeta(\boldsymbol{r}_2, \hat{\boldsymbol{n}}_2, \boldsymbol{r}_3, \hat{\boldsymbol{n}}_3) \\
&w(\hat{\boldsymbol{n}}_2, \hat{\boldsymbol{n}}_4) z(\boldsymbol{r}_4, \hat{\boldsymbol{n}}_4) e^{-\beta(V(\boldsymbol{r}_1-\boldsymbol{r}_2)+V(\boldsymbol{r}_2-\boldsymbol{r}_3)+V(\boldsymbol{r}_3-\boldsymbol{r}_4)+V(\boldsymbol{r}_1-\boldsymbol{r}_3)+V(\boldsymbol{r}_1-\boldsymbol{r}_4)+V(\boldsymbol{r}_2-\boldsymbol{r}_4))} + \\
&\int\int\int\int\int \mathrm{d}^3\boldsymbol{r}_1 \mathrm{d}^2\hat{\boldsymbol{n}}_1 \mathrm{d}^3\boldsymbol{r}_2 \mathrm{d}^2\hat{\boldsymbol{n}}_2 \mathrm{d}^3\boldsymbol{r}_3 \mathrm{d}^2\hat{\boldsymbol{n}}_3 \mathrm{d}^3\boldsymbol{r}_4 \mathrm{d}^2\hat{\boldsymbol{n}}_4 \mathrm{d}^3\boldsymbol{r}_5 \mathrm{d}^2\hat{\boldsymbol{n}}_5\, z(\boldsymbol{r}_1, \hat{\boldsymbol{n}}_1) \xi(\hat{\boldsymbol{n}}_1, \hat{\boldsymbol{n}}_2, \hat{\boldsymbol{n}}_3) \\
&\times \zeta(\boldsymbol{r}_2, \hat{\boldsymbol{n}}_2, \boldsymbol{r}_3, \hat{\boldsymbol{n}}_3) w(\hat{\boldsymbol{n}}_2, \hat{\boldsymbol{n}}_4) z(\boldsymbol{r}_4, \hat{\boldsymbol{n}}_4)) w(\hat{\boldsymbol{n}}_3, \hat{\boldsymbol{n}}_5) z(\boldsymbol{r}_5, \hat{\boldsymbol{n}}_5) e^{-\beta(V(\boldsymbol{r}_1-\boldsymbol{r}_2)+V(\boldsymbol{r}_2-\boldsymbol{r}_3)+\ldots+V(\boldsymbol{r}_4-\boldsymbol{r}_5))} + \\
&\int\int\int\int\int \mathrm{d}^3\boldsymbol{r}_1 \mathrm{d}^2\hat{\boldsymbol{n}}_1 \mathrm{d}^3\boldsymbol{r}_2 \mathrm{d}^2\hat{\boldsymbol{n}}_2 \mathrm{d}^3\boldsymbol{r}_3 \mathrm{d}^2\hat{\boldsymbol{n}}_3 \mathrm{d}^3\boldsymbol{r}_4 \mathrm{d}^2\hat{\boldsymbol{n}}_4 \mathrm{d}^3\boldsymbol{r}_5 \mathrm{d}^2\hat{\boldsymbol{n}}_5\, z(\boldsymbol{r}_1, \hat{\boldsymbol{n}}_1) \xi(\hat{\boldsymbol{n}}_1, \hat{\boldsymbol{n}}_2, \hat{\boldsymbol{n}}_3) \\
&\times \zeta(\boldsymbol{r}_2, \hat{\boldsymbol{n}}_2, \boldsymbol{r}_3, \hat{\boldsymbol{n}}_3) \xi(\hat{\boldsymbol{n}}_2, \hat{\boldsymbol{n}}_4, \hat{\boldsymbol{n}}_5) \zeta(\boldsymbol{r}_4, \hat{\boldsymbol{n}}_4, \boldsymbol{r}_5, \hat{\boldsymbol{n}}_5) e^{-\beta(V(\boldsymbol{r}_1-\boldsymbol{r}_2)+V(\boldsymbol{r}_2-\boldsymbol{r}_3)+\ldots+V(\boldsymbol{r}_4-\boldsymbol{r}_5))} + \ldots
\end{aligned} \tag{5.10}$$

We rewrite (5.10) as:

$$\begin{aligned}
\mathfrak{Z} = 1 + \sum_{N=1}^{\infty} \Bigg(& \int \dots \int \mathrm{d}^3\boldsymbol{r}_1 \mathrm{d}^2\hat{\boldsymbol{n}}_1 \mathrm{d}^3\boldsymbol{r}_2 \mathrm{d}^2\hat{\boldsymbol{n}}_2 \dots \mathrm{d}^3\boldsymbol{r}_{N-1} \mathrm{d}^2\hat{\boldsymbol{n}}_{N-1} \mathrm{d}^3\boldsymbol{r}_N \mathrm{d}^2\hat{\boldsymbol{n}}_N \, z(\boldsymbol{r}_1, \hat{\boldsymbol{n}}_1) w(\hat{\boldsymbol{n}}_1, \hat{\boldsymbol{n}}_2) \\
& \times z(\boldsymbol{r}_2, \hat{\boldsymbol{n}}_2) \dots z(\boldsymbol{r}_{N-1}, \hat{\boldsymbol{n}}_{N-1}) w(\hat{\boldsymbol{n}}_{N-1}, \hat{\boldsymbol{n}}_N) z(\boldsymbol{r}_N, \hat{\boldsymbol{n}}_N) e^{-\frac{1}{2}\beta \sum_i^N \sum_j^N V(\boldsymbol{r}_i - \boldsymbol{r}_j)} \\
& + \int \dots \int \mathrm{d}^3\boldsymbol{r}_1 \mathrm{d}^2\hat{\boldsymbol{n}}_1 \mathrm{d}^3\boldsymbol{r}_2 \mathrm{d}^2\hat{\boldsymbol{n}}_2 \mathrm{d}^3\boldsymbol{r}_3 \mathrm{d}^2\hat{\boldsymbol{n}}_3 \mathrm{d}^3\boldsymbol{r}_4 \mathrm{d}^2\hat{\boldsymbol{n}}_4 \, z(\boldsymbol{r}_1, \hat{\boldsymbol{n}}_1) \xi(\hat{\boldsymbol{n}}_1, \hat{\boldsymbol{n}}_2, \hat{\boldsymbol{n}}_3) \zeta(\boldsymbol{r}_2, \hat{\boldsymbol{n}}_2, \boldsymbol{r}_3, \hat{\boldsymbol{n}}_3) \\
& \times w(\hat{\boldsymbol{n}}_2, \hat{\boldsymbol{n}}_4) z(\boldsymbol{r}_4, \hat{\boldsymbol{n}}_4) \dots z(\boldsymbol{r}_{N-1}, \hat{\boldsymbol{n}}_{N-1}) w(\hat{\boldsymbol{n}}_{N-1}, \hat{\boldsymbol{n}}_N) z(\boldsymbol{r}_N, \hat{\boldsymbol{n}}_N) e^{-\frac{1}{2}\beta \sum_i^N \sum_j^N V(\boldsymbol{r}_i - \boldsymbol{r}_j)} \\
& + \int \dots \int \mathrm{d}^3\boldsymbol{r}_1 \mathrm{d}^2\hat{\boldsymbol{n}}_1 \mathrm{d}^3\boldsymbol{r}_2 \mathrm{d}^2\hat{\boldsymbol{n}}_2 \mathrm{d}^3\boldsymbol{r}_3 \mathrm{d}^2\hat{\boldsymbol{n}}_3 \mathrm{d}^3\boldsymbol{r}_4 \mathrm{d}^2\hat{\boldsymbol{n}}_4 \mathrm{d}^3\boldsymbol{r}_5 \mathrm{d}^2\hat{\boldsymbol{n}}_5 \mathrm{d}^3\boldsymbol{r}_6 \mathrm{d}^2\hat{\boldsymbol{n}}_6 \\
& z(\boldsymbol{r}_1, \hat{\boldsymbol{n}}_1) \xi(\hat{\boldsymbol{n}}_1, \hat{\boldsymbol{n}}_2, \hat{\boldsymbol{n}}_3) \zeta(\boldsymbol{r}_2, \hat{\boldsymbol{n}}_2, \boldsymbol{r}_3, \hat{\boldsymbol{n}}_3) \xi(\hat{\boldsymbol{n}}_2, \hat{\boldsymbol{n}}_4, \hat{\boldsymbol{n}}_5) \zeta(\boldsymbol{r}_4, \hat{\boldsymbol{n}}_4, \boldsymbol{r}_5, \hat{\boldsymbol{n}}_5) w(\hat{\boldsymbol{n}}_4, \hat{\boldsymbol{n}}_6) \\
& \times z(\boldsymbol{r}_6, \hat{\boldsymbol{n}}_6) \dots z(\boldsymbol{r}_{N-1}, \hat{\boldsymbol{n}}_{N-1}) w(\hat{\boldsymbol{n}}_{N-1}, \hat{\boldsymbol{n}}_N) z(\boldsymbol{r}_N, \hat{\boldsymbol{n}}_N) e^{-\frac{1}{2}\beta \sum_i^N \sum_j^N V(\boldsymbol{r}_i - \boldsymbol{r}_j)} + \dots \\
& + \int \dots \int \mathrm{d}^3\boldsymbol{r}_1 \mathrm{d}^2\hat{\boldsymbol{n}}_1 \mathrm{d}^3\boldsymbol{r}_2 \mathrm{d}^2\hat{\boldsymbol{n}}_2 \mathrm{d}^3\boldsymbol{r}_3 \mathrm{d}^2\hat{\boldsymbol{n}}_3 \mathrm{d}^3\boldsymbol{r}_4 \mathrm{d}^2\hat{\boldsymbol{n}}_4 \mathrm{d}^3\boldsymbol{r}_5 \mathrm{d}^2\hat{\boldsymbol{n}}_5 \, z(\boldsymbol{r}_1, \hat{\boldsymbol{n}}_1) \xi(\hat{\boldsymbol{n}}_1, \hat{\boldsymbol{n}}_2, \hat{\boldsymbol{n}}_3) \\
& \times \zeta(\boldsymbol{r}_2, \hat{\boldsymbol{n}}_2, \boldsymbol{r}_3, \hat{\boldsymbol{n}}_3) \xi(\hat{\boldsymbol{n}}_2, \hat{\boldsymbol{n}}_4, \hat{\boldsymbol{n}}_5) \zeta(\boldsymbol{r}_4, \hat{\boldsymbol{n}}_4, \boldsymbol{r}_5, \hat{\boldsymbol{n}}_5) \dots \xi(\hat{\boldsymbol{n}}_{N-3}, \boldsymbol{n}_{N-1}, \hat{\boldsymbol{n}}_N) \\
& \times \zeta(\boldsymbol{r}_{N-1}, \hat{\boldsymbol{n}}_{N-1}, \boldsymbol{r}_N, \hat{\boldsymbol{n}}_N) e^{-\frac{1}{2}\beta \sum_i^N \sum_j^N V(\boldsymbol{r}_i - \boldsymbol{r}_j)} \Bigg)
\end{aligned} \tag{5.11}$$

The grand partition function given by (5.8) can not be computed easily in order to calculate the relevant quantities that will enable us to find the effect of confinement on the branching networks in the presence of mutual monomers interactions. So, in the current situation, we use the mean field-theorical approach to make the problem tractable.

5.1.4 Expression of the grand partition in term of a mean field

The self-consistent procedure or technique consist of considering the average value of total pair interactions acting on any individual segment of the chain(s) as an external field $\phi(\boldsymbol{r})$ created by the other segments of the chain. The H-S transformation is one of the technique use in the mean field theory to decouple these mutual interactions between the chain segments. In this theory, we can express the term that stands for the pair interactions of the chain segments in the definition of the grand canonical partition function as functional of the auxiliary field $\phi(\boldsymbol{r})$. For that we need to write the weight of the interacting potential in term of the microscopic chain segment density $\rho(\boldsymbol{r})$ ($\rho(\boldsymbol{r})$ allows to write the double sum over the pair interactions in term of integrals or in continuous form while keeping the spatial correlation between chain segments.)

$$\rho(\boldsymbol{r}) = \sum_k \delta(\boldsymbol{r} - \boldsymbol{r}_k) \tag{5.12}$$

as:

$$e^{-\frac{1}{2}\beta \sum_i \sum_j V(\boldsymbol{r}_i - \boldsymbol{r}_j)} = e^{-\frac{1}{2}\beta \left(\int \mathrm{d}^3\boldsymbol{r} \int \mathrm{d}^3\boldsymbol{r}' \rho(\boldsymbol{r}) V(\boldsymbol{r} - \boldsymbol{r}') \rho(\boldsymbol{r}') \right)} \tag{5.13}$$

Equation (5.13) is equivalent to the following Gaussian integral equation (H-S transformation):

$$e^{-\frac{1}{2}\beta \left(\int \mathrm{d}^3\boldsymbol{r} \int \mathrm{d}^3\boldsymbol{r}' \rho(\boldsymbol{r}) V(\boldsymbol{r} - \boldsymbol{r}') \rho(\boldsymbol{r}') \right)} = \mathcal{N}_\phi \int D\phi e^{-\frac{1}{2}\beta \left(\int \mathrm{d}^3\boldsymbol{r} \int \mathrm{d}^3\boldsymbol{r}' \phi(\boldsymbol{r}) V^{-1}(\boldsymbol{r} - \boldsymbol{r}') \phi(\boldsymbol{r}') \right) + i \int \mathrm{d}^3\boldsymbol{r} \phi(\boldsymbol{r}) \rho(\boldsymbol{r})} \tag{5.14}$$

where $\phi(\boldsymbol{r})$ is the mean field and $\mathcal{N}_\phi$ the normalisation factor. Replacing equation (5.12) in equation (5.14), we may rewrite the term $e^{i\int \mathrm{d}^3\boldsymbol{r}\phi(\boldsymbol{r})\rho(\boldsymbol{r})}$ as:

$$e^{i\int \mathrm{d}^3\boldsymbol{r}\phi(\boldsymbol{r})\rho(\boldsymbol{r})} = \prod_k e^{\mathrm{i}\phi(\boldsymbol{r}_k)} \tag{5.15}$$

So the grand canonical partition functions for Confined linear actin chain becomes

$$\begin{aligned}\mathfrak{Z} = \mathcal{N}_{\phi,1}\sum_{N=0}^{\infty}\int \mathrm{D}\phi \int \mathrm{d}^3\boldsymbol{r}_1\mathrm{d}^2\hat{\boldsymbol{n}}_1\mathrm{d}^3\boldsymbol{r}_2\mathrm{d}^2\hat{\boldsymbol{n}}_2\ldots\mathrm{d}^3\boldsymbol{r}_N\mathrm{d}^2\hat{\boldsymbol{n}}_N\, z(\boldsymbol{r}_1,\hat{\boldsymbol{n}}_1)e^{\imath\phi(\boldsymbol{r}_1)}w(\hat{\boldsymbol{n}}_1,\hat{\boldsymbol{n}}_2)\\ \times z(\boldsymbol{r}_2,\hat{\boldsymbol{n}}_2)e^{\imath\phi(\boldsymbol{r}_2)}\ldots w(\hat{\boldsymbol{n}}_{N-1},\hat{\boldsymbol{n}}_N)z(\boldsymbol{r}_N,\hat{\boldsymbol{n}}_N)e^{\imath\phi(\boldsymbol{r}_N)}e^{-\frac{1}{2}\beta\left(\int \mathrm{d}^3\boldsymbol{r}\int \mathrm{d}^3\boldsymbol{r}'\phi(\boldsymbol{r})V^{-1}(\boldsymbol{r}-\boldsymbol{r}')\phi(\boldsymbol{r}')\right)}.\end{aligned} \tag{5.16}$$

and the grand canonical partition function for confined branching actin network is:

$$\begin{aligned}\mathfrak{Z} = \mathcal{N}_{\phi,2}\sum_{N=0}^{\infty}\int \mathrm{D}\phi\Bigg(\int\ldots\int \mathrm{d}^3\boldsymbol{r}_1\mathrm{d}^2\hat{\boldsymbol{n}}_1\mathrm{d}^3\boldsymbol{r}_2\mathrm{d}^2\hat{\boldsymbol{n}}_2\ldots\mathrm{d}^3\boldsymbol{r}_{N-1}\mathrm{d}^2\hat{\boldsymbol{n}}_{N-1}\mathrm{d}^3\boldsymbol{r}_N\mathrm{d}^2\hat{\boldsymbol{n}}_N\\ e^{\imath\phi(\boldsymbol{r}_1)}z(\boldsymbol{r}_1,\hat{\boldsymbol{n}}_1)w(\hat{\boldsymbol{n}}_1,\hat{\boldsymbol{n}}_2)e^{\imath\phi(\boldsymbol{r}_2)}z(\boldsymbol{r}_2,\hat{\boldsymbol{n}}_2)\ldots e^{\imath\phi(\boldsymbol{r}_{N-1})}z(\boldsymbol{r}_{N-1},\hat{\boldsymbol{n}}_{N-1})w(\hat{\boldsymbol{n}}_{N-1},\hat{\boldsymbol{n}}_N)\\ \times e^{\imath\phi(\boldsymbol{r}_N)}z(\boldsymbol{r}_N,\hat{\boldsymbol{n}}_N) + \int\ldots\int \mathrm{d}^3\boldsymbol{r}_1\mathrm{d}^2\hat{\boldsymbol{n}}_1\mathrm{d}^3\boldsymbol{r}_2\mathrm{d}^2\hat{\boldsymbol{n}}_2\mathrm{d}^3\boldsymbol{r}_3\mathrm{d}^2\hat{\boldsymbol{n}}_3\mathrm{d}^3\boldsymbol{r}_4\mathrm{d}^2\hat{\boldsymbol{n}}_4\\ e^{\imath\phi(\boldsymbol{r}_1)}z(\boldsymbol{r}_1,\hat{\boldsymbol{n}}_1)\xi(\hat{\boldsymbol{n}}_1,\hat{\boldsymbol{n}}_2,\hat{\boldsymbol{n}}_3)e^{\imath\phi(\boldsymbol{r}_2)}\zeta(\boldsymbol{r}_2,\hat{\boldsymbol{n}}_2,\boldsymbol{r}_3,\hat{\boldsymbol{n}}_3)e^{\imath\phi(\boldsymbol{r}_3)}w(\hat{\boldsymbol{n}}_2,\hat{\boldsymbol{n}}_4)\\ \times e^{\imath\phi(\boldsymbol{r}_4)}z(\boldsymbol{r}_4,\hat{\boldsymbol{n}}_4)\ldots e^{\imath\phi(\boldsymbol{r}_{N-1})}z(\boldsymbol{r}_{N-1},\hat{\boldsymbol{n}}_{N-1})w(\hat{\boldsymbol{n}}_{N-1},\hat{\boldsymbol{n}}_N)e^{\imath\phi(\boldsymbol{r}_N)}z(\boldsymbol{r}_N,\hat{\boldsymbol{n}}_N)\\ + \int\ldots\int \mathrm{d}^3\boldsymbol{r}_1\mathrm{d}^2\hat{\boldsymbol{n}}_1\mathrm{d}^3\boldsymbol{r}_2\mathrm{d}^2\hat{\boldsymbol{n}}_2\mathrm{d}^3\boldsymbol{r}_3\mathrm{d}^2\hat{\boldsymbol{n}}_3\mathrm{d}^3\boldsymbol{r}_4\mathrm{d}^2\hat{\boldsymbol{n}}_4\mathrm{d}^3\boldsymbol{r}_5\mathrm{d}^2\hat{\boldsymbol{n}}_5\mathrm{d}^3\boldsymbol{r}_6\mathrm{d}^2\hat{\boldsymbol{n}}_6\\ e^{\imath\phi(\boldsymbol{r}_1)}z(\boldsymbol{r}_1,\hat{\boldsymbol{n}}_1)\xi(\hat{\boldsymbol{n}}_1,\hat{\boldsymbol{n}}_2,\hat{\boldsymbol{n}}_3)e^{\imath\phi(\boldsymbol{r}_2)}\\ \times\zeta(\boldsymbol{r}_2,\hat{\boldsymbol{n}}_2,\boldsymbol{r}_3,\hat{\boldsymbol{n}}_3)e^{\imath\phi(\boldsymbol{r}_3)}\xi(\hat{\boldsymbol{n}}_2,\hat{\boldsymbol{n}}_4,\hat{\boldsymbol{n}}_5)e^{\imath\phi(\boldsymbol{r}_4)}\zeta(\boldsymbol{r}_4,\hat{\boldsymbol{n}}_4,\boldsymbol{r}_5,\hat{\boldsymbol{n}}_5)e^{\imath\phi(\boldsymbol{r}_5)}w(\hat{\boldsymbol{n}}_4,\hat{\boldsymbol{n}}_6)\\ \times e^{\imath\phi(\boldsymbol{r}_6)}z(\boldsymbol{r}_6,\hat{\boldsymbol{n}}_6)\ldots e^{\imath\phi(\boldsymbol{r}_{N-1})}z(\boldsymbol{r}_{N-1},\hat{\boldsymbol{n}}_{N-1})w(\hat{\boldsymbol{n}}_{N-1},\hat{\boldsymbol{n}}_N)z(\boldsymbol{r}_N,\hat{\boldsymbol{n}}_N)e^{\imath\phi(\boldsymbol{r}_N)} + \ldots\\ + \int\ldots\int \mathrm{d}^3\boldsymbol{r}_1\mathrm{d}^2\hat{\boldsymbol{n}}_1\mathrm{d}^3\boldsymbol{r}_2\mathrm{d}^2\hat{\boldsymbol{n}}_2\mathrm{d}^3\boldsymbol{r}_3\mathrm{d}^2\hat{\boldsymbol{n}}_3\mathrm{d}^3\boldsymbol{r}_4\mathrm{d}^2\hat{\boldsymbol{n}}_4\mathrm{d}^3\boldsymbol{r}_5\mathrm{d}^2\hat{\boldsymbol{n}}_5\\ e^{\imath\phi(\boldsymbol{r}_1)}z(\boldsymbol{r}_1,\hat{\boldsymbol{n}}_1)\xi(\hat{\boldsymbol{n}}_1,\hat{\boldsymbol{n}}_2,\hat{\boldsymbol{n}}_3)e^{\imath\phi(\boldsymbol{r}_2)}\zeta(\boldsymbol{r}_2,\hat{\boldsymbol{n}}_2,\boldsymbol{r}_3,\hat{\boldsymbol{n}}_3)e^{\imath\phi(\boldsymbol{r}_3)}\xi(\hat{\boldsymbol{n}}_2,\hat{\boldsymbol{n}}_4,\hat{\boldsymbol{n}}_5)e^{\imath\phi(\boldsymbol{r}_4)}\\ \zeta(\boldsymbol{r}_4,\hat{\boldsymbol{n}}_4,\boldsymbol{r}_5,\hat{\boldsymbol{n}}_5)e^{\imath\phi(\boldsymbol{r}_5)}\ldots\xi(\hat{\boldsymbol{n}}_{N-3},\boldsymbol{n}_{N-1},\hat{\boldsymbol{n}}_N)\\ \times e^{\imath\phi(\boldsymbol{r}_{N-1})}\zeta(\boldsymbol{r}_{N-1},\hat{\boldsymbol{n}}_{N-1},\boldsymbol{r}_N,\hat{\boldsymbol{n}}_N)e^{\imath\phi(\boldsymbol{r}_N)}\Bigg)\, e^{-\frac{1}{2}\beta\left(\int \mathrm{d}^3\boldsymbol{r}\int \mathrm{d}^3\boldsymbol{r}'\phi(\boldsymbol{r})V^{-1}(\boldsymbol{r}-\boldsymbol{r}')\phi(\boldsymbol{r}')\right)}.\end{aligned} \tag{5.17}$$

Where $\mathcal{N}_{\phi,1}$ and $\mathcal{N}_{\phi,2}$ are the normalization factor and $\int \mathrm{D}\phi$ the functional integration over the external field ϕ.

In the section that follows we use the grand partition function for confined branching networks with mutual interacting segments, that we have obtained to derive the densities distributions of the filaments segments and consequently deduce the resulting non linear integral equations.

5.2 Density distributions

We are now in the mean-field space and we wish to compute the density distributions of the segments of the actin filaments. As defined previously the total density of filaments segments composing the actin networks confined in a finite region is given by:

$$\varrho(\boldsymbol{r},\hat{\boldsymbol{n}}) = \varrho_z(\boldsymbol{r},\hat{\boldsymbol{n}}) + 2\varrho_\zeta(\boldsymbol{r},\hat{\boldsymbol{n}}). \tag{5.18}$$

Where

$$\varrho_z(\boldsymbol{r},\hat{\boldsymbol{n}}) = \frac{z(\boldsymbol{r},\hat{\boldsymbol{n}})}{\mathfrak{Z}}\frac{\delta\mathfrak{Z}}{\delta z(\boldsymbol{r},\hat{\boldsymbol{n}})} \tag{5.19}$$

is the average density distribution of the filaments segments not involved in branching points and

$$\varrho_\zeta(\boldsymbol{r},\hat{\boldsymbol{n}}) = \frac{\zeta(\boldsymbol{r},\hat{\boldsymbol{n}}',\hat{\boldsymbol{n}}'')}{\mathfrak{Z}}\frac{\delta\mathfrak{Z}}{\delta\zeta(\boldsymbol{r},\hat{\boldsymbol{n}}',\hat{\boldsymbol{n}}'')} \tag{5.20}$$

the average density distribution of branching points. Let rewrite the grand partition function for confined branching network as function of a functional $F(\phi(\boldsymbol{r}))$ as

$$\mathfrak{Z} = \int \mathrm{D}\phi\, e^{-F(\phi)} \tag{5.21}$$

where

$$\begin{aligned}
F(\phi) = &-\ln\mathcal{N}_{\phi,2} - \ln\left(\sum_{N=0}^{\infty}\left(\int\ldots\int \mathrm{d}^3\boldsymbol{r}_1\mathrm{d}^2\hat{\boldsymbol{n}}_1\mathrm{d}^3\boldsymbol{r}_2\mathrm{d}^2\hat{\boldsymbol{n}}_2\ldots\mathrm{d}^3\boldsymbol{r}_{N-1}\mathrm{d}^2\hat{\boldsymbol{n}}_{N-1}\mathrm{d}^3\boldsymbol{r}_N\mathrm{d}^2\hat{\boldsymbol{n}}_N\right.\right.\\
&\times e^{\imath\phi(\boldsymbol{r}_1)}z(\boldsymbol{r}_1,\hat{\boldsymbol{n}}_1)w(\hat{\boldsymbol{n}}_1,\hat{\boldsymbol{n}}_2)e^{\imath\phi(\boldsymbol{r}_2)}z(\boldsymbol{r}_2,\hat{\boldsymbol{n}}_2)\ldots e^{\imath\phi(\boldsymbol{r}_{N-1})}z(\boldsymbol{r}_{N-1},\hat{\boldsymbol{n}}_{N-1})w(\hat{\boldsymbol{n}}_{N-1},\hat{\boldsymbol{n}}_N)\\
&\times e^{\imath\phi(\boldsymbol{r}_N)}z(\boldsymbol{r}_N,\hat{\boldsymbol{n}}_N) + \int\ldots\int \mathrm{d}^3\boldsymbol{r}_1\mathrm{d}^2\hat{\boldsymbol{n}}_1\mathrm{d}^3\boldsymbol{r}_2\mathrm{d}^2\hat{\boldsymbol{n}}_2\mathrm{d}^3\boldsymbol{r}_3\mathrm{d}^2\hat{\boldsymbol{n}}_3\mathrm{d}^3\boldsymbol{r}_4\mathrm{d}^2\hat{\boldsymbol{n}}_4\\
&e^{\imath\phi(\boldsymbol{r}_1)}z(\boldsymbol{r}_1,\hat{\boldsymbol{n}}_1)\xi(\hat{\boldsymbol{n}}_1,\hat{\boldsymbol{n}}_2,\hat{\boldsymbol{n}}_3)e^{\imath\phi(\boldsymbol{r}_2)}\zeta(\boldsymbol{r}_2,\hat{\boldsymbol{n}}_2,\boldsymbol{r}_3,\hat{\boldsymbol{n}}_3)e^{\imath\phi(\boldsymbol{r}_3)}w(\hat{\boldsymbol{n}}_2,\hat{\boldsymbol{n}}_4)e^{\imath\phi(\boldsymbol{r}_4)}z(\boldsymbol{r}_4,\hat{\boldsymbol{n}}_4)\\
&\times\ldots e^{\imath\phi(\boldsymbol{r}_{N-1})}z(\boldsymbol{r}_{N-1},\hat{\boldsymbol{n}}_{N-1})w(\hat{\boldsymbol{n}}_{N-1},\hat{\boldsymbol{n}}_N)e^{\imath\phi(\boldsymbol{r}_N)}z(\boldsymbol{r}_N,\hat{\boldsymbol{n}}_N)\\
&+\int\ldots\int \mathrm{d}^3\boldsymbol{r}_1\mathrm{d}^2\hat{\boldsymbol{n}}_1\mathrm{d}^3\boldsymbol{r}_2\mathrm{d}^2\hat{\boldsymbol{n}}_2\mathrm{d}^3\boldsymbol{r}_3\mathrm{d}^2\hat{\boldsymbol{n}}_3\mathrm{d}^3\boldsymbol{r}_4\mathrm{d}^2\hat{\boldsymbol{n}}_4\mathrm{d}^3\boldsymbol{r}_5\mathrm{d}^2\hat{\boldsymbol{n}}_5\mathrm{d}^3\boldsymbol{r}_6\mathrm{d}^2\hat{\boldsymbol{n}}_6\\
&e^{\imath\phi(\boldsymbol{r}_1)}z(\boldsymbol{r}_1,\hat{\boldsymbol{n}}_1)\xi(\hat{\boldsymbol{n}}_1,\hat{\boldsymbol{n}}_2,\hat{\boldsymbol{n}}_3)e^{\imath\phi(\boldsymbol{r}_2)}\zeta(\boldsymbol{r}_2,\hat{\boldsymbol{n}}_2,\boldsymbol{r}_3,\hat{\boldsymbol{n}}_3)\\
&e^{\imath\phi(\boldsymbol{r}_3)}\xi(\hat{\boldsymbol{n}}_2,\hat{\boldsymbol{n}}_4,\hat{\boldsymbol{n}}_5)e^{\imath\phi(\boldsymbol{r}_4)}\zeta(\boldsymbol{r}_4,\hat{\boldsymbol{n}}_4,\boldsymbol{r}_5,\hat{\boldsymbol{n}}_5)e^{\imath\phi(\boldsymbol{r}_5)}w(\hat{\boldsymbol{n}}_4,\hat{\boldsymbol{n}}_6)e^{\imath\phi(\boldsymbol{r}_6)}\\
&\times z(\boldsymbol{r}_6,\hat{\boldsymbol{n}}_6)\ldots e^{\imath\phi(\boldsymbol{r}_{N-1})}z(\boldsymbol{r}_{N-1},\hat{\boldsymbol{n}}_{N-1})w(\hat{\boldsymbol{n}}_{N-1},\hat{\boldsymbol{n}}_N)z(\boldsymbol{r}_N,\hat{\boldsymbol{n}}_N)e^{\imath\phi(\boldsymbol{r}_N)}+\ldots\\
&+\int\ldots\int \mathrm{d}^3\boldsymbol{r}_1\mathrm{d}^2\hat{\boldsymbol{n}}_1\mathrm{d}^3\boldsymbol{r}_2\mathrm{d}^2\hat{\boldsymbol{n}}_2\mathrm{d}^3\boldsymbol{r}_3\mathrm{d}^2\hat{\boldsymbol{n}}_3\mathrm{d}^3\boldsymbol{r}_4\mathrm{d}^2\hat{\boldsymbol{n}}_4\mathrm{d}^3\boldsymbol{r}_5\mathrm{d}^2\hat{\boldsymbol{n}}_5\\
&e^{\imath\phi(\boldsymbol{r}_1)}z(\boldsymbol{r}_1,\hat{\boldsymbol{n}}_1)\xi(\hat{\boldsymbol{n}}_1,\hat{\boldsymbol{n}}_2,\hat{\boldsymbol{n}}_3)e^{\imath\phi(\boldsymbol{r}_2)}\zeta(\boldsymbol{r}_2,\hat{\boldsymbol{n}}_2,\boldsymbol{r}_3,\hat{\boldsymbol{n}}_3)e^{\imath\phi(\boldsymbol{r}_3)}\xi(\hat{\boldsymbol{n}}_2,\hat{\boldsymbol{n}}_4,\hat{\boldsymbol{n}}_5)e^{\imath\phi(\boldsymbol{r}_4)}\\
&\zeta(\boldsymbol{r}_4,\hat{\boldsymbol{n}}_4,\boldsymbol{r}_5,\hat{\boldsymbol{n}}_5)e^{\imath\phi(\boldsymbol{r}_5)}\ldots\xi(\hat{\boldsymbol{n}}_{N-3},\boldsymbol{n}_{N-1},\hat{\boldsymbol{n}}_N)\\
&\left.\left.\times e^{\imath\phi(\boldsymbol{r}_{N-1})}\zeta(\boldsymbol{r}_{N-1},\hat{\boldsymbol{n}}_{N-1},\boldsymbol{r}_N,\hat{\boldsymbol{n}}_N)e^{\imath\phi(\boldsymbol{r}_N)}\right)\right) + \frac{1}{2}\beta\int\mathrm{d}^3\boldsymbol{r}\int\mathrm{d}^3\boldsymbol{r}'\phi(\boldsymbol{r})V^{-1}(\boldsymbol{r}-\boldsymbol{r}')\phi(\boldsymbol{r}').
\end{aligned} \tag{5.22}$$

and for linear confined actin chains we have:

$$\mathfrak{Z} = \int \mathrm{D}\,\phi e^{-F_1(\phi)} \tag{5.23}$$

Where

$$\begin{aligned} F_1(\phi) = -\ln\Bigg(&\mathcal{N}_{\phi,1}\sum_{N=0}^{\infty}\int \mathrm{D}\phi \int \mathrm{d}^3\boldsymbol{r}_1\mathrm{d}^2\hat{\boldsymbol{n}}_1\mathrm{d}^3\boldsymbol{r}_2\mathrm{d}^2\hat{\boldsymbol{n}}_2\ldots\mathrm{d}^3\boldsymbol{r}_N\mathrm{d}^2\hat{\boldsymbol{n}}_N z(\boldsymbol{r}_1,\hat{\boldsymbol{n}}_1)\\ &\times e^{\imath\phi(\boldsymbol{r}_1)}w(\hat{\boldsymbol{n}}_1,\hat{\boldsymbol{n}}_2)z(\boldsymbol{r}_2,\hat{\boldsymbol{n}}_2)e^{\imath\phi(\boldsymbol{r}_2)}\ldots w(\hat{\boldsymbol{n}}_{N-1},\hat{\boldsymbol{n}}_N)z(\boldsymbol{r}_N,\hat{\boldsymbol{n}}_N)e^{\imath\phi(\boldsymbol{r}_N)}\Bigg)\\ &+\frac{1}{2}\beta\int \mathrm{d}^3\boldsymbol{r}\int \mathrm{d}^3\boldsymbol{r}'\phi(\boldsymbol{r})V^{-1}(\boldsymbol{r}-\boldsymbol{r}')\phi(\boldsymbol{r}'). \end{aligned} \tag{5.24}$$

The grand partition functions for both linear filaments and branched networks are complex expression. In order to calculate the functional derivative of $\mathfrak{Z}$, we need to find an analytical expression for the functional integral over ϕ (equations (5.21) and (5.23)) which is not a Gaussian which is thus hard to do. SCFT or mean-field approximation also known as saddle point approximation method is a suitable analytical techniques that we use in order to approximate the grand partition function. It consist to an assumption that there exist a single field $\phi = \phi_0$ (especially in the grand canonical ensemble) that contribute most to the value of the grand partition function. So we can treat ϕ_0 as a local minima of F, meaning that we can expand the functional $F(\phi)$ around ϕ_0 leading to a Gaussian integrals of equation (5.22) (the expression of the grand partition function for confined branching actin network) and of (5.24) (the expression of the grand partition function for confined linear actin filament) which after computation give for branching network:

$$\tilde{\mathfrak{Z}} = e^{-\tilde{F}(\phi_0)}\sqrt{\frac{2\pi}{\tilde{F}''(\phi_0)}} \sim e^{-\tilde{F}(\phi_0)} \tag{5.25}$$

where $\tilde{F}$ is F at $\phi(\boldsymbol{r}) = \phi_0(\boldsymbol{r}) = \phi_0$.

For confined single linear chain:

$$\tilde{\mathfrak{Z}} = e^{-\tilde{F}_1(\phi_0)}\sqrt{\frac{2\pi}{\tilde{F}_1''(\phi_0)}} \sim e^{-\tilde{F}_1(\phi_0)} \tag{5.26}$$

where $\tilde{F}_1$ is F_1 at $\phi(\boldsymbol{r}) = \phi_0(\boldsymbol{r}) = \phi_0$.

This approximation method has a great advantage that it allows to obtain the relevant informations about the physics of the system of study. It is thus commonly and successively used to facilitate the computation of the average field in inhomogeneous complex polymer systems mainly in the grand canonical ensemble.

Using the equation (5.25) and (5.26), we calculate the average density distribution of the actin segments of the branching networks ϱ or of branching points ϱ_ζ and the average density of segments that are not involved in branching points ϱ_z. Following the same calculation scheme of the functional derivative as in the Appendix A.1, we obtain:

$$\tilde{\varrho}_z(\boldsymbol{r},\hat{\boldsymbol{n}}) = \frac{\Phi(\boldsymbol{r},[\phi_0(\boldsymbol{r})],\hat{\boldsymbol{n}})z(\boldsymbol{r},\hat{\boldsymbol{n}})e^{\mathrm{i}\phi_0(\boldsymbol{r})}\Psi(\boldsymbol{r},[\phi_0(\boldsymbol{r})],\hat{\boldsymbol{n}})}{\left(1+\int \mathrm{d}^3\boldsymbol{r}\mathrm{d}^2\hat{\boldsymbol{n}}ze^{\mathrm{i}\phi_0}\Psi(\boldsymbol{r},[\phi_0(\boldsymbol{r})],\hat{\boldsymbol{n}})\right)} \tag{5.27}$$

and

$$\tilde{\varrho}_\zeta(\boldsymbol{r},\hat{\boldsymbol{n}}) = \frac{\Phi(\boldsymbol{r},[\phi_0(\boldsymbol{r})],\hat{\boldsymbol{n}})\zeta(\boldsymbol{r},\hat{\boldsymbol{n}})e^{\mathrm{i}\phi_0(\boldsymbol{r})}\Psi(\boldsymbol{r},[\phi_0(\boldsymbol{r})],\hat{\boldsymbol{n}})\Psi(\boldsymbol{r},[\phi_0(\boldsymbol{r})],\hat{\boldsymbol{n}})}{\left(1+\int \mathrm{d}^3\boldsymbol{r}\mathrm{d}^2\hat{\boldsymbol{n}}ze^{\mathrm{i}\phi_0}\Psi(\boldsymbol{r},[\phi_0(\boldsymbol{r})],\hat{\boldsymbol{n}})\right)} \tag{5.28}$$

Where $\Psi(\boldsymbol{r},[\phi_0(\boldsymbol{r})],\hat{\boldsymbol{n}})$ and $\Phi(\boldsymbol{r},[\phi_0(\boldsymbol{r})],\hat{\boldsymbol{n}})$ are given by the following non-linear integral equations:

$$\Psi(\boldsymbol{r},\hat{\boldsymbol{n}}) = 1+\int_{\boldsymbol{r},\hat{\boldsymbol{n}}'} \mathrm{d}^3\boldsymbol{r}'\mathrm{d}^2\hat{\boldsymbol{n}}'w(\hat{\boldsymbol{n}},\hat{\boldsymbol{n}}')e^{\mathrm{i}\phi_0(\boldsymbol{r})}z(\boldsymbol{r},\hat{\boldsymbol{n}})\Psi(\boldsymbol{r},\hat{\boldsymbol{n}}')+$$
$$\int_{\boldsymbol{r}',\hat{\boldsymbol{n}}'}\int_{\boldsymbol{r}'',\hat{\boldsymbol{n}}''} \mathrm{d}^3\boldsymbol{r}'\mathrm{d}^2\hat{\boldsymbol{n}}'\mathrm{d}^3\boldsymbol{r}''\mathrm{d}^2\hat{\boldsymbol{n}}''\xi(\hat{\boldsymbol{n}},\hat{\boldsymbol{n}}',\hat{\boldsymbol{n}}'')\zeta(\boldsymbol{r}',\hat{\boldsymbol{n}}',\boldsymbol{r}'',\hat{\boldsymbol{n}}'')e^{\mathrm{i}(\phi_0(\boldsymbol{r}')+\phi_0(\boldsymbol{r}''))}\Psi(\mathbf{r}',\hat{\boldsymbol{n}}')\Psi(\boldsymbol{r}'',\hat{\boldsymbol{n}}'') \tag{5.29}$$

and

$$\Phi(\boldsymbol{r},\hat{\boldsymbol{n}}) = 1+\int_{\boldsymbol{r},\hat{\boldsymbol{n}}'} \mathrm{d}^3\boldsymbol{r}'\mathrm{d}^2\hat{\boldsymbol{n}}'\tilde{z}(\boldsymbol{r},\hat{\boldsymbol{n}})e^{\mathrm{i}\phi_0(\boldsymbol{r})}w(\hat{\boldsymbol{n}},\hat{\boldsymbol{n}}')\Psi(\mathbf{r},\hat{\boldsymbol{n}}')+$$
$$\int_{\boldsymbol{r}',\hat{\boldsymbol{n}}'}\int_{\boldsymbol{r}'',\hat{\boldsymbol{n}}''} \mathrm{d}^3\boldsymbol{r}'\mathrm{d}^2\hat{\boldsymbol{n}}'\mathrm{d}^3\boldsymbol{r}''\mathrm{d}^2\hat{\boldsymbol{n}}''\xi(\hat{\boldsymbol{n}},\boldsymbol{n}',\boldsymbol{n}'')\tilde{\zeta}(\boldsymbol{r}',\boldsymbol{n}',\boldsymbol{r}'',\hat{\boldsymbol{n}}'')e^{\mathrm{i}(\phi_0(\boldsymbol{r}')+\phi_0(\boldsymbol{r}''))}\Psi(\boldsymbol{r}',\boldsymbol{n}')\Phi(\boldsymbol{r}'',\hat{\boldsymbol{n}}''). \tag{5.30}$$

One of the remaining task in the calculation of the density distributions is to find the mean-field ϕ_0. ϕ_0 is a minimum of F so:

$$\frac{\delta F(\phi)}{\delta\phi}|_{\phi=\phi_0} = 0 \tag{5.31}$$

Equation (5.31) is the fundamental equation of the mean-field approximation. We calculate the functional derivative of F with respect to ϕ (in the way as calculating the functional derivative of $\mathfrak{Z}$) and take $\phi=\phi_0$ We obtain:

$$\begin{aligned}\frac{\delta\tilde{F}(\phi)}{\delta\phi}\,|_{\phi=\phi_0} = &\int \mathrm{d}^3\boldsymbol{r}'V^{-1}(\boldsymbol{r}-\boldsymbol{r}')\phi_0((r))\\ &-\mathrm{i}\left(\frac{\Phi(\boldsymbol{r},[\phi_0(\boldsymbol{r})],\hat{\boldsymbol{n}})z(\boldsymbol{r},\hat{\boldsymbol{n}})e^{\mathrm{i}\phi_0(\boldsymbol{r})}\Psi(\boldsymbol{r},[\phi_0(\boldsymbol{r})],\hat{\boldsymbol{n}})}{\left(1+\int \mathrm{d}^3\boldsymbol{r}\mathrm{d}^2\hat{\boldsymbol{n}}ze^{\mathrm{i}\phi_0}\Psi(\boldsymbol{r},[\phi_0(\boldsymbol{r})],\hat{\boldsymbol{n}})\right)}+\right.\\ &\left.2\frac{\Phi(\boldsymbol{r},[\phi_0(\boldsymbol{r})],\hat{\boldsymbol{n}})\zeta(\boldsymbol{r},\hat{\boldsymbol{n}})e^{\mathrm{i}\phi_0(\boldsymbol{r})}\Psi(\boldsymbol{r},[\phi_0(\boldsymbol{r})],\hat{\boldsymbol{n}})\Psi(\boldsymbol{r},[\phi_0(\boldsymbol{r})],\hat{\boldsymbol{n}})}{\left(1+\int \mathrm{d}^3\boldsymbol{r}\mathrm{d}^2\hat{\boldsymbol{n}}ze^{\mathrm{i}\phi_0}\Psi(\boldsymbol{r},[\phi_0(\boldsymbol{r})],\hat{\boldsymbol{n}})\right)}\right).\end{aligned} \tag{5.32}$$

We see that the second term on right hand is equal to the total average density distribution of filament segments $\varrho(\boldsymbol{r})],\hat{\boldsymbol{n}})$. So equation (5.31) becomes

$$\int \mathrm{d}^3\boldsymbol{r}'V^{-1}(\boldsymbol{r}-\boldsymbol{r}')\phi_0((r)) - \mathrm{i}\tilde{\varrho}(\boldsymbol{r},\hat{\boldsymbol{n}})) = 0 \tag{5.33}$$

which is a very well known equation called Poisson-Boltzmann equation. We then find ϕ_0 to be :

$$\mathrm{i}\phi_0(\boldsymbol{r}) = \int \mathrm{d}^3\boldsymbol{r}' V(\boldsymbol{r}-\boldsymbol{r}')\tilde{\varrho}(\boldsymbol{r},\hat{\boldsymbol{n}})). \tag{5.34}$$

So we can now replace the mean field ϕ_0 in all the equations where it is used by its equivalent expression. We consider β to be equal to 1. The grand canonical partition function and the integral equations are thus rewritten as functional of the total density distribution $\tilde{\varrho}(\boldsymbol{r},\hat{\boldsymbol{n}}))$ for the numerical implementation.

5.2.1 Numerical solving of the non-linear functional integral equation of Ψ and Φ

We wish to compute self-consistently Ψ and Φ in order to calculate the grand canonical partition functions, the average densities, the degree of polymerization and the order parameter fields of confined actin filament and branching networks were the excluded volume effect between chain segments is present. We model the actin chains and the confining region on triangular lattices (2d for 2d networks and 3d for 3d networks). So we rewrite here the non-linear integral equation given by equations (5.29) and (5.30) in the simplified discrete form and we replace the mean-field $i\phi$ by its equivalent expression (given by equation (5.34)) which is function of the total average density of segments of the confined branching network as:

$$\Psi(\boldsymbol{r},[\varrho],\hat{\boldsymbol{n}}) = 1 + \sum_{\hat{\boldsymbol{n}}'} \mathrm{d}^3\mathbf{r}' w(\boldsymbol{r},\hat{\boldsymbol{n}},\boldsymbol{r}',\hat{\boldsymbol{n}}') z(\boldsymbol{r},\hat{\boldsymbol{n}}') e^{\int \mathrm{d}^3\boldsymbol{r}'\tilde{\varrho}(\boldsymbol{r})V(\boldsymbol{r}-\boldsymbol{r}')}\Psi(\mathbf{r},\hat{\boldsymbol{n}}') + \sum_{\hat{\boldsymbol{n}}'}\sum_{\hat{\boldsymbol{n}}''} \mathrm{d}^3\boldsymbol{r}'\mathrm{d}^3\boldsymbol{r}''\xi(\boldsymbol{r},\hat{\boldsymbol{n}},\boldsymbol{n}',\boldsymbol{n}'')\zeta(\boldsymbol{r}',\boldsymbol{n}',\boldsymbol{n}'')e^{2\int \mathrm{d}^3\boldsymbol{r}'\tilde{\varrho}(\boldsymbol{r}',\hat{\boldsymbol{n}}')V(\boldsymbol{r}-\boldsymbol{r}')}\Psi(\boldsymbol{r}',\boldsymbol{n}')\Psi(\boldsymbol{r}'',\hat{\boldsymbol{n}}'') \tag{5.35}$$

and

$$\Phi(\boldsymbol{r},[\tilde{\varrho}],\hat{\boldsymbol{n}}) = 1 + \sum_{\hat{\boldsymbol{n}}'} \mathrm{d}^3\mathbf{r}' w(\boldsymbol{r},\hat{\boldsymbol{n}},\boldsymbol{r}',\hat{\boldsymbol{n}}') \tilde{z}(\boldsymbol{r},\hat{\boldsymbol{n}}') e^{\int \mathrm{d}^3\boldsymbol{r}'\tilde{\varrho}(\boldsymbol{r})V(\boldsymbol{r}-\boldsymbol{r}')}\Psi(\mathbf{r},\hat{\boldsymbol{n}}') + \sum_{\hat{\boldsymbol{n}}'}\sum_{\hat{\boldsymbol{n}}''} \mathrm{d}^3\boldsymbol{r}'\mathrm{d}^3\boldsymbol{r}''\xi(\boldsymbol{r},\hat{\boldsymbol{n}},\boldsymbol{n}',\boldsymbol{n}'')\tilde{\zeta}(\boldsymbol{r}',\boldsymbol{n}',\boldsymbol{n}'')e^{2\int \mathrm{d}^3\boldsymbol{r}'\tilde{\varrho}(\boldsymbol{r}',\hat{\boldsymbol{n}}')V(\boldsymbol{r}-\boldsymbol{r}')}\Psi(\boldsymbol{r}',\boldsymbol{n}')\Phi(\boldsymbol{r}'',\hat{\boldsymbol{n}}''). \tag{5.36}$$

where

$$\zeta(\boldsymbol{r}',\hat{\boldsymbol{n}}',\hat{\boldsymbol{n}}'') = \zeta_0 \times \begin{cases} 1, & \text{if} \quad \boldsymbol{r}' \in \mathbb{L} \text{ and } \boldsymbol{r}' - \ell\hat{\boldsymbol{n}}' \in \mathbb{L} \\ \text{and} & \boldsymbol{r}' - \ell\hat{\boldsymbol{n}}'' \in \mathbb{L} \\ 0, & \text{otherwise} \end{cases} \tag{5.37}$$

Thus Ψ and Φ are functionals of the total density and consequently is the grand partition function.

We use the same numerical procedure that we present in Chapter 3 for non-interacting network filament segments, to solve the non-linear functional integral equation for $\Psi(\boldsymbol{r},[\tilde{\varrho}],\hat{\boldsymbol{n}})$ and $\Phi(\boldsymbol{r},[\tilde{\varrho}],\hat{\boldsymbol{n}})$ given by equations (5.35) and (5.36), except that in the current case, beside the

self-consistent choice of initial guess of Ψ and Φ, we also choose an initial guess for the total density ϱ which we also choose self-consistently in order to enable convergence of our numerical solution.
We are now going to present and discuss the numerical results of the model.

5.3 Results and discussion

For our numerical calculations we have chosen the following site-to-site interaction potential

$$V(\boldsymbol{r},\hat{\boldsymbol{n}},\boldsymbol{r}',\hat{\boldsymbol{n}}') = V_0\hat{\boldsymbol{n}}\cdot\hat{\boldsymbol{n}}'\delta_{|\boldsymbol{r}-\boldsymbol{r}'|=1}. \tag{5.38}$$

which we term polarising potential since we have chosen it to be function of both the position and the orientations of the chain segments ($V(\boldsymbol{r}-\boldsymbol{r}') \to V(\boldsymbol{r},\hat{\boldsymbol{n}},\boldsymbol{r}',\hat{\boldsymbol{n}}')$). We have for $V_0 < 0$ the interaction favour the alignments of adjacent segments (like ferromagnetic interactions) and for $V_0 > 0$ the interaction favor opposite polarization.

We have obtained the density profiles and radial order field profiles of the three structural and architectural types of networks namely networks of actin dominated by short linear filaments with few branching, network dominated by long linear filaments and the highly branched networks under confinement and in the presence of the excluded volume effect between monomer segments.
We have also computed the average number density of the filament segments. We got similar results for networks confined in various geometries (cube, triangle, square, rectangle and sphere) and the results for 3d networks (networks modelled on 3d triangular lattice) and 2d networks (networks modelled on 2d triangular lattice) are similar. However the results we present here are for networks modelled on 2d triangular lattice and confined to a spherical geometry. We use the same parameter values that we use in Chapter 4 of this thesis (lattice is of size 100×100, the ratio of the persistence length and the diameter of the sphere $\ell_{\mathrm{p}}/D = 1/2$).

5.3.1 Branched networks

5.3.1.1 Short-range aligning interactions ($V_0 < 0$)

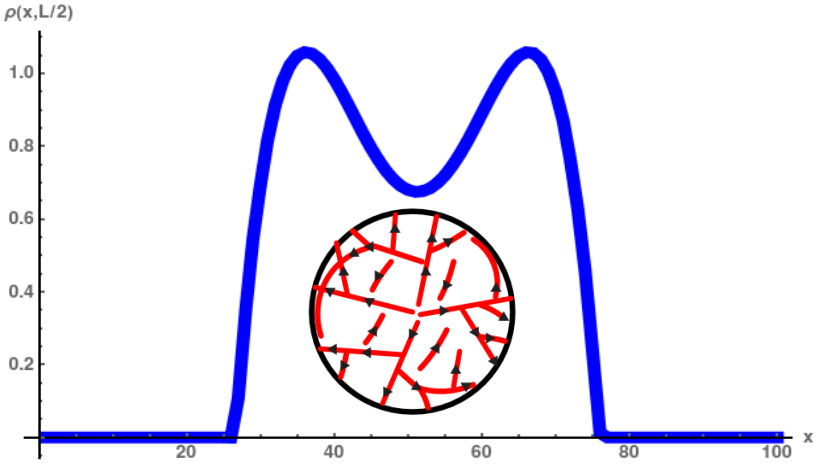

Figure 5.1: Graph of the density profile of the branched actin networks confined in a spherical cell without any mutual monomers interactions, $V_0 = 0.0$. $z = 0.516$ and $\zeta = 0.06$. The density profile shows a deflection near the centre of the sphere meaning that the filament segments of the network inside the confining sphere are inhomogeneously distributed. We have a hight density at the cell periphery and a low distribution as we go from the vicinity of the cell to the middle of the cell. The inset is a cartoon representing the spherical geometry confining the network of actin filaments in red on the graph and it is there to illustrate the type of the networks for which the this density profile is obtained.

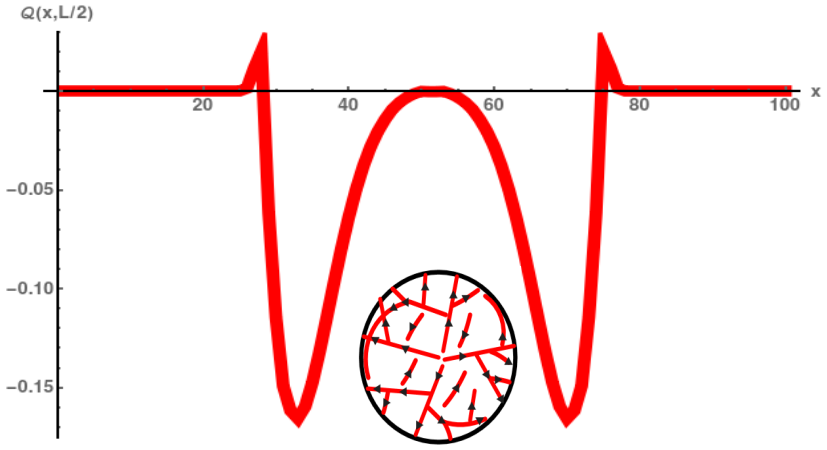

Figure 5.2: Graph of the radial order parameter field profile of the branched actin networks confined in a spherical cell without any mutual monomers interactions, $V_0 = 0.0$. $z = 0.516$ and the branching parameter $\zeta = 0.06$. The order parameter field profile shows that the filament branch and align radially to the cell wall i.e they point perpendicular to the cell wall or membrane. The inset is a cartoon representing the spherical geometry confining the network of actin filaments in red on the graph and it is there to illustrate the type of the networks for which the this density profile is obtained.

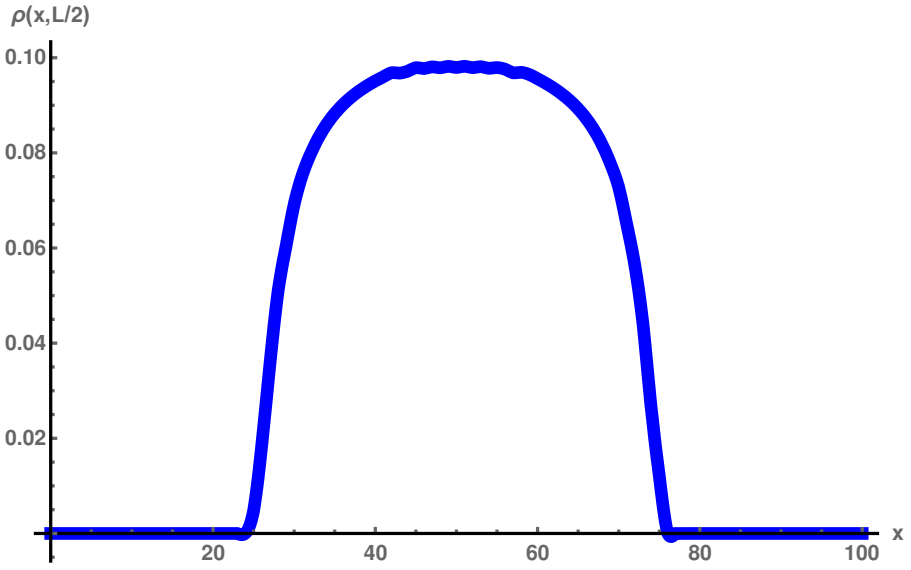

Figure 5.3: Graph of the density profile of the branched actin networks confined in a spherical cell in the presence of attractive mutual monomers interaction potential with strength $V_0 = -1$, $z_0 = 0.516$ and $\zeta_0 = 0.06$. The deflection in the middle of the profile of the density has decreased meaning that in the presence of the small attractive interactions between monomers, the filaments concentrated initially close to the cell membrane attract each other and start becoming homogeneously distributed.

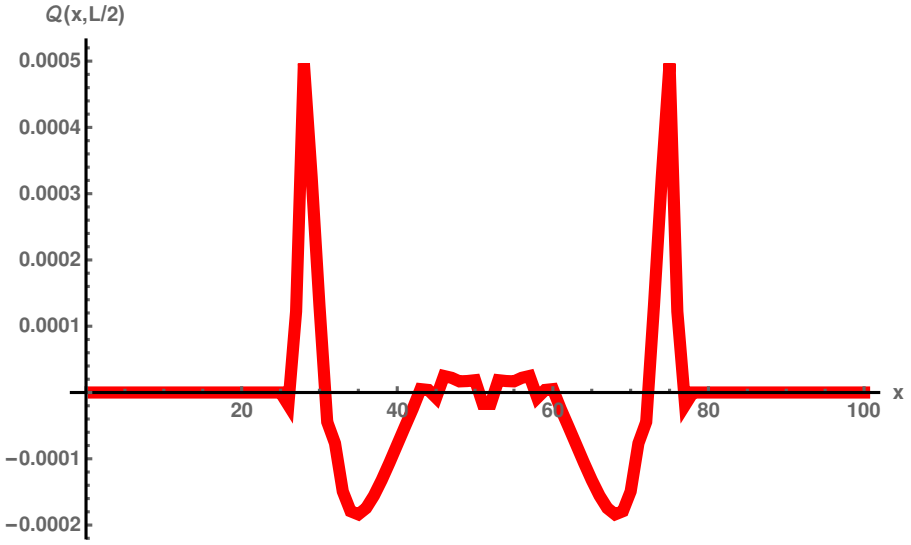

Figure 5.4: Graph of the radial order field profile of the branched actin networks confined in a spherical cell in the presence of attractive mutual monomers interactions, $V_0 = -1$. The filament elongation parameter $z = 0.515$ and the branching parameter $\zeta = 0.06$. The order parameter field profile becomes positive on average. The graph shows that the filaments of branched networks close to the cell membrane have preference of aligning parallel to the cell wall as we introduce a small attractive interaction while the filaments near the centre stay radial or perpendicular to the wall. This profile is similar to the profile of the networks with comparable length scales ($L \sim D \sim \ell_p$).

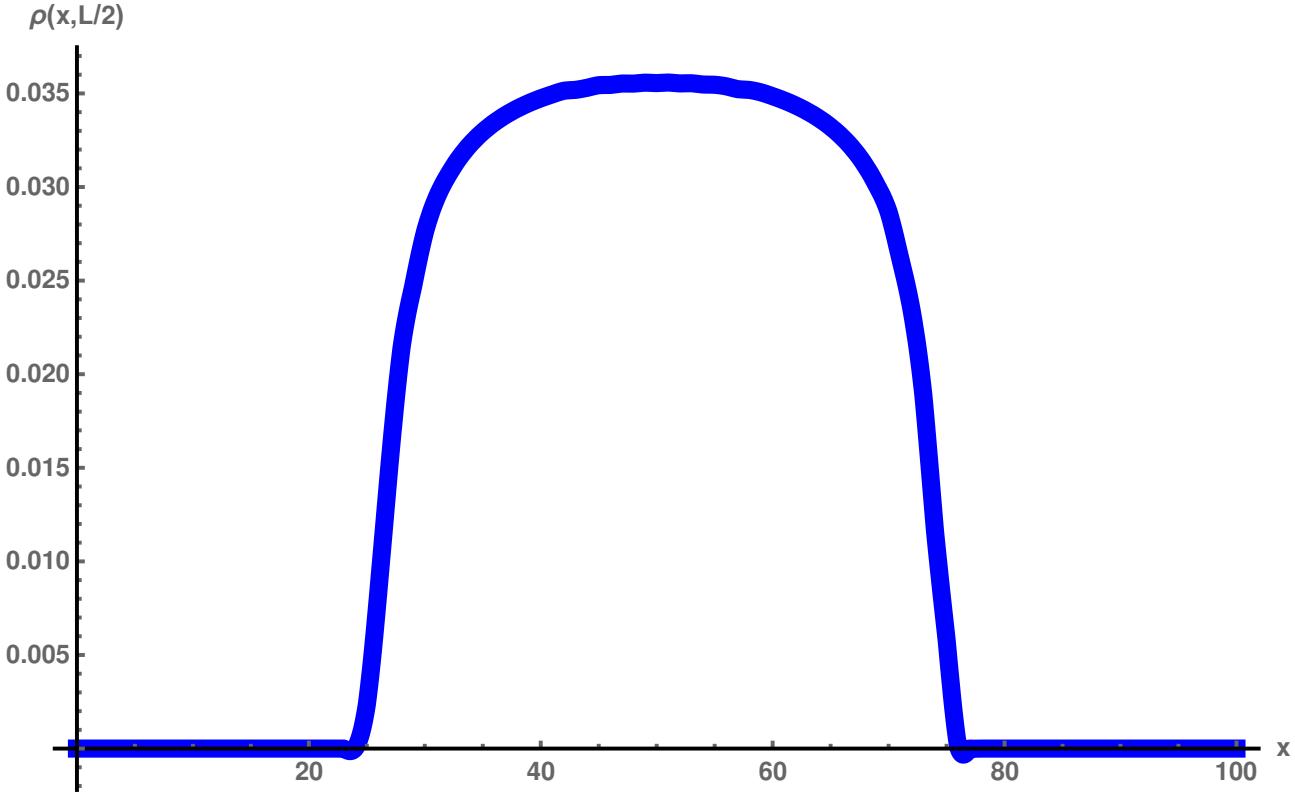

Figure 5.5: Graph of the density profile of the branched actin networks confined in a spherical cell at high attractive interaction strength $|V_0|$, $V_0 = -5$. The filament elongation parameter $z = 0.516$ and the branching parameter $\zeta = 0.06$. Here the density profile of filament segments of the branched networks becomes relatively flat near the centre of the spherical cell at high attractive interaction potential strength.

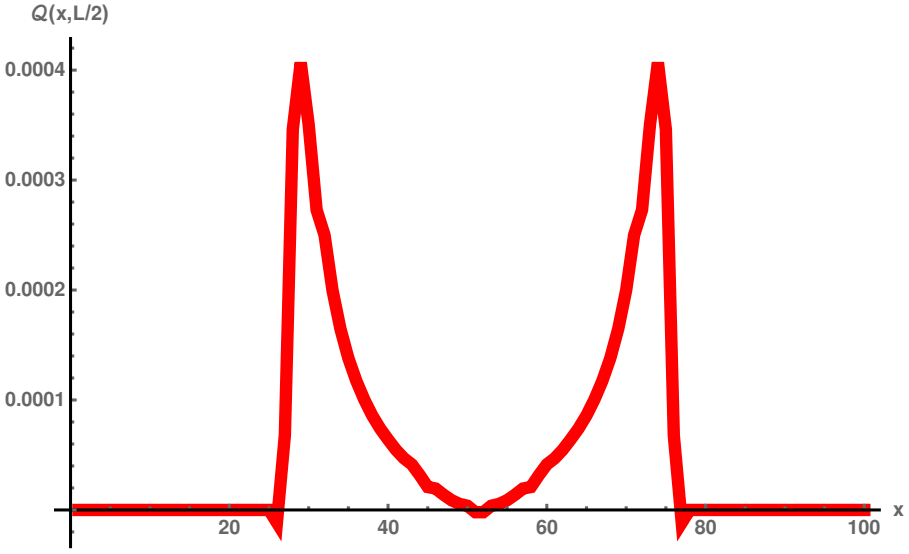

Figure 5.6: Graph of the radial order field profile of the branched actin networks confined in a spherical cell at high attractive interaction strength $|V_0|$, $V_0 = -5$. The filament elongation parameter $z = 0.515$ and the branching parameter $\zeta = 0.06$. The order parameter field profile become on average positive at the cell periphery and isotropic in the middle of the confining cell meaning that filaments close to the cell membrane or wall wrap arround the cell edges.

5.3.1.2 Interactions for $V_0 > 0$

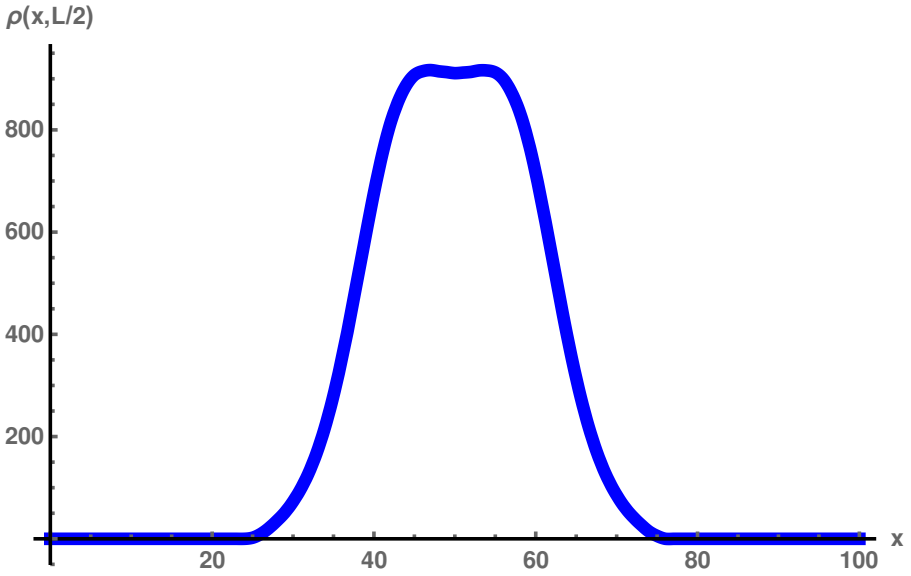

Figure 5.7: Graph of the density profile of the branched actin networks confined in a spherical cell in the presence of repulsive interaction with strength $V_0 = 0.00098$. The filament elongation parameter $z = 0.516$ and the branching parameter $\zeta = 0.06$. At this value of interaction strength $V_0 > 0$, the filament segments of the branched networks start becoming more concentrate near the centre of the sphere while less close to cell wall. This suggest that the filaments or the filament segments repel from the cell membrane and occupy the middle of the sphere.

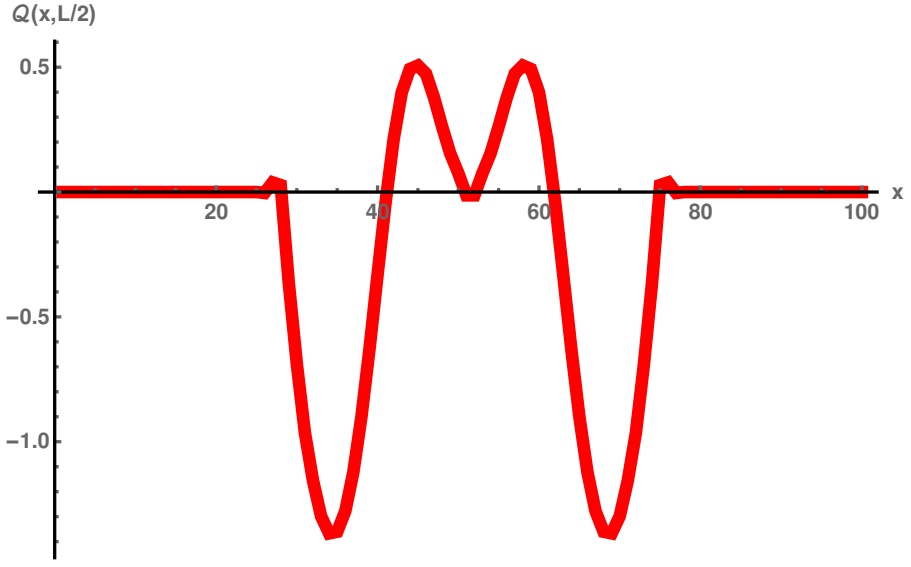

Figure 5.8: Graph of the radial order field profile of the branched actin networks confined in a spherical cell as we increase the interaction strength $V_0 > 0$, $V_0 = 0.00098$. The filament elongation parameter $z = 0.515$ and the branching parameter $\zeta = 0.06$. At this value interaction strength, the order parameter field profile become positive near the centre and stay negative close the cell membrane. So, the filament segments that are near the centre align parallel to the membrane while those close to membrane stay perpendicular to the cell membrane.

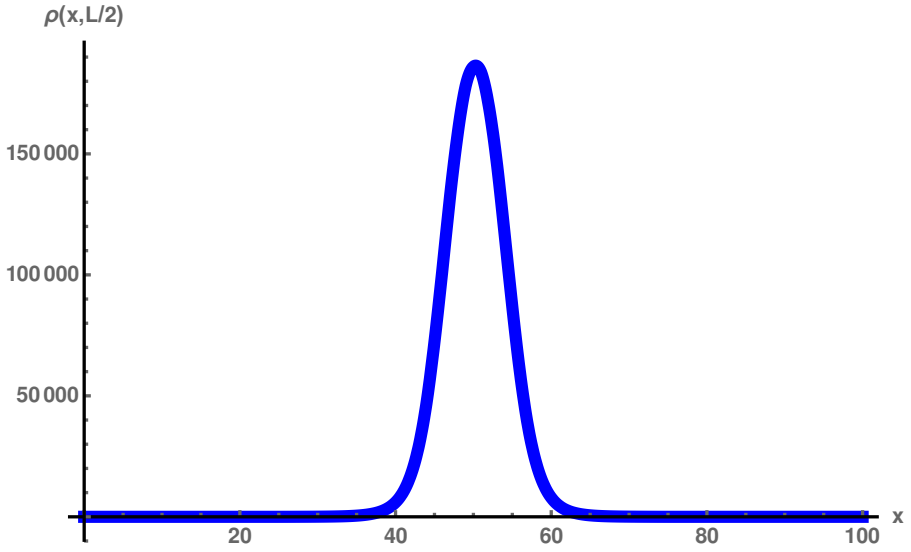

Figure 5.9: Graph of the density profile of the branched actin networks confined in a spherical cell in the presence of interaction with strength $V_0 = 0.001$. The filament elongation parameter $z = 0.516$ and the branching parameter $\zeta = 0.06$. At this value of interaction strength, the filament segments of the branched networks show a high concentration of the filament segments near the centre of the sphere while very little close to cell wall. This suggest that most of the confined filaments or the filament segments of the network occupy the middle of the sphere.

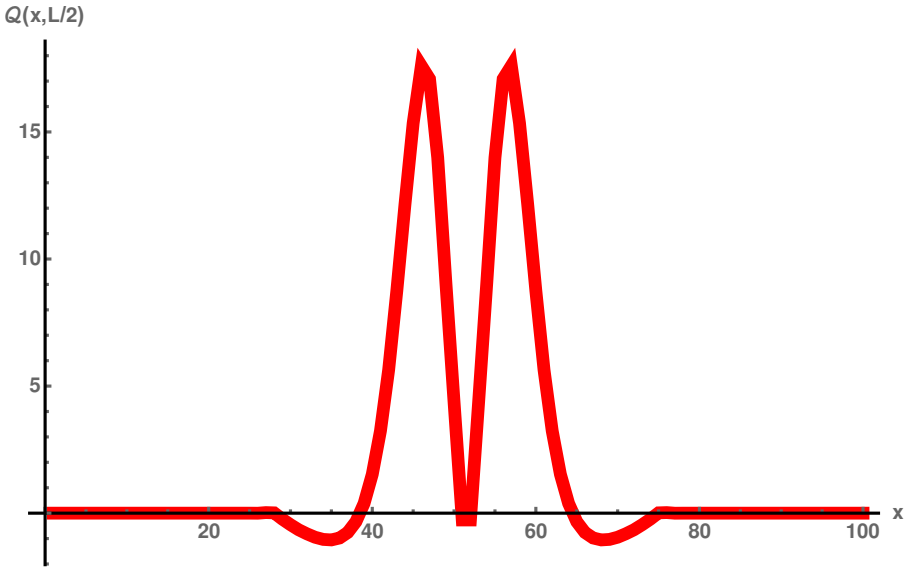

Figure 5.10: Graph of the radial order field profile of the branched actin networks confined in a spherical cell as we increase the repulsive interaction strength, $V_0 = 0.001$. The filament elongation parameter $z = 0.515$ and the branching parameter $\zeta = 0.06$. At this value of interaction strength $V_0 > 0$, the order parameter field profile become on average positive. It indicates that the filament segments at high concentration near the centre are aligned parallel to the membrane only very few stay perpendicular or radial to the cell membrane.

The first remark is that, whether $V_0 > 0$ or $V_0 < 0$, the profiles of the order parameters that

we have obtained show that, the confined branched actin networks in general align parallel to the cell wall.
For $V_0 > 0$ interaction, the density and order profiles show that, the filaments of the branched networks repel from the cell membrane or wall by bending and they occupy the space near the centre of the sphere. So one can predict that there the confining cell exert a repulsive force on the branched networks since the branched networks grow and point straight to the cell membrane. The repulsive force that the interaction potential creates sum up with the cell membrane repulsive force and cause the branched networks (which show strong resistance to the effect of confinements in the absence of any kind of mutual interaction) to bend and causing the branched networks to move away from the wall and concentrate near the centre of the cell.

While for $V_0 < 0$ interaction potential, the profiles of the average density and the order parameter field of the networks show that, filaments become more concentrated near the centre as we increase the strength of the interaction and they have preference of aligning parallel to the cell membrane near its edges. The profiles of the networks we observe are thus similar to the the profiles of the networks dominated by short filaments.

In the section that follows we investigate the effect of the two type of interactions (repulsive and attractive) on the branching networks dominated by long linear filaments.

5.3.2 Networks dominated by long linear filaments

5.3.2.1 Short-range aligning interactions ($V_0 < 0$)

We observe that in the presence of attractive mutual interaction potential between segments of the branching networks dominated by long linear filaments and for small value of the interaction strength ($|V_0| \leq 1$), the order parameter profile shows that the filaments or segments near the centre start aligning perpendicular to the cell wall or membrane while the segments that are close to the cell membrane keeps their parallel alignment and this profile is similar to the the profile of the networks with comparable length scales ($L \sim D \sim \ell_p$). This may be due to the fact that the short-range aligning interaction cause long linear filaments to shrink.
For $|V_0| > 1$, the density profiles is convex-shaped with a plateau near the centre of the sphere and it shows that the filaments of the networks are mostly located near the centre of the spherical cell as we increase the interaction strength and the filaments have preference of aligning parallel to the membrane or wall of the confining cell. Again, we see that this behaviour of the networks is similar to the behaviour of the network dominated by short filaments with no interactions between filament segments.

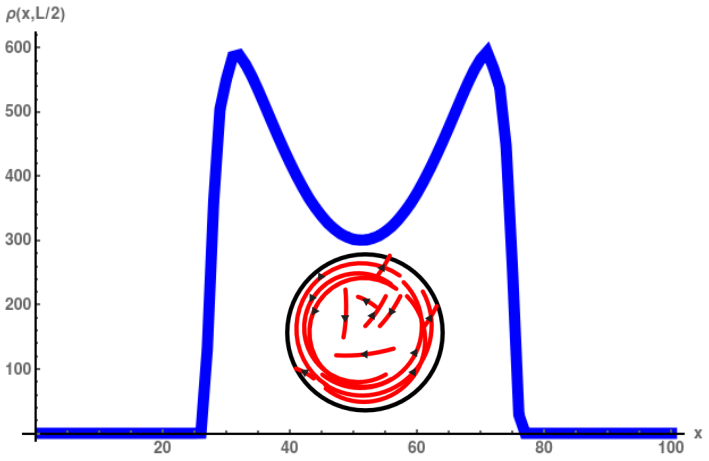

Figure 5.11: Graph of the density profile of the branching actin networks dominated by long linear filaments confined in a spherical cell without any mutual monomers interactions, $V_0 = 0$. $z = 0.75$ and $\zeta = 0.0016$. The density profile shows a deflection near the centre of the sphere meaning that the filament segments of the network inside the confining sphere are inhomogeneously distributed. We have a hight density at the cell periphery and a low distribution as we go from the vicinity of the cell to the middle of the cell. The inset is a cartoon representing the spherical geometry confining the network of actin filaments in red on the graph and it is there to illustrate the type of the networks for which this density profile is obtained.

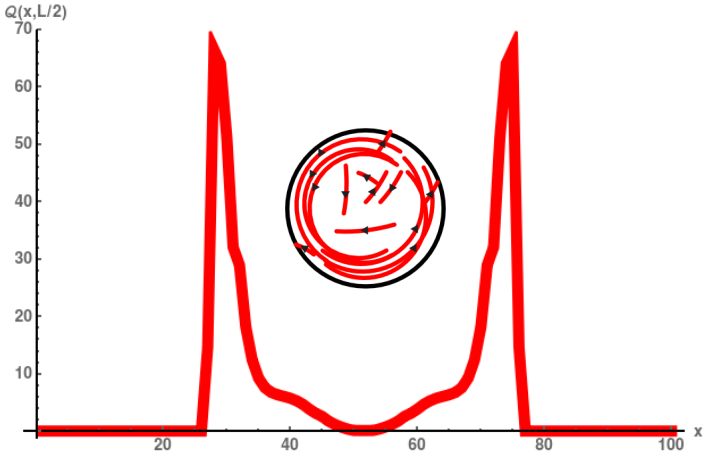

Figure 5.12: Graph of the radial order paramenter field profile of the branching actin networks dominated by long linear filaments confined in a spherical cell without any mutual monomers interactions, $V_0 = 0$. $z = 0.75$ and $\zeta = 0.001$. The order parameter field is positive at the periphery of confining region while 0 in the centre of the sphere. This indicates that long linear filaments bend and wrap around the cell while the few shorter filaments that are in the middle of the cell are isotropically distributed. The inset is a cartoon representing the spherical geometry confining the network of actin filaments in red on the graph and it is there to illustrate the type of the networks for which the this density profile is obtained.

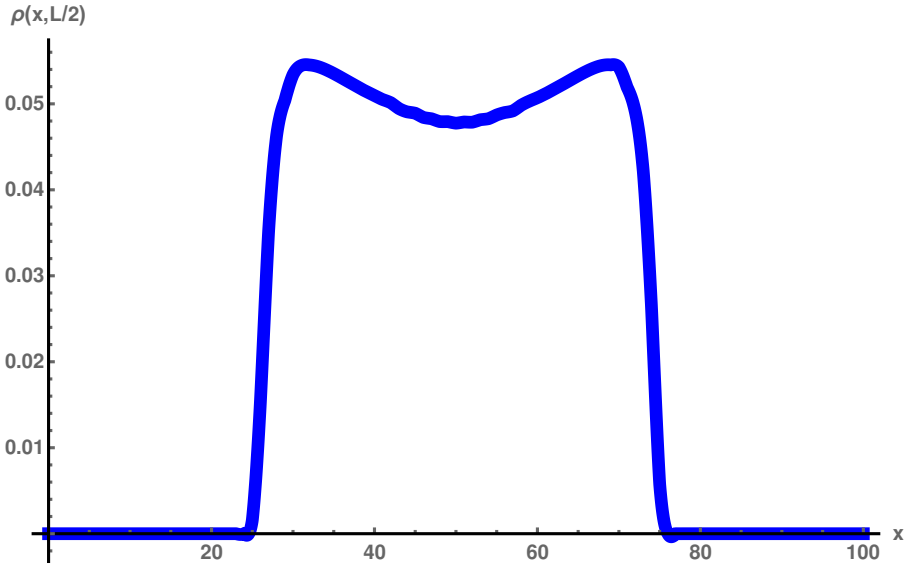

Figure 5.13: Graph of the density profile of the branching actin networks dominated by long linear filaments confined in a spherical cell in the presence of attractive monomers interactions potential with strength $V_0 = -1$. $z = 0.75$ and $\zeta = 0.001$. The deflection in the middle of the profile of the density has decreased meaning that the networks segments are becoming homogeneously distributed inside the cell.

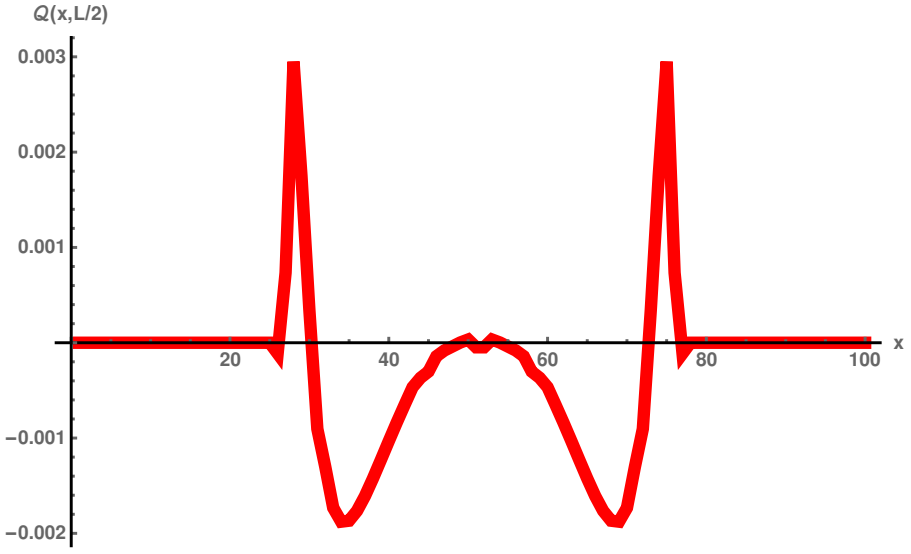

Figure 5.14: Graph of the radial order field profile of the branched actin networks confined in a spherical cell at high attractive interaction strength $|V_0|$, $V_0 = -1$. $z = 0.75$ and $\zeta = 0.001$. The order parameter field profile near the centre of the sphere becomes negative while positive near the cell wall indicating that there is a competition between parallel and perpendicular alignment of the filaments. This profile is similar to the profile of the networks with comparable length scales ($L \sim D \sim \ell_{\mathrm{p}}$).

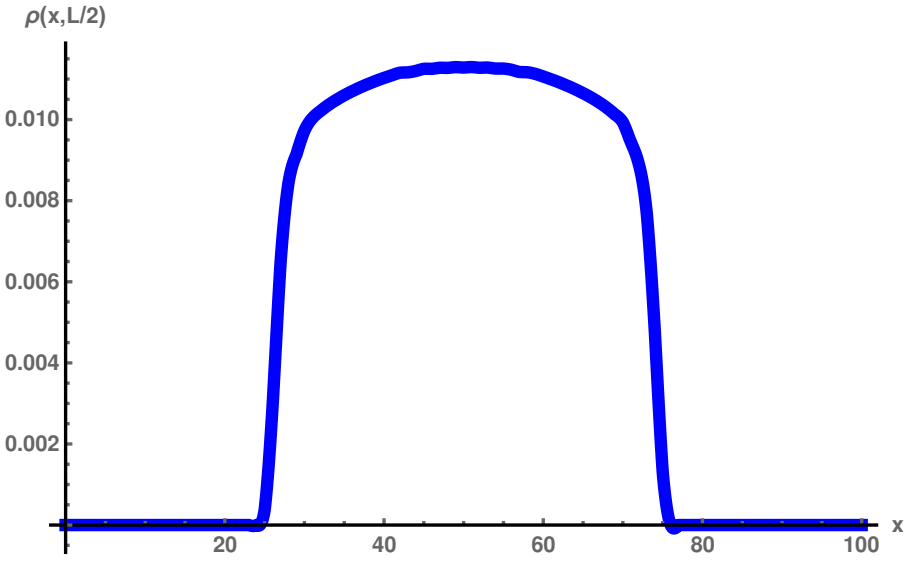

Figure 5.15: Graph of the density profile of the branching actin networks dominated by long linear filaments confined in a spherical cell in the presence of attractive monomers interactions potential with strength $V_0 = -5$. $z = 0.75$ and $\zeta = 0.001$. The profile of the density of segments shows that the network segments becomes more dense near the centre of the cell. This profile is similar to the density profile of the networks dominated by short filaments.

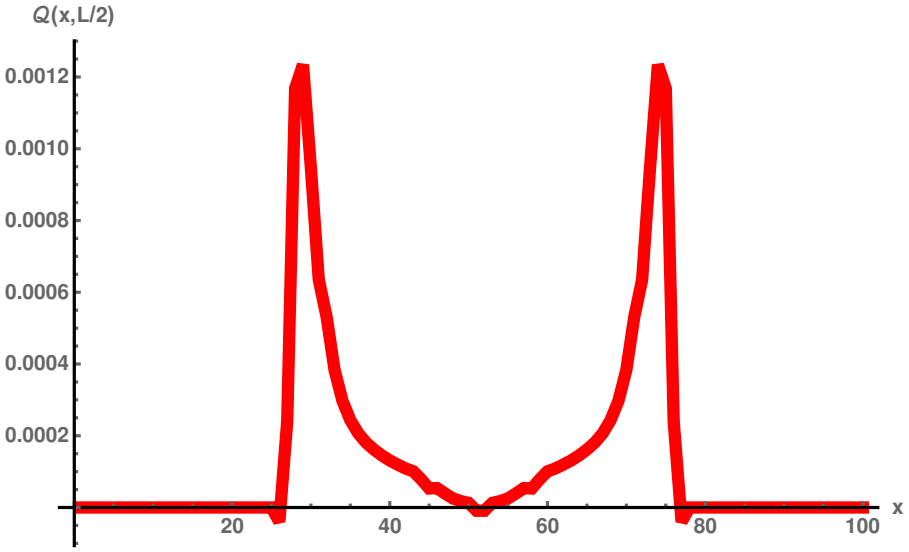

Figure 5.16: Graph of the radial order field profile of the branched actin networks confined in a spherical cell at high attractive interaction strength $|V_0|$, $V_0 = -5$. $z = 0.75$ and $\zeta = 0.001$. The order parameter field profile is positive close to spherical cell wall or membrane and 0 near the centre indicating that filament segments near the cell membrane align parallel to the membrane and those near the centre are isotropically distributed.

5.3.2.2 Repulsive interactions ($V_0 > 0$)

We observe no significant change or no differences between the profiles of the networks dominated by long linear filaments for no mutual interactions between segments and their profiles

in the presence of repulsive interaction potential, by comparing Figure 5.11 and Figure 5.12, Figure 5.17 and Figure 5.18. This may be due to the force created by the interactions in the network system in order to bend the long linear filaments and keep them wrapped around the cell in the cell periphery.

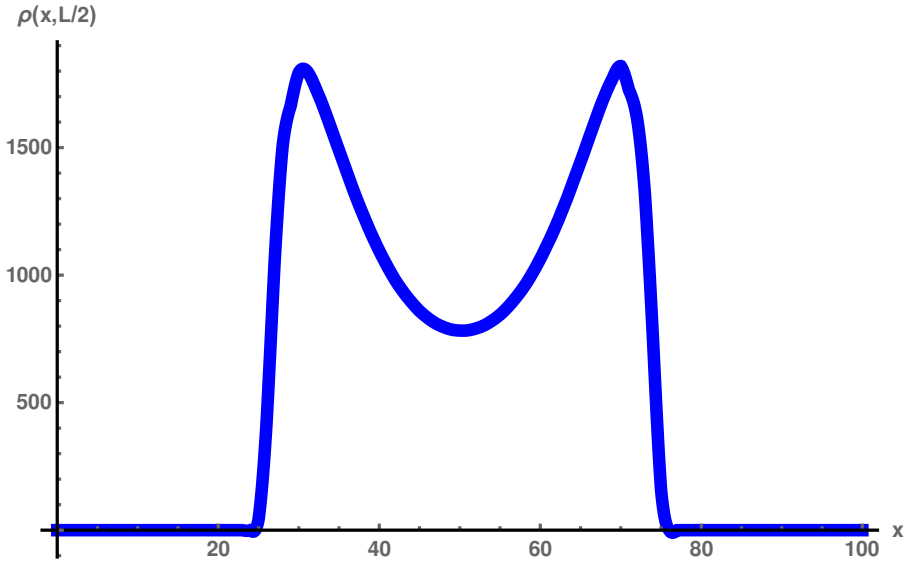

Figure 5.17: Graph of the density profile of the branched actin networks confined in a spherical cell at high attractive interaction strength $|V_0|$, $V_0 = 0.001$. The filament elongation parameter $z = 0.75$ and the branching parameter $\zeta = 0.001$. Here the density of filament segments of the branched networks is convex-shaped at high short-range aligning interaction.

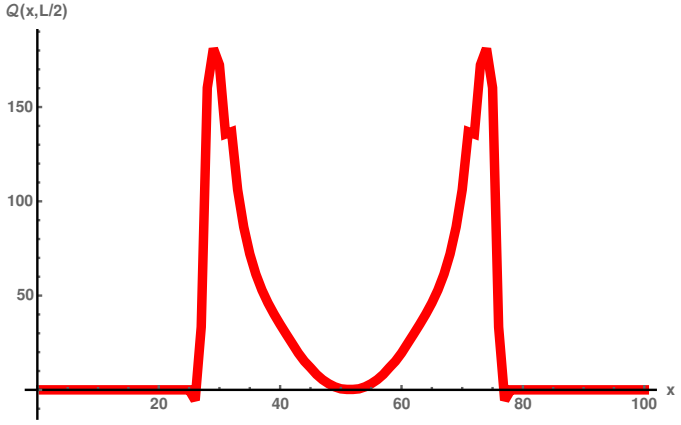

Figure 5.18: Graph of the density profile of the branching actin networks dominated by long linear filaments confined in a spherical cell in the presence of attractive monomers interactions potential with strength $V_0 = 0.001$. $z = 0.75$ and $\zeta = 0.001$. The order parameter field profile is positive. This shows that the long linear filaments with actin monomers mutual interactions stay wrapped around the cell. We predict that this is due to the fact that, the repulsive forces between monomers sum up to the repulsive force from the cell membrane to keep the long linear filaments of the networks bent in order to minimize the free energy of the system.

We present next the effect of the excluded volume effect on networks dominated by short

filaments.

5.3.3 Networks dominated by short filaments

5.3.3.1 Short-range aligning interactions ($V_0 < 0$)

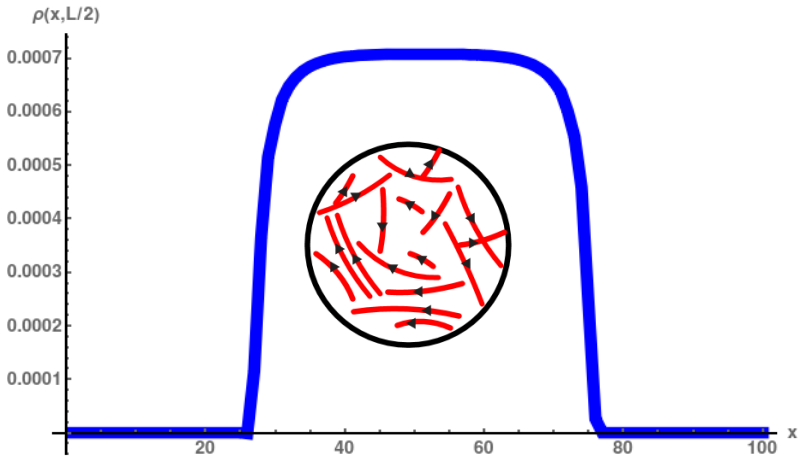

Figure 5.19: Graph of the density profile of networks dominated by short filaments confined in a spherical cell without any mutual monomers interactions i.e here we set the interacting potential to 0 ($V_0 = 0$). $z = 0.5$ and $\zeta = 0.001$. We have relatively flat average density distribution of network segments near the centre of the spherical cell. The inset is a cartoon representing the spherical geometry confining the network of actin filaments in red on the graph and it is there to illustrate the type of the networks for which the this density profile is obtained.

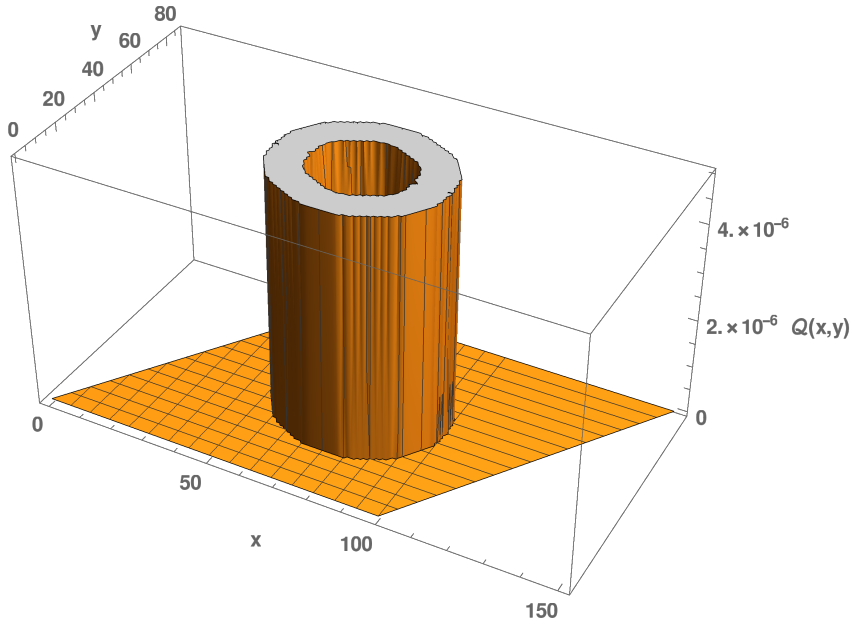

Figure 5.20: Graph of the radial order field profile of networks dominated by short filaments confined in a spherical cell without any mutual monomers interactions i.e here we set the interacting potential to 0 ($V_0 = 0$). The filament elongation parameter $z = 0.515$ and the branching parameter $\zeta = 0.06$. The order parameter field profile shows that the filaments that are close to the cell wall are aligned parallel to it while those near the centre of the confining sphere are isotropically distributed.

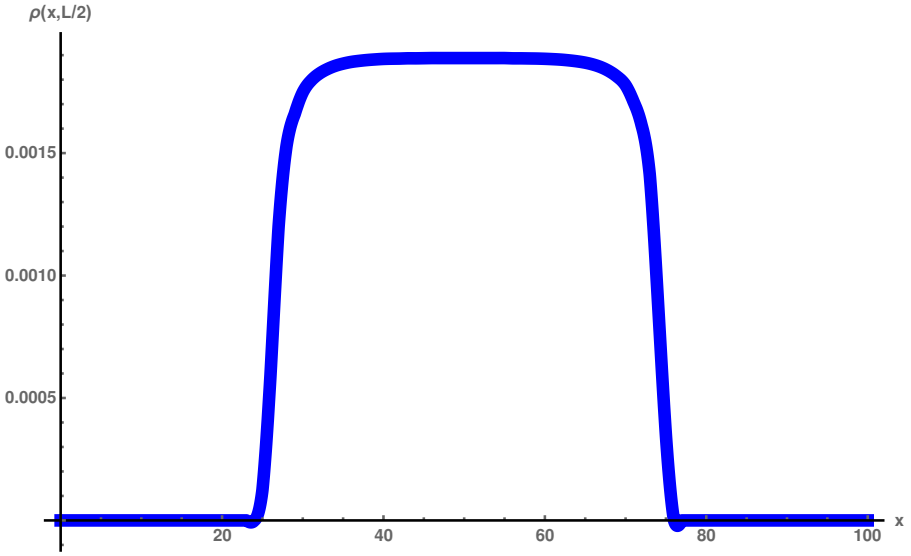

Figure 5.21: Graph of the density profile of networks dominated by short filaments confined in a spherical cell in the presence of $V_0 < 0$ mutual monomers interactions with $V_0 = -5$. $z = 0.5$ and $\zeta = 0.001$. We have convex-shaped average density distribution of the network segments. There is no significant change compared to the case of no monomers mutual interactions.

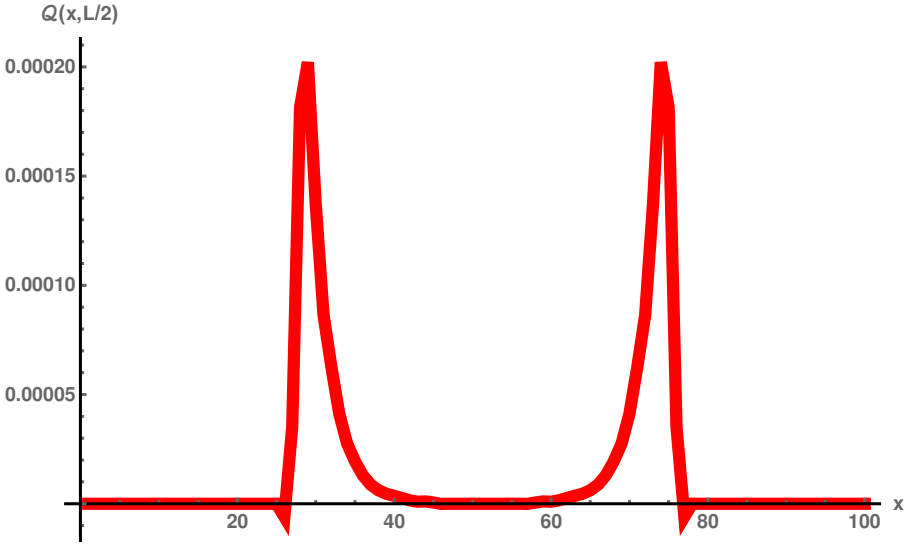

Figure 5.22: Graph of the radial order field profile of networks dominated by short filaments confined in a spherical cell in the presence of attractive mutual monomers interactions with $V_0 = -5$. The filament elongation parameter $z = 0.515$ and the branching parameter $\zeta = 0.06$. The order parameter field profile shows that the filaments that are close to the cell wall are aligned parallel to it while the filaments close to the centre are isotropically distributed. The networks is thus not influenced by the presence of the $V_0 < 0$ interaction between filaments segments.

There is no significant change in the profile of the networks dominated by shorts filaments. This indicate that the effect from the cell membrane are short range. Unless the filament are in contact with the membrane they don't fill confining membrane effects confirming the fact that

the spatial organization of the networks dominated by short filaments are weakly influenced by the confinement effect.

5.3.3.2 $V_0 > 0$ interactions ($V_0 > 0$)

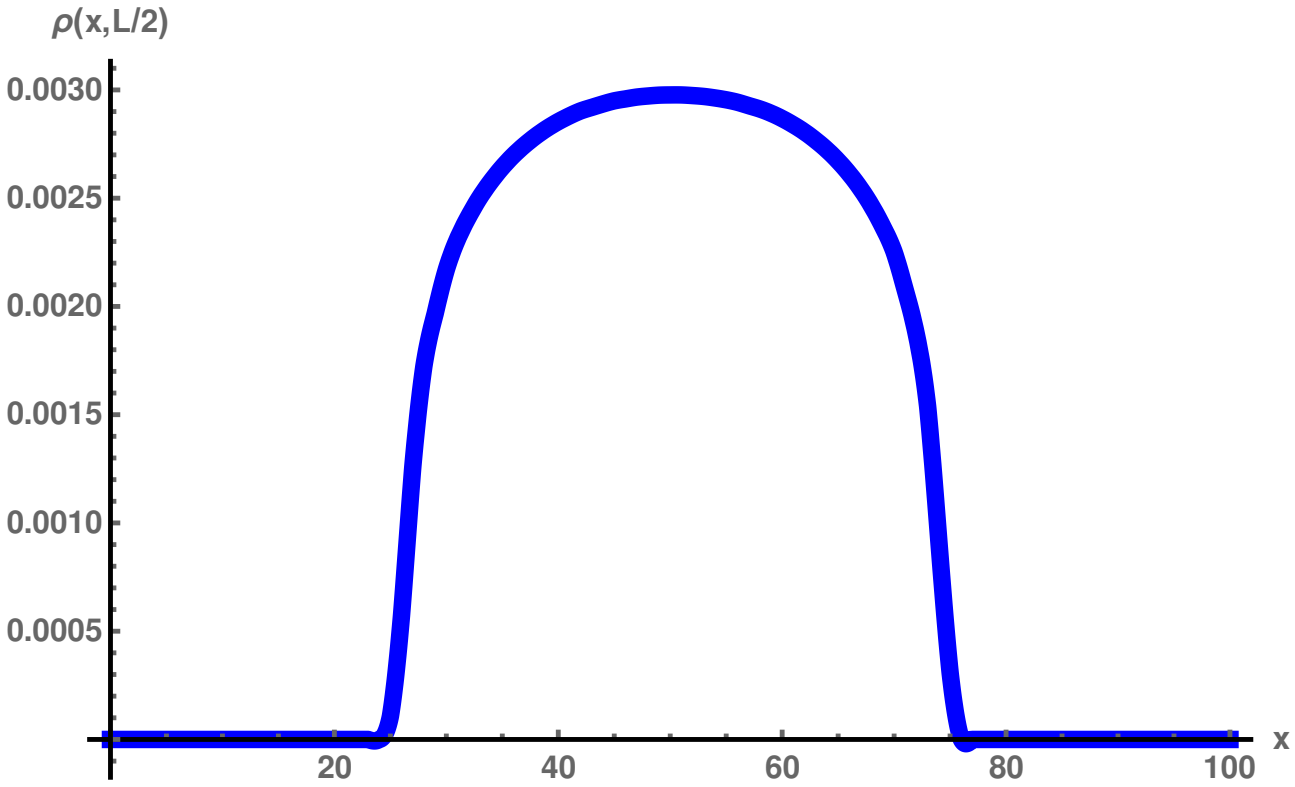

Figure 5.23: Graph of the density profile of networks dominated by short filaments confined in a spherical cell in the presence of repulsive mutual monomers interactions with $V_0 = 13$. $z = 0.5$ and $\zeta = 0.001$. We have homogeneous average density distribution profile of the network segments. There is no significant change compare to the case of no mutual interaction.

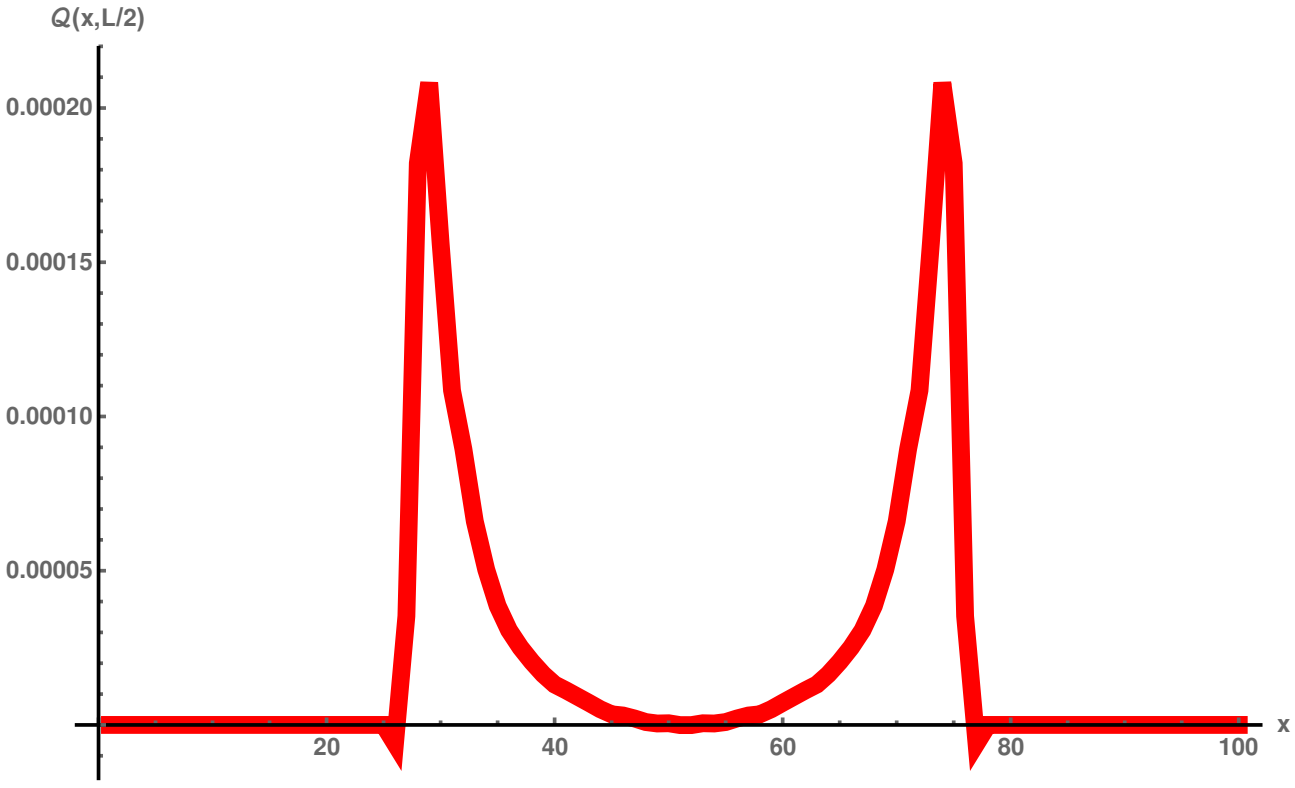

Figure 5.24: Graph of the radial order field profile of networks dominated by short filaments confined in a spherical cell in the presence of $V_0 > 0$ mutual monomers interactions with $V_0 = 13$. The filament elongation parameter $z = 0.515$ and the branching parameter $\zeta = 0.06$. The order parameter field profile shows that the filaments that are close to the cell wall are aligned parallel to it while the filaments close to the centre are isotropically distributed.

We remark that the confinement effects on networks dominated by short filaments do not change in the presence of the excluded volume effects between the chain segments.

5.4 Conclusion

The confined semiflexible polymers with mutual interactions between chain segments have been widely modelled and theory and simulations are developed in order to investigate how the confinement influence the thermodynamic properties and behaviour of these filaments in the presence of of the excluded volume effect [14, 44, 67, 73, 81, 114–118]. However none of them has clearly investigated what are the confinement effects on the spatial organization, orientational ordering and conformation of branching actin networks with mutual chains monomers interactions. In this chapter we have modelled the branching actin networks under confinement in the presence of mutual actin monomers interaction at thermodynamic equilibrium in the grand ensemble. Using the SCFT approximation, we have been able to establish a relationship between the mean field and the total density of filament segments. This allowed the numerical implementation of the non-linear integral equations which couple with the density of the filaments. From there we have computed the density profiles and order parameters fields which shows that in the presence of $V_0 > 0$ mutual interaction potential between monomers of the actin filaments, the rigid confining cell membrane strongly influence the branched networks by bending its filaments while it has no effect on networks dominated by long linear filaments and on the networks dominated by short filaments. We argued that this may be due to the fact that the repulsive potential from the networks add up to the one of the cells membranes in order to bend the branching filaments and the long linear filaments while they have no effects on the short filaments because of their small sizes. While short-range aligning interaction potential ($V_0 < 0$) induce change in the structural organization of the filaments of branched networks and the networks dominated by long linear filaments which then adopt the networks dominated by short filaments behaviour.

These quantitative predictions enhance our understanding of how the Arp2/3-based branched actin networks with excluded volume effect between network segments self-organize spatially and how they align in inside living eukaryotic cells under the effect of cell membrane confinement. This might help to understand some of the physiological processes or mechanical phenomena of cells in which branching actin networks are involved. This model is also important for authors that are thinking of conceiving artificial living cells [119] for medical purposes since one has to identify the structural properties of each component of a living tissue cell and their and role in the cell functions.

In the next chapter, we aim to look at the contribution of the structural properties of branching actin cytoskeletal networks under the cell membrane confinement to the elastic properties and stability of the cell.

Part III

Contribution of confined branching cytoskeletal actin networks to the mechanical properties of tissue cells.

Chapter 6

From structural equilibrium properties of actin networks to the elastic stability of cells

6.1 Introduction

Eukaryotic cells of living tissues are susceptible to physical deformations while maintaining their cellular integrity and function [120]. For example, cells that form epithelial tissues covering the internal and external surfaces of organs such as skin cells or intestines can exhibit elastic behaviour under a wide variety of circumstances as they interact with their substrates or with neighbouring cells. The elastic properties of cells is important in wound healing as well as immune suppression in tumours and in regulating the forces between tissues cells [120–122]. The ability of the cell to resist deformation and to change shape during movement is mainly ensured by the elasticity of actin cytoskeletal networks, the major constituents of the cell cytoskeleton. There are a variety of actin networks. These differences are observed in their architectures and structures. Actin-related binding proteins and the cell membrane confinement effect on actin filaments' spatial organisation and orientation are responsible of these differences in actin networks architectures and structure [123]. The cell membrane confines the cytoskeletal network and controls its growth, its structural and its mechanical behaviour. In turn cytoskeletal filaments especially actin filament networks provide the cells with its mechanical stability and organization [124]. The macroscopic mechanical properties and shape of the cell and its interaction with its neighbouring cells depend mostly on the architecture, structure and elasticity of actin networks [17, 123, 125–129].

Researches suggests that the stability of normal motile cells and their elastic shape changes to internally and externally generated force is closely related to the coupling between the cell-sized confinement and spatial and orientational ordering of branching actin cytoskeleton [13, 89, 104, 130], branching obtained via the Arp2/3 protein complex. Branching actin cy-

toskeleton is thus essential for understanding cells and tissue mechanical function.

The biological importance of knowing how tissue cells keep their mechanical integrity and function at cellular length scale as well as the challenges of understanding how these functions relates to the structure and architectures of system of self-organizing networks, we believe is best illustrated by the study of the structural and elastic properties of branching actin networks inside confining regions. While the structure and physical properties of biological cells must ultimately be described by the known laws of chemistry and physics, how to theoretically establish a quantitative relationship between the networks structural properties and the cell mechanical properties is still not well explored. The aim of our model is to help to elucidate and make quantitative predictions on structural and elastic contribution of the actin cytoskeleton to the elastic properties of the cell and of a collection of cells (Tissues). What are the forces that branching cytoskeletal networks contribute to ensure the mechanical stability of the cell at thermodynamics equilibrium is one of the question that we will treat in course of this chapter.

In the first section of this chapter, we would like to know if branching actin networks growing inside cells cells that have rigid wall (case of plant cells) in two dimensions (Figure 6.1), are stable against compressive and stretching forces. So, we investigate on the stability of the growing and branching networks of actin filaments inside confining region. This stability implies also the stability of our confining cytoskeletal networks model. We then determine the elastic properties of the networks confined in the two dimensional cell or box by calculating the forces exerted between two neighbouring cells with rigid movable membrane or wall separating them. We compute also the Young modulus of the networks as function of the the stiffness of the networks.

In the second section we investigate the energy cost for confined branching networks and for confining semi-flexible membrane to keep the system in thermodynamic equilibrium. This allows us to confirm the elastic stability of actin networks inside cells with elastic membrane. We also explore the relationship between the network structures and the cell membrane elasticity by measuring the density and order field profiles.

In the third section, we consider two neighbouring cells with an elastic membrane separating them and we investigate the stability of the networks again stretchering or compression forces. We measure also the force exerted between the two cells and the young modulus of the networks . We have also looked at the stability of a collection of cells.

In the fourth and last section we investigate the stability of the cell against shear. We also look at the structure of the networks as we shear the confining region with a rigid membrane. Computational and theoretical approaches are used to help capture the physics that we have outlined above.

6.2 Stability and force balance of branching actin networks confined by rigid cell wall

In this section we first investigate the stability of branching actin filamentous networks inside confining regions. We also calculate the forces exerted by these networks.
We model a system of two equal-sized cells with rigid walls that are in contact with each other and inside each of them grow a two dimensional (2d) actin cytoskeletal networks, Figure 6.1. 2d modelling of cytoskeletal networks is very relevant for plant cells. In fact, beside the fact that plant cells possess a very rigid wall and some with a rectangular shape, over ninety percent of the cytoplasm of plant cell is occupied by a very large vacuole leaving the cytoskeleton in a very thin space [18, 131].
Both cells contain identical networks and are separated by a rigid membrane.
We apply small perturbation on the partition membrane which serves as a piston between the two cells. The displacement of the partition stretches the left hand cell affinely while compressing the right hand cell, Figure 6.2. In what follows, we compute the new grand partition function of the system of the two cells allowing us to calculate the Gibbs free energy.

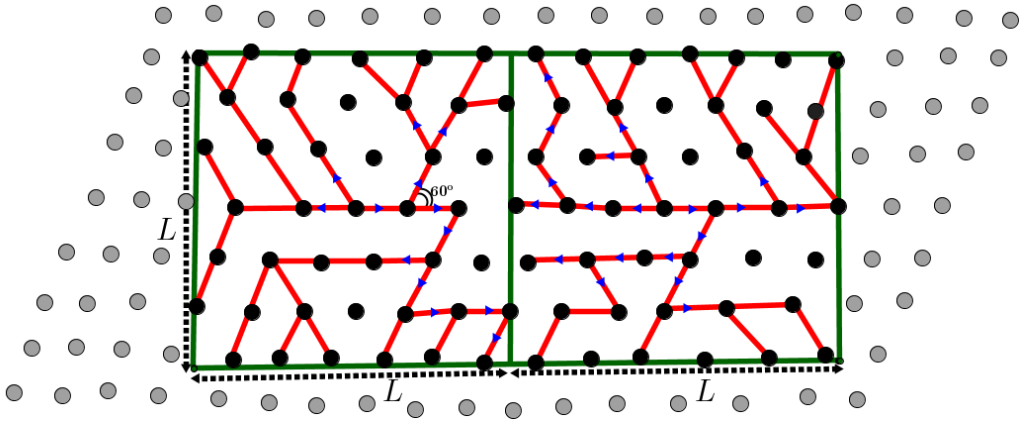

Figure 6.1: 2D Depiction of branched actin networks (in red) growing inside two square-shaped cells separated by a rigid wall or membrane. Actin filament filaments segment occupy the two triangular lattice. The black dots are the sites of the lattice and they indicate the position of the networks segments. The dots in grey are the lattice sites that are not occupied. The wall of the cells are in green.

6.2.1 Stability: Calculation of the Gibbs free energy

Here, the stability of confined branched cytoskeletal networks is discussed. Branched actin networks are formed at the leading edge of the cell and due to it their highly dense structure and branched architecture and their spatial organisation is strongly influenced by the confinement effect from the cell membrane. It is thus useful to investigate the stability of such networks.
To determine the stability of the actin networks under confinement, we compute the Gibbs free energy of the system in Figure 6.2. The Gibbs free energy G is the thermodynamic potential

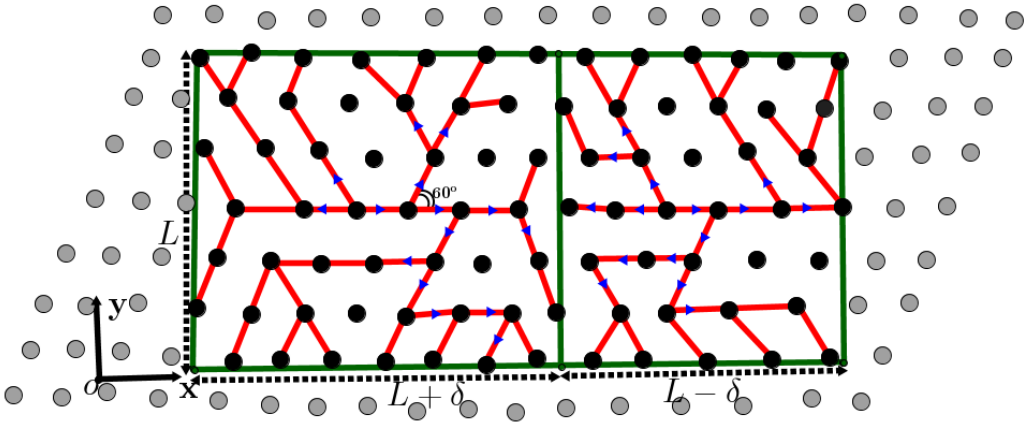

Figure 6.2: Movable partition membrane. It can be interpreted as a piston between separating the content of the two cells. Small displacement of this partition compresses the cytoskeletal networks at the right hands while the networks in the left cell fills the larger volume.

energy which measures the stability of a system. We check whether a small perturbation or displacement of the interface raises or lowers the free energy of the network system. In the present context, if the free energy is increased by the perturbation, the network system is stable. If the free energy is lowered by the perturbation, the network system is inherently unstable and will change the cell morphology. To calculate the Gibbs free energy we need to calculate the grand partition function of the system, the density distributions of actin networks and the average number density of filament segments. The grand partition $\mathfrak{Z}$ function of the system of the two cells is given by the product of the partition function of the cell in left hand side $\mathfrak{Z}(L+\delta)$ and the partition of the cell on right hand side $\mathfrak{Z}(L-\delta)$ of the Figure 6.2, where the grand canonical partition function of each cell is the same as the one we de define in Chapter 3 of this thesis for branching networks.

$$\mathfrak{Z} = \mathfrak{Z}(L+\delta) \times \mathfrak{Z}(L-\delta) \tag{6.1}$$

Where we write in shorthand notation

$$\mathfrak{Z}(L+\delta) = 1 + \int_{x,y,\hat{\boldsymbol{n}}} z(x,y,\hat{\boldsymbol{n}},\delta)\Psi(x,y,\hat{\boldsymbol{n}},\delta), \tag{6.2}$$

$$\mathfrak{Z}(L-\delta) = 1 + \int_{x,y,\hat{\boldsymbol{n}}} z(x,y,\hat{\boldsymbol{n}},-\delta)\Psi(x,y,\hat{\boldsymbol{n}},-\delta) \tag{6.3}$$

$$\mathfrak{Z}(L+\delta) = 1 + \int_{x,y,\hat{\boldsymbol{n}}} z(x,y,\hat{\boldsymbol{n}},\delta)\Psi(x,y,\hat{\boldsymbol{n}},\delta) \tag{6.4}$$

and we define z to be:

$$z(x,y,\hat{\boldsymbol{n}},\delta) = z_0\Theta(L+\delta-x,\hat{\boldsymbol{n}})\Theta(L-y,\hat{\boldsymbol{n}})\Theta(x,\hat{\boldsymbol{n}})\Theta(y,\hat{\boldsymbol{n}}) \tag{6.5}$$

and

$$z(x,y,\hat{\boldsymbol{n}},-\delta) = z_0\Theta(L-\delta-x,\hat{\boldsymbol{n}})\Theta(L-y,\hat{\boldsymbol{n}})\Theta(x,\hat{\boldsymbol{n}})\Theta(y,\hat{\boldsymbol{n}}), \tag{6.6}$$

which gives the confinement.

Let us now compute the Gibbs free energy of the network system as function of the displacement of the partition membrane δ. It is the sum of the Gibbs free energy of the stretched cell and the one of the compressed cell. It is given by:

$$G(\delta) = G(L+\delta) + G(L-\delta) = \mu(N_{-\delta} + N_{\delta}) \tag{6.7}$$

where

$$N_{\delta} = \int_0^L \int_0^L \mathrm{d}x\,\mathrm{d}y\varrho(x+\delta, y) \tag{6.8}$$

and

$$N_{-\delta} = \int_0^L \int_0^L \mathrm{d}x\,\mathrm{d}y\varrho(x-\delta, y) \tag{6.9}$$

are the average numbers of segments of the network, $\varrho(x+\delta, y)$ and $\varrho(x-\delta, y)$ are the average density distributions of cytoskeletal filament segments confined inside respectively the stretched and compressed cells. μ is the chemical potential. The average number of segments and the density distributions are obtained by adjusting the chemical potential activities, z_0 for filament elongation and ζ_0 for filament branching.

We plot the numerical calculation of $G(\delta)$ as function of the displacement δ, Figure 6.3. We see

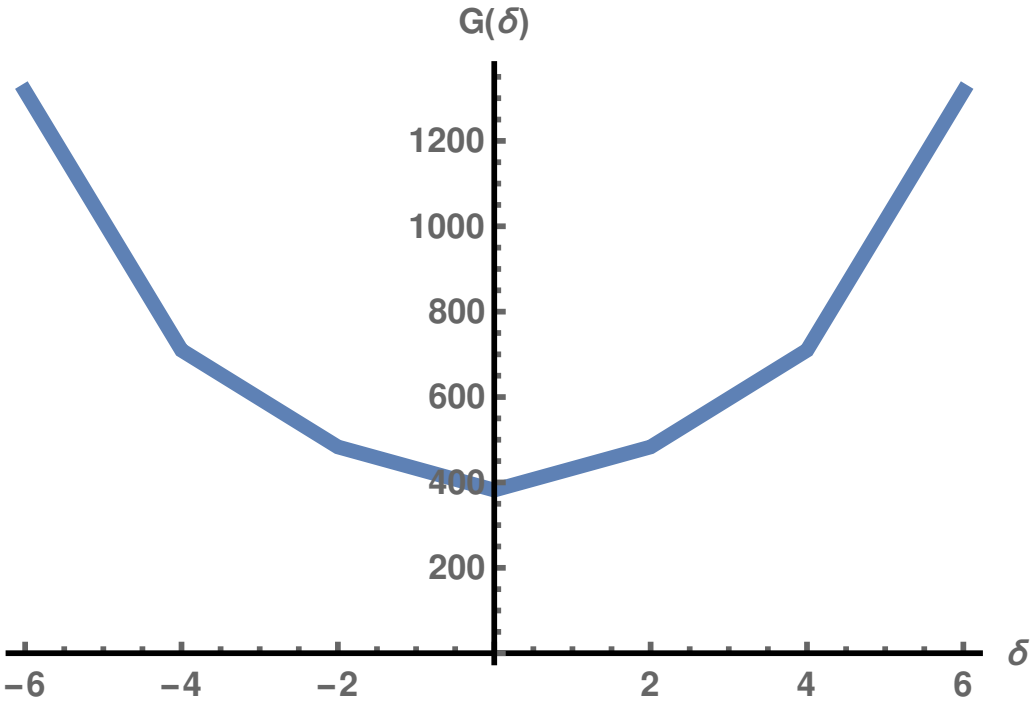

Figure 6.3: Plot of the Gibbs free energy of the system of branching cytoskeletal networks under compressive strains. We have obtained this graph for the ratio between the persistence length of the filaments and the square side length $\ell_p/L = 1.2$, $z_0 = 0.54$ and $\zeta_0 = 0.064$. We observe an the increase of Gibbs free energy meaning that the system is stable against compressions.

that the Gibbs free energy of the system increases as we increase the stretching and compressive

strain. The strong compression of the networks in the right cell raises the free energy in order to keep the system in thermodynamic equilibrium. Cytoskeletal networks that grow in cells that have rigid walls are thus stable against compressive forces. This result has been reported also for the case of spherical confined polymer networks where they showed that the stability of proteinic macromolecules noticeably increases under strong confinement, compared to that in bulk [19, 132]. This result also confirms the stability of our model.
It is also essential to know how much force each cell can exerts or contributes in order to ensure the stability of the cell within the tissue. So we aim to in what follow we compute the the compressive forces exerted by each cell and then deduce the force difference between tissue cells. We compute also the networks elastic response or Young modulus.

6.2.2 Competition between compressed and the stretched networks

Using the relationship between the partition function and the pressure exerted by a system of networks in the grand canonical ensemble (6.10), we compute the difference in force between the two cells and the Young modulus of the branching actin networks. This lead to the characterization of the elastic properties of branched actin networks in confined regions.

$$\langle P \rangle V = k_B T \ln \mathfrak{Z}. \tag{6.10}$$

Where P is the pressure in the network system and V the volume. For 2d systems, we talk about area A of the system instead of the volume V. For a network in square cell of side length L, the force exerted by the network system is given by:

$$F(L) = \langle P \rangle \frac{A}{L}. \tag{6.11}$$

We compute numerically the compressive and stretching forces exerted respectively by compressed and stretched cells as function of the applied strain. We then compute the difference between the two forces as follows:

$$DF(\delta) = F(L+\delta) - F(L-\delta) = k_B T \left(\frac{\ln(\mathfrak{Z}(L+\delta))}{L+\delta} - \frac{\ln(\mathfrak{Z}(L-\delta))}{L-\delta} \right). \tag{6.12}$$

We have also computed the difference in forces that are exerted between these two perturbed cellular networks and plotted it on the graph of Figure 6.4. It shows that the compressed cell or networks exert higher force in order to bring the system back to its equilibrium position at $\delta = 0$, a kind of spring elastic behaviour as spring always go back to its equilibrium position when it is subjected to stretching or to compression. This result confirm also the stability of the network system.
Moreover, it is also important to be able to quantify the ability of the networks to help the cell resists mechanical cues. For that we measure the elastic response or Young bending modulus of the networks.

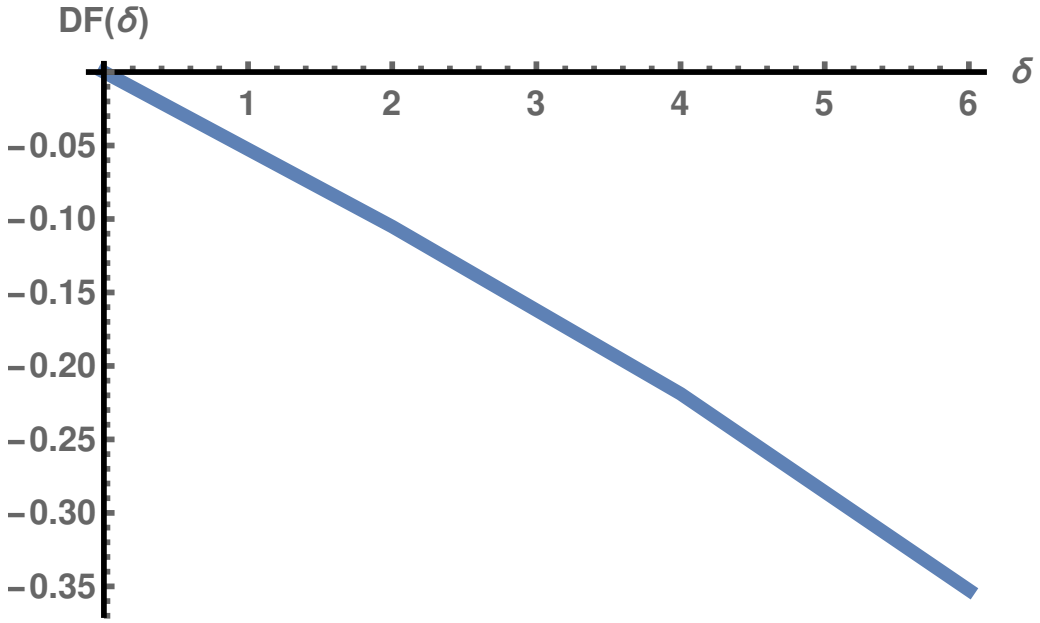

Figure 6.4: Plot of the difference in force between compressed and stretched cell as function strain δ. The networks behave like spring under compression.

6.2.3 Young modulus

We would like to know how well the cystoskeletal network system stand up to tension which the cell membrane is permanently subjected to. So we measure the Young modulus of the networks as function of the network stiffness (the branching parameter ζ) for stain going to 0. The Young modulus E is given by:

$$E = -\frac{\partial DF(\delta)}{\partial \delta}|_{\delta=0}. \tag{6.13}$$

The Young modulus increases linearly with about 7% as we increase ζ from 0. However ζ is increased in the limit of the model validity domain $((1-z_0)^2 \geq 4\zeta_0)$ which is the limit beyond which our numerical calculation diverges. This means that the networks in this case respond affinely to compressive stresses. Recall that the increase of ζ, increases the branching of cytoskeletal filaments. Though, the increasing of the elastic modulus is not large, it shows that branching increases the stiffness of the networks and thus the ability of the networks to withstand the strain This result allows us to confirm the stability of our model. We can now extend it to the case of cell with semi-flexible walls or membranes in order to mimic the mechanical behaviour of cells that have semi-flexible membranes.

6.3 Networks growing inside cells with elastic membrane

Living cells especially in animals have elastic membranes which allow them to cope with the mechanical or elastic behaviour of the cytoskeletal networks to change shape in order to adapt to their environment. However, normal cells seek to keep their volume conserved, unless it is

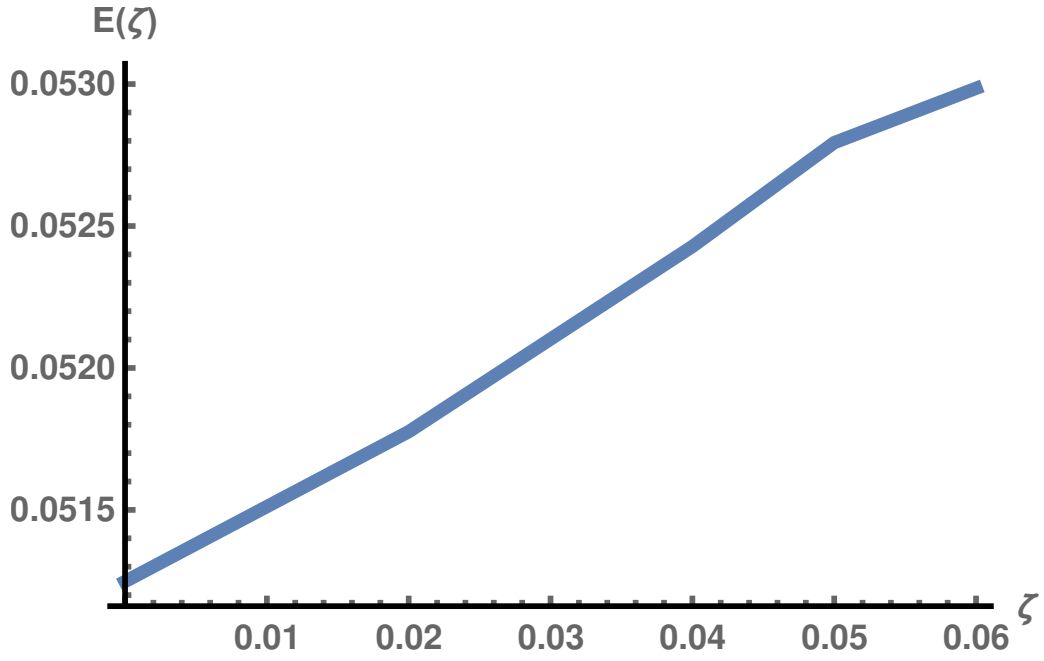

Figure 6.5: Plot of the young modulus of the networks, showing a slow variation as we increase the branching strength ζ. $E(\zeta)$ *varies about* 7% *from* 0.0512 *to* 0.0530.

an invasion due to a tumour (cancer) [87, 133–138]. To take into account this aspect of normal cells in our model, we consider a cell that have a rectangular shape made of membrane that can bend in one direction and we investigate on how to make a choice of the elastic bending modulus of the membrane such that cells of our model will not expand or shrink infinitely. Recall that in our model we are trying to mimic and determine the structure and elastic properties of cells in an equilibrium state that have already establish mature branched actin networks in their interior.

In this section we first investigate the thermodynamic equilibrium of confined branching cytoskeletal networks and we explore the relationship between the structure and architecture of the networks and the elastics properties of the confining cell as one compresses or stretches it. Secondly we investigate on the stability of the confined networks against the compression from neighbouring cell and we compute the pressures or forces transmitted across the elastic cell membranes. Thermodynamic equilibrium calculations under the grand canonical ensemble are done in order to achieve this, as previously.

6.3.1 Energy cost for the cytoskeletal networks and for the cell membrane

We compute the work done by the cytoskeletal networks and the cell membranes in order to minimize the energy cost for the equilibrium of the system. It represents the work required during a reversible thermodynamic process or the energy cost for the system, to give the cell its final volume or shape (i.e the cell is brought out of equilibrium) while keeping on average, a constant pressure in the system. The choice of the bending modulus of the membrane is very

important for the energy cost to be minimized. It means that we need to determine the range of the value of the bending modulus for which the free energy of the system is minimum or for which the work done by both the networks and the elastic membrane is maximum without inducing significant change in the membrane curvature. For that, we introduce a perturbation leading the cell membrane to bend in x directions and get a convex shape in the two directions, Figure 6.6. This is a very simplified version of what might occur, when a cell starts growing in a tissue. We also want to check wheter such deformation is stable with respect to neighbouring cells.

We measure numerically the work done by the confined system as function of the amplitude of the membrane curvature. The shape of the bent side is parametrised by 1d curve $h(y)$ such that the bent side is fixed at its end point i.e $h(L) = 0 = h(0)$ and $h''(L) = 0 = h''(0)$. The free

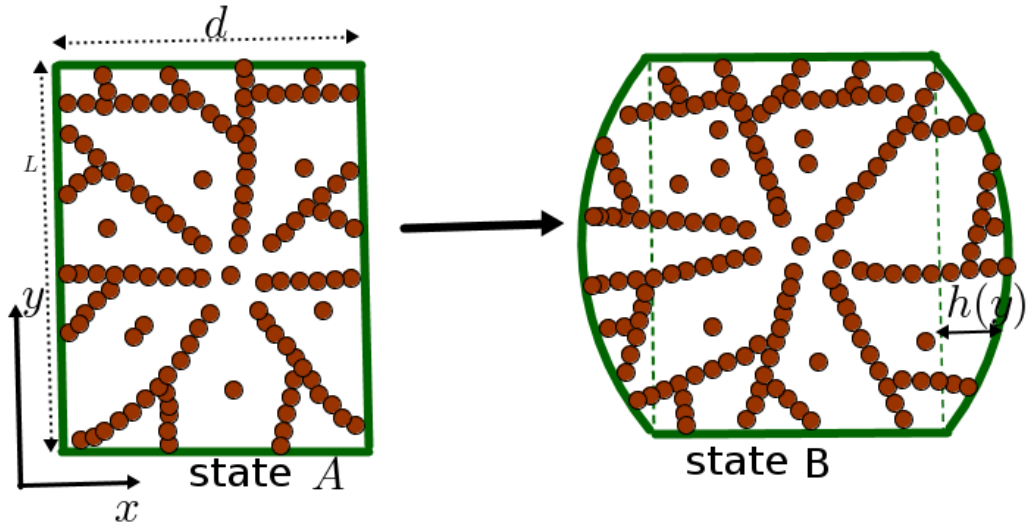

Figure 6.6: The wall of the cell in the x directions are semi-flexible. State A: cell in the unperturbed state. state B: cell in the perturbed state.

energy of the system can be seen as the work W_h done by the cell system during the deformation and is given by the relation in equation (6.10):

$$W_h = \langle P \rangle V = k_B T \ln \mathfrak{Z} \tag{6.14}$$

Where $\mathfrak{Z}$ is the annealed average of the grand partition function $\mathfrak{Z}(L + h(y))$ over all possible configurations of h as:

$$\mathfrak{Z} = \int_h \mathrm{D}h\, \mathfrak{Z}(d + h(y)) P[h] \tag{6.15}$$

Where $\int_h \mathrm{D}h$, $P[h]$ is the distribution function associated to $h(y)$ and is given by:

$$P[h] = \mathcal{N} e^{-\frac{\kappa}{2}\int_0^L \mathrm{d}y (h''(y))^2} \tag{6.16}$$

where $\mathcal{N}$ is the normalization factor and κ the membrane bending modulus.

$$\mathfrak{Z}(L + h(y)) = 1 + \int z(x, y, \hat{\boldsymbol{n}}, h(y)) \Psi(x, y, \hat{\boldsymbol{n}}, h(y)) \tag{6.17}$$

and

$$z(x, y, \hat{\boldsymbol{n}}, h(y)) = z_0 \Theta(d + h(y) - x, \hat{\boldsymbol{n}}) \Theta(L - y, \hat{\boldsymbol{n}}) \Theta(x, \hat{\boldsymbol{n}}) \Theta(y, \hat{\boldsymbol{n}}) \tag{6.18}$$

We do not use the functionals, we rather make the following choice for $h(y)$ for our numerical computation:

$$h(y) = h_0 \sin\left(\frac{\pi}{L} y\right) \tag{6.19}$$

where h_0 represents the amplitude of the deformation. We plot the work as function of the curvature amplitude. We see that, as we make the membrane stiff enough by increasing its bending modulus, the maximum work of the networks is quickly reached without inducing a large change in the membrane curvature, see Figure 6.7. This means that the minimal free energy of the confined system or the minimum energy cost required to keep or bring the system in equilibrium, is obtained for large value of bending modulus (for our model, $\kappa \geq 100$). We can then argue that for cells and their networks to keep their thermodynamic equilibrium, cells membranes need to be stiff enough. It is necessary to have a stiff membrane in order to maintain the equilibrium and finite cell size. This allow us to make good choice of the bending modulus of the cell membrane for our further calculations. And then look at the density and orientation or order profiles of actin networks at this cell as the cell membrane bends and increase the cell volume.

Next we explore the relationship between the structure and architecture of the confined branched networks and the elastic properties of the cell. For that we plot the density and order profiles of the networks and we analyse our observations.

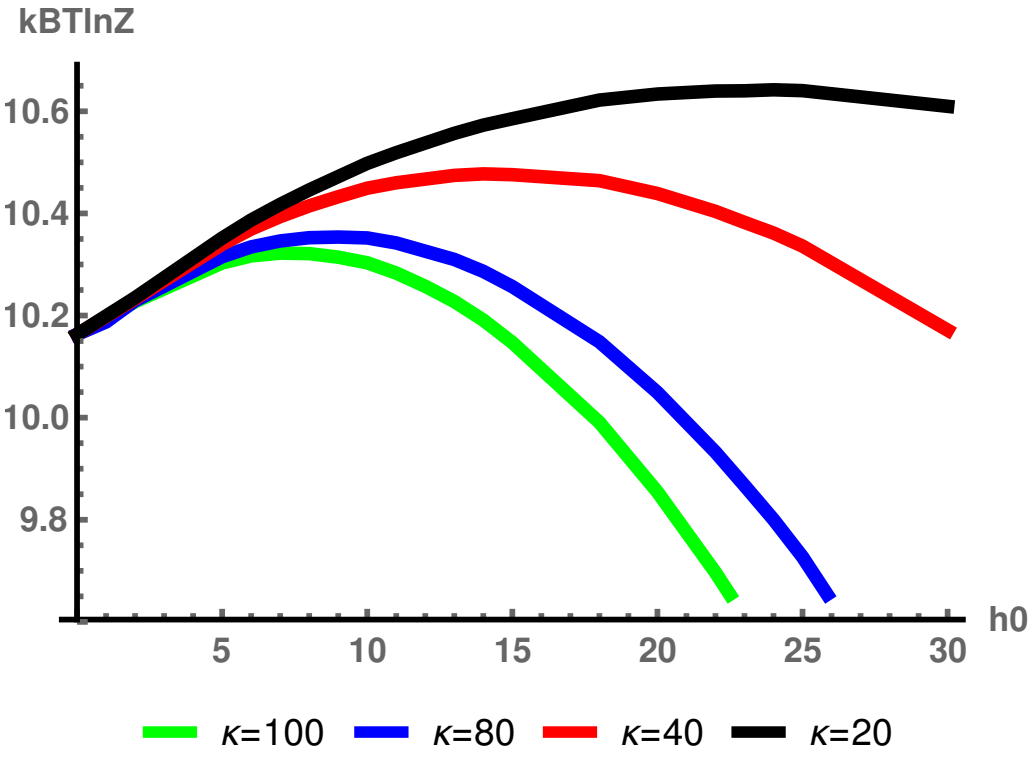

Figure 6.7: Graphs showing the work done by the branching actin networks and the cell membrane. The result is obtained for $\ell_p/L = 1.2$, $z_0 = 0.5$ and $\zeta_0 = 0.06$. As we increase the value of κ, the work done by both the network and the membrane quickly reach the maximum without inducing significant change in the cell membrane curvature. So the minimum energy cost for which the cell stay at equilibrium is obtained for large value of bending modulus κ.

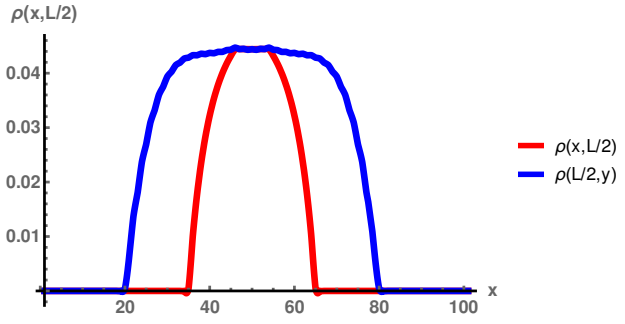

Figure 6.8: This is the density profile of the networks through the centre of the cell for $h_0 = 0$, $\kappa = 100$, $\ell_p/L = 1.2$, $z_0 = 0.5$ *and* $\zeta_0 = 0.06$.

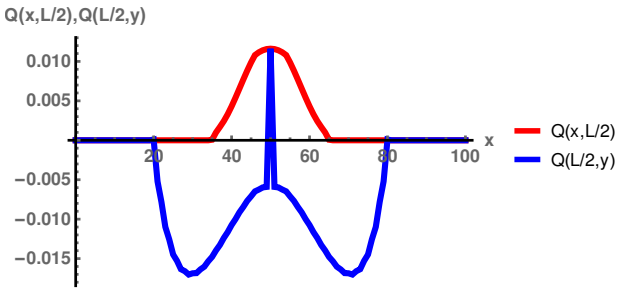

Figure 6.9: Order field of the networks for $h_0 = 0$, $\kappa = 100$, $\ell_p/L = 1.2$, $z_0 = 0.5$ *and* $\zeta_0 = 0.06$.

6.3.2 Confined network structure and cell membrane elasticity

We investigate here the relationship between the structural and elastic properties of the cells. We have density and the order parameter fields through the middle of the cell for different values of h_0 at fixed $\kappa = 100$, $\ell_p/L = 1.2$, $z_0 = 0.5$ and $\zeta_0 = 0.06$. The profiles allow predictions of how the networks structure and architecture couple with the cell membrane elasticity to lead to the emergent mechanical properties of tissue cells. The filaments grows inside cell that have a rectangular shape. Figure 6.8 to Figure 6.19 shows the structure of the networks and

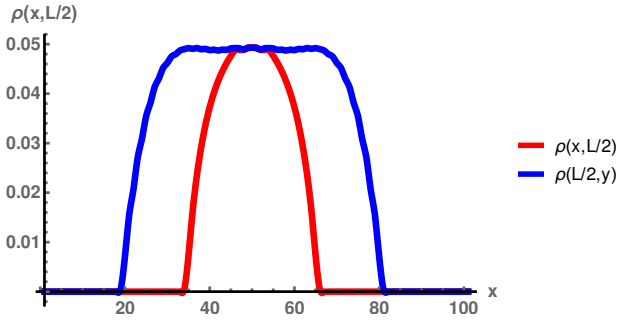

Figure 6.10: density profile of the networks for $h_0 = 1$, $\kappa = 100$, $\ell_p/L = 1.2$, $z_0 = 0.5$ *and* $\zeta_0 = 0.06$.

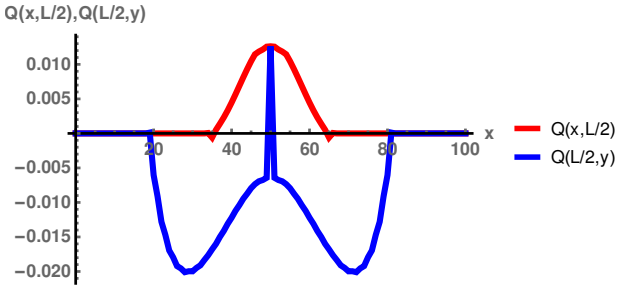

Figure 6.11: Order field of the networks for $h_0 = 1$, $\kappa = 100$, $\ell_p/L = 1.2$, $z_0 = 0.5$ *and* $\zeta_0 = 0.06$.

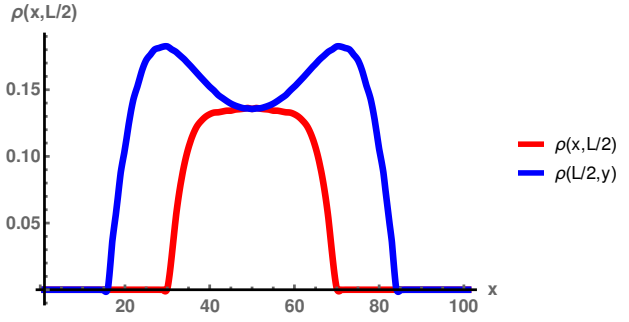

Figure 6.12: density profile of the networks for $h_0 = 5$, $\kappa = 100$, $\ell_p/L = 1.2$, $z_0 = 0.5$ *and* $\zeta_0 = 0.06$.

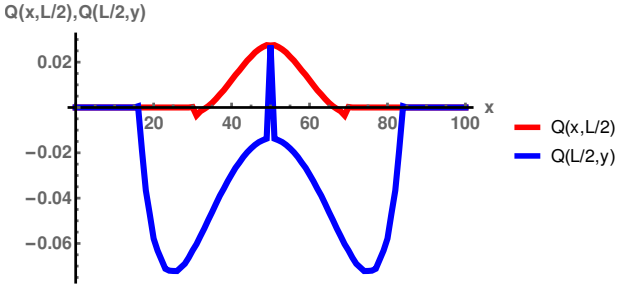

Figure 6.13: Order field of the networks for $h_0 = 5$, $\kappa = 100$, $\ell_p/L = 1.2$, $z_0 = 0.5$ *and* $\zeta_0 = 0.06$.

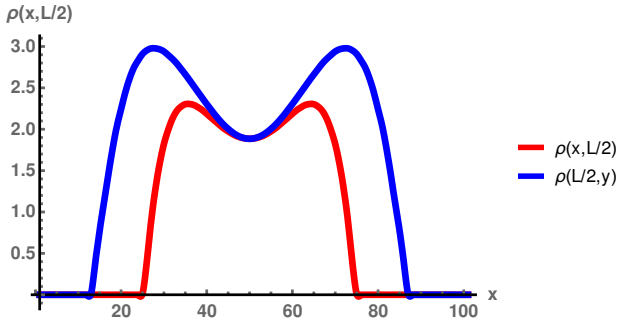

Figure 6.14: density profile of the networks for $h_0 = 10$, $\kappa = 100$, $\ell_p/L = 1.2$, $z_0 = 0.5$ *and* $\zeta_0 = 0.06$.

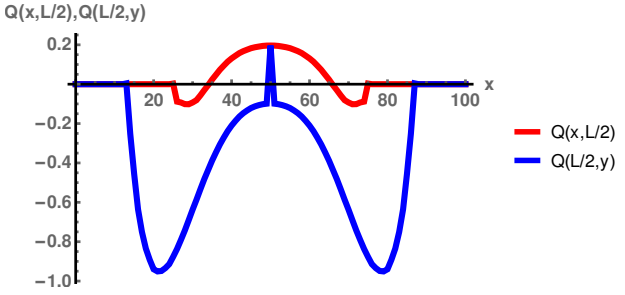

Figure 6.15: Order field of the networks for $h_0 = 10$, $\kappa = 100$, $\ell_p/L = 1.2$, $z_0 = 0.5$ *and* $\zeta_0 = 0.06$.

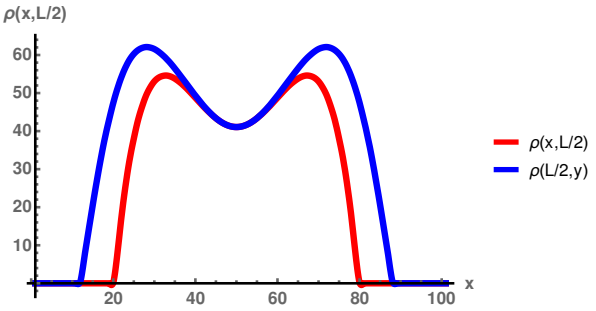

Figure 6.16: density profile of the networks for $h_0 = 15$, $\kappa = 100$, $\ell_p/L = 1.2$, $z_0 = 0.5$ *and* $\zeta_0 = 0.06$.

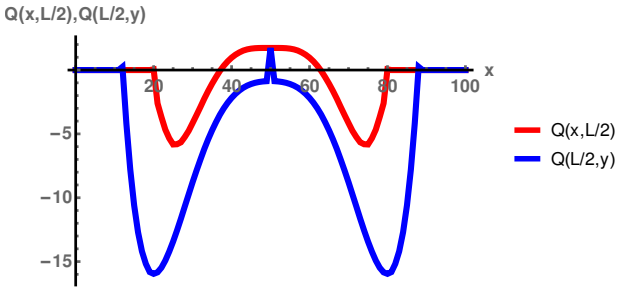

Figure 6.17: Order field of the networks for $h_0 = 15$, $\kappa = 100$, $\ell_p/L = 1.2$, $z_0 = 0.5$ *and* $\zeta_0 = 0.06$.

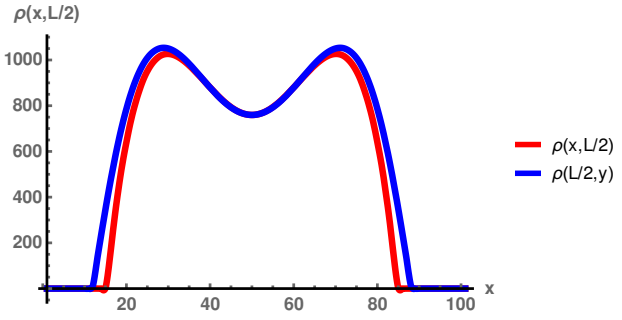

Figure 6.18: density profile of the networks for $h_0 = 20$, $\kappa = 100$, $\ell_p/L = 1.2$, $z_0 = 0.5$ *and* $\zeta_0 = 0.06$.

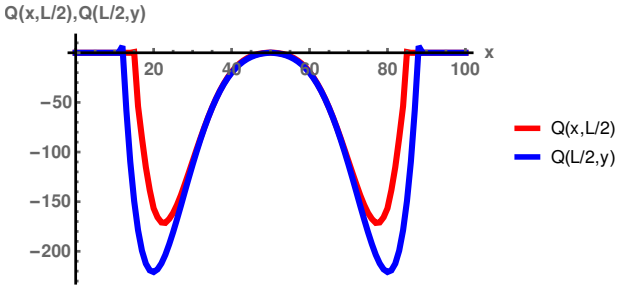

Figure 6.19: Order field of the networks for $h_0 = 20$, $\kappa = 100$, $\ell_p/L = 1.2$, $z_0 = 0.5$ *and* $\zeta_0 = 0.06$.

the alignment of the network filament segments relative to the cell walls.

For small h_0, we observe a network dominated by linear filaments with high anisotropy in the middle of the cell meaning the order parameter field profiles through the centre (in x and y directions) are non-zero in the middle of the cell. This may be due to the non assymmetry of the rectangular shape.

The order profile through the middle in the y direction shows that the filament align perpendicular to the cell membrane in the y direction while the order parameter through the middle in x direction shows that filaments align parallel to the cell wall in x direction. We observe also a higher density of filament segments along y direction with slight homogeneity in the density distribution. This may be explained by the fact that the long filament that are formed seek to align along the longer directions of the confining region in order to minimize the system free energy.

We observe that, as we increase the amplitude of the curvature h_0, the cell becomes more symmetric. The filaments then grow and is highly branched at the cell periphery while isotropic near the centre of the cell. The inhomogeneous density profile that we have obtained shows this observation.

So the order and the density profiles plotted above give us informations about the interplay between the filament architecture and structure and the cell membrane elasticity. The cell

membrane elasticity favour the branching inducing changes in the structure and architecture of the filaments of the networks. The change in the structure and architecture of the networks in turn allows the cell to change or to take a desired shape. However the stiffness of the cell membrane allows the cell to always keep its size finite.

As predicted previously, the orientation of network segments is induced by the confinement effect that the cell membrane introduce. Results show a strong competition between the stiffness of the branched networks and the cell membrane stiffness even in the case of cell with rigid membrane. It is thus important to study the stability of tissue cells with semiflexible membrane against compression and it is the content of our next subsection.

6.3.3 Stability of cell with elastic membrane in the tissues against compression

We consider a tissue or a collection of cells and we want to study the stability of a cell and their confined branching networks against compressive forces. Examples of epithelial tissue under external load show that the tissue may locally respond to the load by either expanding (stretching) or shrinking (compression) or both at the same time. Each cell of the tissue thus contributes to the tissue mechanical behaviour.
For the cell to respond to the mechanical cue or to move, actin monomers under the action of the Arp2/3 protein complex, form orientationally ordered and branched structures at the cell periphery. Are these networks and their confining cells stable against compression within the tissue?
We study two cases of elastic deformation of the tissue cell due to compression.

6.3.3.1 Case 1: tissue cells bulging in opposite directions along x axis

In this case, we consider a very simple example of a collection of cells in which some cells grows against their neighbour cells forming a sheet or tissue of alternating expanded-compressed cells. We want to check wheter such deformation is stable with respect to neighbouring cells.

We consider Figure 6.20 A)and we introduce perturbations which leads cells to bend in x directions and then get a convex shape, as shown by Figure 6.20 C). Figures 6.21 to Figure 6.24 are respectively the shapes and density profiles of the stretched and the compressed cell.

We calculate numerically the Gibbs free energy as a function the amplitude h_0 of the membrane curvature and the plot is presented is Figure 6.25. The increase in the Gibbs free energy shows that in the present case of study, the system is stable against compression or stretching. Are tissues cells still stable is they are all compressed in the same direction?

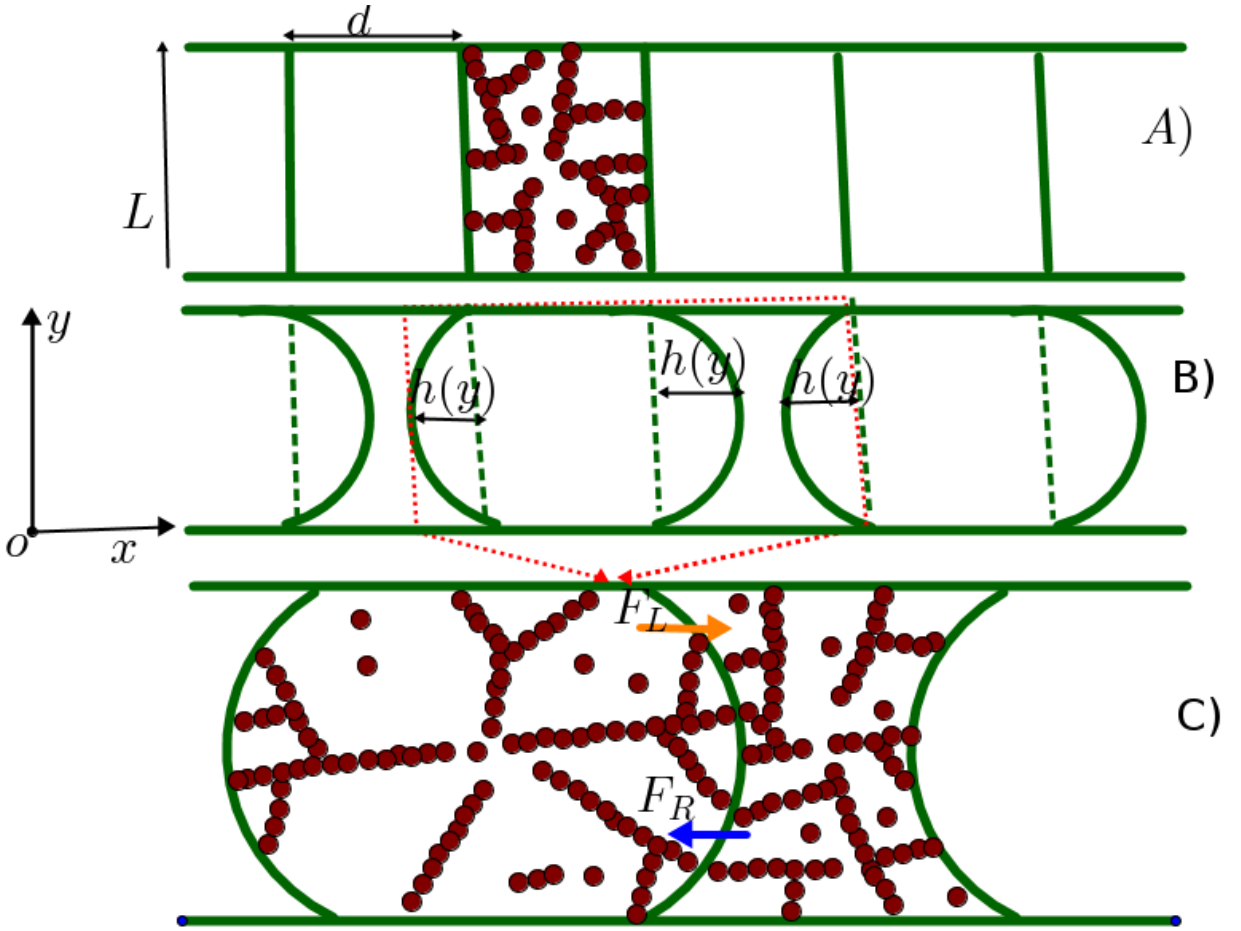

Figure 6.20: Tissue cells confining branching cytoskelatal networks: A) in unperturbed state, B) in perturbed state causing the membranes to bent in the two opposit directions of x about $h(y)$ leading to the increase of the size of a cell against its neighbour, C) Two neighbouring deformed cells: stretched cell and compressed cell

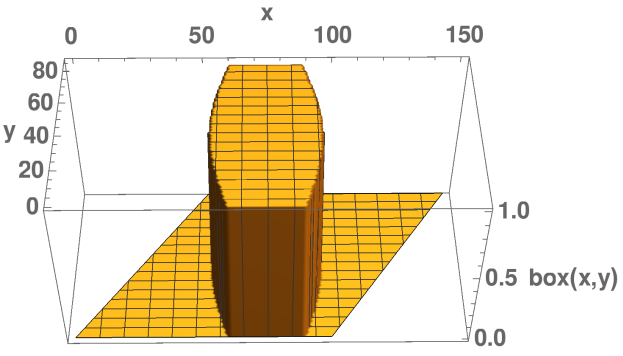

Figure 6.21: Shape of the cell with no network or chains.

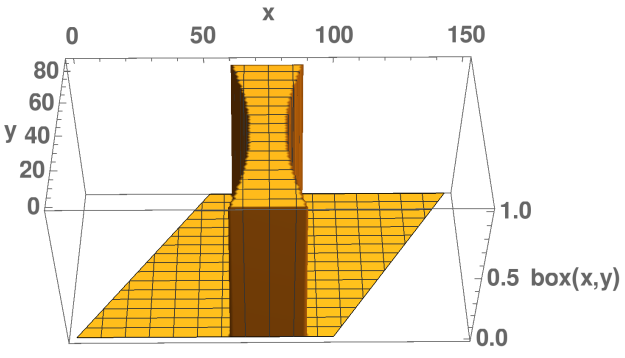

Figure 6.22: Shape of the compressed cell with no chains, the cell is compressed by neighbour cells leading it to take a concave shape.

6.3.3.2 Case 2: tissue cells bulging in the same direction along x axis

Here, all the cells of the tissue are deformed or bent in the same direction. Figure 6.26 is a cartoon of deformation of cell or a collection of cells or tissue and Figure 6.27 and Figure 6.28

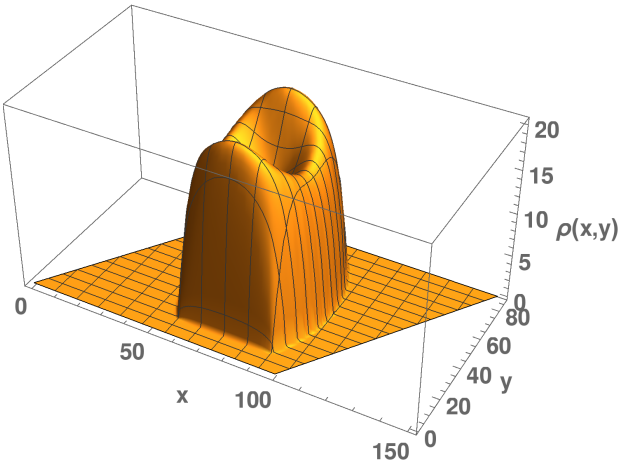

Figure 6.23: Profile in the presence of filaments in the convex cell. The graph is a three dimensional representation of the density profile of the convex cell.

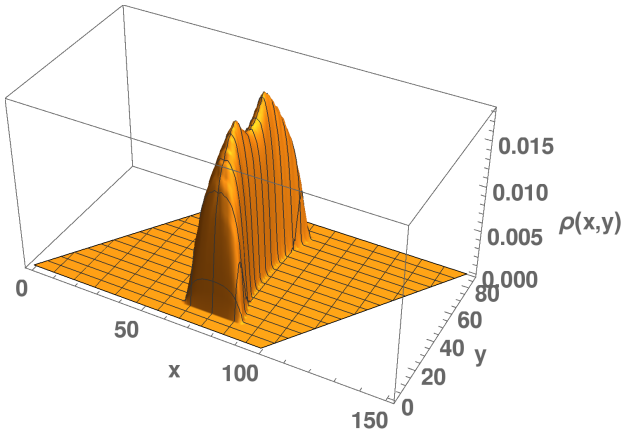

Figure 6.24: The graph is obtained for a concave cell in the presence of filaments inside the cell. It is a three dimensional representation of the average density profile of segments.

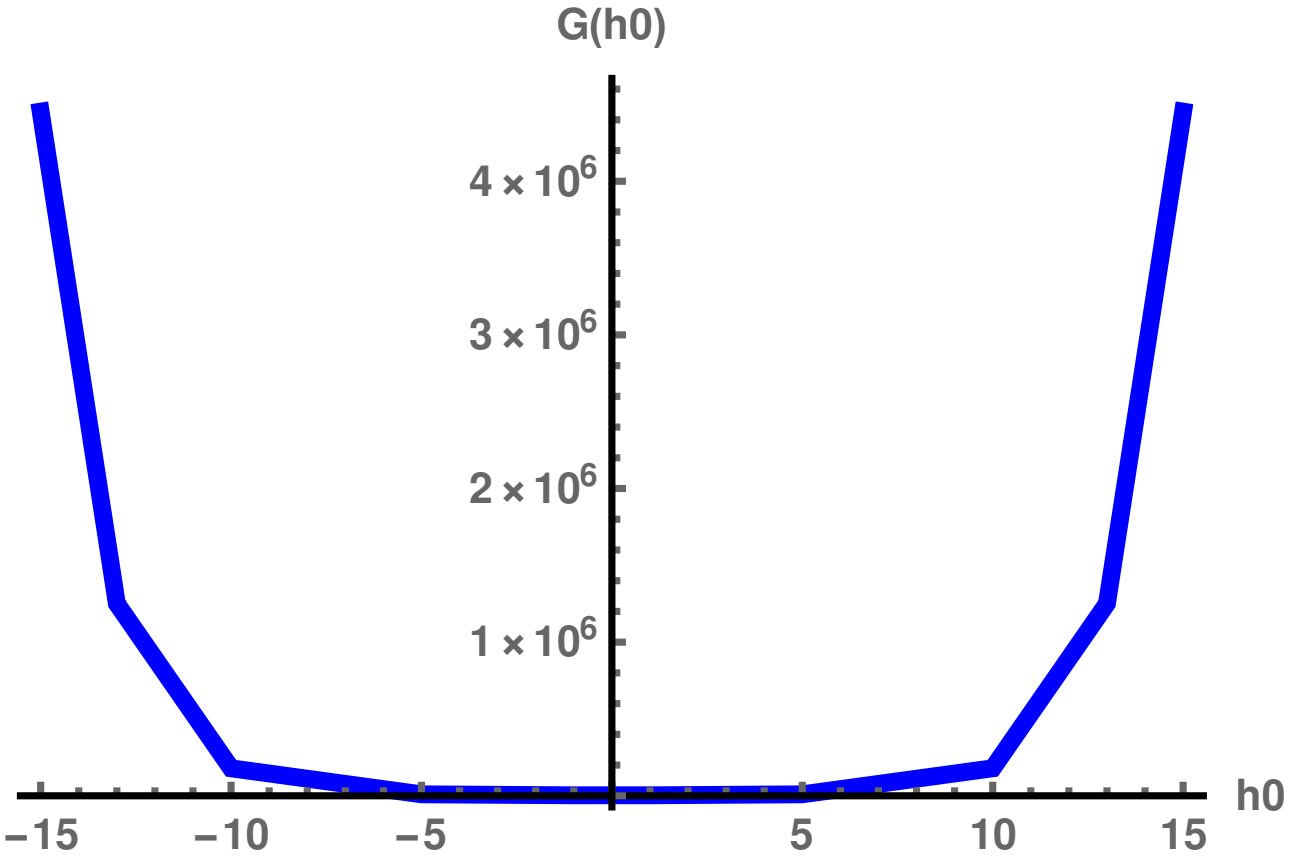

Figure 6.25: Graph of the Gibbs free energy as a function of the amplitude of the bending curvature. The graph shows an increase of the free energy as we increase the perturbation. So this type of deformation applied to of cell confining the branching networks does not impact on the stability of the cell and their networks within the tissue. Here $\ell_p/L = 1.2$, $z_0 = 0.5$ and $\zeta_0 = 0.06$, $\kappa = 100$

shows respectively the profile of the deformed cell and the density profile of filaments segment distribution in tree dimensional representation.

We numerically compute the Gibbs free energy of the system and plot it as function of the amplitude of the perturbation, Figure 6.29. The total Gibbs free energy is the sum of the free energy from all cells of the tissue.

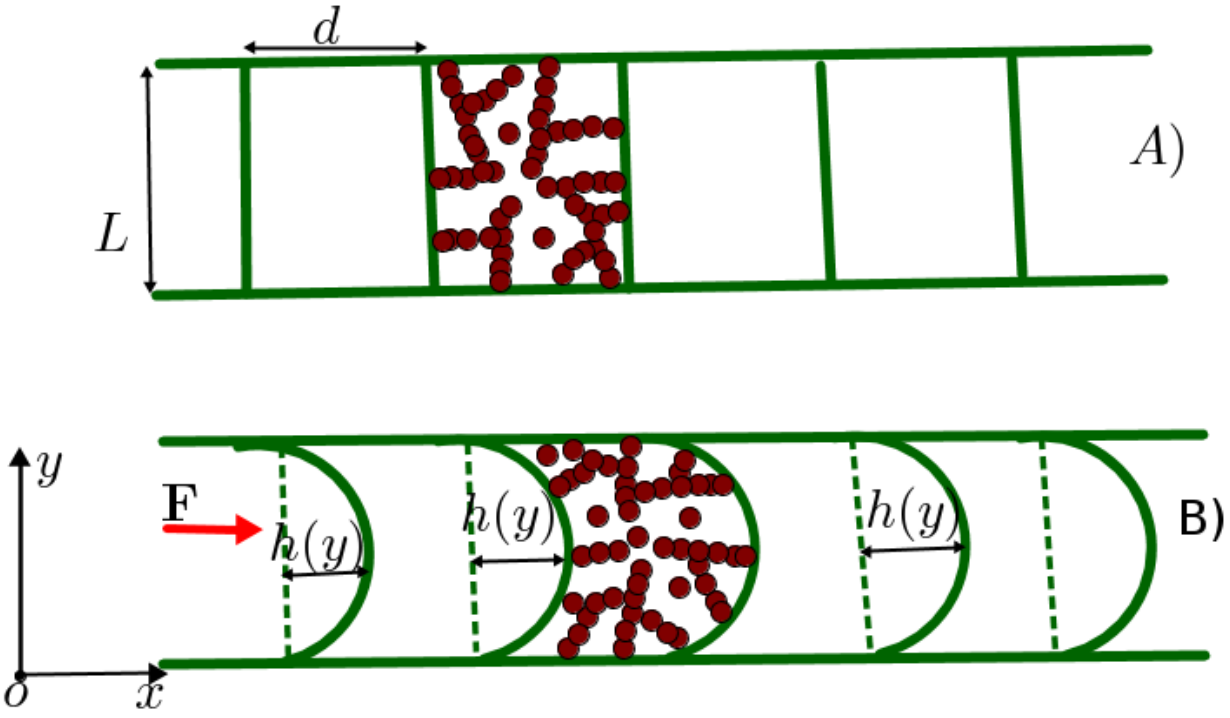

Figure 6.26: Depiction of a collection of cells in which branching cytoskelatal filament network is confined: A) unperturbed state, B) Cell are bent in the same direction under a compressive force.

We have observed in both studied cases that the deformations applied to the confining cells of the collection of cells are not influenced by the cells stability. We thus can conclude that our theoretical model suggest the stabity for tissue cells against compression.

In the next part we are concerned about the pressure balance and the forces that the networks and the cell membranes contribute in order to ensure the stability of tissue cells under compression.
So, in this part we determine the pressure balance between two neighbouring cells of a tissue for the two cases studied above. We also measure the difference in force between two deformed cells of the tissue as function of the amplitude of the membrane curvature $h(y)$, for a given fixed bending modulus of the membrane. We finish with the young modulus of the networks which we calculate as function of the networks stiffness parameter ζ (which increase increases the degree of branching).

density profiles.pdf

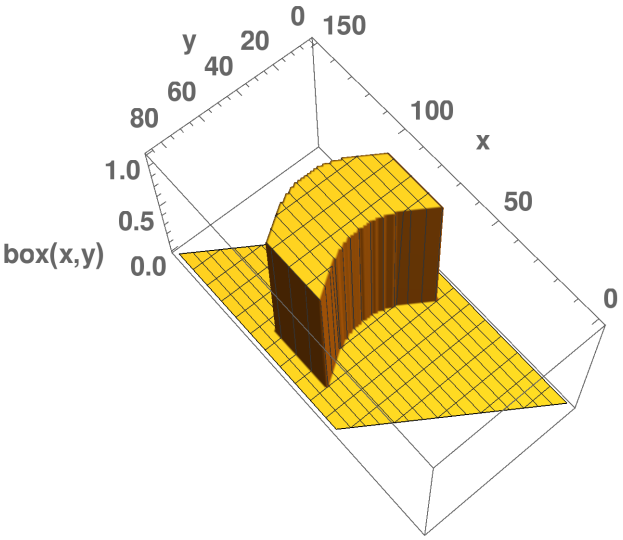

Figure 6.27: The bent cell shape with no chains.

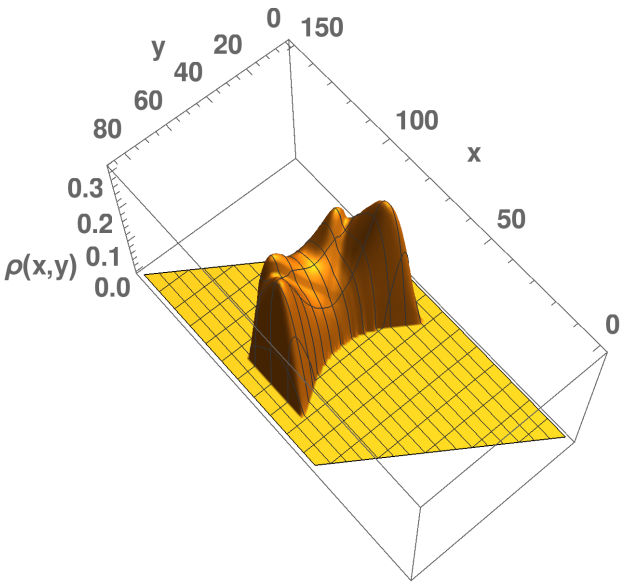

Figure 6.28: The density profile in three dimensional representation for $\ell_p/L = 1.2$, $z_0 = 0.5$ and $\zeta_0 = 0.06$, $\kappa = 100$

6.3.4 Forces and pressure balance

We investigate how confined branched networks and the cell membrane contribute to control the elastic properties of the cells in order for it to keep its size finite.
In order to get this information, we measure the pressure and force balance between two cells confining the branched cytoskeletal networks of the tissue under compression, see depiction in C) of Figure 6.20, where one cell is under compression force (right cell) and the other under stretching force (left cell). The system parameter values are chosen here for the numerical calculation to be: $\ell_p/L = 1.2$, $z_0 = 0.5$ and $\zeta_0 = 0.06$, $\kappa = 100$.

6.3.4.1 Case 1

The total areas A_{sc} and A_{cc} for respectively the stretched (convex shape) and compressed cells (concave) 6.20 are:

$$A_{sc} = L\left(d + 4\frac{h_0}{\pi}\right) \tag{6.20}$$

and

$$A_{cc} = L\left(d - 4\frac{h_0}{\pi}\right) \tag{6.21}$$

The pressures excerted in each of them is given by:

$$P_{sc}(h) = \langle P_L \rangle = \frac{k_B T \ln(\mathfrak{Z}(d + h(y)))}{L(d + 4\frac{h_0}{\pi})} \tag{6.22}$$

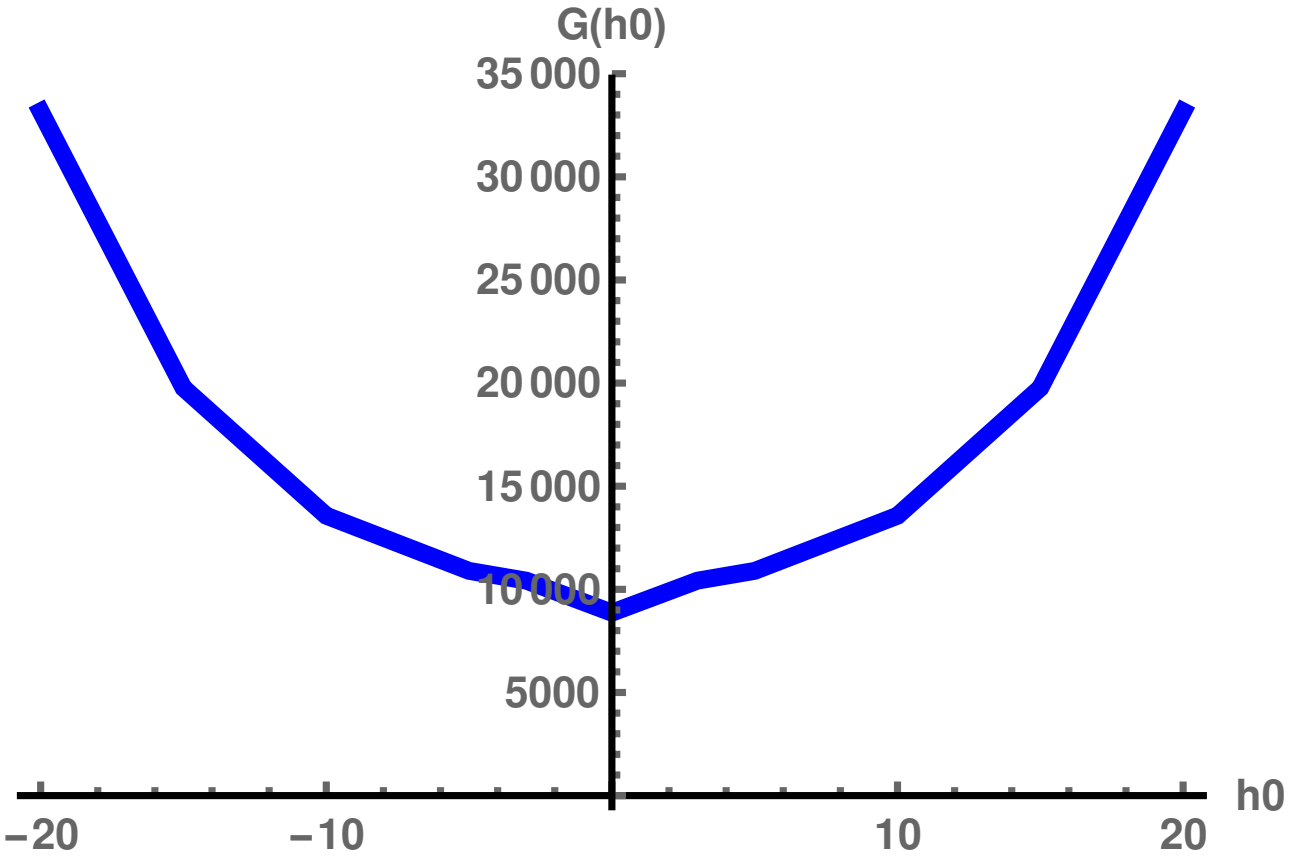

Figure 6.29: We plot the Gibbs free energy of the system of tissue cell bent or deformed in the same direction as function of the amplitude of the bending curvature. The graph shows that the cells are stable against the type of deformation. This calculation is obtained for $\ell_p/L = 1.2$, $z_0 = 0.5$ and $\zeta_0 = 0.06$, $\kappa = 100$

and

$$P_{cc}(h) = \langle P_R \rangle = \frac{k_B T \ln(\mathfrak{Z}(d - h(y)))}{L(d - 4\frac{h_0}{\pi})} \tag{6.23}$$

The difference in force is given by:

$$DF(\delta h) = L(P_{sc} - P_{cc}) \tag{6.24}$$

We observed that there is a mechanical balance between the stretched and compressed cell. We predict that, for a tissue under external compressive and stretching forces, branching cytoskeletal networks and the cell membrane via their elasticity allows the compressed cells to push against the stretched cell in order for the cells to keep their elastic stability. This suggests that the pressure excerted and thus the elasticity of the branching networks matches the cell membrane stiffness and this allows the cell to keep its elastic equilibrium which is very important to keep the cell's mechanical integrity. Our results is in aggrement with the previous studies on the matter [139]

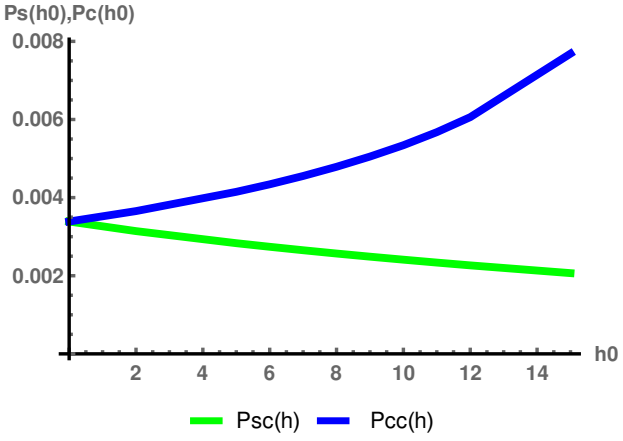

Figure 6.30: The graphs of pressure in the stretched cell P_{sc} and P_{cc} the pressure in the compressed cell. We obseve that, while the pressure is decreasing inside the stretched cell, it is highly increasing inside the compressed. This ensure the elastic stability of cells under compression with the tissue.

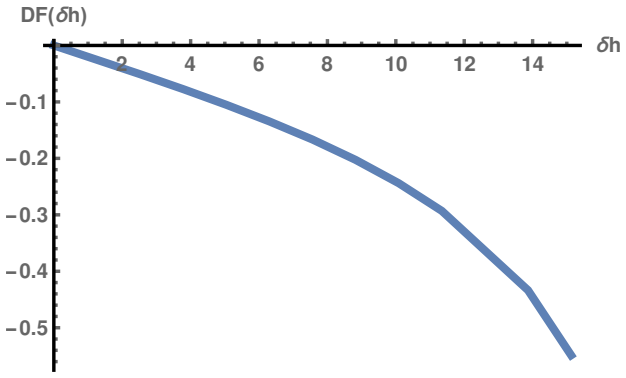

Figure 6.31: Difference in force between the compressed and stretched cell as function of h. It becomes non linear as the membrane curvature increases. The non affine response of the networks due to the effect of the membrane elasticity with. However, the compressed networks exhibit an elastic spring-like behaviour.

6.3.4.2 Case 2 (6.26)

Here we compute numerically the pressure exerted by a system of tissue cells that is deformed by all bending in the same direction. The cell are of the same size and this type of deformation have no change in the area of the cell. The average pressure $\langle P_{total} \rangle$, here is given by the sum of pressure from each cell of the collection. For a number N of cells, since cells are of the same size $(A = L * d)$, P is given by

$$P(h) = \langle P_{total} \rangle = N k_B T \frac{\ln(\mathfrak{Z}(d + h(y)))}{A} \tag{6.25}$$

We plot the pressure as function of the bending amplitude, Figure 6.32. We observe that as the amplitude of the deformation increases, the total pressure of the system decreases. This result may be explained by a low contribution of both the networks and the cell membranes to the system energy as the deformation amplitude increases. In our understanding this will avoid tissue cells to bulge indefinitely and get out of equilibrium since the deformation favor the filaments growth and branching only in one direction.

We are not sure why the pressure in Figure 6.32 6.32 decreases (slightly), and we guest it requires further investigation to understand this.

To achieve this study of the elastic properties of tissue cells and their confined networks under compression, we calculate the Young modulus of the networks.

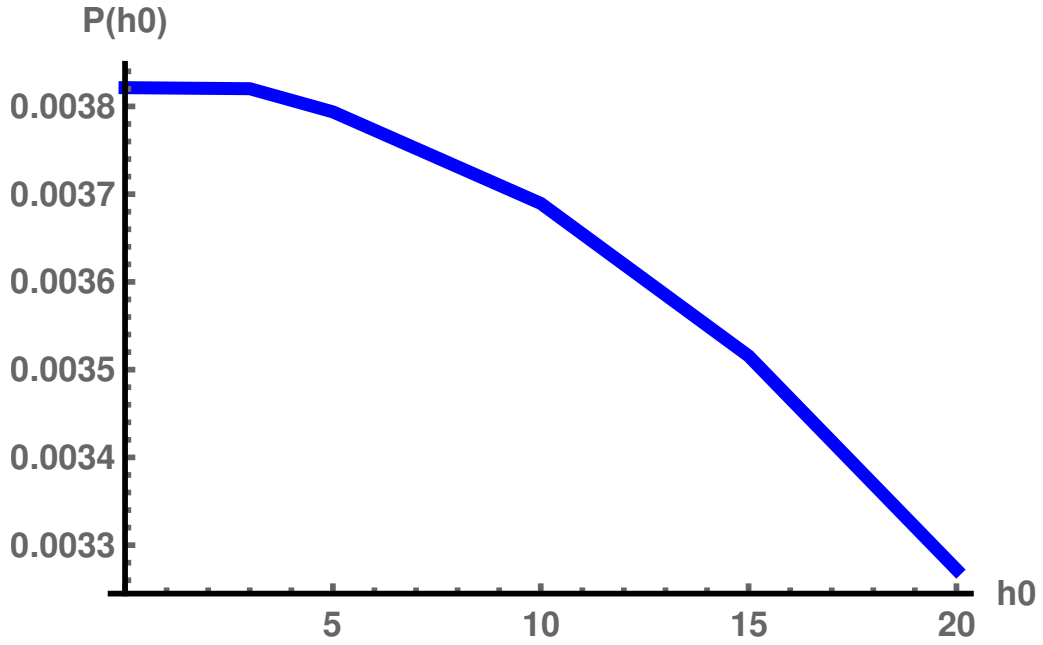

Figure 6.32: Total pressure exerted by a collection of N cells deformed in the same direction. The pressure decreases as the curvature of the bending amplitude increases. This can be explained by the fact that the bending of the cells in the same direction favour the network growth and branching in the direction which may lead to a non reversible deformation of the tissue. The decrease in system free energy thus pressure allows the tissue cells and their tissues to keep a finite size or shape.

6.3.5 The Young modulus of the networks

We have calculated numerically the young modulus of the netorks under compression and we plot it on Figure 6.33 As the stiffness of the networks increases, the Young modulus of the networks also increases in order to allow the cell to resist to large stretching or compression. These results are very important and enable one to have and idea of what the confined cytoskeletal networks contribute to the elasticity of cells and their tissues.

6.4 Are our tissue cells stable against shear?

Here we investigate on the stability of the tissue cell confining branching actin networks against shear. Can we indefinitely shear eukaryotic cells within a tissue?

To answer this question we model the shearing of a cell with square shape and rigid wall confining the branching cytoskeletal networks. Figure 6.34 shows a cartoon of tissue cell under shear deformation.

Graphs from Figure 6.35 to Figure 6.38 present, respectively, the profiles of the square shape cell in unperturbed state versus the shape of the cell under shear and the filaments segments density profiles inside non sheared cell versus sheared cell. The profiles of the density are obtained for $\ell_p/L = 1.2$, $z_0 = 0.5$ and $\zeta_0 = 0.06$. We first measure the free energy of a system of sheared cell numerically as function of the shear angle and then we do analytical calculations

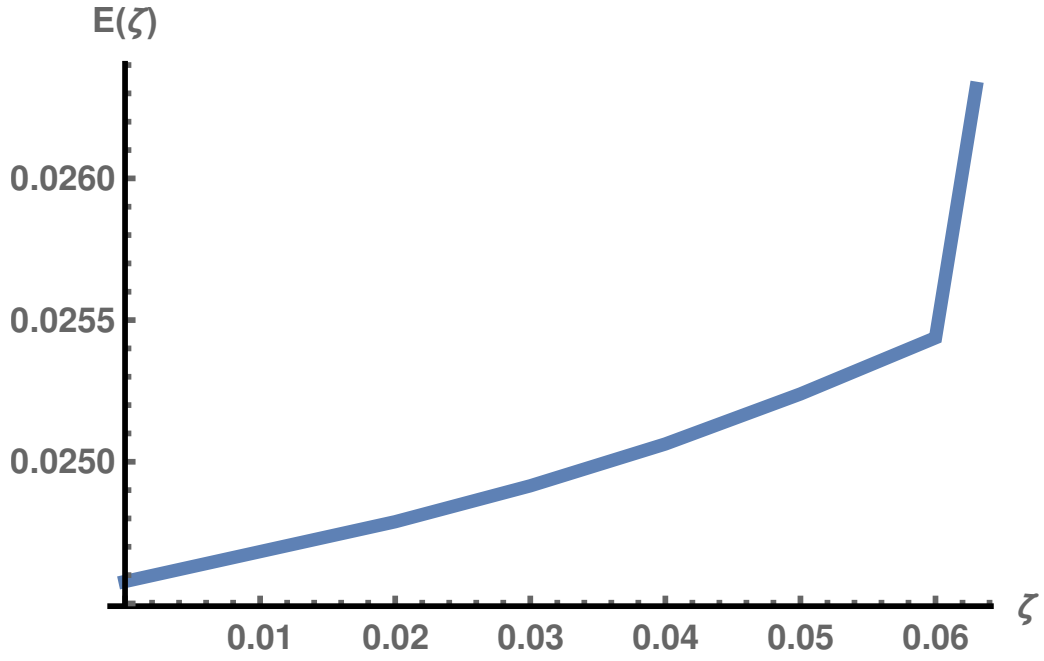

Figure 6.33: Graph of the Young modulus of the network system (Figure 6.20 C)). The graph shows a slow variation of the the Young modulus for the degree of branching parameter ζ between 0 and 0.06. Beyong $\zeta = 0.06$ the Young modulus increases strongly and non affinely , suggesting that beyond this value there is an excess branching of filaments making the networks very stiff. So this strong increase come from the increase of the networks stiffness. And beyond $\zeta = 0.063$ there is a failure in our networks system, leading to divergence of our model. The non affine increase of the Young modulus may be due to the elastic behaviour of the cell membrane.

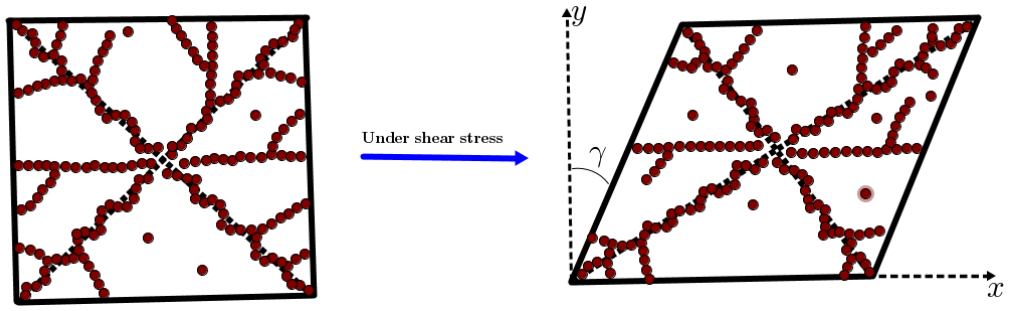

Figure 6.34: Depiction of the confined branching cytoskeletal networks inside square cell under shear strain

to understand our findings better.

6.4.1 numerical results

We compute numerically the Gibbs free energy for two different confining geometry of cells under shear: we model a 2d networks confined in a cell with square shape and a 2d networks in a cell with rectangular shape. The reason for modelling the networks in different geometry is that we want to make sure that the geometry of the cell does not influence the result that we obtain.

We plot the free energy for both square and the rectangular cells under shear. The following

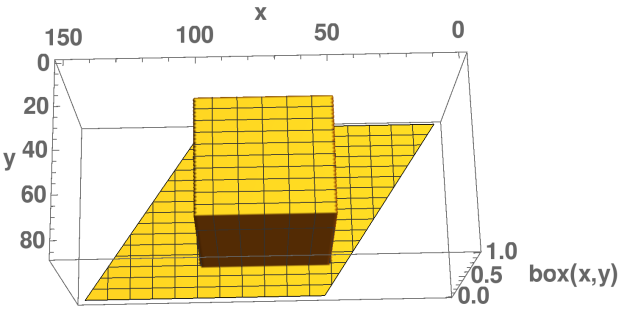

Figure 6.35: Profile of the non deformed square cell with no chains

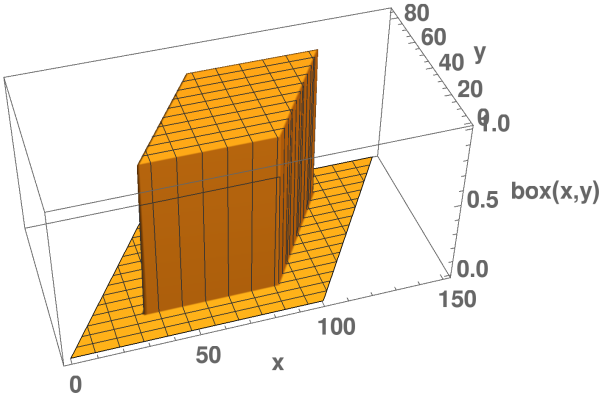

Figure 6.36: Profile of the shear square cell (rhombus cell) with no chains

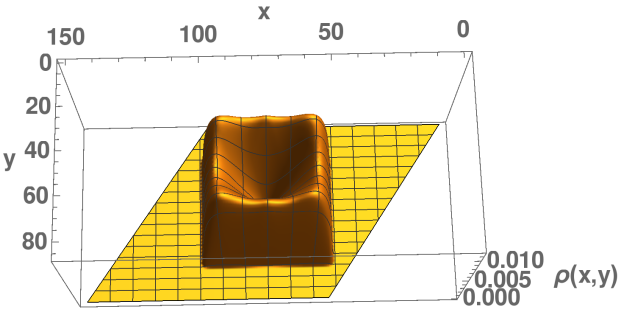

Figure 6.37: Three dimensional-representation or plot of the density profile of filament segments confined in square cell, $\ell_p/L = 1.2$, $z_0 = 0.5$ and $\zeta_0 = 0.06$.

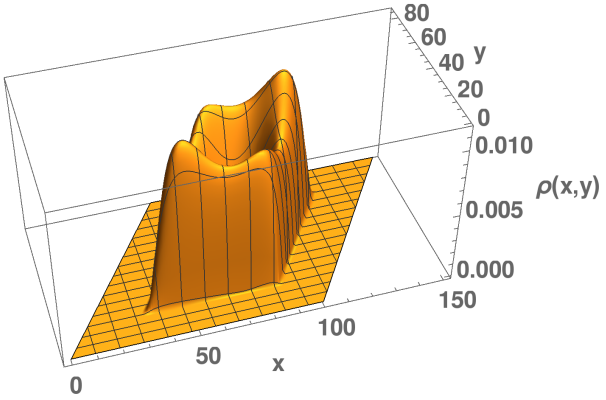

Figure 6.38: Three-dimensional representation of the density profile of filament segments confined in square cell under shear, $\ell_p/L = 1.2$, $z_0 = 0.5$ and $\zeta_0 = 0.06$.

graphs in Figure 6.39 are plot of the free energy for sheared square and sheared rectangular cells that we have obtained from our numerical calculations.

This result suggest that eukaryotic cells are stable again shear up to a critical shear strain or angle of about $\pi/6$. Above this value of the strain, we observe the instability in the cell mechanical response. We wish to understand the origin of the instability around this point. So we choose to plot the density and order field profile of filament segments along the diagonals of the cell with square shape in order to explore the stucture and spatial arrangement of the filaments as one shears the cell.

The plot of Figure 6.40 and Figure 6.41 allows us to predict that as we shear the cell filaments prefer to occupy the longer diagonal and the remaining along the short diagonal bend in order to minimize the system free energy.

To confirm our predictions, we do analytical calculations in the following part and compare

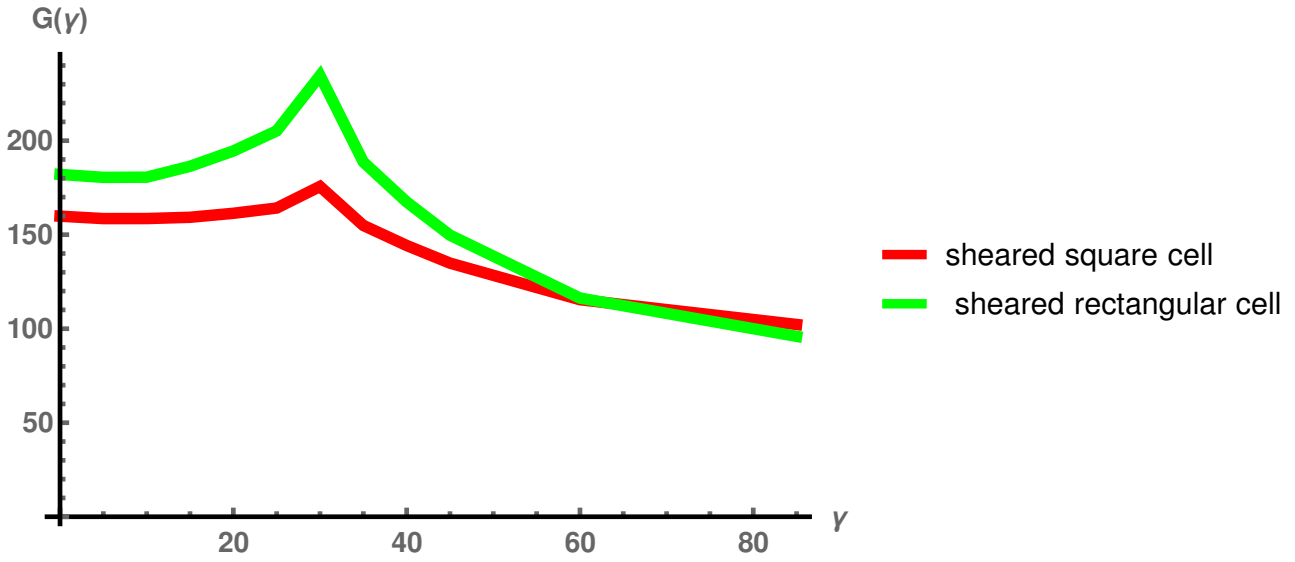

Figure 6.39: Graph of the free energy from numerical calculations for $\ell_p/L = 1.2$, $\ell_p/d = 1.4$ for square and rectangular cell, $z_0 = 0.5$ and $\zeta_0 = 0.06$. As the shear strain increases, the free energy show the stability of the confined actin networks up to a value of strain of $\pi/6$. It means that there exists a transition between the stability and the instability of the cell at shear angle $\pi/6$

it with the numerical result. We wish to calculate analytically the critical shear angle above which the semi-flexible filament networks under confinement become unstable .

6.4.2 Analytical model and calculation of the free energy of confined semiflexible polymer filaments under shear

To start, we consider a semi-flexible filament of length L_c pinned at both ends by compressive forces, Figure 6.42.

We use the Kratky and Porod model for semi-flexible filament called worm-like chain to model the chain. It is a continuum model in which the polymer chain is parametrised by a space curve $\boldsymbol{r}(s)$. The Hamiltonian of the system of the chain is given by:

$$H[\boldsymbol{r}(s)] = \frac{k_b}{2}\int_0^{L_c} \mathrm{d}s \left(\frac{\mathrm{d}^2\boldsymbol{r}(s)}{\mathrm{d}s^2}\right)^2. \tag{6.26}$$

where k_b is the bending modulus of the filament.

To calculate the free energy of the system, we need to calculate the constrained partition function. The constrained partition function is the probability that the ends of the filament of contour length L_c is separated by the vector $\boldsymbol{R} = \boldsymbol{r}(L_c) - \boldsymbol{r}(0)$. Under a compression force at the end of the filament, the filament can deform and take various configurations. We define here the partition function associated to the configuration in which the end-to-end distance of the filament is equal to x where $x = \boldsymbol{R}/L_c$.

$$Z = \mathcal{N}\int \mathcal{D}\boldsymbol{r} e^{-\beta H[\boldsymbol{r}]}. \tag{6.27}$$

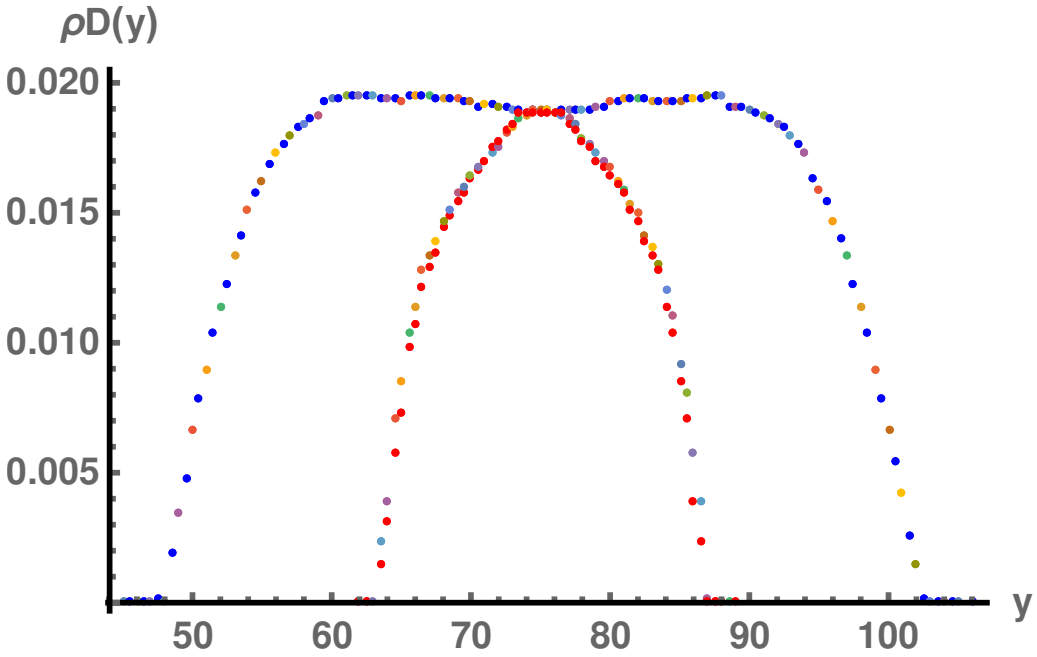

Figure 6.40: we plot the profile of the average density of segments along the long diagonal versus short diagonal of the sheared square cell for $\ell_p/L = 1.2$, $z_0 = 0.5$ and $\zeta_0 = 0.06$. The graph in blue respectively red dots are the profiles of the segments density distribution along the long diagonal respectively the short diagonal. We see an heterogeneous and high density of filament segments along the longer diagonals while the segment density is low along the shorter diagonals. filaments are more dense close to the cell wall due to the filaments branching

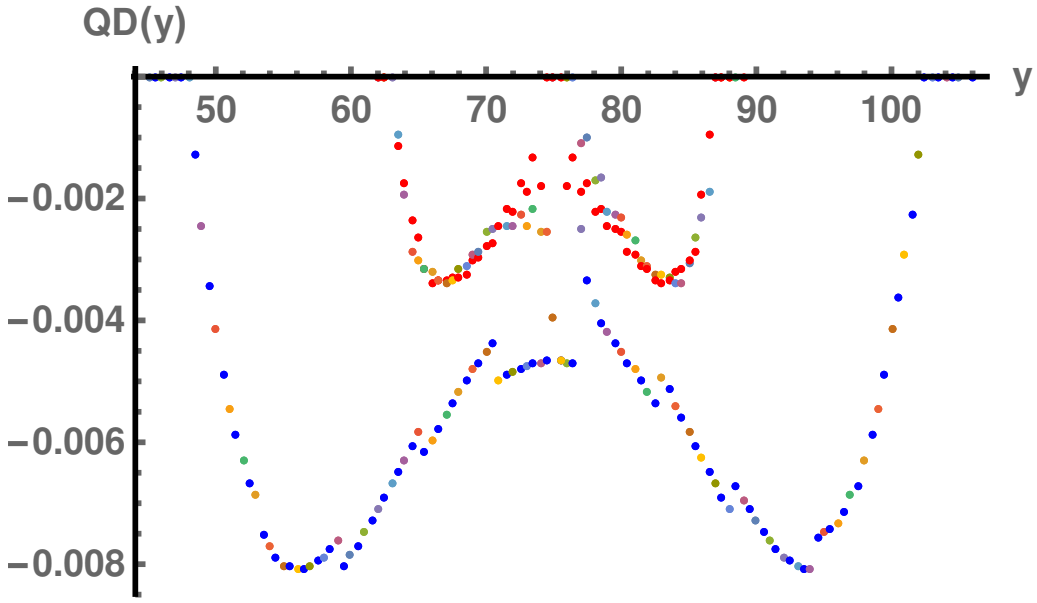

Figure 6.41: The graph in blue respectively red are order parameter field profiles along the long respectively short diagonal. The order profiles show that filament branches and point perpendicular to the cell wall.

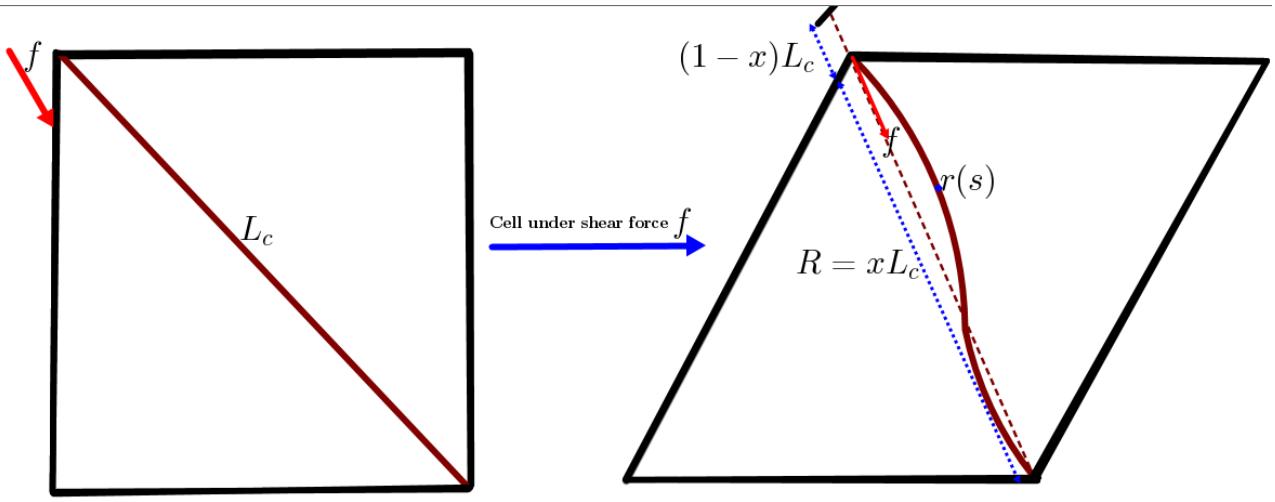

Figure 6.42: Depiction of semiflexible filament pinned at both ends along the diagonal of sheared square by compressive force due to the applied shear force f, L_c is the contour length of the chain

Where $\mathcal{N}$ is the normalization factor and $\beta = 1/k_B T$.

To calculate this partition function and get interesting physics that we want, we need to consider the constraint of filament rigid local inextensibility:

$$\left(\frac{\mathrm{d}\boldsymbol{r}(s)}{\mathrm{d}s}\right)^2 = 1. \tag{6.28}$$

and the constraint that the filament is in the configurations where the space-curve start at 0 and end at x:

$$x = \frac{\boldsymbol{r}(L_c) - \boldsymbol{r}(0)}{L_c}. \tag{6.29}$$

which serve as boundary conditions. The local in-extensibility approach defined above make the integral in equation (7.63) hard to solve. To simplify this integral in order to make it analytically tractable, we use a mean field approach that consist of converting the rigid local in-extensibility constraint into global constraint which is:

$$\langle |\mathrm{d}\boldsymbol{r}(s)/\mathrm{d}s| \rangle = 1. \tag{6.30}$$

Z then becomes:

$$Z = \mathcal{N} \int \mathcal{D}\boldsymbol{r} e^{-\beta H[\mathbf{r}]} \delta(\langle (\mathrm{d}\boldsymbol{r}(s)/\mathrm{d}s)^2 \rangle - 1). \tag{6.31}$$

As proved in Ref [140, 141], the partition function depends only on the parameter t given by:

$$t = \frac{\beta k_b (1 - x^2)}{2L_c}. \tag{6.32}$$

so that:

$$Z(t) = \mathcal{N} \int \mathrm{d}\phi e^{\mathrm{i}t\phi} \left(\frac{\sqrt{\mathrm{i}\phi}}{\sin\sqrt{\mathrm{i}\phi}}\right)^{\frac{d}{2}}. \tag{6.33}$$

where ϕ is an auxilliary field.
The integral in 3D is performed numerically and the interpolation gives the partition function Z of the form:

$$Z(t) = e^{-\pi^2 t - \frac{1}{\pi t}} \tag{6.34}$$

This allows then to calculate the free energy F for the system. It is given by:

$$F = k_B T \ln Z(t). \tag{6.35}$$

As function of filament extension, we have in the absence of any compressive force:

$$F(x) = \frac{\beta k_b \pi^2 (1 - x^2)}{2L_c} + \frac{2L_c}{\pi k_b \beta (1 - x^2)} \tag{6.36}$$

The first term in the free energy is the energetic contribution due to the filament bending and the second term is the cotribution from both energetic and entropic effect.
In the presence of a constant compressive force f, this force does the work $fL_c x$ to move the ends of the filament parallel to $\boldsymbol{R}$. This cork contributes to the free energy. So the total free energy is:

$$F(x) = fL_c x + \frac{\beta k_b \pi^2 (1 - x^2)}{2L^c} + \frac{2L}{\pi k_b \beta (1 - x^2)} \tag{6.37}$$

In the case of no compression, the free energy has a unique minimum near the full extension (the filament is unbuckled) and the equilibrium end-to-end length of the filament is at:

$$x_{\mathrm{e}} = \left(1 - \frac{2L_c}{\beta \pi^{3/2} k_b}\right)^{1/2} = \left(1 - \frac{2L_c}{\pi^{3/2} \ell_{\mathrm{p}}}\right)^{1/2} \tag{6.38}$$

where the persitence length of the filament ℓ_{p} is identified to βk_b.
The filament behave like a spring and the effective spring constant k_{eff} corresponding to the curvature of the free energy at x_e is obtained as:

$$k_{\mathrm{eff}} = 4\pi^{5/2} \frac{\ell_{\mathrm{p}}^2}{\beta L_c^4} \left(1 - \frac{2L_c}{\pi^{3/2} \ell_{\mathrm{p}}}\right) \tag{6.39}$$

The obtained effective spring constant tells us that the stiffness of the filament is regulated by the ratio of the persistence length and the contour length (ℓ_{p}/L_c).

In the next subsection we aim to apply the developed analytical model for a networks of semiflexible filaments confined in cell with square shape and which is under shear stress.

6.4.3 Application of the analytical model to confined cytoskeletal networks under shear in the grand canonical ensemble

Assuming that only the longest spanning filaments most likely feel the applied shear strain and then contribute most to the elasticity of the cell, we reduce our network system to a system of two filaments inside the box. And the longest spanning filaments are along the diagonals

of the box. We investigate which filaments contribute to the elasticity of the box under shear according to their length scale compare to the size of the box, Figure 6.43. We combine the

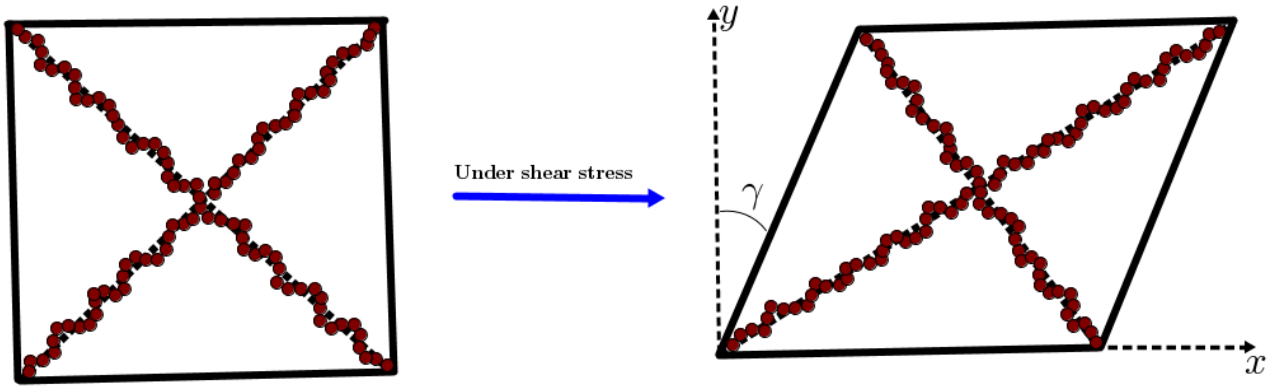

Figure 6.43: Depiction of two semi-flexible filaments confined along the diagonal of a square under shear strain. We model the filaments as springs where each filament has an effective spring coefficient k_{eff}

above results with a certain probability z^N of having the polymer chains with a certain length along the diagonals of the sheared box. z is the fugacity associated to the activity of the bond in the polymer chains and N is the number of bounds in a polymer chain.

We now calculate the contribution to the free energy from each filament as we shear the confining box. We assume that these filaments have a spring-like behaviour when subjected to a strain, with the effective spring coefficient k_{eff} .

Let $N_1 = L_1(\gamma)/\ell$ and $N2 = L_2(\gamma)/\ell$ be respectively the numbers of bonds in the filament along the shorter and longer diagonals as we apply a shear stress to the square box. ℓ is the length of the bond and we choose it to be equal to 1.

$$L_1(\gamma) = d\sqrt{1 - 2\tan\gamma + 1/(\cos\gamma)^2} \tag{6.40}$$

and

$$L_2(\gamma) = d\sqrt{1 + 2\tan\gamma + 1/(\cos\gamma)^2} \tag{6.41}$$

where d is the length of one side of the square box.

The free energy of the system of these two filaments as function of the shear strain γ is given by

$$F(\gamma) = z^{N_1}(F_1(\gamma) + z^{N_2 - N_1}F_2(\gamma)) \tag{6.42}$$

where

$$F_1(\gamma) = z^{N_1}\frac{k_{\text{eff}_1}}{2}(\gamma)(x_1(\gamma) - x_{\text{e}_1}(\gamma))^2 \tag{6.43}$$

and

$$F_2(\gamma) = z^{N_2}\frac{k_{\text{eff}_2}}{2}(\gamma)(x_2(\gamma) - x_{\text{e}_2}(\gamma))^2 \tag{6.44}$$

where $x_1(\gamma) = L_1(\gamma)$ and $x_2(\gamma) = L_2(\gamma)$.

We compute the free energy close to full extension of the filaments ($x = 1$) and we plot the graph Figure 7.2.

We obtain a critical shear angle near $\pi/4$. Beyond this angle the system of semi-flexible filaments along the diagonal are unstable. Comparing the rigidity of both filaments, we argue that as we shear the confining box, the filament along shorter diagonal either bent or loose monomers and become shorter at the same size as the diagonal and thus more rigid , while the filament along longer diagonal continue to grow and become less rigid. So we observe competition between filament growing versus shrinking and bending [54]. So we have these three effects that are contributing to the elasticity of the networks and we predict that the shrinking effect dominates.

The difference between the numerical and analytical near critical angle may be due to the fact that we have considered for our analytical calculations that the free energy of the system is dominated by the energy of the filaments that are along the diagonals of the confining square region.

6.5 Conclusion

In this chapter we have studied the stability confined branching cytoskeletal networks in finite cells and the contribution of these networks on the elastic and structure properties of cells within tissue. We explore the relationship between the cell cytoskeletal networks structures, architecture and their elastic properties and those of the cells. We have focused on the case of tissues cells under compression and cells under shear.
We have obtained that for cells with rigid or elastic membrane, in the presence of compressive forces, the cells and their networks are stable. We have been able to measure the forces exerted by the branching cytoskeletal actin networks and the cell membranes to allows the cells to keep their mechanical equilibrium.
While for the shear, our numerical and analytical calculations showed that the cytoskeletal networks under cellular confinement are not indefinitely stable against shear. The numerical results showed that the instability occur near $\pi/6$ and the analytical calculation give an angle near $\pi/4$ above which the instability occur. We thus deduce that the shear critical angle is situated between angles $\pi/6$ and $\pi/4$.

This study is relevant for improving our understanding of certain physiological and mechanical behaviour of cells and the models we built here can be tested experimentally. This we hope might bring more light in living cell biology and also help in the diagnosis and healing of certain

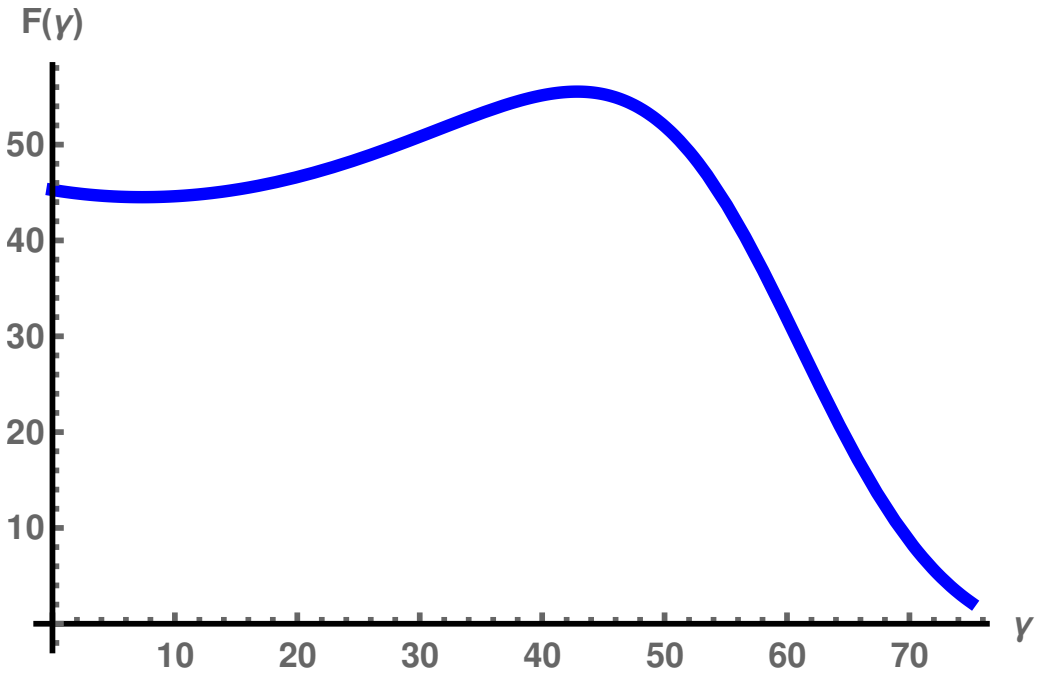

Figure 6.44: Graph of the free energy from analytical calculations. We observe an instability of the system occurring above a shear angle of $\pi/4$.

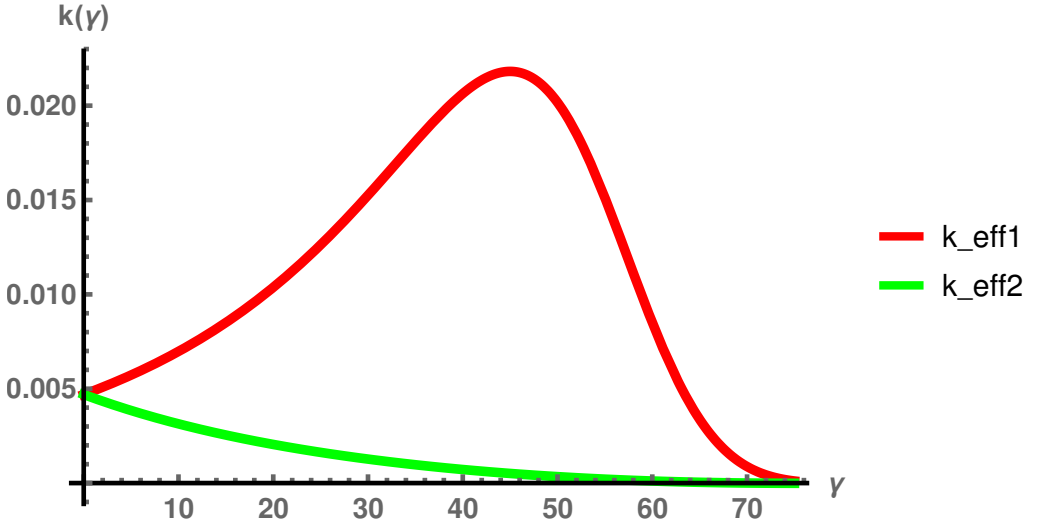

Figure 6.45: Red: effective bending modulus of the filament along the shorter diagonal of the box as function of shear angle. Green: effective bending modulus of the filament along the the longer diagonal of the box as function of shear angle. The graph of the bending rigidities shows that the effective bending rigidity of the filament along the shorter diagonal increases with increasing of the shear strain or shear angle up to a critical angle of $\pi/4$ then start decreasing. While the rigidity of the filament along the longer diagonal decrease with increasing of the shear strain. This implies that the filament along the shorter filament contribute most to the free energy, ensuring thus the stability of the system.

cellular diseases such as cancer whose spreading and formation of metastasis are known to be mainly monitored by the forces that actin cytoskeleton generates [22, 87].

In the chapter that follows, we use an alternative approach to investigate the mechanical or elastic properties of cell comprising branching actin cytoskeletal networks.

Chapter 7

Modelling of cells as a reinforced composite material: an alternative mean field approach

7.1 Introduction

In this chapter, we use an alternative mean field approach to investigate the elastic properties of branching actin networks. We model the living cell and its branching cytoskeletal networks as an elastic composite material. The model is based on the linear theory of disordered fibre-reinforced composites developped by Cates and Edwards [72]. They used the Green function formalism to study some of the physical properties of elastic media reinforced by linear rigid polymer filaments. Their formalism is convenient for our system of study since branching cytoskeletal actin networks are actin are stiff.

In the first section we present their model for a system of linear filaments embbeded in an elastic medium and in the next section we introduce a small modification of the formalism to adapt it to a system of a medium reinforced by stiff star-like branched semiflexible polymer network. The work here though follows Cates and Edwards [72] very closely with only small addition.

7.2 Green function formalism: fibre-fibre and fibre-matrix Interactions

We give in this section a summary of the approach developped by Cates and Edwards [72]. They developed a formalism that enabled them to calculate he effective elastic Green function of an elastic matrix composite in which is embedded the elastic fibres at low volume fraction fibre in the presence of disorder . The behaviour or response of the fibre-matrix system to

an external force **F** is studied. They aim to predict the possible occurrence of de-bonding or fibres breakage in the composites material. Thus the load in the fibres, the shear stress at the fibre-matrix interface, the elastic and bulk moduli have to be determined. To do so a cell model is considered. It consist of a study of a single fibre embedded in the elastic medium Figure 7.2. The effective Green function for the single fibre system is determined.The knowledge of the The effective Green function which characterize the hydrodynamics interactions between fibres and its matrix, permit to evaluate the amount of deformation or displacement of a fibre matrix which is under load and to evaluate the stress induced by the stress fibre in the matrix.The contribution of all fibres is then determined using the total effective green function which also has to be calculated.

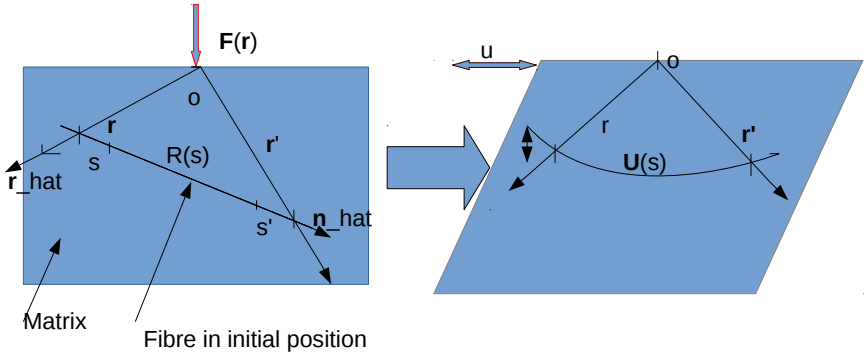

Figure 7.1: *a displacement of a fibre-matrix composite under an external force*

The fibre on Figure 7.2 has a length l, it is taken to be straight i.e with small radius $r_0 \ll l$, a cross section a, s is the length along the fibre. $\mathbf{R}(s)$ is the equilibrium position of the fibre which undergoes a displacement $\mathbf{U}(s)$ $E_f = E_m + E$ its Young modulus, E_m is the Young modulus of the matrix. The matrix is isotropic with shear modulus μ, bulk modulus B and Poisson ratio $\sigma = \frac{3B-2\mu}{6B+2\mu}$, $E_m = 2\mu(1+\sigma)$.

The total displacement or deformation $\mathbf{u}(\mathbf{r})$ of the fibre-matrix when a force distribution $\mathbf{F}(\mathbf{r})$ is applied on the matrix is equal to the sum of displacement of the matrix without fibre and

the displacement when the fibre is present. The deformation $\mathbf{u}(\mathbf{r})$ satisfies the Stokes equation and is:

- In the absence of any fibre in the matrix

$$\mathbf{u}(\mathbf{r}) = \int \mathbf{G}_0(\mathbf{r}-\mathbf{r}')\mathbf{F}(\mathbf{r}')\mathrm{d}^3\mathbf{r}' \tag{7.1}$$

with

$$\mathbf{G}_0(\mathbf{r}) = \frac{1}{16\pi\mu|\mathbf{r}|}\left\{\left(\frac{3-4\sigma}{1-\sigma}\right)\mathbf{I} + \frac{\hat{\mathbf{r}}\hat{\mathbf{r}}}{1-\sigma}\right\} \tag{7.2}$$

the Green function. $\hat{\mathbf{r}}$ is the unit vector along $\mathbf{r}$.
For $E_f > E_m$ there is an extra force $\sigma(s)$ induced by the stress created inside the fire, acting on the matrix defined by:

$$\sigma(s) = \mathbf{\Delta}(s)\mathbf{U}(s) \quad \text{or} \quad \sigma(s) = \mathbf{\Delta}.\mathbf{U} \quad \text{with} \quad \mathbf{\Delta}(s) = -Ea\mathbf{nn}\frac{\partial^2}{\partial s^2} \tag{7.3}$$

where $\mathbf{n}$ is the unit vector along the fibre axis. We have as boundary conditions for a well bonded fibre:

$$\mathbf{u}(\mathbf{R}(s)) = \mathbf{U}(s) \Leftrightarrow \mathbf{U}(s) = \int \delta(\mathbf{R}(s)-\mathbf{r})\mathbf{u}(\mathbf{r})\mathrm{d}^3\mathbf{r} \tag{7.4}$$

- In the presence of any fibre in the matrix, the displacement $\mathbf{u}(\mathbf{r})$ becomes:

$$\mathbf{u}(\mathbf{r}) = \int \mathbf{G}_0(\mathbf{r}-\mathbf{r}')\mathbf{F}(\mathbf{r}')\mathrm{d}^3\mathbf{r}' + \int \mathbf{G}_0(\mathbf{r}-\mathbf{R}(s))\sigma(s)\mathrm{d}s \tag{7.5}$$

which we can rewrite:

$$\mathbf{u}(\mathbf{r}) = \int \mathbf{G}_0(\mathbf{r}\text{-}\mathbf{r}')\mathbf{F}(\mathbf{r}')\mathrm{d}^3\mathbf{r}' + \int\int \mathbf{G}_0(\mathbf{r}-\mathbf{r}'(s))\delta(\mathbf{R}(s)-\mathbf{r}')\sigma(s)\mathrm{d}s\mathrm{d}^3\mathbf{r}'$$

We also define

$$\delta(\mathbf{R}(s)-\mathbf{r}) = \phi(s,\mathbf{r})$$

Now all the calculations will be done in Fourier space and we will look for the way to eliminate σ and $\mathbf{U}$. Using the Fourier Transform (FT) of a convolution ($FT(f*g) = FT(f).FT(g)$), we have:

$$\mathbf{U}(s) = \int \phi(s,\mathbf{k})\mathbf{u}(\mathbf{k})\mathrm{d}^3\mathbf{k} = \phi\mathbf{u} \tag{7.6}$$

$$\mathbf{u}(\mathbf{k}) = \mathbf{G}_0(\mathbf{k})\cdot\mathbf{F}(\mathbf{k}) + \mathbf{G}_0(\mathbf{k})\int \phi(s,\mathbf{k})\sigma(s)\mathrm{d}s = \mathbf{G}_0.\mathbf{F} + \mathbf{G}_0\phi\sigma \tag{7.7}$$

Let us calculate $\mathbf{G}_0(\mathbf{k})$ the FT of $\mathbf{G}_0(\mathbf{r})$

$$\mathbf{G}_0(\mathbf{r}) = \frac{1}{16\pi\mu|\mathbf{r}|}\left\{\left(\frac{3-4\sigma}{1-\sigma}\right)\mathbf{I} + \frac{\hat{\mathbf{r}}\hat{\mathbf{r}}}{1-\sigma}\right\} = P\frac{\mathbf{I}}{|\mathbf{r}|} + Q\frac{\hat{\mathbf{r}}\hat{\mathbf{r}}}{|\mathbf{r}|} = Pf(\mathbf{r}) + Qg(\mathbf{r})$$

where $P = \frac{3-4\sigma}{16\pi\mu(1-\sigma)} = \frac{6B+14\mu}{16\pi\mu(3B+4\mu)}$; $Q = \frac{1}{16\pi\mu(1-\sigma)} = \frac{6B+2\mu}{16\pi\mu(3B+4\mu)}$; $f(\mathbf{r}) = \frac{\mathbf{I}}{|\mathbf{r}|}$ and $g(\mathbf{r}) = \frac{\hat{\mathbf{r}}\hat{\mathbf{r}}}{|\mathbf{r}|}$.
After computing the fourier transform of f and g (see appendix A.4.1)we get

$$\mathbf{G}_0(\mathbf{k}) = P\tilde{f}(\mathbf{r}) + Q\tilde{g}(\mathbf{r})$$

where $\tilde{f}$ and $\tilde{f}$ are the Fourier transforms of f and g. We obtain the expression for $\mathbf{G}_0(\mathbf{k})$ as

$$\boldsymbol{G}_0(\boldsymbol{k}) = \frac{1}{\mu k^2}(\boldsymbol{I} - \hat{\boldsymbol{k}}\hat{\boldsymbol{k}}) + \frac{\boldsymbol{I}}{B + \frac{4\mu}{3}}\hat{\boldsymbol{k}}\hat{\boldsymbol{k}} \tag{7.8}$$

where $k = |\mathbf{k}|$

The expression of U becomes:

$$U(s) = \int \phi(s,\mathbf{k})\mathbf{G}_0(\mathbf{k}).\mathbf{F}(\mathbf{k}) + \int\int \phi(s,\mathbf{k})\mathbf{G}_0(\mathbf{k})\phi(s',\mathbf{k})\sigma(s')\mathrm{d}s'\mathrm{d}^3\mathbf{k} \tag{7.9}$$

$$\mathbf{R}(s) = s\mathbf{n} \Longrightarrow \int \phi(s,\mathbf{k})\mathbf{G}_0(\mathbf{k})\phi(s',\mathbf{k})\mathrm{d}^3\mathbf{k} = \mathbf{G}_0(s\mathbf{n} - s'\mathbf{n})$$

Thus

$$U(s) = \int \phi(s,\mathbf{k})\mathbf{G}_0(\mathbf{k}) \cdot \mathbf{F}(\mathbf{k}) + \int \mathbf{G}_0(s\mathbf{n} - s'\mathbf{n})\boldsymbol{\Delta}(s') \cdot \mathbf{U}(s')\mathrm{d}s' \tag{7.10}$$

This last equation can be written as:

$$[q|U] + \sum_{q'}[q|\mathbf{G}_0|q']\boldsymbol{\Delta}(q') \cdot [q'|\mathbf{U}] = \int [q|\phi(\mathbf{k})]\mathbf{G}_0(\mathbf{k}) \cdot \mathbf{F}(\mathbf{k}) \tag{7.11}$$

or

$$U + \phi\mathbf{G}_0\phi\boldsymbol{\Delta} \cdot \mathbf{U} = \phi\mathbf{G}_0 \cdot \mathbf{F} \tag{7.12}$$

Now, to calculate the quantity $\phi\mathbf{G}_0\phi\boldsymbol{\Delta}$ we introduce the notion of the Hermitian product:

$$[f|q] = \int_0^\ell \psi_q(s)f(s)\mathrm{d}s \quad \text{and} \quad [q|\mathbf{G}_0|q] = \int_0^\ell\int_0^\ell \psi_q(s)\mathbf{G}_0(s\mathbf{n} - s'\mathbf{n})\psi_{q'}(s')\mathrm{d}s\mathrm{d}s' \tag{7.13}$$

where ψ_q are the eigenfunctions of $\boldsymbol{\Delta}$ ($\boldsymbol{\Delta}(q) = Eaq^2\mathbf{nn}$) defined by $\psi_q(s) = (\frac{2}{l})^{\frac{1}{2}}\cos(qs)$ in the case where there is no force across the fibre end-faces.

To solve the equation (7.12), the fibre Green function $\mathscr{G}_0(q,q')$ is used:

$$\sum_{q'}(\delta_{qq'}\mathbf{I} + [q|\mathbf{G}_0|q']\boldsymbol{\Delta}(q'))\mathscr{G}_0(q,q'') = \delta_{qq''}\mathbf{I} \tag{7.14}$$

or

$$(\mathbf{I}+\phi\mathbf{G}_0\phi\boldsymbol{\Delta})\mathscr{G}_0=\mathbf{I}\Longrightarrow\mathscr{G}_0(q,q')=\frac{\mathbf{I}}{\mathbf{I}+\phi\mathbf{G}_0\phi\boldsymbol{\Delta}}=\delta_{qq'}\mathscr{G}_0(q) \tag{7.15}$$

Let us calculate $\mathscr{G}_0(q,q')$

$$[q|\mathbf{G}_0|q']\boldsymbol{\Delta}(q')=n\cdot[q|\mathbf{G}_0|q']\cdot n\boldsymbol{\Delta}(q') \tag{7.16}$$

where $n\cdot[q|\mathbf{G}_0|q']\cdot n=\mathbf{G}_0(q,q')$ is the scalar form of $[q|\mathbf{G}_0|q']$.

$$\mathbf{G}_0(q,q')=\int_0^\ell\int_0^\ell\psi_q(s)\mathbf{n}\cdot\mathbf{G}_0(s\mathbf{n}-s'\mathbf{n})\cdot\mathbf{n}\psi_{q'}(s')\mathrm{d}s\mathrm{d}s' \tag{7.17}$$

We now calculate $\mathbf{n}\cdot\mathbf{G}_0(s\mathbf{n}-s'\mathbf{n})\cdot\mathbf{n}$:

$$\begin{aligned}\mathbf{n}\cdot\mathbf{G}_0(\mathbf{sn\text{-}s'n})\cdot\mathbf{n}&=\mathbf{n}\cdot\left(P\frac{\boldsymbol{I}}{|\mathbf{n}s-s'\mathbf{n}|}+Q\frac{(s\mathbf{n}-s'\mathbf{n})(s\mathbf{n}-s'\mathbf{n})}{|s\mathbf{n}-s'\mathbf{n}|^3}\right)\cdot\mathbf{n}\\&=\mathbf{n}\cdot\left(P\frac{\boldsymbol{I}}{|s-s'|}+Q\frac{\mathbf{nn}(s-s')^2}{|s-s'|^3}\right)\cdot\mathbf{n}\end{aligned} \tag{7.18}$$

Then we get:

$$\mathbf{n}\cdot\mathbf{G}_0(s\mathbf{n}-s'\mathbf{n})\cdot\mathbf{n}=\frac{1}{4\pi\mu}\frac{1}{|s-s'|};$$

such that

$$\mathbf{G}_0(q,q')=\frac{2}{\ell}\int_0^\ell\int_0^\ell\frac{\cos(qs)\cos(q's')}{4\pi\mu|s-s'|}\mathrm{d}s\mathrm{d}s'.$$

After some integration process the first integral gives for $q=q'$

$$\mathbf{G}_0(q,q')=\frac{1}{4\pi^2\mu}\int_{-\pi}^{\pi}\left\{\frac{-\sin(m|y|)}{m|y|}+(\pi-|y|)\frac{\cos(m|y|)}{|y|}\right\}\mathrm{d}y$$

This integral diverge for $q=q'$ and is finite for $q\neq q'$ The interesting case is the divergence part. Only the divergent term $\frac{1}{4\pi^2\mu}\int_{-\pi}^{\pi}\pi\frac{\cos(m|y|)}{|y|}dy$ bring the shear in the fibre matrix system.Thus only this term is consider. Two cases are observed: the presence of screening ($k\ll l^{-1}$) where the short length cut-off in the separation of s-s' is set to $\frac{1}{2}r_0$ so that the effective elastics equations will be matched, which is compared with the absence of the screening ($k\ll l^{-1}$) case.

$$\mathbf{G}_0(q,q')=\frac{\delta_{qq'}}{2\pi\mu}\int_{\frac{r_0}{2l}}^{\pi}\frac{\cos(my)}{y}e^{-\frac{yl}{\xi}}\mathrm{d}y$$

Using Euler gamma integral and taking the lower limit to 0 and the upper limit to infinity ($\int_0^{+\infty}\frac{1}{y}(\frac{1}{y+1}-e^{-y})\mathrm{d}y\Longrightarrow\int_0^{\infty}\frac{\cos y}{y}e^{-y}\mathrm{d}y=-\gamma-\int_0^{+\infty}(-\frac{1}{y}+\frac{1}{y+1})\mathrm{d}y$)

we get

$$\mathbf{G}_0(q,q')=\frac{\delta_{qq'}}{2\pi\mu}\left[-\gamma+\ln\left(\frac{2\ell}{r_0}\right)\right]$$

$\gamma' = \frac{1}{2}e^{\gamma}$ and $\ell = \frac{m\pi}{q}$. So

$$\mathbf{G}_0(q,q') = \frac{\delta_{qq'}}{2\pi\mu}\ln\left(\frac{\pi}{\gamma' r_0 q}\right) = \delta_{qq'}K_0(q) \tag{7.19}$$

Then

$$\mathscr{G}_0(q,q') = \delta_{qq'}(\boldsymbol{I} + Eaq^2K_0(q))^{-1} \tag{7.20}$$

Using the relation

$$\delta_{qq'}\left[C\boldsymbol{I} + D\mathbf{n}_i\mathbf{n}_i\right]^{-1} = \frac{\delta_{qq'}}{C}\left[\boldsymbol{I} - \frac{D}{D+C}\mathbf{n}_i\mathbf{n}_i\right] \tag{7.21}$$

We have:

$$\mathscr{G}_0(q,q') = \delta_{qq'}\left\{(\mathbf{I}-\mathbf{nn}) + \frac{\mathbf{nn}}{\mathbf{I}+K_0(q)Eaq^2}\right\} \tag{7.22}$$

From equation (7.12), we have:

$$\mathbf{U} = \frac{\phi\mathbf{G}_0.\mathbf{F}}{\mathbf{I}+\phi\mathbf{G}_0\phi\boldsymbol{\Delta}} \Longrightarrow \mathbf{U} = \mathscr{G}_0\phi\mathbf{G}_0.\mathbf{F} \tag{7.23}$$

Then

$$\sigma = \boldsymbol{\Delta}\mathscr{G}_0\phi\mathbf{G}_0.\mathbf{F} \tag{7.24}$$

and

$$\mathbf{u} = \mathbf{G}_0(\mathbf{k}).\mathbf{F}\mathbf{k} - \sum_q \mathbf{G}_0(\mathbf{k})[\phi(\mathbf{k}) \mid q]\boldsymbol{\Delta}(q)\mathscr{G}_0(q)\int [q \mid \phi(\mathbf{k}')]\mathbf{G}_0(\mathbf{k}').\mathbf{F}(\mathbf{k}')\mathrm{d}^3\mathbf{k}' \tag{7.25}$$

In short hand writing, we have:

$$\mathbf{u} = \mathbf{G}_0.\mathbf{F} - \mathbf{G}_0\phi\boldsymbol{\Delta}\mathscr{G}_0\phi\mathbf{G}_0.\mathbf{F} \tag{7.26}$$

The total average response of the fibre-matrix system to an applied force of wave vector $\mathbf{k}$ is:

$$\langle\mathbf{u}\rangle = \langle\mathbf{G}_0(\mathbf{k}).\mathbf{F}\mathbf{k} - \sum_q \mathbf{G}_0(\mathbf{k})[\phi(\mathbf{k}) \mid q]\boldsymbol{\Delta}(q)\mathscr{G}_0(q)\int [q \mid \phi(\mathbf{k}')]\mathbf{G}_0(\mathbf{k}').\mathbf{F}(\mathbf{k}')\mathrm{d}^3\mathbf{k}'\rangle \tag{7.27}$$

In this latter equation, there is the average quantity $\langle[\phi(\mathbf{k}) \mid q][q \mid \phi(\mathbf{k}')]\rangle$ which we compute in the following.

$$\langle[\phi(\mathbf{k}) \mid q][q \mid \phi(\mathbf{k}')]\rangle = \frac{2}{V\ell}\int_{-\infty}^{+\infty}\int_0^{\ell}\int_0^{\ell}\psi_q(s)\psi_q(s')\phi(s,\mathbf{k})\phi(s',\mathbf{k})\mathrm{d}s\mathrm{d}s'\mathrm{d}x \tag{7.28}$$

where x is the centre of mass position of the fibre.

$$\langle[\phi(\mathbf{k}) \mid q][q \mid \phi(\mathbf{k}')]\rangle = \frac{2}{\ell}\delta(\boldsymbol{k}-\boldsymbol{k}')\int_0^\ell\int_0^\ell \cos(qs)\cos(qs')e^{i\boldsymbol{k}\cdot\mathbf{n}(s-s')}\mathrm{d}s\mathrm{d}s' \tag{7.29}$$

or

$$\langle[\phi(\mathbf{k}) \mid q][q \mid \phi(\mathbf{k}')]\rangle = \frac{2}{\ell}\delta(\boldsymbol{k}-\boldsymbol{k}')\left(\int_0^\ell \cos(qs)e^{i\boldsymbol{k}\cdot\mathbf{n}s}\mathrm{d}s\right)\left(\int_0^\ell \cos(qs')e^{-i\boldsymbol{k}\cdot\mathbf{n}s'}\mathrm{d}s'\right) \tag{7.30}$$

Let calculate each term in the parenthesis.

$$\begin{aligned}
\int_0^\ell \cos(qs)e^{i\boldsymbol{k}\cdot\mathbf{n}s}\mathrm{d}s &= \int_0^\ell \cos(qs)(\cos(qs)+\mathrm{i}\sin(qs))\mathrm{d}s \\
&= \frac{1}{2}\int_0^\ell (\cos(q+\boldsymbol{k}\cdot\mathbf{n})s+\cos(q-\boldsymbol{k}\cdot\mathbf{n})s) \\
&+ \frac{1}{2}\int_0^\ell \mathrm{i}\,(\sin(q+\boldsymbol{k}\cdot\mathbf{n})s-\sin(q-\boldsymbol{k}\cdot\mathbf{n})s)\,\mathrm{d}s \\
&= \frac{1}{2}\frac{\sin(q+\boldsymbol{k}\cdot\mathbf{n})\ell}{q+\boldsymbol{k}\cdot\mathbf{n}}+\frac{1}{2}\frac{\sin(q-\boldsymbol{k}\cdot\mathbf{n})\ell}{q-\boldsymbol{k}\cdot\mathbf{n}} \\
&- \mathrm{i}\frac{1}{2}\left\{\frac{\cos(q+\boldsymbol{k}\cdot\mathbf{n})\ell}{q+\boldsymbol{k}\cdot\mathbf{n}}-\frac{\cos(q-\boldsymbol{k}\cdot\mathbf{n})\ell}{q-\boldsymbol{k}\cdot\mathbf{n}}+\frac{2\boldsymbol{k}\cdot\mathbf{n}}{(\boldsymbol{k}\cdot\mathbf{n})^2-q^2}\right\} \\
&= \frac{\boldsymbol{k}\cdot\mathbf{n}}{(\boldsymbol{k}\cdot\mathbf{n})^2-q^2}\left(\cos\pi m\sin(\boldsymbol{k}\cdot\mathbf{n}\ell)-\mathrm{i}(\cos\pi m\cos(\boldsymbol{k}\cdot\mathbf{n}\ell)-1)\right)
\end{aligned} \tag{7.31}$$

In the same way we find:

$$\int_0^\ell \cos(qs')e^{-i\boldsymbol{k}\cdot\mathbf{n}s'}\mathrm{d}s' = \frac{\boldsymbol{k}\cdot\mathbf{n}}{(\boldsymbol{k}\cdot\mathbf{n})^2-q^2}\left(\cos\pi m\sin(\boldsymbol{k}\cdot\mathbf{n}\ell)+\mathrm{i}(\cos\pi m\cos(\boldsymbol{k}\cdot\mathbf{n}\ell)-1)\right) \tag{7.32}$$

So

$$\langle[\phi(\mathbf{k}) \mid q][q \mid \phi(\mathbf{k}')]\rangle = \frac{4}{\ell}\delta(\boldsymbol{k}-\boldsymbol{k}')\left(\frac{\boldsymbol{k}\cdot\mathbf{n}}{(\boldsymbol{k}\cdot\mathbf{n})^2-q^2}\right)^2(-1)^{m+1}\cos(\boldsymbol{k}\cdot\mathbf{n}\ell) \tag{7.33}$$

$$= -\frac{4}{\ell}\delta(\boldsymbol{k}-\boldsymbol{k}')\left(\frac{\boldsymbol{k}\cdot\mathbf{n}}{(\boldsymbol{k}\cdot\mathbf{n})^2-q^2}\right)^2(-1)^m\left\{1-2\sin^2\frac{\boldsymbol{k}\cdot\mathbf{n}\ell}{2}\right\} \tag{7.34}$$

$$= \frac{8}{\ell}\delta(\boldsymbol{k}-\boldsymbol{k}')\left[\frac{\boldsymbol{k}\cdot\mathbf{n}\sin\left\{\frac{1}{2}\boldsymbol{k}\cdot\mathbf{n}\ell+\frac{\pi}{4}(1-(-1)^m)\right\}}{\boldsymbol{k}\cdot\mathbf{n}-q^2}\right]^2 \tag{7.35}$$

$$\sim \delta(\mathbf{k}-\mathbf{k}')\phi^2(\mathbf{k},q)) \tag{7.36}$$

We now express the average deformation of the linear fiber reinforced elastic medium as

$$\langle \mathbf{u} \rangle = [\mathbf{G}_0 - \mathbf{G}_0 \langle \phi \boldsymbol{\Delta} \mathscr{G}_0 \phi \rangle \mathbf{G}_0] \, \mathbf{F} \tag{7.37}$$

We then obtain the effective Green function $\mathbf{G}$ for a single fiber α as:

$$\mathbf{G} = \mathbf{G}_0 - \mathbf{G}_0 \langle \phi \boldsymbol{\Delta} \mathscr{G}_0 \phi \rangle \mathbf{G}_0 = \mathbf{G}_0 - \mathbf{G}_0 \langle \mathbf{T}^\alpha \rangle \mathbf{G}_0 \tag{7.38}$$

where $\mathbf{T}^\alpha = \phi \boldsymbol{\Delta} \mathscr{G}_0 \phi$ and α the single fibre.

For many fibres, we have:

$$\mathbf{G} = \mathbf{G}_0 - \mathbf{G}_0 \sum_\alpha \langle \mathbf{T}^\alpha \rangle \mathbf{G}_0 + \mathbf{G}_0 \sum_{\alpha \neq \beta} \langle \mathbf{T}^\alpha \mathbf{G}_0 \mathbf{T}^\beta \rangle \mathbf{G}_0 - \mathbf{G}_0 \sum_{\alpha \neq \beta} \sum_{\gamma \neq \beta} \langle \mathbf{T}^\alpha \mathbf{G}_0 \mathbf{T}^\beta \mathbf{G}_0 \mathbf{T}^\gamma \rangle \mathbf{G}_0 \tag{7.39}$$

The fibres are not correlated in their center of mass so one can write:
$\langle \mathbf{T}^\alpha \mathbf{G}_0 \mathbf{T}^\beta \rangle = \langle \mathbf{T}^\alpha \rangle \mathbf{G}_0 \langle \mathbf{T}^\beta \rangle$, thus:

$$\mathbf{G} = \mathbf{G}_0 - \mathbf{G}_0 \mathbf{T} \mathbf{G}_0 + \mathbf{G}_0 \mathbf{T} \mathbf{G}_0 \mathbf{T} \mathbf{G}_0 - ..... = \mathbf{G}_0 (1 - \mathbf{T}(\mathbf{G}_0 - \mathbf{G}_0 \mathbf{T} \mathbf{G}_0 + ...)) \Longrightarrow \tag{7.40}$$

$$\mathbf{G} = \mathbf{G}_0 (1 - \mathbf{T}\mathbf{G}) \Longrightarrow \mathbf{G} = \frac{\mathbf{G}_0}{1 + \mathbf{T}} \Longrightarrow \mathbf{G}^{-1} = \mathbf{G}_0^{-1} + \mathbf{G}_0^{-1} \mathbf{T} \mathbf{G}_0^{-1} + \mathbf{T}^{-1} \tag{7.41}$$

For an incompressible medium, $\mathbf{G}_0^{-1}$ exist if B is finite. $\mathbf{G}^{-1}$ is the expansion of the inverse of the Green function in fibre number N. The terms in the $\mathbf{G}$ expression are second order in T because there is repeated occurrence of a given fibre (e.g: the third order in T, $\langle \mathbf{T}^\alpha \mathbf{G}_0 \mathbf{T}^\beta \mathbf{G}_0 \mathbf{T}^\gamma \rangle$, contains $\langle \mathbf{T}^\alpha \mathbf{G}_0 \mathbf{T}^\beta \mathbf{G}_0 \mathbf{T}^\alpha \rangle$ which is second order, not third in the fibre number density).
The self-consistence approximation of Edward and Freed is then used to rewrite the following equations:

$$\mathbf{G}^{-1} = \mathbf{G}_0^{-1} + \Sigma \quad \text{where} \quad \Sigma = N \langle \phi \boldsymbol{\Delta} \mathscr{G}_0 \phi \rangle \tag{7.42}$$

and also the elastic interaction $[q|\mathbf{G}_0|q']$ between the normal modes q and q' of a given fibre is replaced in the defining equation of the fibre Green function $\mathcal{G}$ by the screened interaction $[q|\mathbf{G}|q']$ which depends on the final $\mathbf{G}$

$$\sum_{q'} (\delta_{qq'} \mathbf{I} + [q|\mathbf{G}|q'] \boldsymbol{\Delta}(q')) \mathscr{G}_0(q, q") = \delta_{qq"} \mathbf{I} \tag{7.43}$$

$[q|\mathbf{G}|q']$ remains diagonal for q and q' up to $\frac{1}{r_0}$ That is an implicit averaging over the positions of the neighbouring fibres, all embedded in an effective elastic medium and under screening properties at short distance, but is simply elastic for $l \gg l_c$ the critical length.In fact the elastic

interaction between two well separated point on a fibre is screened by the neighbouring fibre. One expect to have:$\mathbf{G}(\mathbf{k}) \sim \frac{1}{k^2+\xi^{-2}}$ where ξ is the screening length.

In the next section we model the cell as an elastic medium embbeded with a composite of star filaments and do do the calculation of the effective green function of the system following the calculations done above for a system of linear filaments.

7.3 Calculation of the effective elastic Green of the system of elastic cell reinforced by a composite of star fibers

We Construct a mechanical model to study the mechanicals interactions between cytoskeletal's filament (Which we assume to be in form of star) networks and their cell matrix when these are subjected to external forces. It enables us to measure the force transmitted by the networks to the cell. As mention earlier we are using continuum mechanics of deformation theory by Edward and Cates to calculate the effective elastic Green function which will allows us to predict the elastic or mechanical properties of living eukaryotic cells.

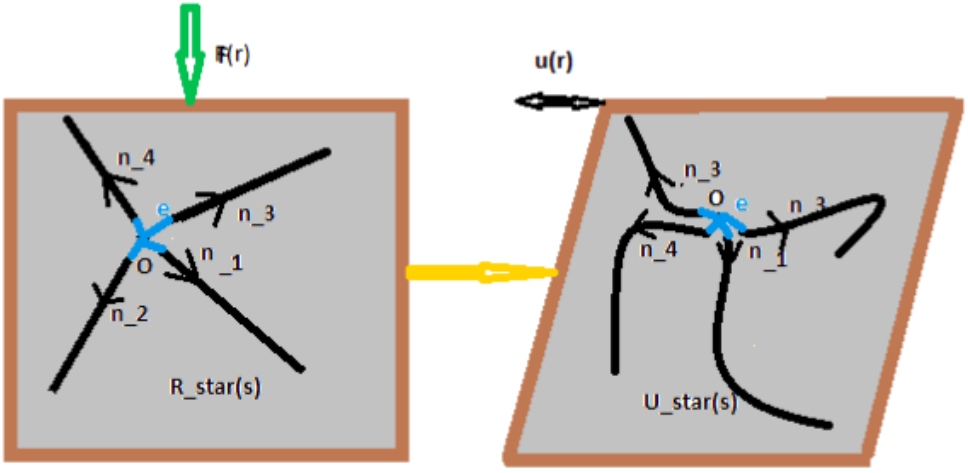

Figure 7.2: *An example of star-like branched semiflexible polymer made up of four linear fibre or polymer chains is embeded in the cell matrix.* $\boldsymbol{n} = \boldsymbol{n}_i$ *are the units vectors of each filament in the star, filaments are of same length and have one of their end connected at the same points forming thus a star filament with* $e = \epsilon$ *the centre of mass of the star.* s *is the arclength,* $\boldsymbol{R}(s)$ *is the initial position of the star of filaments in the medium which undergo a displacement* $\boldsymbol{U}(s)$ *when an external force is applied*

We define the position vector $\mathbf{R}(s)$ of the star-like branched semiflexible polymer made up of four linear fibre or polymer chains, see Figure 7.2 of length ℓ_1, ℓ_2, ℓ_3 and ℓ_4 with $\ell_1 = \ell_2 = \ell_3 = \ell_4 = \ell$ as:

$$\mathbf{R}(s) = \begin{cases} \mathbf{r}_0 + s\mathbf{n}_1 & \text{if } s \in [0, \ell_1] \\ \mathbf{r}_0 + s\mathbf{n}_2 & \text{if } s \in [0, \ell_2] \\ \mathbf{r}_0 + s\mathbf{n}_3 & \text{if } s \in [0, \ell_3] \\ \mathbf{r}_0 + s\mathbf{n}_4 & \text{if } s \in [0, \ell_4] \end{cases} . \tag{7.44}$$

To ease the calculations, we will rather consider star semiflexible polymers with functionality 3. So we rewrite the position vector $\mathbf{R}(s)$ as:

$$\mathbf{R}(s) = \begin{cases} \mathbf{r}_0 + s\mathbf{n}_1 & \text{if } s \in [0, \ell_1] \\ \mathbf{r}_0 + s\mathbf{n}_2 & \text{if } s \in [0, \ell_2] \\ \mathbf{r}_0 + s\mathbf{n}_3 & \text{if } s \in [0, \ell_3] \end{cases} . \tag{7.45}$$

In the absence of star in the cell, the deformation of the cell matrix under an external forces F is:

$$\mathbf{u}(\mathbf{r}) = \int \mathbf{G}_0(\mathbf{r} - \mathbf{r}')\mathbf{F}(\mathbf{r}')\mathrm{d}^3\mathbf{r}' \tag{7.46}$$

where $\mathbf{G}_0$ is the response function between two points $\mathbf{r}$ and $\mathbf{r}'$ of the matrix called the Green function. It is defined as

$$\mathbf{G}_0(\mathbf{r}) = \frac{1}{16\pi\mu|\mathbf{r}|}\left\{\left(\frac{3-4\sigma}{1-\sigma}\right)\mathbf{I} + \frac{\hat{\mathbf{r}}\hat{\mathbf{r}}}{1-\sigma}\right\} = \alpha_1\frac{\mathbf{I}}{|\mathbf{r}|} + \beta_1\frac{\hat{\mathbf{r}}\hat{\mathbf{r}}}{|\mathbf{r}|} \tag{7.47}$$

where

$$\alpha_1 = \frac{3-4\sigma}{16\pi\mu(1-\sigma)} = \frac{6B+14\mu}{16\pi\mu(3B+4\mu)}$$

and

$$\beta_1 = \frac{1}{16\pi\mu(1-\sigma)} = \frac{6B+2\mu}{16\pi\mu(3B+4\mu)}$$

$$|\mathbf{r}| = |\mathbf{r}_1 - \mathbf{r}_2| = |\mathbf{n}s - \mathbf{n}'s'|$$

The separation between two different points of star filaments (both points may be on the same branch or one on branch A and other one on branch B of the star)

As defined before, $\mathbf{r}_1$ and $\mathbf{r}_2$ are the position vectors of two different filaments of the star.

$$\frac{\mathbf{I}}{|\mathbf{r}|} = \frac{\mathbf{I}}{\sqrt{s^2 + s'^2 - 2s's\cos\theta}}$$

with θ the angle between the unit vectors $\mathbf{n}$.

$$\frac{\hat{\mathbf{r}}\hat{\mathbf{r}}}{|\mathbf{r}|} = \frac{\mathbf{n}\mathbf{n}s^2 + \mathbf{n}'\mathbf{n}'s'^2 - \mathbf{n}\mathbf{n}'ss' - \mathbf{n}'\mathbf{n}ss'}{\{s^2 + s'^2 - 2s's\cos\theta\}^{\frac{3}{2}}}$$

In the presence of the star in the matrix, the external forces acting on the matrix lead to the displacement of the whole cell system (cell matrix and the star filaments). Star filament When they are deformed,induce an extra force per unit length $\sigma(s)$ on the cell matrix if the Young modulus of star filaments E_f is greater than than the young modulus of the matrix E_m. The displacement of the star is defined by:

$$\mathbf{U}(s) = \mathbf{u}(\mathbf{R}(s)) \tag{7.48}$$

$$\mathbf{U}(s) = \begin{cases} \mathbf{u}(\mathbf{R}_1(s_1)) \\ \mathbf{u}(\mathbf{R}_2(s_2)) \\ \mathbf{u}(\mathbf{R}_3(s_3)) \end{cases} \tag{7.49}$$

Where $\mathbf{R}_i(s_i)$ is the position vector of a filament i of the star.

The stress created inside each fiber of the star is defined by:

$$\sigma_i(s_i) = \mathbf{\Delta}_i(s_i)\mathbf{U}_i(s_i) \quad \text{or} \quad \sigma_i(s_i) = \mathbf{\Delta}_i.\mathbf{U}_i \quad \text{with} \quad \mathbf{\Delta}(s) = -Ea\mathbf{n}_i\mathbf{n}_j\frac{\partial^2}{\partial s_i^2} \tag{7.50}$$

$$\mathbf{U}_i(s_i) = \int \delta(\mathbf{R}_i(s_i) - \mathbf{r})\mathbf{u}(\mathbf{r})\mathrm{d}^3\mathbf{r} = \int \phi_i(s_i, \mathbf{r})\mathbf{u}(\mathbf{r})\mathrm{d}^3\mathbf{r} = \phi_i\mathbf{u} \tag{7.51}$$

Then the deformation of the matrix in the presence of star of fiber is:

$$\mathbf{u}(\mathbf{r}) = \int \mathbf{G}_0(\mathbf{r}\text{-}\mathbf{r}')\mathbf{F}(\mathbf{r}')\mathrm{d}^3\mathbf{r}' + \sum_{i=1}^{3}\int\int \mathbf{G}_0(\mathbf{r} - \mathbf{r}')\delta(\mathbf{R}_i(s_i) - \mathbf{r}')\sigma_i(s_i)\mathrm{d}s_i\mathrm{d}^3\mathbf{r}' \tag{7.52}$$

The Fourier transform with respect to a special $\mathbf{r}$ of $\delta(\mathbf{R}_i(s_i) - \mathbf{r})$ is:

$$\delta(\mathbf{R}_i(s_i) - \mathbf{r}) = \phi_i(s_i, \mathbf{r})$$

$$\mathbf{u}(\mathbf{k}) = \mathbf{G}_0(\mathbf{k}) \cdot \mathbf{F}(\mathbf{k}) + \sum_{i=1}^{3}\mathbf{G}_0(\mathbf{k})\int_{s_i} \phi_i(s_i, \mathbf{k})\sigma_i(s_i)\mathrm{d}s_i \tag{7.53}$$

or in short hand writing

$$\mathbf{u}(\mathbf{k}) = \mathbf{G}_0 \cdot \mathbf{F} + \sum_{i=1}^{3} \mathbf{G}_0 \cdot \phi_i \sigma_i \tag{7.54}$$

$$\mathbf{U}_j(s_j) = \int \phi_j(s_j, \mathbf{k}) \mathbf{u}(\mathbf{k}) \mathrm{d}^3\mathbf{k} \quad \text{with} \quad j = 1, 2, 3 \tag{7.55}$$

Substituting equation (7.53) in equation (7.55) we have:

$$\begin{aligned} \mathbf{U}_j(s_j) &= \int \phi_j(s_j, \mathbf{k}) \mathbf{G}_0(\mathbf{k}) \mathbf{F}(\mathbf{k}) \mathrm{d}^3\mathbf{k} \\ &\quad + \sum_{i=1}^{3} \int_{\mathbf{k}} \int_{s_i} \phi_j(s_j, \mathbf{k}) \mathbf{G}_0(\mathbf{k}) \phi_i(s_i, \mathbf{k}) \\ &= \int \phi_j(s_j, \mathbf{k}) \mathbf{G}_0(\mathbf{k}) \mathbf{F}(\mathbf{k}) \mathrm{d}^3\mathbf{k} - \sum_{i=1}^{3} \int \mathbf{G}_0(s_j \mathbf{n}_j - s_i \mathbf{n}_i)) \boldsymbol{\Delta}_i(s_i) \cdot \mathbf{U}_i(s_i) \mathrm{d}s_i \end{aligned} \tag{7.56}$$

Equation (7.56) can be expanded as a Fourier series on the eigenfunctions φ_q of Δ and assuming that there is no force accross the fiber end points, the eigenfunctions found to be:

$$\varphi_q(s) = \left(\frac{2}{\ell}\right)^{\frac{1}{2}} \cos(qs)$$

where $s \in [0, \ell]$ and $q = \frac{m\pi}{\ell}$.

The following Hermitian products $[f|q]$ and $[q|F|q']$ are defined in order to calculate the equation (7.56),

$$[f|q] = \int_0^l \varphi_q(s) f(s) \mathrm{d}s \quad \text{and} \quad [q|F|q'] = \int_0^l \int_0^l \varphi_q(s') \varphi_q(s) F(s, s') \mathrm{d}s \mathrm{d}s' \tag{7.57}$$

The equation (7.56) then can be written as:

$$\begin{cases} [q|\mathbf{U}_1] + \sum_{q'} \sum_{i=1}^{3} [q|\mathbf{G}_{01i}|q'] \boldsymbol{\Delta}_i \cdot [q|\mathbf{U}_i] = \int \phi_1(s_1, \mathbf{k}) \mathbf{G}_0(\mathbf{k}) \mathbf{F}(\mathbf{k}) \mathrm{d}^3\mathbf{k} \\ [q|\mathbf{U}_2] + \sum_{q'} \sum_{i=1}^{3} [q|\mathbf{G}_{02i}|q'] \boldsymbol{\Delta}_i \cdot [q|\mathbf{U}_i] = \int \phi_2(s_1, \mathbf{k}) \mathbf{G}_0(\mathbf{k}) \mathbf{F}(\mathbf{k}) \mathrm{d}^3\mathbf{k} \\ [q|\mathbf{U}_3] + \sum_{q'} \sum_{i=1}^{3} [q|\mathbf{G}_{03i}|q'] \boldsymbol{\Delta}_i \cdot [q|\mathbf{U}_i] = \int \phi_3(s_3, \mathbf{k}) \mathbf{G}_0(\mathbf{k}) \mathbf{F}(\mathbf{k}) \mathrm{d}^3\mathbf{k} \end{cases}$$

we rewrite the system in the following matrix form as:

$$\begin{pmatrix} [q|\mathbf{U}_1] \\ [q|\mathbf{U}_2] \\ [q|\mathbf{U}_3] \end{pmatrix} + \begin{pmatrix} \sum_{q'} [q|\mathbf{G}_{011}|q'] \boldsymbol{\Delta}_1 & \sum_{q'} [q|\mathbf{G}_{012}|q'] \boldsymbol{\Delta}_2 & \sum_{q'} \cdot [q|\mathbf{G}_{013}|q'] \boldsymbol{\Delta}_3 \\ \sum_{q'} [q|\mathbf{G}_{021}|q'] \boldsymbol{\Delta}_1 & \sum_{q'} [q|\mathbf{G}_{022}|q'] \boldsymbol{\Delta}_2 & \sum_{q'} [q|\mathbf{G}_{023}|q'] \boldsymbol{\Delta}_3 \\ \sum_{q'} [q|\mathbf{G}_{031}|q'] \boldsymbol{\Delta}_1 & \sum_{q'} [q|\mathbf{G}_{032}|q'] \boldsymbol{\Delta}_2 & \sum_{q'} [q|\mathbf{G}_{033}|q'] \boldsymbol{\Delta}_3 \end{pmatrix} \begin{pmatrix} [q|\mathbf{U}_1] \\ [q|\mathbf{U}_2] \\ [q|\mathbf{U}_3] \end{pmatrix} = \tag{7.58}$$

$$\begin{pmatrix} \int \phi_1(s_1,\mathbf{k})\mathbf{G}_0(\mathbf{k})\mathbf{F}(\mathbf{k})\mathrm{d}^3\mathbf{k} \\ \int \phi_2(s_1,\mathbf{k})\mathbf{G}_0(\mathbf{k})\mathbf{F}(\mathbf{k})\mathrm{d}^3\mathbf{k} \\ \int \phi_3(s_3,\mathbf{k})\mathbf{G}_0(\mathbf{k})\mathbf{F}(\mathbf{k})\mathrm{d}^3\mathbf{k} \end{pmatrix}$$

or in short

$$\begin{pmatrix} [q|\mathbf{U}_1] \\ [q|\mathbf{U}_2] \\ [q|\mathbf{U}_3] \end{pmatrix} + \begin{pmatrix} \sum_{q'}[q|\mathbf{G}_{011}|q']\boldsymbol{\Delta}_1 & \sum_{q'}[q|\mathbf{G}_{012}|q']\boldsymbol{\Delta}_2 & \sum_{q'}\cdot[q|\mathbf{G}_{013}|q']\boldsymbol{\Delta}_3 \\ \sum_{q'}[q|\mathbf{G}_{021}|q']\boldsymbol{\Delta}_1 & \sum_{q'}[q|\mathbf{G}_{022}|q']\boldsymbol{\Delta}_2 & \sum_{q'}[q|\mathbf{G}_{023}|q']\boldsymbol{\Delta}_3 \\ \sum_{q'}[q|\mathbf{G}_{031}|q']\boldsymbol{\Delta}_1 & \sum_{q'}[q|\mathbf{G}_{032}|q']\boldsymbol{\Delta}_2 & \sum_{q'}[q|\mathbf{G}_{033}|q']\boldsymbol{\Delta}_3 \end{pmatrix} \begin{pmatrix} [q|\mathbf{U}_1] \\ [q|\mathbf{U}_2] \\ [q|\mathbf{U}_3] \end{pmatrix} = \tag{7.59}$$

$$\begin{pmatrix} \phi_1\mathbf{G}_0\cdot\mathbf{F} \\ \phi_2\mathbf{G}_0\cdot\mathbf{F} \\ \phi_3\mathbf{G}_0\cdot\mathbf{F} \end{pmatrix}$$

Let us call

$$\mathbb{A}_{qq'} = \begin{pmatrix} \sum_{q'}[q|\mathbf{G}_{011}|q']\boldsymbol{\Delta}_1 & \sum_{q'}[q|\mathbf{G}_{012}|q']\boldsymbol{\Delta}_2 & \sum_{q'}\cdot[q|\mathbf{G}_{013}|q']\boldsymbol{\Delta}_3 \\ \sum_{q'}[q|\mathbf{G}_{021}|q']\boldsymbol{\Delta}_1 & \sum_{q'}[q|\mathbf{G}_{022}|q']\boldsymbol{\Delta}_2 & \sum_{q'}[q|\mathbf{G}_{023}|q']\boldsymbol{\Delta}_3 \\ \sum_{q'}[q|\mathbf{G}_{031}|q']\boldsymbol{\Delta}_1 & \sum_{q'}[q|\mathbf{G}_{032}|q']\boldsymbol{\Delta}_2 & \sum_{q'}[q|\mathbf{G}_{033}|q']\boldsymbol{\Delta}_3 \end{pmatrix} \tag{7.60}$$

with

$$\mathbf{U} = \begin{pmatrix} [q|\mathbf{U}_1] \\ [q|\mathbf{U}_2] \\ [q|\mathbf{U}_3] \end{pmatrix} \tag{7.61}$$

and

$$\mathbf{H} = \begin{pmatrix} \phi_1\mathbf{G}_0\cdot\mathbf{F} \\ \phi_2\mathbf{G}_0\cdot\mathbf{F} \\ \phi_3\mathbf{G}_0\cdot\mathbf{F} \end{pmatrix} \tag{7.62}$$

For us to determine the stress $\boldsymbol{\sigma}$ created inside the star filaments and their deformation $\mathbf{u}(\mathbf{r})$, we need to solve equation (7.59). So we introduce $\mathscr{G}(q,q')$ which is a fibre Green function defined as:

$$\sum_{q'}(\mathbb{I}\delta_{qq'} + \mathbb{A}_{qq'})\mathscr{G}(q',q'') = \mathbb{I}\delta_{qq''} \tag{7.63}$$

as

$$\mathbf{U} = \mathscr{G}\mathbf{H} \tag{7.64}$$

$$\mathscr{G}(q,q') = \delta_{qq'}(\mathbb{I} + \mathbb{A}_{qq'})^{-1}$$

or in short:

$$\mathscr{G} = (\mathbb{I} + \mathbb{A}_{qq'})^{-1}$$

We want now to calculate the matrix $\mathbb{A}_{qq'}$ elements.
The diagonal components are already known from Cates and Edwards article [72] and are equal to $\delta_{qq'}K(q)Eaq^2\mathbf{n}_i\mathbf{n}_i$. It is left to calculate the off-diagonal components of which are $\sum_{q'}\mathbf{n}_i\cdot[q|\mathbf{G}_0|q']\cdot\mathbf{n}_j\boldsymbol{\Delta}_i$, $(i,j=1,2,3)$.

$$[q|\mathbf{G}_0|q'] = \int_0^\ell\int_0^\ell \psi_q(s)\mathbf{G}_0(\mathbf{n}s-\mathbf{n})\psi_{q'}(s')\mathrm{d}s\mathrm{d}s' \tag{7.65}$$

The scalar form of $[q|\mathbf{G}_0|q']\Delta$ is:

$$[q|\mathbf{G}_0|q']\Delta_i = \boldsymbol{n}_i\cdot[q|\mathbf{G}_0|q']\cdot\boldsymbol{n}_i\Delta_i$$

.

$$\mathbf{G}_0(q,q') = \mathbf{n}\cdot[q|\mathbf{G}_0|q']\cdot\mathbf{n}' = \mathbf{n}\cdot\left(\int_0^\ell\int_0^\ell \psi_q(s)\mathbf{G}_0\{\mathbf{n}s-\mathbf{n}'s'\}\psi_{q'}(s')\mathrm{d}s\mathrm{d}s'\right)\cdot\mathbf{n} \tag{7.66}$$

$$\mathbf{G}_0(q,q') = \frac{2(\alpha+\beta)}{\ell}\int_0^\ell\int_0^\ell \frac{\cos qs\cos q's'}{\{s^2+s'^2-2ss'\cos\theta\}^{\frac{1}{2}}}\mathrm{d}s\mathrm{d}s' + \tag{7.67}$$

$$\frac{2\beta sin^2(\theta)}{\ell}\int_0^\ell\int_0^\ell \frac{s'^2\cos qs\cos q's'}{\{s^2+s'^2-2ss'\cos\theta\}^{\frac{3}{2}}}\mathrm{d}s\mathrm{d}s'$$

We introduce Change of variables:

$qs = \frac{m\pi}{\ell}s = mt \Longrightarrow t = \frac{\pi}{l}v$ and $t' = \frac{\pi}{l}s'$; $(t,t')\in[0,\pi]\times[0,\pi]$
$\mathbf{G}_0(q,q')$ becomes

$$\mathbf{G}_0(q,q') = \frac{2(\alpha+\beta)}{\pi}\int_0^\pi\int_0^\pi \frac{\cos mt\cos m't'}{\{t^2+t'^2-2tt'\cos\theta\}^{\frac{1}{2}}}\mathrm{d}t'\mathrm{d}t + \tag{7.68}$$

$$\frac{2\beta sin^2\theta}{\pi}\int_0^\pi\int_0^\pi \frac{t'^2\cos mt\cos(m't')}{(t^2+t'^2-2tt'\cos\theta)^{\frac{3}{2}}}\mathrm{d}t\mathrm{d}t'$$

We do again the following change of variables:

$$\begin{cases} Z = t-t' \\ S = \frac{1}{2}(t+t') \end{cases} \Longrightarrow \begin{cases} t = S+\frac{Z}{2} \\ t' = S-\frac{Z}{2} \end{cases} \tag{7.69}$$

where the Jacobian $J=1$;

$$\begin{cases} 0 \le t \le \pi \\ 0 \le t' \le \pi \end{cases} \Longrightarrow \begin{cases} -\frac{Z}{2} \le S \le \pi - \frac{Z}{2} \\ \frac{Z}{2} \le S \le \pi + \frac{Z}{2} \end{cases} \Longrightarrow \frac{|Z|}{2} \le S \le \pi - \frac{|Z|}{2} \tag{7.70}$$

Let Z_1 and S_1 be the lower limits of the integrals and Z_2 and S_2 the upper limits.

$$\begin{cases} Z_1 = Z_{\min} = t_{\min} - t'_{\max} = -\pi \\ Z_2 = Z_{\max} = t_{\max} - t'_{\min} = \pi \end{cases} \tag{7.71}$$

$(S_1, S_2) \times (Z_1, Z_2) \in [\frac{|Z|}{2}, \pi - \frac{|Z|}{2}] \times [-\pi, \pi]$.
We rewrite $\mathbf{G}_0(q, q')$ with $\alpha + \beta = \frac{1}{4\pi\mu}$ as:

$$\mathbf{G}_0(q, q') = \frac{\sqrt{2}\cos\theta}{2\mu\pi^2} \int_{Z_1}^{Z_2} \int_{S_1}^{S_2} \frac{\cos m'(S - \frac{Z}{2}) \cos m(S + \frac{Z}{2})}{\{4S^2(1 - \cos\theta) + Z^2(1 + \cos\theta)\}^{\frac{1}{2}}} \mathrm{d}S\mathrm{d}Z - \tag{7.72}$$

$$\frac{2\sqrt{2}\beta\sin^2\theta}{\pi} \int_{Z_1}^{Z_2} \int_{S_1}^{S_2} \frac{\cos m'(S - \frac{Z}{2}) \cos m(S + \frac{Z}{2})(S^2 - \frac{Z^2}{4})}{\{4S^2(1 - \cos\theta) + Z^2(1 + \cos\theta)\}^{\frac{3}{2}}} \mathrm{d}S\mathrm{d}Z$$

We wish to calculate analytically $\mathbf{G}_0(q, q')$. But we need to approximate these terms.
We computed $\mathbf{G}_0(q, q')$ numerically and we realised that the off-diagonals terms are a lot smaller than diagonal terms, in spite of numerical problems with oscillatory functions . We remark that the first term in the expression of $\mathbf{G}_0(q, q')$ becomes non-negligible at the lowest modes $m = m' = 0$.

So the following approximation $m = m' = 0$ applies to equation 7.3 in the calculation of $\mathbf{G}_0(q, q')$.
We define

$$\mathbf{G}_0(q, q')|_{q=q'=0} = \Phi(\theta) \tag{7.73}$$

where

$$\Phi(\theta) = \frac{\sqrt{2}}{2\mu\pi^2} \int_{-\pi}^{\pi} \int_{S_1}^{S_2} \frac{1}{\{4S^2(1 - \cos\theta) + Z^2(1 + \cos\theta)\}^{\frac{1}{2}}} \mathrm{d}S\mathrm{d}Z - \tag{7.74}$$

$$\frac{2\sqrt{2}\beta\sin^2\theta}{\pi} \int_{-\pi}^{\pi} \int_{S_1}^{S_2} \frac{(S^2 - \frac{\sigma^2}{4})}{\{4S^2(1 - \cos\theta) + Z^2(1 + \cos\theta)\}^{\frac{3}{2}}} \mathrm{d}S\mathrm{d}Z$$

After the first integration we have:

$$\Phi(\theta) = \frac{\sqrt{2}}{4\pi^2\mu a_1^{\frac{1}{2}}} \left(1 - \frac{\sin^2\theta}{16a_1(1 - \sigma)}\right) \int_{-\pi}^{\pi} \mathrm{d}Z \left[\ln[2a_1 S + a_1\sqrt{4S^2 + \frac{b_1}{a_1}Z^2}]\right]_{S_1}^{S_2} + \tag{7.75}$$

$$\frac{\sqrt{2}}{16\pi^2\mu a_1^{\frac{1}{2}}(1-\sigma)}\int_{-\pi}^{\pi}\mathrm{d}Z\left[\frac{S}{\sqrt{4S^2+\frac{b_1}{a_1}Z^2}}\right]_{S_1}^{S_2}$$

where $a = 1-\cos\theta$ and $b = 1+\cos\theta$

$$\Phi(\theta) = \frac{1}{\mu\pi}\ln\left(\frac{2-a_1}{\sqrt{2a_1}-a_1}\right)+\frac{\sqrt{2a_1}-2}{16\pi\mu(1-\sigma)} \tag{7.76}$$

We now come back into equation (7.59) in order to solve it for $\boldsymbol{U}$.

Thus, let us write:

$$\mathbb{A}_{qq'} = \mathbb{A}(q)\delta_{qq'}$$

$$\mathbb{A}(q) = \delta_{qq'}K(q)Eaq^2\Phi(\theta)\begin{pmatrix}\frac{\mathbf{n}_1\mathbf{n}_1}{\Phi(\theta)} & \mathbf{n}_2\mathbf{n}_2 & \mathbf{n}_3\mathbf{n}_3\\ \mathbf{n}_1\mathbf{n}_1 & \frac{\mathbf{n}_2\mathbf{n}_2}{\Phi(\theta)} & \mathbf{n}_3\mathbf{n}_3\\ \mathbf{n}_1\mathbf{n}_1 & \mathbf{n}_2\mathbf{n}_2 & \frac{\mathbf{n}_3\mathbf{n}_3}{\Phi(\theta)}\end{pmatrix} \tag{7.77}$$

Let now calculate $\mathscr{G}$. We introduce the diagonal matrix $\mathbb{D}$.

$$\mathscr{G} = (\mathbb{I}+\mathbb{A})^{-1} = (\mathbb{I}+\mathbb{A}-\mathbb{D}+\mathbb{D})^{-1} \tag{7.78}$$

$$\mathscr{G} = [(\mathbb{I}+\mathbb{D})^{-1}(\mathbb{I}+(\mathbb{I}+\mathbb{D})^{-1}(\mathbb{A}-\mathbb{D})]^{-1} = [(\mathbb{I}+(\mathbb{I}+\mathbb{D})^{-1}(\mathbb{A}-\mathbb{D})]^{-1}(\mathbb{I}+\mathbb{D})^{-1} \tag{7.79}$$

The intra-fibre hydrodynamics interactions (The interactions between the segments of the same branch or fibre of the star) are much stronger than the inter fibre interactions (Interaction between segments of different fibres). So

$$(\mathbb{I}+\mathbb{D})^{-1}(\mathbb{A}-\mathbb{D}) \ll 1 \tag{7.80}$$

Thus we can do Taylor expansion of $\mathscr{G}$

$$\begin{aligned}\mathscr{G} &= [(\mathbb{I}-(\mathbb{I}+\mathbb{D})^{-1}(\mathbb{A}-\mathbb{D})+(\mathbb{I}-\mathbb{D})^{-2}(\mathbb{A}-\mathbb{D})^2+(\mathbb{I}+\mathbb{D})^{-3}(\mathbb{A}-\mathbb{D})^3-\cdots\\ &\quad +(-1)^p(\mathbb{I}+\mathbb{D})^{-p}(\mathbb{A}-\mathbb{D})^p](\mathbb{I}+\mathbb{D})^{-1}\\ &= \mathbb{P}-\mathbb{P}\mathbb{M}\mathbb{P}+\mathbb{P}^2\mathbb{M}^2\mathbb{P}-\cdots+(-1)^p\mathbb{P}^p\mathbb{M}^p\mathbb{P}\end{aligned}$$

where

$$\mathbb{P} = (\mathbb{I}+\mathbb{D})^{-1} = \delta_{qq'}\begin{pmatrix}(\mathbb{I}+\mathbf{n}_1\mathbf{n}_1K(q)Eaq^2)^{-1} & 0 & 0\\ 0 & (\mathbb{I}+\mathbf{n}_2\mathbf{n}_2K(q)Eaq^2)^{-1} & 0\\ 0 & 0 & (\mathbb{I}+\mathbf{n}_3\mathbf{n}_3K(q)Eaq^2)^{-1}\end{pmatrix} \tag{7.81}$$

and

$$\mathbb{M} = \delta_{qq'} K(q) E a q^2 \Phi(\theta) \begin{pmatrix} 0 & \mathbf{n}_2\mathbf{n}_2 & \mathbf{n}_3\mathbf{n}_3 \\ \mathbf{n}_1\mathbf{n}_1 & 0 & \mathbf{n}_3\mathbf{n}_3 \\ \mathbf{n}_1\mathbf{n}_1 & \mathbf{n}_2\mathbf{n}_2 & 0 \end{pmatrix} \tag{7.82}$$

From the relation

$$\delta_{qq'} \left[C\boldsymbol{I} + D\mathbf{n}_i\mathbf{n}_i \right]^{-1} = \frac{\delta_{qq'}}{C} \left[\boldsymbol{I} - \frac{D}{D+C} \mathbf{n}_i\mathbf{n}_i \right] \tag{7.83}$$

we have:

$$\delta_{qq'} \left[\boldsymbol{I} + \mathbf{n}_i\mathbf{n}_i K(q) E a q^2 \right]^{-1} = \delta_{qq'} \left[(\boldsymbol{I} - \mathbf{n}_i\mathbf{n}_i) + \frac{\mathbf{n}_i\mathbf{n}_i}{1 + K(q) E a q^2} \right] = \boldsymbol{\mathcal{G}}_{0ii}(q, q') \tag{7.84}$$

$$\mathbb{PMP} = \frac{K(q) E a q^2 \Phi(\theta)}{1 + K(q) E a q^2} \begin{pmatrix} 0 & \mathbf{n}_2\mathbf{n}_2 - \frac{K(q) E a q^2 \cos\theta}{1 + K(q) E a q^2} \mathbf{n}_1\mathbf{n}_2 & \mathbf{n}_3\mathbf{n}_3 - \frac{K(q) E a q^2 \cos\theta}{1 + K(q) E a q^2} \mathbf{n}_1\mathbf{n}_3 \\ \mathbf{n}_1\mathbf{n}_1 - \frac{K(q) E a q^2 \cos\theta}{1 + K(q) E a q^2} \mathbf{n}_2\mathbf{n}_1 & 0 & \mathbf{n}_3\mathbf{n}_3 - \frac{K(q) E a q^2 \cos\theta}{1 + K(q) E a q^2} \mathbf{n}_2\mathbf{n}_3 \\ \mathbf{n}_1\mathbf{n}_1 - \frac{K(q) E a q^2 \cos\theta}{1 + K(q) E a q^2} \mathbf{n}_3\mathbf{n}_1 & \mathbf{n}_2\mathbf{n}_2 - \frac{K(q) E a q^2 \cos\theta}{1 + K(q) E a q^2} \mathbf{n}_3\mathbf{n}_2 & 0 \end{pmatrix} \tag{7.85}$$

Let the first, second and third diagonal elements of $\mathbb{P}$ be called respectively $\boldsymbol{\mathcal{G}}_{011}(q)$,$\boldsymbol{\mathcal{G}}_{022}(q)$ and $\boldsymbol{\mathcal{G}}_{033}(q)$.

Then we get the first order expression for $\boldsymbol{\mathcal{G}}$ that we call:

$$\begin{aligned} \boldsymbol{\mathcal{G}}(q, q') &= \begin{pmatrix} \boldsymbol{\mathcal{G}}_{11} & \boldsymbol{\mathcal{G}}_{12} & \boldsymbol{\mathcal{G}}_{13} \\ \boldsymbol{\mathcal{G}}_{21} & \boldsymbol{\mathcal{G}}_{22} & \boldsymbol{\mathcal{G}}_{23} \\ \boldsymbol{\mathcal{G}}_{31} & \boldsymbol{\mathcal{G}}_{32} & \boldsymbol{\mathcal{G}}_{33} \end{pmatrix} \\ &= \frac{K(q) E a q^2 \Phi(\theta)}{1 + K(q) E a q^2} \\ &\quad \begin{pmatrix} \left[\frac{K(q) E a q^2 \Phi(\theta)}{1 + K(q) E a q^2} \right]^{-1} \boldsymbol{\mathcal{G}}_{011}(q) & \mathbf{n}_2\mathbf{n}_2 - \frac{K(q) E a q^2 \cos\theta}{1 + K(q) E a q^2} \mathbf{n}_1\mathbf{n}_2 & \mathbf{n}_3\mathbf{n}_3 - \frac{K(q) E a q^2 \cos\theta}{1 + K(q) E a q^2} \mathbf{n}_1\mathbf{n}_3 \\ \mathbf{n}_1\mathbf{n}_1 - \frac{K(q) E a q^2 \cos\theta}{1 + K(q) E a q^2} \mathbf{n}_2\mathbf{n}_1 & \left[\frac{K(q) E a q^2 \Phi(\theta)}{1 + K(q) E a q^2} \right]^{-1} \boldsymbol{\mathcal{G}}_{022}(q) & \mathbf{n}_3\mathbf{n}_3 - \frac{K(q) E a q^2 \cos\theta}{1 + K(q) E a q^2} \mathbf{n}_2\mathbf{n}_3 \\ \mathbf{n}_1\mathbf{n}_1 - \frac{K(q) E a q^2 \cos\theta}{1 + K(q) E a q^2} \mathbf{n}_3\mathbf{n}_1 & \mathbf{n}_2\mathbf{n}_2 - \frac{K(q) E a q^2 \cos\theta}{1 + K(q) E a q^2} \mathbf{n}_3\mathbf{n}_2 & \left[\frac{K(q) E a q^2 \Phi(\theta)}{1 + K(q) E a q^2} \right]^{-1} \boldsymbol{\mathcal{G}}_{033}(q) \end{pmatrix} \end{aligned} \tag{7.86}$$

We can now express $\mathbf{U}$, $\boldsymbol{\sigma}$ and $\mathbf{u}(\mathbf{r})$.

$$\begin{aligned} \boldsymbol{U} &= \begin{pmatrix} \boldsymbol{\mathcal{G}}_{11} & \boldsymbol{\mathcal{G}}_{12} & \boldsymbol{\mathcal{G}}_{13} \\ \boldsymbol{\mathcal{G}}_{21} & \boldsymbol{\mathcal{G}}_{22} & \boldsymbol{\mathcal{G}}_{21} \\ \boldsymbol{\mathcal{G}}_{31} & \boldsymbol{\mathcal{G}}_{32} & \boldsymbol{\mathcal{G}}_{33} \end{pmatrix} \begin{pmatrix} \phi_1 \\ \phi_2 \\ \phi_3 \end{pmatrix} \boldsymbol{G}_0 \cdot \boldsymbol{F} \\ &= \begin{pmatrix} \boldsymbol{\mathcal{G}}_{11}\phi_1 + \boldsymbol{\mathcal{G}}_{12}\phi_2 + \boldsymbol{\mathcal{G}}_{13}\phi_3 \\ \boldsymbol{\mathcal{G}}_{21}\phi_1 + \boldsymbol{\mathcal{G}}_{22}\phi_2 + \boldsymbol{\mathcal{G}}_{21}\phi_3 \\ \boldsymbol{\mathcal{G}}_{31}\phi_1 + \boldsymbol{\mathcal{G}}_{32}\phi_2 + \boldsymbol{\mathcal{G}}_{33}\phi_3 \end{pmatrix} \boldsymbol{G}_0 \cdot \boldsymbol{F} \end{aligned} \tag{7.87}$$

Thus

$$\boldsymbol{\sigma} = -\boldsymbol{\Delta} \cdot \boldsymbol{U} = -\begin{pmatrix} \Delta_1 \cdot U_1 \\ \Delta_2 \cdot U_2 \\ \Delta_1 \cdot U_3 \end{pmatrix} = -\begin{pmatrix} \boldsymbol{\sigma}_1 \\ \boldsymbol{\sigma}_2 \\ \boldsymbol{\sigma}_3 \end{pmatrix} \tag{7.88}$$

$$\boldsymbol{\sigma} = \begin{pmatrix} \Delta_1(\boldsymbol{\mathcal{G}}_{11}\phi_1 + \boldsymbol{\mathcal{G}}_{12}\phi_2 + \boldsymbol{\mathcal{G}}_{13}\phi_3) \\ \Delta_2(\boldsymbol{\mathcal{G}}_{21}\phi_1 + \boldsymbol{\mathcal{G}}_{22}\phi_2 + \boldsymbol{\mathcal{G}}_{21}\phi_3) \\ \\ \Delta_3(\boldsymbol{\mathcal{G}}_{31}\phi_1 + \boldsymbol{\mathcal{G}}_{32}\phi_2 + \boldsymbol{\mathcal{G}}_{33}\phi_3) \end{pmatrix} \boldsymbol{G}_0 \cdot \boldsymbol{F} \tag{7.89}$$

And then

$$\boldsymbol{u} = \boldsymbol{G}_0 \cdot \boldsymbol{F} + \sum_{i=1}^{3} \boldsymbol{G}_0 \phi_i \boldsymbol{\sigma}_i \tag{7.90}$$

$$= \boldsymbol{G}_0 \cdot \boldsymbol{F} - \boldsymbol{G}_0 \left(\sum_{i=1}^{3} \phi_i \Delta_i \boldsymbol{\mathcal{G}}_{ii} \phi_i + \sum_{i,j=1_{i \neq j}}^{3} \phi_i \Delta_i \boldsymbol{\mathcal{G}}_{ij} \phi_j \right) \boldsymbol{G}_0 \cdot \boldsymbol{F} \tag{7.91}$$

$$\begin{aligned} = \boldsymbol{G}_0 \cdot \boldsymbol{F} - \boldsymbol{G}_0 (&\phi_1\Delta_1\boldsymbol{\mathcal{G}}_{11}\phi_1 + \phi_1\Delta_1\boldsymbol{\mathcal{G}}_{12}\phi_2 + \phi_1\Delta_1\boldsymbol{\mathcal{G}}_{13}\phi_3 + \phi_2\Delta_2\boldsymbol{\mathcal{G}}_{21}\phi_1 \\ &+\phi_2\Delta_2\boldsymbol{\mathcal{G}}_{22}\phi_2 + \phi_2\Delta_2\boldsymbol{\mathcal{G}}_{23}\phi_3 + \phi_3\Delta_3\boldsymbol{\mathcal{G}}_{31}\phi_1 + \phi_3\Delta_3\boldsymbol{\mathcal{G}}_{32}\phi_2 + \phi_3\Delta_3\boldsymbol{\mathcal{G}}_{33}\phi_1) \boldsymbol{G}_0 \cdot \boldsymbol{F} \end{aligned} \tag{7.92}$$

More explicitly:

$$\begin{aligned} \boldsymbol{u} = \boldsymbol{G}_0 \cdot \boldsymbol{F} - \boldsymbol{G}_0 \Bigg(&\frac{Eaq^2}{1 + K(q)Eaq^2} \left[\phi_1\mathbf{n}_1\mathbf{n}_1\phi_1 + \phi_2\mathbf{n}_2\mathbf{n}_2\phi_2 + \phi_3\mathbf{n}_3\mathbf{n}_3\phi_3\right] + \\ &\frac{K(q)\Phi(\theta)(Eaq^2)^2\cos\theta}{(1 + K(q)Eaq^2)^2} \left[\phi_1\mathbf{n}_1\mathbf{n}_2\phi_2 + \phi_1\mathbf{n}_1\mathbf{n}_3\phi_3 \right. \\ &\left. + \phi_2\mathbf{n}_2\mathbf{n}_1\phi_1\phi_2\mathbf{n}_2\mathbf{n}_3\phi_3 + \phi_3\mathbf{n}_3\mathbf{n}_1\phi_1 + \phi_3\mathbf{n}_3\mathbf{n}_2\phi_2\right] \Bigg) \boldsymbol{G}_0 \cdot \boldsymbol{F} \end{aligned} \tag{7.93}$$

or

$$\boldsymbol{u} = \boldsymbol{G}_0 \cdot \boldsymbol{F} - \boldsymbol{G}_0 \left(\frac{Eaq^2}{1 + K(q)Eaq^2} \sum_{i=1}^{3} \phi_i \mathbf{n}_i \mathbf{n}_i \phi_i + \frac{K(q)\Phi(\theta)(Eaq^2)^2\cos\theta}{(1 + K(q)Eaq^2)^2} \sum_{i,j=1_{i \neq j}}^{3} \phi_i \mathbf{n}_i \mathbf{n}_j \phi_j \right) \boldsymbol{G}_0 \cdot \boldsymbol{F} \tag{7.94}$$

We now can calculate the average response or deformation $\boldsymbol{u}$ ($\langle \boldsymbol{u} \rangle$) over the total number of star polymers in the cell medium. Average $\boldsymbol{u}$ means average the correlation factors $[q|\phi_i][\phi_i|q']$ ($\langle [q|\phi_i][\phi_i|q'] \rangle$) and $\phi_i \Delta_1 \boldsymbol{\mathscr{G}}_{ij} \phi_j < [q|\phi_i][\phi_j|q']$.

$$\phi_i = \phi_i(s, \boldsymbol{k}) = F.T(\delta(\boldsymbol{R}(s) - \boldsymbol{r})) = \frac{1}{(2\pi)^3} \int_{-\infty}^{\infty} \delta(\boldsymbol{R}(s) - \boldsymbol{r}) e^{i\boldsymbol{k}\cdot\boldsymbol{r}} \mathrm{d}^3\boldsymbol{r} = e^{i\boldsymbol{k}\cdot\boldsymbol{R}(s)} \tag{7.95}$$

We take $\boldsymbol{r}$ (here $\boldsymbol{r} = \boldsymbol{r}_0$) as the center of mass position of the star. So we define

$$\langle |\phi_i][\phi_j|q'] \rangle = \frac{1}{V} \int_{-\infty}^{+\infty} \mathrm{d}^3\boldsymbol{r} [q|\phi_i][\phi_j|q'] \tag{7.96}$$

where V is the system volume.

$$\langle |\phi_i][\phi_j|q'] \rangle = \frac{2}{V\ell} \int_0^\ell \int_0^\ell \int_{-\infty}^{\infty} \cos(qs) \cos q' s' e^{i(\mathbf{r}+s\mathbf{n})\boldsymbol{k}} e^{-i(\mathbf{r}+s'\mathbf{n}'))\boldsymbol{k}'} \mathrm{d}^3\boldsymbol{r} \mathrm{d}s \mathrm{d}s' \tag{7.97}$$

using the definition

$$\frac{1}{V} \int_{-\infty}^{\infty} \mathrm{d}^3\boldsymbol{r} e^{\mathrm{i}(\boldsymbol{k}-\boldsymbol{k}')\cdot\boldsymbol{r}} = \delta(\boldsymbol{k} - \boldsymbol{k}') \tag{7.98}$$

for $i = j$ i.e $\boldsymbol{n} = \boldsymbol{n}'$ we have the first correlation quantity

$$\langle [\phi_i(\mathbf{k}) \mid q][q \mid \phi_i(\mathbf{k}')] \rangle = \frac{2}{\ell} \delta(\boldsymbol{k} - \boldsymbol{k}') \int_0^\ell \int_0^\ell \cos(qs) \cos(qs') e^{i\boldsymbol{k}\cdot\mathbf{n}(s-s')} \mathrm{d}s \mathrm{d}s' \tag{7.99}$$

or

$$\langle [\phi_i(\mathbf{k}) \mid q][q \mid \phi_i(\mathbf{k}')] \rangle = \frac{2}{\ell} \delta(\boldsymbol{k} - \boldsymbol{k}') \left(\int_0^\ell \cos(qs) e^{i\boldsymbol{k}\cdot\mathbf{n}s} \mathrm{d}s \right) \left(\int_0^\ell \cos(qs') e^{-i\boldsymbol{k}\cdot\mathbf{n}s'} \mathrm{d}s' \right) \tag{7.100}$$

Let uscalculate each term in the parenthesis.

$$\begin{aligned} \int_0^\ell \cos(qs) e^{\mathrm{i}\boldsymbol{k}\cdot\mathbf{n}s} \mathrm{d}s &= \int_0^\ell \cos(qs)(\cos(qs) + \mathrm{i}\sin(qs)) \mathrm{d}s & (7.101) \\ &= \frac{\boldsymbol{k}\cdot\mathbf{n}}{(\boldsymbol{k}\cdot\mathbf{n})^2 - q^2} (\cos\pi m \sin(\boldsymbol{k}\cdot\mathbf{n}\ell) - \mathrm{i}(\cos\pi m \cos(\boldsymbol{k}\cdot\mathbf{n}\ell) - 1)) & (7.102) \\ & & (7.103) \end{aligned}$$

In the same way we find:

$$\int_0^\ell \cos(qs') e^{-i\boldsymbol{k}\cdot\mathbf{n}s'} \mathrm{d}s' = \frac{\boldsymbol{k}\cdot\mathbf{n}}{(\boldsymbol{k}\cdot\mathbf{n})^2 - q^2} (\cos\pi m \sin(\boldsymbol{k}\cdot\mathbf{n}\ell) + \mathrm{i}(\cos\pi m \cos(\boldsymbol{k}\cdot\mathbf{n}\ell) - 1)) \tag{7.104}$$

So

$$\langle[\phi_i(\mathbf{k}) \mid q][q \mid \phi_i(\mathbf{k}')]\rangle = \frac{4}{\ell}\delta(\boldsymbol{k}-\boldsymbol{k}')\left(\frac{\boldsymbol{k}\cdot\mathbf{n}}{(\boldsymbol{k}\cdot\mathbf{n})^2-q^2}\right)^2(-1)^{m+1}\cos(\boldsymbol{k}\cdot\mathbf{n}\ell) \tag{7.105}$$

$$= -\frac{4}{\ell}\delta(\boldsymbol{k}-\boldsymbol{k}')\left(\frac{\boldsymbol{k}\cdot\mathbf{n}}{(\boldsymbol{k}\cdot\mathbf{n})^2-q^2}\right)^2(-1)^{m}\left\{1-2\sin^2\frac{\boldsymbol{k}\cdot\mathbf{n}\ell}{2}\right\} \tag{7.106}$$

We have already shown that

$$\langle[\phi_i(\mathbf{k}) \mid q][q \mid \phi_i(\mathbf{k}')]\rangle = \frac{8}{\ell}\delta(\boldsymbol{k}-\boldsymbol{k}')\left[\frac{\boldsymbol{k}\cdot\mathbf{n}\sin\left\{\frac{1}{2}\boldsymbol{k}\cdot\mathbf{n}\ell+\frac{\pi}{4}(1-(-1)^m)\right\}}{\boldsymbol{k}\cdot\mathbf{n}-q^2}\right]^2 \tag{7.107}$$

The second correlation quantity corresponds to $\boldsymbol{n}\neq\boldsymbol{n}'$:

$$\langle|\phi_i][\phi_j|q']\rangle = \delta(\boldsymbol{k}-\boldsymbol{k}')\frac{2}{\ell}\int_0^\ell\int_0^\ell\cos(qs)\cos q's'e^{i((\mathbf{n}\cdot\boldsymbol{k}s-\mathbf{n}'\cdot\boldsymbol{k}s')}\mathrm{d}s\mathrm{d}s' \tag{7.108}$$

We rewrite for brevity

$$\langle[\phi(\mathbf{k}) \mid q][q' \mid \phi(\mathbf{k}')]\rangle = \delta(\boldsymbol{k}-\boldsymbol{k}')\phi_i(\boldsymbol{k})\phi_j(\boldsymbol{k}) \tag{7.109}$$

$$\phi_i(\boldsymbol{k})\phi_j(\boldsymbol{k}) = \frac{2}{\ell}\left(\int_0^\ell\cos(qs)e^{i((\mathbf{n}\cdot\boldsymbol{k}s}\mathrm{d}s\right)\left(\int_0^\ell\cos(qs)e^{-i((\mathbf{n}'\cdot\boldsymbol{k}s'}\mathrm{d}s'\right) \tag{7.110}$$

Thus, we can now do the averaging

$$\langle\boldsymbol{u}\rangle = \left[\boldsymbol{G}_0-\boldsymbol{G}_0\rangle\boldsymbol{T}^\lambda_{\mathrm{star}}\langle\boldsymbol{G}_0\right]\cdot\boldsymbol{F} \tag{7.111}$$

with

$$\boldsymbol{T}^\lambda_{star} = \sum_{i=1}^{3}\phi_i\Delta_i\boldsymbol{\mathscr{G}}_{ii}\phi_i + \sum_{i,j=1_{i\neq j}}^{3}\phi_i\Delta_i\boldsymbol{\mathscr{G}}_{ij}\phi_j \tag{7.112}$$

Where λ denote the single star in the matrix. The effective Green function is then defined as

$$\boldsymbol{G}_{star} = \boldsymbol{G}_0 - \boldsymbol{G}_0\left\{\sum_{i=1}^{3}\phi_i\Delta_i\boldsymbol{\mathscr{G}}_{ii}\phi_i + \sum_{i,j=1_{i\neq j}}^{3}\phi_i\Delta_i\boldsymbol{\mathscr{G}}_{ij}\phi_j\right\}\boldsymbol{G}_0 \tag{7.113}$$

Where λ denote the single star in the matrix and For a star fibre of density N, in the matrix,

$$\boldsymbol{G}_{star} = \boldsymbol{G}_0^{-1} + \Sigma \tag{7.114}$$

where

$$\Sigma = N\left\langle \sum_{i=1}^{3} \phi_i \Delta_i \boldsymbol{\mathscr{G}}_{ii} \phi_i + \sum_{i,j=1_{i\neq j}}^{3} \phi_i \Delta_i \boldsymbol{\mathscr{G}}_{ij} \phi_j \right\rangle \tag{7.115}$$

Taking into account all q modes, Σ become:

$$\Sigma \cong N\left\langle \sum_{q,q'} \left(\sum_{i=1}^{3} \phi_i^2(\boldsymbol{k},q)\Delta_i \boldsymbol{\mathscr{G}}_{ii} + \sum_{i,j=1_{i\neq j}}^{3} \phi_i(\boldsymbol{k})\phi_j(\boldsymbol{k})\Delta_i \boldsymbol{\mathscr{G}}_{ij} \right) \right\rangle \tag{7.116}$$

$$\Sigma \cong N\left\langle \sum_{q,q'} \left(\frac{Eaq^2}{1+K(q)Eaq^2} \sum_{i=1}^{3} \phi_i^2 \mathbf{n}_i\mathbf{n}_i + \frac{K(q)\Phi(\theta)(Eaq^2)^2}{(1+K(q)Eaq^2)^2}\cos\theta \sum_{i,j=1_{i\neq j}}^{3} \phi_i(\boldsymbol{k})\phi_j(\boldsymbol{k})\mathbf{n}_i\mathbf{n}_j \right) \right\rangle \tag{7.117}$$

a here is different from $a = 1-\cos\theta$ (the one define above).

$$\Sigma \cong N\left\langle \sum_{q,q'} \left(\sum_{i=1}^{3} \phi_i^2(\boldsymbol{k},q)\Delta_i \boldsymbol{\mathscr{G}}_{ii} + \sum_{i,j=1_{i\neq j}}^{3} \phi_i(\boldsymbol{k})\phi_j(\boldsymbol{k})\Delta_i \boldsymbol{\mathscr{G}}_{ij} \right) \right\rangle \tag{7.118}$$

$$\Sigma \cong N\left\langle \sum_{q,q'} \left(\frac{Eaq^2}{1+K(q)Eaq^2} \sum_{i=1}^{3} \phi_i^2 \mathbf{n}_i\mathbf{n}_i + \frac{K(q)\Phi(\theta)(Eaq^2)^2}{(1+K(q)Eaq^2)^2}\cos\theta \sum_{i,j=1_{i\neq j}}^{3} \phi_i(\boldsymbol{k})\phi_j(\boldsymbol{k})\mathbf{n}_i\mathbf{n}_j \right) \right\rangle \tag{7.119}$$

To avoid confusion between imaginary i and the i labelling the number of fibres in the star, we set $i = \alpha$ and $j = \beta$

So for a density P of fibres in the stars:

$$\sum_{\alpha=1}^{P} \phi_\alpha^2 \mathbf{n}_\alpha\mathbf{n}_\alpha = \sum_{\alpha=1}^{P} \frac{8}{\ell}\mathbf{n}_\alpha\mathbf{n}_\alpha \left[\frac{\boldsymbol{k}\cdot\mathbf{n}_\alpha \sin\left\{\frac{1}{2}\boldsymbol{k}\cdot\mathbf{n}_\alpha\ell + \frac{\pi}{4}(1-(-1)^m)\right\}}{\boldsymbol{k}\cdot\mathbf{n}_\alpha - q^2} \right]^2 \longrightarrow_{k\to 0} \sum_{\alpha=1}^{P} \frac{8(\boldsymbol{k}\cdot\mathbf{n}_\alpha)^2\mathbf{n}_\alpha\mathbf{n}_\alpha}{\ell q^4} \tag{7.120}$$

$$\sum_{\alpha,\beta=1_{\alpha\neq\beta}}^{P} \phi_\alpha(\boldsymbol{k})\phi_\beta(\boldsymbol{k})\mathbf{n}_\alpha\mathbf{n}_\beta = \sum_{\alpha,\beta=1_{\alpha\neq\beta}}^{P} \frac{2\mathbf{n}_\alpha\mathbf{n}_\beta}{\ell(\mathbf{n}_\alpha\cdot\boldsymbol{k})(\mathbf{n}_\beta\cdot\boldsymbol{k})}\left(e^{i\boldsymbol{k}\cdot(\mathbf{n}_\alpha-\mathbf{n}_\beta)\ell} - e^{i\boldsymbol{k}\cdot\mathbf{n}_\alpha\ell} - e^{-i\boldsymbol{k}\cdot\mathbf{n}_\beta\ell} + 1\right) \tag{7.121}$$

7.4 Conclusion

In this Chapter, we presented an alternative mean field approach which one can use in order to get information about the elastic properties of cells and their cytoskeleton. We used the

model of an elastic medium embedding star like actin filaments following the work of Cates and Edwards [72]. Our variation here is to place stars of filaments rather than single linear filaments, using the ideas of the other authors. However we need some approximation in order to take the calculations further in this model. This is one of our objective for furture works.

Chapter 8

Conclusion and outlook

8.1 Conclusion

The mechanical properties and stability of living eukaryotics cells within a living tissue depend mainly on the structure, spatial organisation and orientational ordering of their cytoskeleton. The structure, spatial organization and ordering of the cytoskeleton are in turn controlled by the effect of confinement that the cell membrane introduces. Actin is the most abundant network of the cell cytoskeleton and contributes most to the cell mechanical stability through its dense and branched structural networks inside the cell. In this thesis we showed a quantitative study of the effect of confinement on the structure, spatial organisation and orientation of filaments or segments of branching actin networks that enabled us to investigate on the contribution of confined branching actin networks to the mechanical stability of the living tissue cells at equilibrium thermodynamics. The quantitative study consisted of modelling the branching actin networks confined inside a geometrical cell and measuring the density profiles, the order parameter field profiles and the degree of polymerisation of segments of the filaments of the actin networks. The model is based on a monomer ensemble formalism for semiflexible linear polymers inside confining region [1, 2, 44] with tools in statistical mechanics.

In Chapter 1 of this thesis we motivated the study we did in this thesis and the background of the coarse-grained modelling techniques from polymer physics used to investigate the properties of the mechanical properties of cells and their cytoskeleton. In Chapter 2, we have introduced the model for linear semiflexible actin networks. We neglected any kind of interaction between monomers of the chains. We defined the grand canonical partition function for the confined linear chains which we use to derive the expression of the average densities and the mean numbers of segments inside the confining regions. We have also defined a radial order parameter that measures the filaments segment orientation inside the confining region. In Chapter 3, we extended the model including branching in the system of confined linear chains where the

branching mimics the tree-like networks that form via Arp2/3 protein complex inside living cells. Here again we defined a grand canonical partition function for the branching networks and derived the expression for the average density distributions of the networks. The obtained densities depend on recursive non-linear coupled integral equations. We developed then a self-consistent numerical method which enabled us to solve these equations and then we computed the density profiles, the order parameter field profiles and the average degree of polymerisation for three different type of branching actin networks including network dominated by short actin filaments, networks dominated by long linear filaments and the branched network. We present the quantitative results of the computations in Chapter 4 for the three type of networks that we have modelled. These results enabled us to understand how the cell membrane effect on the actin networks depending on their topolology or their architecture and how does the structure and conformations vary.

The cell membrane confinement strongly influence the branching actin networks dominated by long linear filaments and leads to their wrapping around the cell in order to minimize the free energy of the cell system and this results are in agreement with other previous works [41, 54, 55, 57, 57, 63]. The branched networks are also strongly influenced by the confinements effects but they do not bend. They point straight to the confining cell membrane or wall. We argued that this may be due to the stiffness that the branching introduce [71]. In Chapter 5, we include the mutual monomer interactions in the model of the confined branching networks. We define again a grand canonical partition function for the system. Using a SCFT and a mean-field theoretical approximation we derive and compute densities and order profiles like previously. The results of the densities and the radial order parameter field profiles show that in the presence of pair interaction between actin monomers, the filaments of the branched networks and the ones dominated by long linear filaments are subjected to strong confinement and both networks bend around the cell. We then in Chapter 6 of this thesis investigated the relationship between the structural and conformational properties of the branching actin networks and the elastic properties of the cells and their tissues. The calculation of the free energies and forces of a collection of cells enabled us to show that the confined branching actin networks are stable against compressive forces ensuring thus the stability of the cells within the tissue, [139, 142]. However cells under shear are stable until one reaches a critical angle near 30° which we obtain from our numerical calculation, while analytical calculation give us a critical angle near of 45. Beyond these angles the cells become unstable. In Chapter 7, we have introduce an alternative mean field approach in which a cell is treated as a reinforced composite material. We are not yet at the conclusive results. However this method can enable one to investigate the elastic properties of cells. It is an ongoing model and calculation which we think of taking further in our future works.

The results we have obtained are very important for the understanding of the mechanical

instabilities that occur in living epithelial cells and tissues such as intestine. They show the role of the confinements in the mechanical properties of cell. The knowledge of the physical parameters that monitors the stabilities of the cytoskeleton and thus of the cells within tissues is a great asset in the diagnosis and healing of diseases such as cancer since the development, spreading or invasion of cancer cells are often induced by the abnormal mechanical properties of cells [21–23, 28]. Our models can be tested experimentally, and the results are also important in biotechnology, where engineer are trying to build artificial living cells [119]. However these models need to be improved. In fact we have expected a phase transitions in the response of confined branching actin networks under a perturbing external field, which we have not found.

Understanding fully the mechanical properties of living eukaryotic cells and their tissues especially of animals, is one of the most important current objectives of researchers in the field of biophysics due to the increasing number of cell mechanical related diseases. In this thesis we have investigated the elastic properties and stability of the tissue cell by considering that the system is at equilibrium thermodynamics. However it is also important to note that neither the properties of individual cells nor the structures composed of the cells are static. Tissue properties depend also on the growth of new cells, the deaths of others, and exceedingly complex responses to physiological conditions, which may include external stresses [143]. In our models we have not looked at the dynamics of the branching actin networks under confinements. Taking into account the dynamics of the networks in our model can lead us to phase transitions. We have not included also the interaction of the networks with the cell membrane and we are thinking of including it in our future works. We aim to get opportunity to test our models experimentally in other to confirm our numerical results. We will also take further the calculations of the Chapter 7 of this thesis for the results.

Appendix A

Details for calculations in chapters

A.1 Definitions of a functional and functional derivative

In this work we make use of functional and functional derivative. So we would like here to recall what a functional is and how to get its derivative.
A functional is ordinary defined in term of integral of a function. It is thus a function of function written as $F[f]$ or a function of set of functions $F[f_1, f_2, \ldots]$. Some of more general examples of functional are the :

1)
$$F[f(\mathbf{r})] = \int f(\mathbf{r})w(\mathbf{r})\mathrm{d}\mathbf{r} \tag{A.1}$$

2) The action integral of classical mechanics
$$F[f(\mathbf{r})] = \int L(\mathbf{r}, f(\mathbf{r}), \bigtriangledown f(\mathbf{r}))\mathrm{d}\mathbf{r} \tag{A.2}$$

3) nonlocal functional of two functions
$$F[f_1(\mathbf{r}), f_2(\mathbf{r})] = \int w(\mathbf{r}_1)f(\mathbf{r})w(\mathbf{r}_2)\mathrm{d}\mathbf{r}_1\mathrm{d}\mathbf{r}_2 \tag{A.3}$$

The functional derivative is a generalization of the usual derivative. It is often used in the calculus of variations. Instead of differentiating a function with respect to the variable $\mathbf{r}$, one differentiates a functional with respect to function f. The simplest calculation of a functional derivative is given by:

$$\frac{\delta}{\delta f(\mathbf{r}')}F[f(\mathbf{r})] = \lim_{\epsilon \longrightarrow 0} \frac{F[f(\mathbf{r}) + \epsilon\delta(\mathbf{r} - \mathbf{r}')] - F[f(\mathbf{r})]}{\epsilon} \tag{A.4}$$

where δ is the δ-Dirac function and it can be replaced by any arbitrary function according to the objectif of the derivation.

We thus use this definition of the functional derivative to derive the expression of the density distribution of the filament segments in equation (3.29). So in what follows we calculate the functional derivative of the grand canonical partition functions of single linear chain that we have defined in equation (2.7) and of branching networks (which contains both linear and branched filaments) defined in equation 3.14

A.1.1 Density of linear filaments

The average density $\varrho_s(\boldsymbol{r},\hat{\boldsymbol{n}})$ of segments of confined linear chain is defined by:

$$\varrho_s(\boldsymbol{r},\hat{\boldsymbol{n}}) = \frac{z(\boldsymbol{r},\hat{\boldsymbol{n}})}{\mathfrak{Z}}\frac{\delta\mathfrak{Z}}{\delta z(\boldsymbol{r},\hat{\boldsymbol{n}})}. \tag{A.5}$$

in short hand notation we write:

$$\varrho_s(\boldsymbol{r},\hat{\boldsymbol{n}}) = \frac{z}{\mathfrak{Z}}\frac{\delta\mathfrak{Z}}{\delta z}. \tag{A.6}$$

Recall that:

$$\begin{aligned}
\mathfrak{Z}[z(\boldsymbol{r},\hat{\boldsymbol{n}})] = 1 + \int \mathrm{d}^3\boldsymbol{r}_1\mathrm{d}^2\hat{\boldsymbol{n}}_1 z(\boldsymbol{r}_1,\hat{\boldsymbol{n}}_1) + \\
\int\int \mathrm{d}^3\boldsymbol{r}_1\mathrm{d}^2\hat{\boldsymbol{n}}_1\mathrm{d}^3\boldsymbol{r}_2\mathrm{d}^2\hat{\boldsymbol{n}}_2 z(\mathbf{r}_1,\hat{\boldsymbol{n}}_1)w(\boldsymbol{r}_1,\hat{\boldsymbol{n}}_1,\mathbf{r}_2,\hat{\boldsymbol{n}}_2)z(\boldsymbol{r}_2,\hat{\boldsymbol{n}}_2) + \\
\int\int\int \mathrm{d}^3\boldsymbol{r}_1\mathrm{d}^2\hat{\boldsymbol{n}}_1\mathrm{d}^3\boldsymbol{r}_2,\mathrm{d}^2\hat{\boldsymbol{n}}_2\mathrm{d}^3\boldsymbol{r}_3\mathrm{d}^2\hat{\boldsymbol{n}}_3 z(\boldsymbol{r}_1,\hat{\boldsymbol{n}}_1)w(\boldsymbol{r}_1,\hat{\boldsymbol{n}}_1,\boldsymbol{r}_2,\hat{\boldsymbol{n}}_2)z(\boldsymbol{r}_2,\hat{\boldsymbol{n}}_2) \\
w(\boldsymbol{r}_2,\hat{\boldsymbol{n}}_2,\boldsymbol{r}_3,\hat{\boldsymbol{n}}_3)z(\boldsymbol{r}_3,\hat{\boldsymbol{n}}_3) + \\
\int\int\int\int \mathrm{d}^3\boldsymbol{r}_1\mathrm{d}^2\hat{\boldsymbol{n}}_1\mathrm{d}^3\boldsymbol{r}_2,\mathrm{d}^2\hat{\boldsymbol{n}}_2\mathrm{d}^3\boldsymbol{r}_3\mathrm{d}^2\hat{\boldsymbol{n}}_3\mathrm{d}^3\boldsymbol{r}_4\mathrm{d}^2\hat{\boldsymbol{n}}_4 z(\boldsymbol{r}_1,\hat{\boldsymbol{n}}_1)w(\boldsymbol{r}_1,\hat{\boldsymbol{n}}_1,\boldsymbol{r}_2,\hat{\boldsymbol{n}}_2)z(\boldsymbol{r}_2,\hat{\boldsymbol{n}}_2) \\
w(\boldsymbol{r}_2,\hat{\boldsymbol{n}}_2,\boldsymbol{r}_3,\hat{\boldsymbol{n}}_3)z(\boldsymbol{r}_3,\hat{\boldsymbol{n}}_3)w(\boldsymbol{r}_3,\hat{\boldsymbol{n}}_3,\boldsymbol{r}_4,\hat{\boldsymbol{n}}_4)z(\boldsymbol{r}_4,\hat{\boldsymbol{n}}_4) + \\
\ldots + \int\ldots\int \mathrm{d}^3\boldsymbol{r}_1\mathrm{d}^2\hat{\boldsymbol{n}}_1\mathrm{d}^3\boldsymbol{r}_2\mathrm{d}^2\hat{\boldsymbol{n}}_2\ldots\mathrm{d}^3\boldsymbol{r}_N\mathrm{d}^2\hat{\boldsymbol{n}}_N z(\boldsymbol{r}_1,\hat{\boldsymbol{n}}_1)w(\boldsymbol{r}_1,\hat{\boldsymbol{n}}_1,\boldsymbol{r}_2,\hat{\boldsymbol{n}}_2)z(\boldsymbol{r}_2,\hat{\boldsymbol{n}}_2) \\
\ldots w(\boldsymbol{r}_{N-1},\hat{\boldsymbol{n}}_{N-1},\boldsymbol{r}_N,\hat{\boldsymbol{n}}_N)z(\boldsymbol{r}_N,\hat{\boldsymbol{n}}_N) + \ldots
\end{aligned} \tag{A.7}$$

where $\int \mathrm{d}^3\boldsymbol{r}_1\mathrm{d}^2\hat{\boldsymbol{n}}_1 = \int\int \mathrm{d}^3\boldsymbol{r}_1\mathrm{d}^2\hat{\boldsymbol{n}}_1$.

The functional derivative of any functional $\mathfrak{Z}(z(\boldsymbol{r},\hat{\boldsymbol{n}}))$ is:

$$\frac{\delta\mathfrak{Z}[z(\boldsymbol{r},\hat{\boldsymbol{n}})]}{\delta z(\boldsymbol{r},\hat{\boldsymbol{n}})} = \mathbf{lim}_{\epsilon\to 0}\frac{\mathfrak{Z}[z(\boldsymbol{r},\hat{\boldsymbol{n}}) + \epsilon\delta(\boldsymbol{r}-\boldsymbol{r}',\hat{\boldsymbol{n}}-\hat{\boldsymbol{n}}')] - \mathfrak{Z}[z(\boldsymbol{r},\hat{\boldsymbol{n}})]}{\epsilon} \tag{A.8}$$

So we have:

$$
\begin{aligned}
\frac{\delta \mathfrak{Z}[z(\boldsymbol{r},\hat{\boldsymbol{n}})]}{\delta z(\boldsymbol{r},\hat{\boldsymbol{n}})} = & \int \mathrm{d}^3\boldsymbol{r}_1\mathrm{d}^2\hat{\boldsymbol{n}}_1\delta(\boldsymbol{r}-\boldsymbol{r}_1,\hat{\boldsymbol{n}}-\hat{\boldsymbol{n}}_1)+ \\
& \int\int \mathrm{d}^3\boldsymbol{r}_1\mathrm{d}^2\hat{\boldsymbol{n}}_1\mathrm{d}^3\boldsymbol{r}_2\mathrm{d}^2\hat{\boldsymbol{n}}_2\delta(\boldsymbol{r}-\boldsymbol{r}_1,\hat{\boldsymbol{n}}-\hat{\boldsymbol{n}}_1)w(\hat{\boldsymbol{n}}_1,\hat{\boldsymbol{n}}_2)z(\boldsymbol{r}_2,\hat{\boldsymbol{n}}_2)+ \\
& \int\int \mathrm{d}^3\boldsymbol{r}_1\mathrm{d}^2\hat{\boldsymbol{n}}_1\mathrm{d}^3\boldsymbol{r}_2\mathrm{d}^2\hat{\boldsymbol{n}}_2 z(\mathbf{r}_1,\hat{\boldsymbol{n}}_1)w(\hat{\boldsymbol{n}}_1,\hat{\boldsymbol{n}}_2)\delta(\boldsymbol{r}-\boldsymbol{r}_2,\hat{\boldsymbol{n}}-\hat{\boldsymbol{n}}_2)+ \\
& \int\int\int \mathrm{d}^3\boldsymbol{r}_1\mathrm{d}^2\hat{\boldsymbol{n}}_1\mathrm{d}^3\boldsymbol{r}_2,\mathrm{d}^2\hat{\boldsymbol{n}}_2\mathrm{d}^3\boldsymbol{r}_3\mathrm{d}^2\hat{\boldsymbol{n}}_3\delta(\boldsymbol{r}-\boldsymbol{r}_1,\hat{\boldsymbol{n}}-\hat{\boldsymbol{n}}_1)w(\hat{\boldsymbol{n}}_1,\hat{\boldsymbol{n}}_2)z(\boldsymbol{r}_2,\hat{\boldsymbol{n}}_2) \\
& w(\hat{\boldsymbol{n}}_2,\hat{\boldsymbol{n}}_3)z(\boldsymbol{r}_3,\hat{\boldsymbol{n}}_3)+ \\
& \int\int\int \mathrm{d}^3\boldsymbol{r}_1\mathrm{d}^2\hat{\boldsymbol{n}}_1\mathrm{d}^3\boldsymbol{r}_2,\mathrm{d}^2\hat{\boldsymbol{n}}_2\mathrm{d}^3\boldsymbol{r}_3\mathrm{d}^2\hat{\boldsymbol{n}}_3 z(\boldsymbol{r}_1,\hat{\boldsymbol{n}}_1)w(\hat{\boldsymbol{n}}_1,\hat{\boldsymbol{n}}_2)\delta(\boldsymbol{r}-\boldsymbol{r}_2,\hat{\boldsymbol{n}}-\hat{\boldsymbol{n}}_2) \\
& w(\hat{\boldsymbol{n}}_2,\hat{\boldsymbol{n}}_3)z(\boldsymbol{r}_3,\hat{\boldsymbol{n}}_3)+ \\
& \int\int\int \mathrm{d}^3\boldsymbol{r}_1\mathrm{d}^2\hat{\boldsymbol{n}}_1\mathrm{d}^3\boldsymbol{r}_2,\mathrm{d}^2\hat{\boldsymbol{n}}_2\mathrm{d}^3\boldsymbol{r}_3\mathrm{d}^2\hat{\boldsymbol{n}}_3 z(\boldsymbol{r}_1,\hat{\boldsymbol{n}}_1)w(\hat{\boldsymbol{n}}_1,\hat{\boldsymbol{n}}_2)z(\boldsymbol{r}_2,\hat{\boldsymbol{n}}_2) \\
& w(\hat{\boldsymbol{n}}_2,\hat{\boldsymbol{n}}_3)\delta(\boldsymbol{r}-\boldsymbol{r}_3,\hat{\boldsymbol{n}}-\hat{\boldsymbol{n}}_3)+ \\
& \int\int\int\int \mathrm{d}^3\boldsymbol{r}_1\mathrm{d}^2\hat{\boldsymbol{n}}_1\mathrm{d}^3\boldsymbol{r}_2,\mathrm{d}^2\hat{\boldsymbol{n}}_2\mathrm{d}^3\boldsymbol{r}_3\mathrm{d}^2\hat{\boldsymbol{n}}_3\mathrm{d}^3\boldsymbol{r}_4\mathrm{d}^2\hat{\boldsymbol{n}}_4\delta(\boldsymbol{r}-\boldsymbol{r}_1,\hat{\boldsymbol{n}}-\hat{\boldsymbol{n}}_1)w(\hat{\boldsymbol{n}}_1,\hat{\boldsymbol{n}}_2) \\
& z(\boldsymbol{r}_2,\hat{\boldsymbol{n}}_2)w(\boldsymbol{r}_2,\hat{\boldsymbol{n}}_2,\boldsymbol{r}_3,\hat{\boldsymbol{n}}_3)z(\boldsymbol{r}_3,\hat{\boldsymbol{n}}_3)w(\hat{\boldsymbol{n}}_3,\hat{\boldsymbol{n}}_4)z(\boldsymbol{r}_4,\hat{\boldsymbol{n}}_4)+ \\
& \int\int\int\int \mathrm{d}^3\boldsymbol{r}_1\mathrm{d}^2\hat{\boldsymbol{n}}_1\mathrm{d}^3\boldsymbol{r}_2,\mathrm{d}^2\hat{\boldsymbol{n}}_2\mathrm{d}^3\boldsymbol{r}_3\mathrm{d}^2\hat{\boldsymbol{n}}_3\mathrm{d}^3\boldsymbol{r}_4\mathrm{d}^2\hat{\boldsymbol{n}}_4 z(\boldsymbol{r}_1,\hat{\boldsymbol{n}}_1)w(\hat{\boldsymbol{n}}_1,\hat{\boldsymbol{n}}_2) \\
& \delta(\boldsymbol{r}-\boldsymbol{r}_2,\hat{\boldsymbol{n}}-\hat{\boldsymbol{n}}_2)w(\boldsymbol{r}_2,\hat{\boldsymbol{n}}_2,\boldsymbol{r}_3,\hat{\boldsymbol{n}}_3)z(\boldsymbol{r}_3,\hat{\boldsymbol{n}}_3)w(\hat{\boldsymbol{n}}_3,\hat{\boldsymbol{n}}_4)z(\boldsymbol{r}_4,\hat{\boldsymbol{n}}_4)+ \\
& \int\int\int\int \mathrm{d}^3\boldsymbol{r}_1\mathrm{d}^2\hat{\boldsymbol{n}}_1\mathrm{d}^3\boldsymbol{r}_2,\mathrm{d}^2\hat{\boldsymbol{n}}_2\mathrm{d}^3\boldsymbol{r}_3\mathrm{d}^2\hat{\boldsymbol{n}}_3\mathrm{d}^3\boldsymbol{r}_4\mathrm{d}^2\hat{\boldsymbol{n}}_4 z(\boldsymbol{r}_1,\hat{\boldsymbol{n}}_1)w(\hat{\boldsymbol{n}}_1,\hat{\boldsymbol{n}}_2)z(\boldsymbol{r}_2,\hat{\boldsymbol{n}}_2) \\
& w(\hat{\boldsymbol{n}}_2,\hat{\boldsymbol{n}}_3)\delta(\boldsymbol{r}-\boldsymbol{r}_3,\hat{\boldsymbol{n}}-\hat{\boldsymbol{n}}_3)w(\hat{\boldsymbol{n}}_3,\hat{\boldsymbol{n}}_4)z(\boldsymbol{r}_4,\hat{\boldsymbol{n}}_4)+ \\
& \int\int\int\int \mathrm{d}^3\boldsymbol{r}_1\mathrm{d}^2\hat{\boldsymbol{n}}_1\mathrm{d}^3\boldsymbol{r}_2,\mathrm{d}^2\hat{\boldsymbol{n}}_2\mathrm{d}^3\boldsymbol{r}_3\mathrm{d}^2\hat{\boldsymbol{n}}_3\mathrm{d}^3\boldsymbol{r}_4\mathrm{d}^2\hat{\boldsymbol{n}}_4 z(\boldsymbol{r}_1,\hat{\boldsymbol{n}}_1)w(\hat{\boldsymbol{n}}_1,\hat{\boldsymbol{n}}_2)z(\boldsymbol{r}_2,\hat{\boldsymbol{n}}_2) \\
& w(\hat{\boldsymbol{n}}_2,\hat{\boldsymbol{n}}_3)z(\boldsymbol{r}_3,\hat{\boldsymbol{n}}_3)w(\hat{\boldsymbol{n}}_3,\hat{\boldsymbol{n}}_4)\delta(\boldsymbol{r}-\boldsymbol{r}_4,\hat{\boldsymbol{n}}-\hat{\boldsymbol{n}}_4)+\ldots
\end{aligned}
\tag{A.9}
$$

In the following equations we use $\int_{\boldsymbol{r}_1,\hat{\boldsymbol{n}}_1,\boldsymbol{r}_2,\hat{\boldsymbol{n}}_2\ldots\boldsymbol{r}_N,\hat{\boldsymbol{n}}_N+\ldots}$ to mean $\int\ldots\int \mathrm{d}^3\boldsymbol{r}_1\mathrm{d}^2\hat{\boldsymbol{n}}_1\mathrm{d}^3\boldsymbol{r}_2\mathrm{d}^2\hat{\boldsymbol{n}}_2\ldots\mathrm{d}^3\boldsymbol{r}_N\mathrm{d}^2\hat{\boldsymbol{n}}_N\ldots$. We rewrite equation (A.9) with short hand notations as:

$$\begin{aligned}\frac{\delta\Im[z(\boldsymbol{r},\hat{\boldsymbol{n}})]}{\delta z(\boldsymbol{r},\hat{\boldsymbol{n}})} = &\int_{\boldsymbol{r}_1,\hat{\boldsymbol{n}}_1}\langle\boldsymbol{r},\hat{\boldsymbol{n}}|\boldsymbol{r}_1,\hat{\boldsymbol{n}}_1\rangle + \int_{\boldsymbol{r}_2,\hat{\boldsymbol{n}}_2}\langle\boldsymbol{r},\hat{\boldsymbol{n}}|wz|\boldsymbol{r}_2,\hat{\boldsymbol{n}}_2\rangle + \int_{\boldsymbol{r}_1,\hat{\boldsymbol{n}}_1}\langle\boldsymbol{r}_1,\hat{\boldsymbol{n}}_1|zw|\boldsymbol{r},\hat{\boldsymbol{n}}\rangle + \\ &\int_{\boldsymbol{r}_2,\hat{\boldsymbol{n}}_2,\boldsymbol{r}_3,\hat{\boldsymbol{n}}_3}\langle\boldsymbol{r},\hat{\boldsymbol{n}}|wz|\boldsymbol{r}_2,\hat{\boldsymbol{n}}_2\rangle\langle\boldsymbol{r}_2,\hat{\boldsymbol{n}}_2|wz|\boldsymbol{r}_3,\hat{\boldsymbol{n}}_3\rangle + \\ &\int_{\boldsymbol{r}_1,\hat{\boldsymbol{n}}_1,\boldsymbol{r}_3,\hat{\boldsymbol{n}}_3}\langle\boldsymbol{r}_1,\hat{\boldsymbol{n}}_1|zw|\boldsymbol{r},\hat{\boldsymbol{n}}\rangle\langle\boldsymbol{r},\hat{\boldsymbol{n}}|wz|\boldsymbol{r}_3,\hat{\boldsymbol{n}}_3\rangle + \\ &\int_{\boldsymbol{r}_1,\hat{\boldsymbol{n}}_1,\boldsymbol{r}_2,\hat{\boldsymbol{n}}_2}\langle\boldsymbol{r}_1,\hat{\boldsymbol{n}}_1|zw|\boldsymbol{r}_2,\hat{\boldsymbol{n}}_2\rangle\langle\boldsymbol{r}_2,\hat{\boldsymbol{n}}_2|zw|\boldsymbol{r},\hat{\boldsymbol{n}}\rangle + \\ &\int_{\boldsymbol{r}_2,\hat{\boldsymbol{n}}_2,\boldsymbol{r}_3,\hat{\boldsymbol{n}}_3,\boldsymbol{r}_4,\hat{\boldsymbol{n}}_4}\langle\boldsymbol{r},\hat{\boldsymbol{n}}|wz|\boldsymbol{r}_2,\hat{\boldsymbol{n}}_2\rangle\langle\boldsymbol{r}_2,\hat{\boldsymbol{n}}_2|wz|\boldsymbol{r}_3,\hat{\boldsymbol{n}}_3\rangle\langle\boldsymbol{r}_3,\hat{\boldsymbol{n}}_3|wz|\boldsymbol{r}_4,\hat{\boldsymbol{n}}_4\rangle + \\ &\int_{\boldsymbol{r}_1,\hat{\boldsymbol{n}}_1,\boldsymbol{r}_3,\hat{\boldsymbol{n}}_3,\boldsymbol{r}_4,\hat{\boldsymbol{n}}_4}\langle\boldsymbol{r}_1,\hat{\boldsymbol{n}}_1|zw|\boldsymbol{r},\hat{\boldsymbol{n}}\rangle\langle\boldsymbol{r},\hat{\boldsymbol{n}}|wz|\boldsymbol{r}_3,\hat{\boldsymbol{n}}_3\rangle\langle\boldsymbol{r}_3,\hat{\boldsymbol{n}}_3|wz|\boldsymbol{r}_4,\hat{\boldsymbol{n}}_4\rangle + \\ &\int_{\boldsymbol{r}_1,\hat{\boldsymbol{n}}_1,\boldsymbol{r}_2,\hat{\boldsymbol{n}}_2,\boldsymbol{r}_4,\hat{\boldsymbol{n}}_4}\langle\boldsymbol{r}_1,\hat{\boldsymbol{n}}_1|zw|\boldsymbol{r}_2,\hat{\boldsymbol{n}}_2\rangle\langle\boldsymbol{r}_2,\hat{\boldsymbol{n}}_2|zw|\boldsymbol{r},\hat{\boldsymbol{n}}\rangle\langle\boldsymbol{r},\hat{\boldsymbol{n}}|zw|\boldsymbol{r}_4,\hat{\boldsymbol{n}}_4\rangle + \\ &\int_{\boldsymbol{r}_1,\hat{\boldsymbol{n}}_1,\boldsymbol{r}_2,\hat{\boldsymbol{n}}_2,\boldsymbol{r}_3,\hat{\boldsymbol{n}}_3}\langle\boldsymbol{r}_1,\hat{\boldsymbol{n}}_1|zw|\boldsymbol{r}_2,\hat{\boldsymbol{n}}_2\rangle\langle\boldsymbol{r}_2,\hat{\boldsymbol{n}}_2|zw|\boldsymbol{r}_3,\hat{\boldsymbol{n}}_3\rangle\langle\boldsymbol{r}_3,\hat{\boldsymbol{n}}_3|zw|\boldsymbol{r},\hat{\boldsymbol{n}}\rangle + \ldots\end{aligned} \tag{A.10}$$

After integration we have:

$$\begin{aligned}\frac{\delta\Im[z(\boldsymbol{r},\hat{\boldsymbol{n}})]}{\delta z(\boldsymbol{r},\hat{\boldsymbol{n}})} = &1 + \langle\boldsymbol{r},\hat{\boldsymbol{n}}|wz|\mathbf{1}\rangle + \langle\mathbf{1}|zw|\boldsymbol{r},\hat{\boldsymbol{n}}\rangle + \langle\boldsymbol{r},\hat{\boldsymbol{n}}|(wz)^2|\mathbf{1}\rangle + \langle\mathbf{1}|zw|\boldsymbol{r},\hat{\boldsymbol{n}}\rangle\langle\boldsymbol{r},\hat{\boldsymbol{n}}|wz|\mathbf{1}\rangle + \\ &\langle\mathbf{1}|(zw)^2|\boldsymbol{r},\hat{\boldsymbol{n}}\rangle + \langle\boldsymbol{r},\hat{\boldsymbol{n}}|(wz)^3|\mathbf{1}\rangle + \langle\mathbf{1}|zw|\boldsymbol{r},\hat{\boldsymbol{n}}\rangle\langle\boldsymbol{r},\hat{\boldsymbol{n}}|(wz)^2|\mathbf{1}\rangle + \\ &\langle\mathbf{1}|(zw)^2|\boldsymbol{r},\hat{\boldsymbol{n}}\rangle\langle\boldsymbol{r},\hat{\boldsymbol{n}}|wz|\mathbf{1}\rangle + \langle\mathbf{1}|(zw)^3|\boldsymbol{r},\hat{\boldsymbol{n}}\rangle + \ldots\end{aligned} \tag{A.11}$$

$$\begin{aligned}&= [1 + \langle\boldsymbol{r},\hat{\boldsymbol{n}}|wz|\mathbf{1}\rangle + \langle\boldsymbol{r},\hat{\boldsymbol{n}}|(wz)^2|\mathbf{1}\rangle + \langle\boldsymbol{r},\hat{\boldsymbol{n}}|(wz)^3|\mathbf{1}\rangle + \ldots] + \\ &[1 + \langle\boldsymbol{r},\hat{\boldsymbol{n}}|wz|\mathbf{1}\rangle + \langle\boldsymbol{r},\hat{\boldsymbol{n}}|(wz)^2|\mathbf{1}\rangle + \langle\boldsymbol{r},\hat{\boldsymbol{n}}|(wz)^3|\mathbf{1}\rangle + \ldots]\times \\ &[\langle\mathbf{1}|zw|\boldsymbol{r},\hat{\boldsymbol{n}}\rangle + \langle\mathbf{1}|(zw)^2|\boldsymbol{r},\hat{\boldsymbol{n}}\rangle + \langle\mathbf{1}|(zw)^3|\boldsymbol{r},\hat{\boldsymbol{n}}\rangle + \ldots]\end{aligned}$$

Factorizing equation (A.11) gives:

$$\begin{aligned}\frac{\delta\Im[z(\boldsymbol{r},\hat{\boldsymbol{n}})]}{\delta z(\boldsymbol{r},\hat{\boldsymbol{n}})} = &[1 + \langle\boldsymbol{r},\hat{\boldsymbol{n}}|wz|\mathbf{1}\rangle + \langle\boldsymbol{r},\hat{\boldsymbol{n}}|(wz)^2|\mathbf{1}\rangle + \langle\boldsymbol{r},\hat{\boldsymbol{n}}|(wz)^3|\mathbf{1}\rangle + \ldots]\times \\ &[1 + \langle\mathbf{1}|zw|\boldsymbol{r},\hat{\boldsymbol{n}}\rangle + \langle\mathbf{1}|(zw)^2|\boldsymbol{r},\hat{\boldsymbol{n}}\rangle + \langle\mathbf{1}|(zw)^3|\boldsymbol{r},\hat{\boldsymbol{n}}\rangle + \ldots]\end{aligned} \tag{A.12}$$

$$= \sum_{N=0}^{\infty}\langle\boldsymbol{r},\hat{\boldsymbol{n}}|(wz)^N|\mathbf{1}\rangle \times \sum_{N=0}^{\infty}\langle\mathbf{1}|(zw)^N|\boldsymbol{r},\hat{\boldsymbol{n}}\rangle$$

We define the quantities $\Psi(\boldsymbol{r},\hat{\boldsymbol{n}})$ and $\Phi(\boldsymbol{r},\hat{\boldsymbol{n}})$ as:

$$\Psi(\boldsymbol{r},\hat{\boldsymbol{n}}) = \sum_{N=0}^{\infty} \langle \boldsymbol{r},\hat{\boldsymbol{n}}|(wz)^N|\mathbf{1}\rangle \tag{A.13}$$

$$\Phi(\boldsymbol{r},\hat{\boldsymbol{n}}) = \sum_{N=0}^{\infty} \langle \mathbf{1}|(zw)^N|\boldsymbol{r},\hat{\boldsymbol{n}}\rangle \tag{A.14}$$

The sum in equation (A.15) and equation (A.16) are geometric so we rewrite $\Psi(\boldsymbol{r},\hat{\boldsymbol{n}})$ and $\Phi(\boldsymbol{r},\hat{\boldsymbol{n}})$ as:

$$\begin{cases} \Psi(\boldsymbol{r},\hat{\boldsymbol{n}}) = \langle \boldsymbol{r},\hat{\boldsymbol{n}}|(\boldsymbol{I}-wz)^{-1}|\mathbf{1}\rangle \\ \Phi(\boldsymbol{r},\hat{\boldsymbol{n}}) = \langle \mathbf{1}|(\boldsymbol{I}-zw)^{-1}|\boldsymbol{r},\hat{\boldsymbol{n}}\rangle \end{cases} . \tag{A.15}$$

$$\frac{\delta \mathfrak{Z}[z(\boldsymbol{r},\hat{\boldsymbol{n}})]}{\delta z(\boldsymbol{r},\hat{\boldsymbol{n}})} = \Psi(\boldsymbol{r},\hat{\boldsymbol{n}})\Phi(\boldsymbol{r},\hat{\boldsymbol{n}}) \tag{A.16}$$

We can also calculate the functional derivative of the partition function by using the following equations:

$$\mathfrak{Z} = 1 + \int_{\boldsymbol{r},\hat{\boldsymbol{n}}} z(\boldsymbol{r},\hat{\boldsymbol{n}})\Psi(\boldsymbol{r},\hat{\boldsymbol{n}}) \tag{A.17}$$

in short hand notation

$$\mathfrak{Z} = 1 + \int z\Psi \tag{A.18}$$

or

$$\mathfrak{Z} = 1 + \int z\Phi \tag{A.19}$$

with $\Psi(\boldsymbol{r},\hat{\boldsymbol{n}})$ and $\Phi(\boldsymbol{r},\hat{\boldsymbol{n}})$ written in integral form (short hand notation) as:

$$\Psi(\boldsymbol{r},\hat{\boldsymbol{n}}) = \Psi = 1 + \int wz\Psi \tag{A.20}$$

and

$$\Phi(\boldsymbol{r},\hat{\boldsymbol{n}}) = \Phi = 1 + \int zw\Phi \tag{A.21}$$

So we use the equation (A.20) and we have

$$\begin{aligned}
\frac{\delta\mathfrak{Z}}{\delta z} &= \Psi + \int z\,\frac{\delta\Psi}{\delta z} \\
&= \Psi + \int z(w\Psi + wz\frac{\delta\Psi}{\delta z}) \\
&= \Psi + \int zw\,\Psi + \int zwz\,\frac{\delta\Psi}{\delta z} \\
&= \Psi + \int zw\,\Psi + \int zwz\,\frac{\delta\Psi}{\delta z} \\
&= \Psi + \int zw\,\Psi + \int zwzw\,\Psi + \int zwzwz\,\frac{\delta\Psi}{\delta z} \\
&= \Psi + \int zw\,\Psi + \int zwzw\,\Psi + \int zwzwzw\,\Psi + \ldots + \int zwzw\ldots zw\,\Psi + \ldots \\
&= \Psi(1 + \int zw + \int zwzw + \int zwzwzw + \ldots + \int zwzw\ldots zw + \ldots)
\end{aligned} \tag{A.22}$$

We see that according to equation (A.13)

$$\frac{\delta\mathfrak{Z}}{\delta z} = \Psi\Phi\varrho = \frac{z}{\mathfrak{Z}}\Psi\Phi\varrho \tag{A.23}$$

We use this second procedure to calculate the average density of filament segments of confined branching networks.

A.1.2 Average density of segments for branching actin networks

We use here the short hand notation. The total average density of the branching actin networks is given by

$$\varrho = \varrho_z + 2\varrho_\zeta. \tag{A.24}$$

ϱ_z is the density of segments of linear chains of the branching networks i.e the density of the segments that are not involved in branching points. We obtain similar expression as the density expression we obtained in the above equation (A.23) except that in the current case i.e for branching networks:

$$\Psi = 1 + \int wz\Psi + \int \xi\zeta\Psi\Psi \tag{A.25}$$

and

$$\Phi = 1 + \int zw\Phi + \int \xi\zeta\Psi\Phi \tag{A.26}$$

It is left now with the derivation of the expression the average density of segments $2\varrho_\zeta$ involved in branching points.

$$\varrho_\zeta = \frac{\zeta}{\mathfrak{Z}} \frac{\delta \mathfrak{Z}}{\delta \zeta} \tag{A.27}$$

The definition of the grand partition $\mathfrak{Z}$ is given by equation (A.18) or by equation (A.19).

So we calculate in the following the functional derivative of $\mathfrak{Z}$ using its definition given by the equation (A.18).

$$\begin{aligned} \frac{\delta \mathfrak{Z}}{\delta z} &= \int z \frac{\delta \Psi}{\delta \zeta} \\ &= \int z \left(wz \frac{\delta \Psi}{\delta \zeta} + \xi \Psi \Psi + 2\xi\zeta\Psi \frac{\delta \Psi}{\delta \zeta} \right) \\ &= \int z \left(wz \left(wz \frac{\delta \Psi}{\delta \zeta} + \xi \Psi \Psi + 2\xi\zeta\Psi \frac{\delta \Psi}{\delta \zeta} \right) + \right. \\ &\left. \xi \Psi \Psi + 2\xi\zeta\Psi \left(wz \frac{\delta \Psi}{\delta \zeta} + \xi \Psi \Psi + 2\xi\zeta\Psi \frac{\delta \Psi}{\delta \zeta} \right) \right) \end{aligned} \tag{A.28}$$

We recursively expanded the equation (A.28) in the same way as equation (A.22). We expanded also the product $\Psi\Psi\Phi$. We remark that the terms of this equation (A.28) are identic to the terms of the product $\Psi\Psi\Phi$. We then deduced that:

$$\frac{\delta \mathfrak{Z}}{\delta \zeta} = \Psi\Psi\Phi. \tag{A.29}$$

So we find

$$\varrho_\zeta = \frac{\zeta}{\mathfrak{Z}} \Psi\Psi\Phi. \tag{A.30}$$

We then sum the densities to obtain the expression for the total density.

A.2 Density and order profiles for branching actin networks confined in others geometries

The results are similar to the results we have obtained for networks confined in spherical geometry in Chapter 4 of this thesis. So we present here only the profiles of the branching networks in tree-dimensional plots.

A.2.1 Cell with square shape

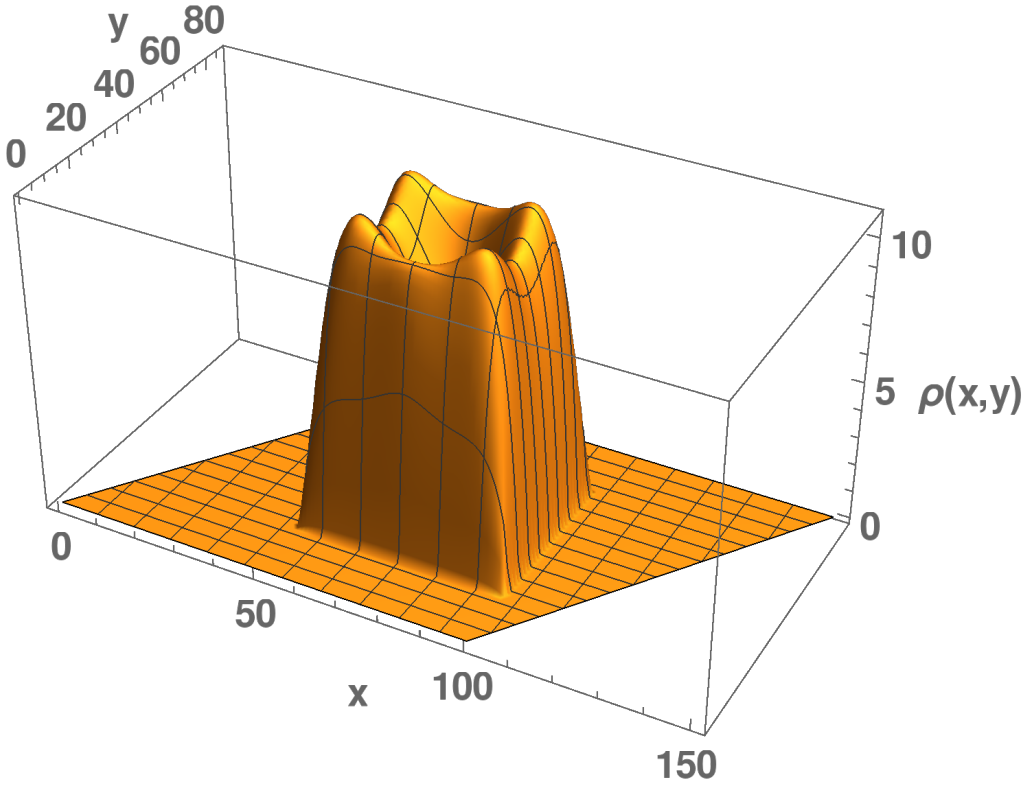

Figure A.1: Three dimensional plot of the density profile of the segments of the branched networks. It is obtained for $(1-z_0)^2 \sim 4\zeta_0$. We plot this density profile for $\zeta_0 = 0.06$ and $z_0 = 0.516$. We observe a huge decrease of the average density of segments in the middle of the square while the profile shows a high density distribution at the periphery of the confining square cell.

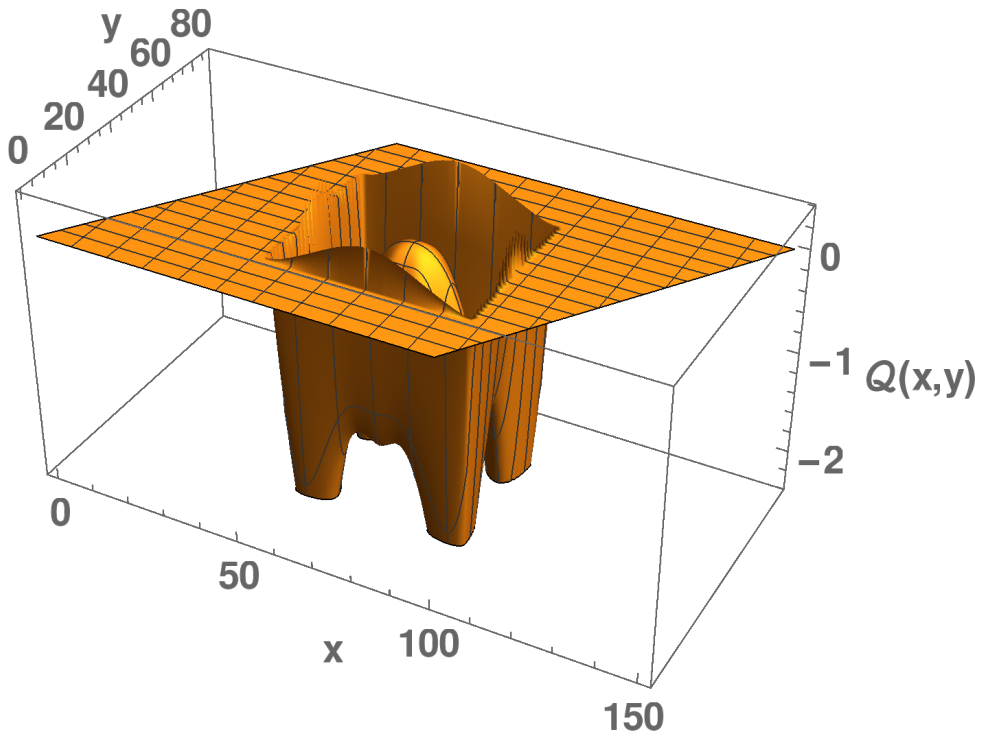

Figure A.2: Radial order parameter field profile of 2d branched networks plotted in three dimension. The profile we show is obtained for $z_0 = 0.516$ and $\zeta_0 = 0.06$. We have negative order parameter field with very small positive values at the vicinity of the cell. This indicate that filaments of segments of the branched networks align perpendicular or point straight to the confining. Only very filament bent. The chain segments are isotropically distributed in the middle of the square.

A.2.2 Cell with triangular shape

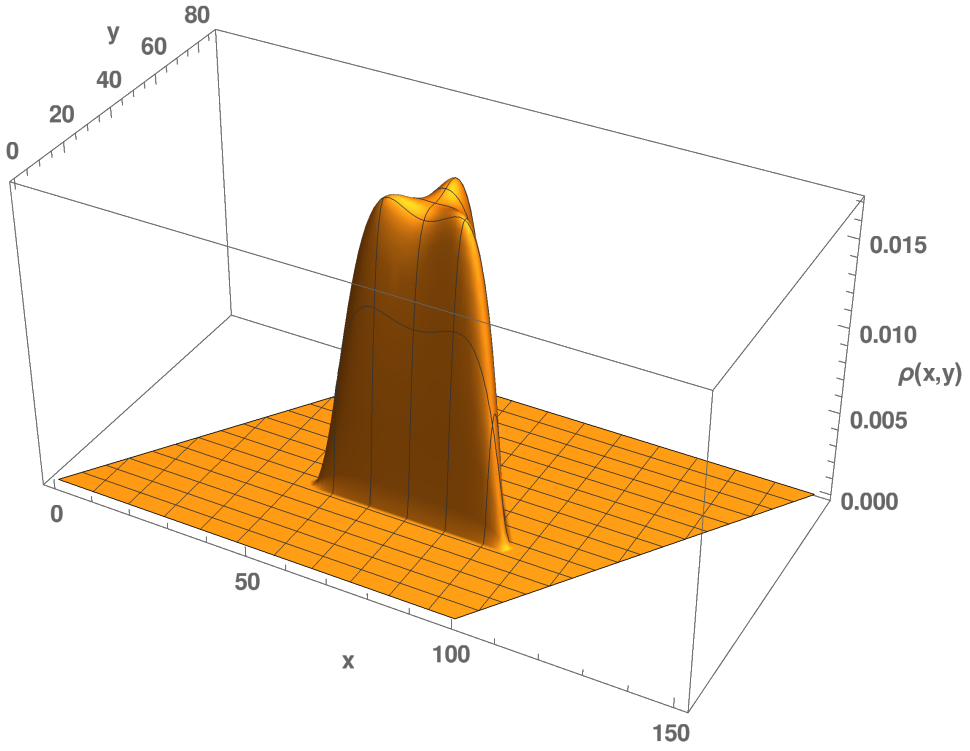

Figure A.3: Three dimensional plot of the density profile of the segments of the branched networks. It is obtained for $(1-z_0)^2 \sim 4\zeta_0$. We plot this density profile for $\zeta_0 = 0.06$ and $z_0 = 0.516$. We observe a huge decrease of the average density of segments in the middle of the square while the profile shows a high density distribution at the periphery of the confining triangular cell.

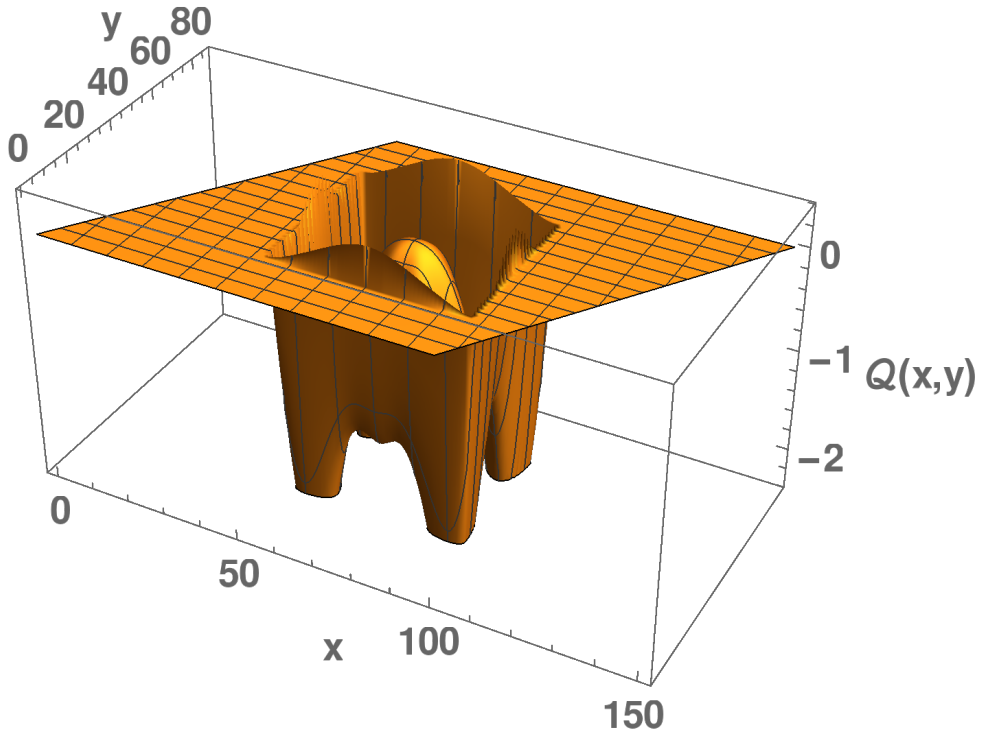

Figure A.4: Radial order parameter field profile of 2d branched networks plotted in three dimension. The profile we show is obtained for $z_0 = 0.516$ and $\zeta_0 = 0.06$. We have negative order parameter field with very small positive values at the vicinity of the cell. This indicate that filaments of segments of the branched networks align perpendicular or point straight to the confining. Only very filament bent. The chain segments are isotropically distributed in the middle of the triangular cell.

A.3 Semiflexible filaments under compressive forces: Derivation of equation (6.33)

Here we follow the general approach as outlined in the papers of Blundell and Terentjev [140, 141] to derive the equation (6.33) and we refer the reader to these papers for more details. We describe the semi-flexible chain as made of discrete stiff monomers bonds. We have N monomers in the chain and each monomers has a distinct discrete position r_k along the chain. The bonds of size b are formed between successive monomers, $b = r_{m+1} - r_m$, Figure A.5. We

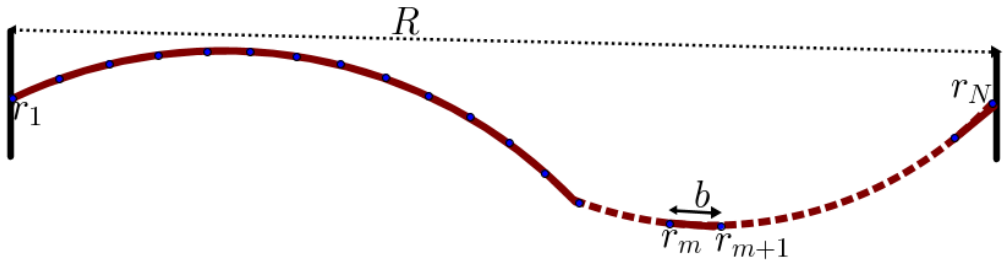

Figure A.5: Descete description of the semi-flexible filament, of contour length L_c. R is the end-to-end distance of the chain and b the bond size.

start rewriting the discrete version of the following equation (equation (6.31)) which is:

$$Z = \mathcal{N} \int \mathcal{D}r e^{-\beta H[r]} \delta(\langle (\mathrm{d}\boldsymbol{r}(s)/\mathrm{d}s)^2 \rangle - 1). \tag{A.31}$$

where $\mathcal{N}$ is the normalization factor.

The first and second derivatives of the space-curve $\boldsymbol{r}(s)$ is written in discrete form as:

$$\boldsymbol{r}'(s) = \lim_{\epsilon \to 0} \frac{r(s+\epsilon) - r(s)}{\epsilon} \overset{\text{discrete}}{\simeq} \frac{r_{m+1} - r_m}{b} = b \frac{\partial r_m}{\partial m} = \dot{r}_m. \tag{A.32}$$

In d dimension:

$$\mathcal{N}\mathcal{D}\boldsymbol{r}(s) = \lim_{N \to \infty} \prod_{m=1}^{N-1} \frac{\mathrm{d}^d r_m}{L_c^d}. \tag{A.33}$$

The discrete version of Z is:

$$Z = \int \prod_{m=1}^{N-1} \frac{\mathrm{d}^d r_m}{L_c^d} e^{-\frac{\beta\kappa}{2} \sum_{m=1}^{N-1} (r_{m+1} - 2r_m + r_{m-1})^2} \prod_{m=1}^{N-1} \delta[(r_{m+1} - r_m)^2 - b^2]. \tag{A.34}$$

The δ-function term in its fourrier transform is:

$$\prod_{m=1}^{N-1} \delta[(r_{m+1} - r_m)^2 - b^2] = \prod_{m=1}^{N-1} \frac{1}{2\pi} \int_{-\infty}^{+\infty} \mathrm{d}\nu_m e^{\mathrm{i}\nu_m ((r_{m+1} - r_m)^2 - b^2)}, \tag{A.35}$$

where ν_m is an auxiliary field. So

$$Z = \int \prod_{m=1}^{N-1} \frac{\mathrm{d}^d r_m}{L_c^d} \mathrm{d}\nu_m e^{\left(\sum_{m=1}^{N-1} \left[-\frac{\beta\kappa b^4}{2} \ddot{r}_m^2 + \mathrm{i}\nu_m b (\dot{r}_m^2 - 1) \right] \right)}. \tag{A.36}$$

We come back to the continuum version of the system and we have

$$\lim_{N \to \infty} \prod_{m=1}^{N-1} L \mathrm{d}\nu_m = D\nu(s). \tag{A.37}$$

In the limit of very large N and b going to 0, the partition function can be written in the path integral form as:

$$Z = \int \mathcal{D}\boldsymbol{r} \mathcal{D}\nu \, e^{\int_0^{L_c} \mathrm{d}s \left(-\frac{u}{2} \ddot{\boldsymbol{r}}(s)^2 + \mathrm{i}\nu(s) (\dot{\boldsymbol{r}}(s)^2 - 1) \right)}, \tag{A.38}$$

where $u = \kappa b^3 \beta$ and is related to the persistence length ℓ_p of a polymer chain in d-dimensions as : $u = \ell_p (d-1)/2$. We use the mean-field approach to make the computation of the partition function analytically possible. The approach is to replace the local in-extensibility constraints $\dot{r} = 1$ with the global constraint $\langle \dot{r} \rangle = 1$.The auxiliary field $\nu(s)$ can also be replaced by its mean value $\bar{\nu}$ which take different value for different configurations. These do not lead the lost of any physics of the problem, rather make the problem analytically tractable.

The integral become now Gaussian and we use the following boundary conditions to compute it.

$$\boldsymbol{r}(0) = 0 \quad \text{and} \quad \boldsymbol{r}(L_c) = \boldsymbol{R} \tag{A.39}$$

where $\boldsymbol{R}$ is the end-to-end distance vector of the filament. We consider that the space-curve is a straight curve with small fluctuations $\boldsymbol{h}(s)$ which vanish at both ends of the filament i.e $\boldsymbol{h}(0) = 0 = \boldsymbol{h}(L_c)$. So we can define

$$\boldsymbol{r}(s) = \frac{s}{L_c}\boldsymbol{R} + \boldsymbol{h}(s). \tag{A.40}$$

$\boldsymbol{r}(s)$ in Fourier series can be written as:

$$\boldsymbol{r}(s) = \frac{s}{L_c}\boldsymbol{R} + \sum_{q=1}^{\infty} \boldsymbol{h}_q \sin\left(\frac{q\pi s}{L_c}\right). \tag{A.41}$$

By doing the Fourier expansion of equation (A.38), we obtain the partion function in the form of series of Gaussian integrals:

$$Z = L_c \int_{-\infty}^{+\infty} \mathrm{d}\bar{\nu} e^{-\imath\bar{\nu}L_c\left(1-\left(\frac{\boldsymbol{R}}{L_c}\right)^2\right)} \int \mathcal{D}h_q e^{\left[-\frac{1}{2}\sum_{q=1}^{\infty}\boldsymbol{h}_q\cdot M_q\cdot\boldsymbol{h}_q\right]}. \tag{A.42}$$

$$Z = L_c \int_{-\infty}^{+\infty} \mathrm{d}\bar{\nu} e^{-\mathrm{i}\bar{\nu}L_c\left(1-\left(\frac{\boldsymbol{R}}{L_c}\right)^2\right)} \prod_{q=1}^{q=\infty} \sqrt{detM_q}, \tag{A.43}$$

where

$$M_q = \boldsymbol{I}_d \left[\frac{uL_c}{2}\left(\frac{q\pi}{L}\right)^4 - \mathrm{i}\bar{\nu}L_c\left(\frac{q\pi}{L}\right)^2\right]. \tag{A.44}$$

After using the identity $\prod_{q=1}^{q=\infty}[1 - x^2/q^2\pi^2]^{-1} = x/sinx$. We then finally come up with the expression of the partition function as:

$$Z = \frac{u}{2L_c} \int_{-\infty}^{+\infty} \mathrm{d}\gamma e^{-\mathrm{i}\gamma\frac{u}{2L_c}\left(1-\left(\frac{\boldsymbol{R}}{L_c}\right)^2\right)} \left[\frac{\sqrt{\mathrm{i}\gamma}}{\sin\sqrt{\mathrm{i}\gamma}}\right]^{d/2}, \tag{A.45}$$

Where $\gamma = 2\bar{\nu}L_c^2/u$. It gives an estimation of the deviation of the chain from its full extension. So it is related to the effective stiffness of the filament.

A.4 Cell as fiber reinforced composite material

A.4.1 Green function

We want to compute fourier transform of the following Green function

$$f(\mathbf{k}) = \int \mathrm{d}^3\mathbf{r} \frac{1}{|\mathbf{r}|} e^{\mathrm{i}\mathbf{k}.\mathbf{r}}$$

In spherical coordinates: $\mathrm{d}^3\mathbf{r} = r^2 \sin\theta \mathrm{d}\theta \mathrm{d}\varphi \mathrm{d}r$ where $r : 0 \to \infty$, $\theta : 0 \to \pi$ and $\varphi : 0 \to 2\pi$. we choose $\mathbf{k}$ to be in the direction of z-axis ($\mathbf{k}.\mathbf{r} = kr\cos\theta$). Thus

$$f(\mathbf{k}) = \int_0^\infty \mathrm{d}r \int_{-1}^1 \mathrm{d}(\cos\theta) \int_0^{2\pi} \mathrm{d}\varphi r^2 \times \frac{1}{r} e^{\mathrm{i}kr\cos\theta}$$

$$f(\mathbf{k}) = \frac{2\pi}{\mathrm{i}k} \int_0^\infty \mathrm{d}r (e^{\mathrm{i}kr} - e^{-\mathrm{i}kr})$$

This integral diverge when r goes to infinity, so since $\frac{1}{|\mathbf{r}|}$ is an interaction, we can regularize it by adding $e^{-\epsilon r}$. Thus

$$f(\mathbf{k}) = \lim_{\epsilon\to 0} \frac{2\pi}{\mathrm{i}k} \int_0^\infty \mathrm{d}r (e^{\mathrm{i}kr-\epsilon r} - e^{-\mathrm{i}kr-\epsilon r}) = \frac{4\pi}{k^2}\mathbf{I}$$

Now we want to calculate the FT of $g(\mathbf{r})$. To calculate it we decompose the tensor $\hat{\boldsymbol{r}}\hat{\boldsymbol{r}}$ in its parallel ($\hat{z}//\hat{k}$) and perpendicular ($(\hat{x},\hat{y})\perp\hat{k}$) components.

$\hat{\boldsymbol{r}} = \hat{x} + \hat{y} + \hat{z} = \hat{i} + \hat{j} + \hat{k}$
We have

$$\begin{aligned} \hat{\boldsymbol{r}}\cdot\hat{\boldsymbol{r}}\hat{\boldsymbol{r}}\cdot\hat{\boldsymbol{r}} &= (\hat{x}+\hat{y}+\hat{k})\cdot\hat{\boldsymbol{r}}\hat{\boldsymbol{r}}\cdot(\hat{x}+\hat{y}+\hat{k}) && \text{(A.46)} \\ &= \begin{pmatrix} \hat{x}\cdot\hat{\boldsymbol{r}}\hat{\boldsymbol{r}}\cdot\hat{x} & \hat{x}\cdot\hat{\boldsymbol{r}}\hat{\boldsymbol{r}}\cdot\hat{y} & \hat{x}\cdot\hat{\boldsymbol{r}}\hat{\boldsymbol{r}}\cdot\hat{z} \\ \hat{y}\cdot\hat{\boldsymbol{r}}\hat{\boldsymbol{r}}\cdot\hat{x} & \hat{y}\cdot\hat{\boldsymbol{r}}\hat{\boldsymbol{r}}\cdot\hat{y} & \hat{y}\cdot\hat{\boldsymbol{r}}\hat{\boldsymbol{r}}\cdot\hat{z} \\ \hat{z}\cdot\hat{\boldsymbol{r}}\hat{\boldsymbol{r}}\cdot\hat{x} & \hat{z}\cdot\hat{\boldsymbol{r}}\hat{\boldsymbol{r}}\cdot\hat{y} & \hat{z}\cdot\hat{\boldsymbol{r}}\hat{\boldsymbol{r}}\cdot\hat{z} \end{pmatrix} && \text{(A.47)} \end{aligned}$$

So

$$g(\mathbf{r}) = \frac{1}{|\boldsymbol{r}|} \begin{pmatrix} \hat{x}\cdot\hat{\boldsymbol{r}}\hat{\boldsymbol{r}}\cdot\hat{x} & \frac{1}{2}\sin^2\theta\cos 2\psi & \frac{1}{2}\sin 2\theta\cos\psi \\ \frac{1}{2}\sin^2\theta\cos 2\psi & \hat{y}\cdot\hat{\boldsymbol{r}}\hat{\boldsymbol{r}}\cdot\hat{y} & \frac{1}{2}\sin 2\theta\sin\psi \\ \frac{1}{2}\sin 2\theta\cos\psi & \frac{1}{2}\sin 2\theta\sin\psi & \hat{z}\cdot\hat{\boldsymbol{r}}\hat{\boldsymbol{r}}\cdot\hat{z} \end{pmatrix} \begin{pmatrix} \hat{\boldsymbol{i}}\hat{\boldsymbol{i}} \\ \hat{\boldsymbol{j}}\hat{\boldsymbol{j}} \\ \hat{\boldsymbol{k}}\hat{\boldsymbol{k}} \end{pmatrix} \quad \text{(A.48)}$$

The Fourier transform of all the off-diagonal components is 0 because $\int_0^{2\pi}\cos(2\psi)\mathrm{d}\psi = \int_0^{2\pi}\cos(\psi)\mathrm{d}\psi = \int_0^{2\pi}\sin(\psi)\mathrm{d}\psi = 0$.
So

$$F.T\{g(\mathbf{r})\} = F.T\left\{ \frac{1}{|\boldsymbol{r}|} \begin{pmatrix} \hat{x}\cdot\hat{\boldsymbol{r}}\hat{\boldsymbol{r}}\cdot\hat{x} & 0 & 0 \\ 0 & \hat{y}\cdot\hat{\boldsymbol{r}}\hat{\boldsymbol{r}}\cdot\hat{y} & 0 \\ 0 & 0 & \hat{z}\cdot\hat{\boldsymbol{r}}\hat{\boldsymbol{r}}\cdot\hat{z} \end{pmatrix} \begin{pmatrix} \hat{\boldsymbol{i}}\hat{\boldsymbol{i}} \\ \hat{\boldsymbol{j}}\hat{\boldsymbol{j}} \\ \hat{\boldsymbol{k}}\hat{\boldsymbol{k}} \end{pmatrix} \right\} \quad \text{(A.49)}$$

From symmetry, $\hat{x}\cdot\hat{\boldsymbol{r}}\hat{\boldsymbol{r}}\cdot\hat{x} = \hat{y}\cdot\hat{\boldsymbol{r}}\hat{\boldsymbol{r}}\cdot\hat{y}$
Thus

$$g(\boldsymbol{k}) = F.T\{g(\mathbf{r})\} = \begin{pmatrix} M & 0 & 0 \\ 0 & M & 0 \\ 0 & 0 & A \end{pmatrix} \begin{pmatrix} \hat{\boldsymbol{i}}\hat{\boldsymbol{i}} \\ \hat{\boldsymbol{j}}\hat{\boldsymbol{j}} \\ \hat{\boldsymbol{k}}\hat{\boldsymbol{k}} \end{pmatrix} = M(\hat{\boldsymbol{i}}\hat{\boldsymbol{i}} + \hat{\boldsymbol{j}}\hat{\boldsymbol{j}}) + A\hat{\boldsymbol{k}}\hat{\boldsymbol{k}} = M(\boldsymbol{I} - \hat{\boldsymbol{k}}\hat{\boldsymbol{k}}) + A\hat{\boldsymbol{k}}\hat{\boldsymbol{k}} \quad \text{(A.50)}$$

where $M = F.T\left\{\frac{1}{|\boldsymbol{r}|}\hat{x}\cdot\hat{\boldsymbol{r}}\hat{\boldsymbol{r}}\cdot\hat{x}\right\}$ and $A = F.T\left\{\frac{1}{|\boldsymbol{r}|}\hat{z}\cdot\hat{\boldsymbol{r}}\hat{\boldsymbol{r}}\cdot\hat{z}\right\} = F.T\left\{\frac{1}{|\boldsymbol{r}|}\hat{\boldsymbol{k}}\cdot\hat{\boldsymbol{r}}\hat{\boldsymbol{r}}\cdot\hat{\boldsymbol{k}}\right\} = F.T\left\{\frac{\cos^2\theta}{|\boldsymbol{r}|}\right\} = -\frac{4\pi}{k^2}$

$$Tr\left(T.F\left\{g(\boldsymbol{r})\right\}\right) = F.T\left\{Tr\left(g(\boldsymbol{r})\right)\right\} \Leftrightarrow T.F\left\{\frac{1}{|\boldsymbol{r}|}\right\} = \frac{4\pi}{k^2} = 2M + A = 2M - \frac{4\pi}{k^2} \tag{A.51}$$

So

$$M = \frac{4\pi}{k^2} \tag{A.52}$$

Thus

$$g(\boldsymbol{k}) = \begin{pmatrix} \frac{4\pi}{k^2} & 0 & 0 \\ 0 & \frac{4\pi}{k^2} & 0 \\ 0 & 0 & -\frac{4\pi}{k^2} \end{pmatrix} \begin{pmatrix} \hat{\boldsymbol{i}}\hat{\boldsymbol{i}} \\ \hat{\boldsymbol{j}}\hat{\boldsymbol{j}} \\ \hat{\boldsymbol{k}}\hat{\boldsymbol{k}} \end{pmatrix} = \frac{4\pi}{k^2}(\boldsymbol{I} - 2\hat{\boldsymbol{k}}\hat{\boldsymbol{k}}) \tag{A.53}$$

Finally we have the expression

$$\boldsymbol{G}_0(\boldsymbol{k}) = \frac{1}{\mu k^2}(\boldsymbol{I} - \hat{\boldsymbol{k}}\hat{\boldsymbol{k}}) + \frac{\boldsymbol{I}}{B + \frac{4\mu}{3}}\hat{\boldsymbol{k}}\hat{\boldsymbol{k}} \tag{A.54}$$

Bibliography

[1] Frisch Harry L. and J. K. Percus. Confined homopolymers. *J. Phys. Chem. B*, 105, 2001.

[2] Müller-Nedebock K. K., Frisch H. L., and Percus J. K. Stiff polymer in monomer ensemble. *Physical Review E*, 67, 2003.

[3] Wolgemuth C. W. Trend: Does cell biology need physicists? *Physics*, 4:4, 2011.

[4] Lombard J. Once upon a time the cell membranes: 175 years of cell boundary research. *Biology Direct*, 9(1):32, 2014.

[5] Israelachvili JN, Marčelja S., and Horn Roger G. Physical principles of membrane organization. *Quarterly Reviews of Biophysics*, 13(2):121–200, 1980.

[6] Bao Gang. and Suresh S. Cell and molecular mechanics of biological materials. *Nature Materials*, 2(11):715, 2003.

[7] Fletcher D. A. and Mullins R. D. Cell mechanics and the cytoskeleton. *EPL (Europhysics Letters)*, 110, 2015.

[8] Fletcher D. A. and Geissler P. L. Active biological materials. *Annual Review of Physical Chemistry*, 60, 2009.

[9] Stricker J., Falzone T., and Gardel M. L. Mechanics of the F-actin cytoskeleton. *Journal of Biomechanics*, 43, 2010.

[10] Tsai F. C. and Koenderink G. H. Shape control of lipid bilayer membranes by confined actin bundles. *Soft Matter*, 11, 2015.

[11] Murata K. and Wolf M. Cryo-electron microscopy for structural analysis of dynamic biological macromolecules. *Biochimica et Biophysica Acta (BBA)-General Subjects*, 2017.

[12] Mason William T. *Fluorescent and luminescent probes for biological activity: a practical guide to technology for quantitative real-time analysis*. Elsevier, 1999.

[13] Silva M. S., Alvarado J., Nguyen J., Georgoulia N., Mulder B. M., and Koenderink G. H. Self-organized patterns of actin filaments in cell-sized confinement. *Soft Matter*, 7, 2011.

[14] Benková Z., Rišpanová L., and Cifra P. Structural behavior of a semiflexible polymer chain in an array of nanoposts. *Polymers*, 9(8):313, 2017.

[15] Bovellan M., Romeo Y., Biro M., Boden A., Chugh P., Yonis A., Vaghela M., Fritzsche M., Moulding D., Thorogate R., et al. Cellular control of cortical actin nucleation. *Current Biology*, 24(14):1628–1635, 2014.

[16] Eggers Daryl K. and Valentine Joan S. Crowding and hydration effects on protein conformation: a study with sol-gel encapsulated proteins1. *Journal of Molecular Biology*, 314(4):911–922, 2001.

[17] Rotsch C. and Radmacher M. Drug-induced changes of cytoskeletal structure and mechanics in fibroblasts: an atomic force microscopy study. *Biophysical Journal*, 78(1):520–535, 2000.

[18] Pujol T., du Roure O., Fermigier M., and Heuvingh J. Impact of branching on the elasticity of actin networks. *Proceedings of the National Academy of Sciences*, 109(26):10364–10369, 2012.

[19] Kunkel J. and Asuri P. Function, structure, and stability of enzymes confined in agarose gels. *PloS One*, 9(1):e86785, 2014.

[20] Ospina Stella A. and Turville S. All-round manipulation of the actin cytoskeleton by hiv. *Viruses*, 10(2):63, 2018.

[21] Olson Michael F. and Sahai E. The actin cytoskeleton in cancer cell motility. *Clinical & Experimental Metastasis*, 26(4):273, 2009.

[22] Kanaan Z., Qadan M., Eichenberger Maurice R., and Galandiuk S. The actin-cytoskeleton pathway and its potential role in inflammatory bowel disease-associated human colorectal cancer. *Genetic Testing and Molecular Biomarkers*, 14(3):347–353, 2010.

[23] Ku NO, Zhou X., Toivola Diana M., and Omary M. Bishr. The cytoskeleton of digestive epithelia in health and disease. *American Journal of Physiology-Gastrointestinal and Liver Physiology*, 277(6):G1108–G1137, 1999.

[24] Panciera T., Azzolin L., Cordenonsi M., and Piccolo S. Mechanobiology of yap and taz in physiology and disease. *Nature Reviews Molecular Cell Biology*, 18(12):758, 2017.

[25] Nerem R. Mi. Vascular fluid mechanics, the arterial wall, and atherosclerosis. *Journal of Biomechanical Engineering*, 114(3):274–282, 1992.

[26] Paszek Matthew J., Zahir N., Johnson Kandice R., Lakins Johnathon N., Rozenberg Gabriela I., Gefen Amit, Reinhart-King Cynthia A., Margulies Susan S., Dembo M., Boettiger D., et al. Tensional homeostasis and the malignant phenotype. *Cancer Cell*, 8(3):241–254, 2005.

[27] C. Wickramarachchi D., Theofilopoulos Argyrios N., and Kono Dwight H. Immune pathology associated with altered actin cytoskeleton regulation. *Autoimmunity*, 43(1):64–75, 2010.

[28] Ailenberg M. and Silverman M. Cytochalasin d disruption of actin filaments in 3t3 cells produces an anti-apoptotic response by activating gelatinase a extracellularly and initiating intracellular survival signals. *Biochimica et Biophysica Acta (BBA)-Molecular Cell Research*, 1593(2-3):249–258, 2003.

[29] Hein S., Kostin S., Heling A., Maeno Y., and Schaper J. The role of the cytoskeleton in heart failure. *Cardiovascular Research*, 45(2):273–278, 2000.

[30] Bansod Yogesh D. and Bursa J. Continuum-based modelling approaches for cell mechanics. *World Academy of Science, Engineering and Technology, International Journal of Biological, Biomolecular, Agricultural, Food and Biotechnological Engineering*, 9(9):969–980, 2015.

[31] Hall Cameron L. *Modelling of some biological materials using continuum mechanics*. PhD thesis, Queensland University of Technology, 2008.

[32] Mofrad Mohammad RK and Kamm Roger D. *Cytoskeletal mechanics: models and measurements in cell mechanics*. Cambridge University Press, 2006.

[33] Polacheck William J. and Chen Christopher S. Measuring cell-generated forces: a guide to the available tools. *Nature methods.*, 13(5):415, 2016.

[34] Alvarado J., Mulder Bela M., and Koenderink Gijsje H. Alignment of nematic and bundled semiflexible polymers in cell-sized confinement. *Soft Matter*, 10(14):2354–2364, 2014.

[35] Tsugawa S., Hervieux N., Hamant O., Boudaoud A., Smith R. S., Li C. B., and Komatsuzaki T. Extracting subcellular fibrillar alignment with error estimation: Application to microtubules. *Biophysical Journal*, 110, 2016.

[36] Addae-Mensah Kweku A. and Wikswo John P. Measurement techniques for cellular biomechanics in vitro. *Experimental Biology and Medicine*, 233(7):792–809, 2008.

[37] Sun Y. and Nelson Bradley J. Mems for cellular force measurements and molecular detection. *International Journal of Information Acquisition*, 1(01):23–32, 2004.

[38] MacKintosh FC. Polymer-based models of cytoskeletal networks. *Cytoskelet Mech Model Meas Cell Mech*, 9(3):152–169, 2006.

[39] Wen Q. and Janmey Paul A. Polymer physics of the cytoskeleton. *Current Opinion in Solid State and Materials Science*, 15(5):177–182, 2011.

[40] Dai L., van der Maarel J., and Doyle Patrick S. Extended de gennes regime of dna confined in a nanochannel. *Macromolecules*, 47(7):2445–2450, 2014.

[41] Gao J., Tang P., Yang Y., and Chen Jeff ZY. Free energy of a long semiflexible polymer confined in a spherical cavity. *Soft Matter*, 10(26):4674–4685, 2014.

[42] Hawkins Rhoda J., Piel M., Faure-Andre G., Lennon-Dumenil AM, Joanny JF, Prost J, and Voituriez R. Pushing off the walls: a mechanism of cell motility in confinement. *Physical review letters*, 102(5):058103, 2009.

[43] Azari A. and Müller-Nedebock K. K. Entropic competition in polymeric systems under geometrical confinement. *EPL (Europhysics Letters)*, 463, 2010.

[44] Pasquali S. and Percus J. K. Mean field and the confined single homopolymer. *Molecular Physics*, 107, 2009.

[45] Gittes F., Mickey B., Nettleton J., and Howard J. Flexural rigidity of microtubules and actin filaments measured from thermal fluctuations in shape. *The Journal of Cell Biology*, 120(4):923–934, 1993.

[46] Ott A., Magnasco M., Simon A., and Libchaber A. Measurement of the persistence length of polymerized actin using fluorescence microscopy. *Physical Review E*, 48(3):R1642, 1993.

[47] Charrier Elisabeth E. and Janmey Paul A. Mechanical properties of intermediate filament proteins. In *Methods in Enzymology*, volume 568, pages 35–57. Elsevier, 2016.

[48] Herrmann H., Bär H., Kreplak L., Strelkov Sergei V., and Aebi U. Intermediate filaments: from cell architecture to nanomechanics. *Nature Reviews Molecular Bell Biology*, 8(7):562, 2007.

[49] Isambert H., Venier P., Maggs Anthony C., Fattoum A., Kassab R., Pantaloni D., and Carlier M-F. Flexibility of actin filaments derived from thermal fluctuations. effect of bound nucleotide, phalloidin, and muscle regulatory proteins. *Journal of Biological Chemistry*, 270(19):11437–11444, 1995.

[50] Svitkina T. M. and Borisy G. G. Arp2/3 complex and actin depolymerizing factor/cofilin in dendritic organization and treadmilling of actin filament array in lamellipodia. *The Journal of Cell Biology*, 145, 1999.

[51] Small J. V., Herzog M., and Anderson K. Actin filament organization in the fish keratocyte lamellipodium. *J. Cell Biol.*, 129, 1995.

[52] Flory Paul J. and Volkenstein M. Statistical mechanics of chain molecules, 1969.

[53] Frey E., Kroy K., Wilhelm J., and Sackmann E. Statistical mechanics of semiflexible polymers: theory and experiment. In *Dynamical Networks in Physics and Biology*, pages 103–119. Springer, 1998.

[54] Liu Y. and Chakraborty B. Shapes of semiflexible polymers in confined spaces. *Physical Biology*, 5(2):026004, 2008.

[55] Köster S., Kierfeld J., and Pfohl T. Characterization of single semiflexible filaments under geometric constraints. *The European Physical Journal E*, 25(4):439–449, 2008.

[56] Sakaue T. Semiflexible polymer confined in closed spaces. *Macromolecules*, 40(14):5206–5211, 2007.

[57] Chen Jeff ZY and Sullivan DE. Free energy of a wormlike polymer chain confined in a slit: crossover between two scaling regimes. *Macromolecules*, 39(22):7769–7773, 2006.

[58] Daoud M. and De Gennes PG. Statistics of macromolecular solutions trapped in small pores. *Journal de Physique*, 38(1):85–93, 1977.

[59] Higuchi Y., Yoshikawa K., and Iwaki T. Confinement causes opposite effects on the folding transition of a single polymer chain depending on its stiffness. *Physical Review E*, 84(2):021924, 2011.

[60] Cifra P. and Bleha T. Shape transition of semi-flexible macromolecules confined in channel and cavity. *The European Physical Journal E*, 32(3):273–279, 2010.

[61] Nikoubashman A., Vega Daniel A., Binder K., and Milchev A. Semiflexible polymers in spherical confinement: Bipolar orientational order versus tennis ball states. *Physical Review Letters*, 118(21):217803, 2017.

[62] Chen Jeff ZY. Theory of wormlike polymer chains in confinement. *Progress in Polymer Science*, 54:3–46, 2016.

[63] Zhang W-Y and Chen Jeff ZY. Tennis-ball state of a self-avoiding wormlike polymer on a spherical surface. *EPL (Europhysics Letters)*, 94(4):43001, 2011.

[64] Wolfe J. Cellular thermodynamics: the molecular and macroscopic views. *eLS,(Chichester: John Wiley & Sons, Ltd.)*, pages 1–13, 2015.

[65] Yang Y., Qiu F., Tang P., and Zhang H. Applications of self-consistent field theory in polymer systems. *Science in China Series B*, 49(1):21–43, 2006.

[66] Edwards Sam F. The statistical mechanics of polymers with excluded volume. *Proceedings of the Physical Society*, 85(4):613, 1965.

[67] Bryk P. and MacDowell Luis G. Self-consistent field/density functional study of conformational properties of polymers at interfaces: Role of intramolecular interactions. *The Journal of Chemical Physics*, 129(10):104901, 2008.

[68] Matsen Mark W. Self-consistent field theory and its applications. *Soft Matter*, 1:87–178, 2006.

[69] Fredrickson G. *The equilibrium theory of inhomogeneous polymers*, volume 134. Oxford University Press on Demand, 2006.

[70] Dolgushev M., Berezovska G., and Blumen A. Branched semiflexible polymers: theoretical and simulation aspects. *Macromolecular Theory and Simulations*, 20(8):621–644, 2011.

[71] Pujol T., du Roure O., Fermigier M., and Heuvingh J. Impact of branching on the elasticity of actin networks. *Proceedings of the National Academy of Sciences*, 109(26):10364–10369, 2012.

[72] Cates Michael E. and Edwards Samuel F. Linear theory of disordered fibre-reinforced composites. *Proc. R. Soc. Lond. A*, 395(1808):89–109, 1984.

[73] Teraoka I. Polymer solutions in confining geometries. *Progress in Polymer Science*, 21(1):89–149, 1996.

[74] Ostermeir K., Alim K., and Frey E. Confinement induces conformational transition of semiflexible polymer rings to figure eight form. *Soft Matter*, 6(15):3467–3471, 2010.

[75] Wang J. and Gao H. A generalized bead-rod model for Brownian dynamics simulations of wormlike chains under strong confinement. *The Journal of Chemical Physics*, 123(8):084906, 2005.

[76] Kratky O. O. Kratky and G. Porod, Recl. Trav. Chim. Pays-Bas 68, 1106 (1949). *Recl. Trav. Chim. Pays-Bas*, 68:1106, 1949.

[77] Yamakawa H. *Modern theory of polymer solutions.* Harper & Row, 1971.

[78] Ganesan V., Khounlavong L., and Pryamitsyn V. Equilibrium characteristics of semiflexible polymer solutions near probe particles. *Physical Review E*, 78(5):051804, 2008.

[79] Lamura A. and Winkler RG. Semiflexible polymers under external fields confined to two dimensions. *The Journal of Chemical Physics*, 137(24):244909, 2012.

[80] Müller-Nedebock K. K. and Frisch H. L. Matrix models of discretely bending, stiff polymers. *Polymer Physics*, 44, 2003.

[81] Teraoka Arlene A. and Teraoka I. *Polymer solutions: an introduction to physical properties.* John Wiley & Sons, 2002.

[82] Baxter Rodney J. *Exactly solved models in statistical mechanics.* Elsevier, 2016.

[83] Svitkina T. Imaging cytoskeleton components by electron microscopy. In *Cytoskeleton Methods and Protocols*, pages 187–206. Springer, 2009.

[84] Reymann A-C, Martiel J-L, Cambier T., Blanchoin L., Boujemaa-Paterski R., and Théry M. Nucleation geometry governs ordered actin networks structures. *Nature Materials*, 9(10):827, 2010.

[85] Letort G., Politi A. Z., Ennomani H., Théry M., Nedelec F., and Blanchoin L. Geometrical and mechanical properties control actin filament organization. *PLoS Computational Biology*, 11, 2015.

[86] Ennomani Hajer, Letort Gaëlle, Guérin Christophe, Martiel Jean-Louis, Cao Wenxiang, Nédélec François, Enrique M, Théry Manuel, and Blanchoin Laurent. Architecture and connectivity govern actin network contractility. *Current Biology*, 26(5):616–626, 2016.

[87] Olson M. F. and Sahai E. The actin cytoskeleton in cancer cell motility. *Clinical and Experimental Metastasis*, 276, 2009.

[88] Chen Christopher S., Mrksich M., Huang S., Whitesides George M., and Ingber Donald E. Geometric control of cell life and death. *Science*, 276(5317):1425–1428, 1997.

[89] Mullins R. Dyche, Heuser John A., and Pollard Thomas D. The interaction of arp2/3 complex with actin: nucleation, high affinity pointed end capping, and formation of branching networks of filaments. *Proceedings of the National Academy of Sciences*, 95(11):6181–6186, 1998.

[90] Quint D. A. and Schwarz J. M. Optimal orientation in branched cytoskeletal networks. *Journal of Mathematical Biology*, 63, 2011.

[91] Borisy G. G. and Svitkina T. M. Actin machinery: pushing the envelope. *Cell Biol.*, 12, 2000.

[92] Gunning Brian ES and Steer Martin W. *Plant cell biology: structure and function*. Jones & Bartlett Learning, 1996.

[93] Clark Andrew G., Dierkes K., and Paluch Ewa K. Monitoring actin cortex thickness in live cells. *Biophysical Journal*, 105(3):570–580, 2013.

[94] Gillespie J. Mayne M. and Jiang M. RNA folding on the 3D triangular lattice. *BMC Bioinformatics*, 10, 2009.

[95] Liu J., Song B., Yao Y., Xue Y., Liu W., and Liu Z. Wang-landau sampling in face-centered-cubic hydrophobic-hydrophilic lattice model proteins. *Physical Review E*, 90(4):042715, 2014.

[96] Newman M. E. and Ziff R. M. Fast Monte Carlo algorithm for site or bond percolation. *Physical Review E*, 64, 2001.

[97] Maly I. V. and Borisy G. G. Self-organization of a propulsive actin network as an evolutionary process. *Proceedings of the National Academy of Sciences*, 98, 2001.

[98] Clausen Mathias P., Colin-York H., Schneider F., Eggeling C., and Fritzsche M. Dissecting the actin cortex density and membrane-cortex distance in living cells by super-resolution microscopy. *Journal of Physics D: Applied Physics*, 50(6):064002, 2017.

[99] Joanny J-F, Kruse K., Prost J., and Ramaswamy S. The actin cortex as an active wetting layer. *The European Physical Journal E*, 36(5):52, 2013.

[100] Le Goff L., Hallatschek O., Frey E., and Amblard F. Tracer studies on f-actin fluctuations. *Physical Review Letters*, 89(25):258101, 2002.

[101] Nakaya K., Imai M., Komura S., Kawakatsu T., and Urakami N. Polymer-confinement-induced nematic transition of microemulsion droplets. *EPL (Europhysics Letters)*, 71(3):494, 2005.

[102] Köster S., Steinhauser D., and Pfohl T. Brownian motion of actin filaments in confining microchannels. *Journal of Physics: Condensed Matter*, 17(49):S4091, 2005.

[103] Cifra P. Weak-to-strong confinement transition of semi-flexible macromolecules in slit and in channel. *The Journal of Chemical Physics*, 136(2):024902, 2012.

[104] Pinot M., Chesnel F., Kubiak JZ, Arnal I., Nedelec FJ, and Gueroui Z. Effects of confinement on the self-organization of microtubules and motors. *Current Biology*, 19(11):954–960, 2009.

[105] Fischman Donald A. An electron microscope study of myofibril formation in embryonic chick skeletal muscle. *The Journal of Cell Biology*, 32(3):557–575, 1967.

[106] Wirtz D. Atilgan E. and Sun S. X. Morphology of the lamellipodium and organization of actin filaments at the leading edge of crawling cells. *Biophysical Journal*, 89, 2005.

[107] Pritchard R. H., Huang Y. Y. S., and Terentjev E. M. Mechanics of biological networks: from the cell cytoskeleton to connective tissue. *Soft Matter*, 10, 2014.

[108] Liu J., Song B., Yao Y., Xue Y., Liu W., and Liu Z. Wang-Landau sampling in face-centered-cubic hydrophobic-hydrophilic lattice model proteins. *Physical Review E*, 90, 2014.

[109] Smyda Mark R. and Harvey Stephen C. The entropic cost of polymer confinement. *The Journal of Physical Chemistry B.*, 116(35):10928–10934, 2012.

[110] Cifra P. and Bleha T. Simulation of chain organization in encapsulated polymers. In *Macromolecular Symposia*, volume 296, pages 336–341. Wiley Online Library, 2010.

[111] Benková Z., Rišpanová L., and Cifra P. Structural behavior of a semiflexible polymer chain in an array of nanoposts. *Polymers*, 9(8):313, 2017.

[112] Iwasa Janet H. and Mullins R. Dyche. Spatial and temporal relationships between actin-filament nucleation, capping, and disassembly. *Current Biology*, 17(5):395–406, 2007.

[113] Du Toit A., De Wet S., Hofmeyr JH, Müller-Nedebock K., and Loos B. The precision control of autophagic flux and vesicle dynamics - a micropattern approach. *Cells*, 7(8):94, 2018.

[114] Yu Y-X and Wu J. Density functional theory for inhomogeneous mixtures of polymeric fluids. *The Journal of Chemical Physics*, 117(5):2368–2376, 2002.

[115] Wei Z., Ning N., Zhang L., Tian M., and Mi J. Density functional theory of polymer structure and conformations. *Polymers*, 8(4):121, 2016.

[116] Paturej J., Milchev A., Egorov Sergei A., and Binder K. Star polymers confined in a nanoslit: A simulation test of scaling and self-consistent field theories. *Soft Matter*, 9(44):10522–10531, 2013.

[117] Cerdà Juan J., Sintes T., and Chakrabarti A. Excluded volume effects on polymer chains confined to spherical surfaces. *Macromolecules*, 38(4):1469–1477, 2005.

[118] Sikorski A. and Romiszowski P. Properties of branched confined polymers. *The Journal of Chemical Physics*, 120(15):7206–7211, 2004.

[119] Xu C., Hu S., and Chen X. Artificial cells: from basic science to applications. *Materials Today*, 19(9):516–532, 2016.

[120] Safran SA, Gov N., Nicolas A., Schwarz US, and Tlusty T. Physics of cell elasticity, shape and adhesion. *Physica A: Statistical Mechanics and its Applications*, 352(1):171–201, 2005.

[121] Ananthakrishnan Revathi, Guck Jochen, Wottawah Falk, Schinkinger Stefan, Lincoln Bryan, Romeyke M., Moon T., and Käs J. Quantifying the contribution of actin networks to the elastic strength of fibroblasts. *Journal of Theoretical Biology*, 242(2):502–516, 2006.

[122] Abreu-Blanco Maria Teresa, Watts James J., Verboon Jeffrey M., and Parkhurst Susan M. Cytoskeleton responses in wound repair. *Cellular and Molecular Life Sciences*, 69(15):2469–2483, 2012.

[123] Huber F., Strehle D., Schnauß J., and Käs J. Formation of regularly spaced networks as a general feature of actin bundle condensation by entropic forces. *New Journal of Physics*, 17(4):043029, 2015.

[124] Kubitschke H, Schnauss J., Nnetu KD, Warmt E., Stange R., and Kaes J. Actin and microtubule networks contribute differently to cell response for small and large strains. *New Journal of Physics*, 19(9):093003, 2017.

[125] Wilhelm J. and Frey E. Elasticity of stiff polymer networks. *Physical Review Letters*, 91(10):108103, 2003.

[126] Huber F., Schnauß J., Rönicke S., Rauch P., Müller K., Fütterer C., and Käs J. Emergent complexity of the cytoskeleton: from single filaments to tissue. *Advances in Physics*, 62(1):1–112, 2013.

[127] Lieleg O., Claessens Mireille MAE, and Bausch Andreas R. Structure and dynamics of cross-linked actin networks. *Soft Matter*, 6(2):218–225, 2010.

[128] Huisman Erik M., van Dillen T., Onck Patrick R., and Van der Giessen E. Three-dimensional cross-linked f-actin networks: relation between network architecture and mechanical behavior. *Physical Review Letters*, 99(20):208103, 2007.

[129] Schmoller KM, Lieleg O., and Bausch AR. Structural and viscoelastic properties of actin/filamin networks: cross-linked versus bundled networks. *Biophysical Journal*, 97(1):83–89, 2009.

[130] Pinot M., Steiner V., Dehapiot B., Yoo B-K, Chesnel F., Blanchoin L., Kervrann C., and Gueroui Z. Confinement induces actin flow in a meiotic cytoplasm. *Proceedings of the National Academy of Sciences*, 109(29):11705–11710, 2012.

[131] Alberts B., Johnson A., Lewis J., Raff M., Roberts K., and Walter P. How cells regulate their cytoskeletal filaments. 2002.

[132] Rathore N., Knotts IV Thomas A., and de Pablo Juan J. Confinement effects on the thermodynamics of protein folding: Monte carlo simulations. *Biophysical Journal*, 90(5):1767–1773, 2006.

[133] Yamaguchi H. and Condeelis J. Regulation of the actin cytoskeleton in cancer cell migration and invasion. *Biochimica et Biophysica Acta (BBA)-Molecular Cell Research*, 1773(5):642–652, 2007.

[134] Friedl P. and Wolf K. Tumour-cell invasion and migration: diversity and escape mechanisms. *Nature Reviews Cancer*, 3(5):362, 2003.

[135] Friedl P. and Gilmour D. Collective cell migration in morphogenesis, regeneration and cancer. *Nature reviews Molecular Cell Biology*, 10(7):445, 2009.

[136] Ramis-Conde I., Chaplain Mark AJ, and Anderson Alexander RA. Mathematical modelling of cancer cell invasion of tissue. *Mathematical and Computer Modelling*, 47(5-6):533–545, 2008.

[137] Szymańska Z., Rodrigo Cristian M., Lachowicz M., and Chaplain Mark AJ. Mathematical modelling of cancer invasion of tissue: the role and effect of nonlocal interactions. *Mathematical Models and Methods in Applied Sciences*, 19(02):257–281, 2009.

[138] Gerisch A. and Chaplain MAJ. Mathematical modelling of cancer cell invasion of tissue: local and non-local models and the effect of adhesion. *Journal of Theoretical Biology*, 250(4):684–704, 2008.

[139] Chicurel Marina E., Chen Christopher S., and Donald E. Ingber. Cellular control lies in the balance of forces. *Current Opinion in Cell Biology*, 10(2):232–239, 1998.

[140] Blundell JR and Terentjev EM. Buckling of semiflexible filaments under compression. *Soft Matter*, 5(20):4015–4020, 2009.

[141] Blundell JR and Terentjev EM. Forces and extensions in semiflexible and rigid polymer chains and filaments. *Journal of Physics A: Mathematical and Theoretical*, 40(36):10951, 2007.

[142] Wang S., Arellano-Santoyo H., Combs Peter A., and Shaevitz Joshua W. Actin-like cytoskeleton filaments contribute to cell mechanics in bacteria. *Proceedings of the National Academy of Sciences*, 107(20):9182–9185, 2010.

[143] Hannezo E., Prost J., and Joanny J-F. Instabilities of monolayered epithelia: shape and structure of villi and crypts. *Physical Review Letters*, 107(7):078104, 2011.